

BWR STABILITY AND BIFURCATION ANALYSIS USING A NOVEL REDUCED ORDER MODEL AND THE SYSTEM CODE RAMONA

THÈSE N° 2927 (2004)

PRÉSENTÉE À LA FACULTÉ SCIENCES DE BASE

Institut de physique de l'énergie et des particules

SECTION DE PHYSIQUE

ÉCOLE POLYTECHNIQUE FÉDÉRALE DE LAUSANNE

POUR L'OBTENTION DU GRADE DE DOCTEUR ÈS SCIENCES

PAR

Abdelhamid DOKHANE

diplôme de physique théorique, Centre International pour la physique théorique, Trieste, Italie
et de nationalité algérienne

acceptée sur proposition du jury:

Prof. R. Chawla, directeur de thèse
Prof. A. Fasoli, rapporteur
Dr D. Hennig, rapporteur
Prof. Rizwan-Uddin, rapporteur
Prof. G. Verdú, rapporteur

Lausanne, EPFL
2004

This Thesis is dedicated to

*My Parents: Houria and Allaoua,
My Wife Leila,
And my Sons: Aimen & Amine*

ABSTRACT

Boiling water reactor (BWR) stability analysis is usually carried out using large system codes. However, because of the large computational efforts required, such codes cannot in practice be employed for the detailed investigation of the complete manifold of solutions of the nonlinear differential equations describing the BWR system. In this context, reduced order models, containing a minimum number of system equations describing the most important physical phenomena, become necessary to provide deeper insight into the physical mechanisms underlying the different instability phenomena observed in BWRs, *e.g.* in-phase and out-of-phase power oscillations.

A novel analytical, reduced order model has been currently developed to simulate the different types of instabilities encountered in heated channels and BWRs, *viz.* density wave oscillations (DWOs), as well as in-phase and out-of-phase oscillations in the reactor core. The complete model comprises three main parts: spatial lambda-mode neutron kinetics with the fundamental and first azimuthal modes, fuel heat conduction dynamics, and core thermal-hydraulics based on a drift flux model representation of the two-phase flow.

Stability and *semi-analytical* bifurcation analysis is carried out for a purely thermal-hydraulic system (heated channel), as well as for a complete BWR (represented via two-channel nuclear-coupled thermal-hydraulics), using the current reduced order model in conjunction with the bifurcation code BIFDD. The impact of the drift flux parameters on the stability boundary (SB) and nature of bifurcation has thereby been investigated. Results show that both sub- and supercritical Hopf bifurcations are encountered along the stability boundary. Using a drift flux model instead of a homogeneous equilibrium model for the two-phase flow is found to have significant effects on the SB, as well as on the nature of Hopf bifurcation. For independent confirmation of the results of the semi-analytical bifurcation analyses, as well as to evaluate the system behaviour in regions away from the stability boundary, numerical integration has been carried out of the set of ordinary differential equations (ODEs) involved in each case.

With each of the two channels of the currently developed BWR reduced order model representing half of the reactor core, it has been possible to apply it to the investigation of out-of-phase instability phenomena as well. First, the stability limits for in-phase and out-of-phase BWR oscillation modes for a generic case are determined in parameter space. An in-depth investigation is then performed of the properties of the elements of the eigenvectors associated with these two oscillation modes. Results show that analysing the properties of the eigenvectors can provide full information as regards the corresponding oscillation mode

(in-phase or out-of-phase) *without* solving the set of system ODEs. In addition, such analysis conclusively shows that in-phase and out-of-phase oscillation modes in a BWR are *whole-system* mechanisms and not just limited to the excitation of the fundamental and first azimuthal modes of the neutron flux.

In parallel to the generic studies with the reduced order model, a detailed local bifurcation analysis has been performed at two representative operational points for the Leibstadt and Ringhals-1 BWR nuclear power plants using the complex system code RAMONA. The goal in this analysis is to demonstrate how the system solution (behaviour) can, in some situations, vary in a significant manner when a certain parameter, *e.g.* the mass flow rate, is changed by small amounts. First, a *correspondence hypothesis* is proposed, underlining the unique relationship for BWRs between a stable (unstable) limit cycle solution and the occurrence of a supercritical (subcritical) Hopf bifurcation. The RAMONA analysis carried out clearly shows that stability and bifurcation analysis expertise using reduced order models is indeed very important for the understanding and appropriate interpretation of certain complicated nonlinear phenomena that are sometimes observed in simulations using system codes. Thus, the present investigations have revealed, for the first time, the occurrence of a subcritical Hopf bifurcation during BWR stability analysis using a system code. Such a study is thereby shown to allow the determination and characterisation of local stability boundaries within the exclusion area of a BWR's power-flow map.

Finally, in order to assess the applicability (as well as limitations) of the currently developed reduced order in a more quantitative manner, it has been applied to the analysis of a specific Leibstadt operational point. Comparison of the results obtained with those of RAMONA show that, although the current reduced order model could adequately predict certain characteristics, it was not able to correctly predict some others because of the highly simplified reactor core geometry, the uncertainties in evaluating the design and operating parameters, as also the limitations of the feedback reactivity model employed. The main conclusion to be drawn in this context is that, although reduced order models do indeed allow an in-depth understanding of the complex processes determining BWR stability (through the possibility of conducting fast and detailed semi-analytical bifurcation analysis), they need to be considered as *complementary* tools to complex system codes, and *not* as alternatives.

VERSION ABREGEE

Les études de stabilité des Réacteurs à Eau Bouillante (REB) s'appuient généralement sur l'utilisation de puissants codes de simulation appelés codes système. Cependant, une analyse détaillée de l'ensemble des solutions des équations différentielles non linéaires décrivant un système complexe comme le REB nécessite des temps de calcul prohibitifs. Pour ce genre d'analyse, des modèles dits d'ordre réduit, décrivant les principaux phénomènes physiques avec un minimum d'équations, s'avèrent mieux adaptés notamment pour mettre en lumière les mécanismes physiques mis en jeu lors des différentes instabilités observées dans le fonctionnement des REB.

Un nouveau modèle analytique d'ordre réduit a été développé pour simuler les différents types d'instabilités rencontrées dans des canaux chauffants et dans les REB, aussi bien les Oscillations d'Onde de Densité (OOD) que les oscillations de puissance en phase (globale) ou en opposition de phase (azimutalement déphasée) dans le cœur du réacteur. Le modèle complet comporte trois parties : un modèle de neutronique spatiale de type lambda incluant le mode fondamental et le premier mode azimutal, un modèle dynamique de conduction thermique au sein du combustible, et un modèle thermohydraulique basé sur une représentation de type "drift flux" de l'écoulement diphasique dans le cœur.

Des analyses de stabilité et les analyses *semi-analytiques* de bifurcation ont été accomplies pour un système purement thermohydraulique puis un système REB complet (représenté par deux canaux thermohydrauliques avec couplage neutronique) en utilisant conjointement le nouveau modèle d'ordre réduit et le code de bifurcation BIFDD. L'influence des paramètres du modèle "drift flux" sur la limite de stabilité (LS) et sur le type de bifurcation a été étudiée. Les résultats permettent d'observer des bifurcations de Hopf le long de la LS, aussi bien de type sous-critique que de type super-critique. L'utilisation d'un modèle "drift flux", au lieu d'un modèle homogène, pour simuler l'écoulement diphasique, indique un effet appréciable aussi bien sur la LS que sur le type de bifurcation de Hopf. De plus, afin de confirmer d'une manière indépendante les résultats de l'analyse semi-analytique des bifurcations et d'évaluer le comportement du système dans les régions éloignées de la LS, une intégration numérique a été faite, pour chaque cas, à partir de l'ensemble des équations différentielles ordinaires (EDO).

A l'aide de la représentation du cœur du REB par deux canaux parallèles, il a aussi été possible de reproduire et d'étudier des oscillations en opposition de phase. D'abord, les LS pour les oscillations en phase ou en opposition de phase sont déterminées dans l'espace des paramètres. Puis les propriétés des éléments des vecteurs propres associés à ces deux modes

d'oscillations sont analysées de manière détaillée. Les résultats montrent en fait que l'analyse des vecteurs propres seule permet de déterminer directement le mode d'oscillation associé sans qu'il soit nécessaire de résoudre directement le système d'EDO. De plus, ces résultats mettent en lumière que les oscillations en phase et en opposition de phase dans un REB sont en fait des mécanismes *globaux*, et ne sont pas seulement limités à l'excitation du mode fondamental et du premier mode azimutal du flux neutronique.

Parallèlement à ces études génériques avec le modèle d'ordre réduit, une étude de bifurcation pour deux points de fonctionnement représentatifs des REB de Leibstadt et de Ringhals-1 a été effectuée avec le code système RAMONA. Le but de cette étude est de démontrer comment, sous certaines conditions, le comportement du système prédit par le code peut sensiblement varier en fonction de faibles variations de certains paramètres, comme par exemple le débit massique entrant dans le cœur. D'abord, une *hypothèse de correspondance* est proposée, dans laquelle une relation univoque est établie pour les REB entre un cycle limite stable (instable) et une bifurcation de Hopf de type super-critique (sous-critique). Cette étude montre en tout cas clairement qu'une expertise de l'analyse des bifurcations (utilisant des modèles d'ordre réduit) est en effet très importante pour comprendre et interpréter correctement les phénomènes non linéaires observables dans les résultats des codes tel que RAMONA. Ainsi, cette étude a permis d'identifier, pour la première fois, une bifurcation de Hopf de type sous-critique dans une étude de stabilité de REB avec un code système. Elle a aussi permis de déterminer et de caractériser des LS locales à l'intérieur de la zone d'exclusion dans le diagramme débit-puissance d'un REB.

Finalement, afin d'être en mesure d'évaluer d'une manière plus quantitative l'applicabilité (aussi bien que les limitations) du nouveau modèle d'ordre réduit, il a été appliqué à un point de fonctionnement particulier du REB de Leibstadt. Une comparaison des résultats avec ceux obtenus avec RAMONA montre que le modèle d'ordre réduit peut prédire de manière adéquate certaines caractéristiques mais n'est pas capable d'en reproduire certaines autres. La raison provient principalement du trop grand degré de simplification de la modélisation géométrique du cœur, de l'incertitude dans l'évaluation des paramètres de fonctionnement du REB mais aussi des limites du modèle de contre-réaction de réactivité employé. Dans ce contexte, la conclusion principale que l'on peut tirer est la suivante : les modèles d'ordre réduits ne peuvent être considérés comme des *substituts* aux codes système détaillés, mais plutôt comme des outils d'évaluation *complémentaires* qui permettent, par l'utilisation d'analyse *semi-analytique* de bifurcation, une compréhension approfondie des mécanismes complexes déterminant la stabilité des REB.

CONTENTS

1	INTRODUCTION	1
1.1	PREVIOUS WORK	4
1.1.1	Heated Channel Problems	4
1.1.2	Nuclear-Coupled Thermal-hydraulic Instabilities	6
1.1.3	BWR Stability Analysis Using Complex System Codes	7
1.2	PRESENT OBJECTIVES	7
1.3	ORIGINAL CONTRIBUTIONS	9
1.4	THESIS OUTLINE	10
	References	11
2	BWR STABILITY ANALYSIS	15
2.1	CONCEPT OF STABILITY	15
2.2	LINEAR STABILITY ANALYSIS	15
2.2.1	Linear Stability Criteria	17
2.2.2	BWR Models for Linear Stability Analysis	18
2.3	NONLINEAR ANALYSIS	19
2.3.1	Stability Boundary in Mathematical Sense	19
2.3.2	BWR Models for Nonlinear Stability Analysis	21
2.4	EXPERIMENTAL ANALYSIS (TIME SERIES ANALYSIS)	23
2.4.1	Monitoring System	24
2.4.2	Time Series Analysis	26
2.5	SPATIAL MODE INSTABILITIES	27
2.6	HYDRAULIC BOUNDARY CONDITIONS ISSUE	29
2.7	CODES USED IN THIS THESIS	31
2.7.1	System Code RAMONA	32
2.7.2	Bifurcation code BIFDD	35
2.7.3	Reduced order model Fortran code (<i>bwr.f</i>)	35
2.7.4	Matlab program for numerical integration (<i>integration.m</i>)	35
	References	37
3	BIFURCATION ANALYSIS	41
3.1	HOPF BIFURCATION THEORY	41
3.1.1	Center Manifold Reduction	44
3.1.2	Poincaré Normal Form	44
3.2	SEMI-ANALYTICAL BIFURCATION METHOD	45
3.3	CODE BIFDD	46
3.3.1	Numerical Evaluation of Hopf Bifurcation Parameters	47
3.3.2	BIFDD Modification	48
	References	49
4	DEVELOPMENT OF THE NOVEL REDUCED ORDER MODEL	51

4.1	<i>INTRODUCTION</i>	51
4.2	<i>NEUTRON KINETICS</i>	52
4.3	<i>FUEL ROD HEAT CONDUCTION</i>	57
4.4	<i>THERMAL-HYDRAULICS</i>	64
4.5	<i>CORRELATIONS USED</i>	72
4.6	<i>SUMMARY OF THE NEW REDUCED ORDER MODEL</i>	73
	References	74
5	STABILITY AND BIFURCATION ANALYSIS OF A HEATED CHANNEL -----	77
5.1	<i>INTRODUCTION</i>	77
5.2	<i>THE HEATED CHANNEL MODEL</i>	79
5.3	<i>VALIDATION OF THE THERMAL-HYDRAULIC MODEL</i>	80
5.4	<i>DRIFT FLUX VS. HOMOGENEOUS EQUILIBRIUM MODEL</i>	86
	5.4.1 Semi-Analytical Bifurcation Analysis	86
	5.4.2 Numerical Simulation	90
5.5	<i>SENSITIVITY ANALYSIS</i>	96
	5.5.1 Semi-Analytical Bifurcation Analysis	96
	5.5.2 Numerical Simulation	99
5.6	<i>SUMMARY AND CONCLUSIONS</i>	101
	References	101
6	NONLINEAR BWR STABILITY ANALYSIS USING THE CURRENT TWO-CHANNEL REDUCED ORDER MODEL -----	105
6.1	<i>INTRODUCTION</i>	105
6.2	<i>SUMMARY OF THE BWR MODEL</i>	107
6.3	<i>STABILITY LIMITS FOR IN-PHASE AND OUT-OF-PHASE MODES</i>	108
	6.3.1 Semi-analytical Bifurcation Analysis	109
	6.3.2 Numerical Simulation	119
	6.3.3 Conclusions	125
6.4	<i>THE EFFECTS OF USING A DRIFT FLUX VERSUS HOMOGENEOUS EQUILIBRIUM MODEL</i>	126
	6.4.1 Effects of the drift flux parameters on the SB and the nature of Hopf bifurcation..	126
	6.4.2 Effects of the drift flux parameters on the type of oscillation mode.....	133
6.5	<i>SUMMARY AND CONCLUSIONS</i>	134
	References	135
7	BIFURCATION ANALYSIS USING RAMONA -----	137
7.1	<i>INTRODUCTION</i>	137
7.2	<i>THE CORRESPONDENCE HYPOTHESIS: STABLE (UNSTABLE) LIMIT CYCLE Vs. SUPERCRITICAL (SUBCRITICAL) HOPF BIFURCATION</i>	138
7.3	<i>SUBCRITICAL HOPF BIFURCATION USING RAMONA</i>	139
	7.3.1 Results for the Different Leibstadt NPP Operational Points.....	141

7.3.2 Interpretation and Discussion.....	147
7.4 SUPERCRITICAL HOPF BIFURCATION USING RAMONA.....	150
7.4.1 Results for the Different Ringhals-1 NPP Operational Points	151
7.4.2 Interpretation and Discussion.....	154
7.5 SUMMARY AND CONCLUSIONS.....	157
References	159
8 REDUCED ORDER MODEL VS. SYSTEM CODE RAMONA-----	161
8.1 SENSITIVITY ANALYSIS USING THE REDUCED ORDER MODEL.....	162
8.1.1 Effects of Void Feedback Reactivity.....	162
8.1.2 Effects of Pellet-Clad Gap Conductance	164
8.1.3 Effects of Fuel Radial Dimensions	164
8.1.4 Effects of Inlet and Exit Pressure Loss Coefficients.....	164
8.2 STABILITY BEHAVIOUR OF THE KKLC7_REC4 OP USING RAMONA....	169
8.3 STABILITY CHARACTERISTICS OF THE KKLC7_REC4 OP USING THE REDUCED ORDER MODEL.....	171
8.3.1 Semi-analytical Bifurcation Analysis	172
8.3.2 Numerical Simulation.....	174
8.4 COMPARISON OF RESULTS AND DISCUSSION.....	174
8.5 SUMMARY AND CONCLUSIONS.....	177
References	178
9 CONCLUSIONS AND RECOMMENDATIONS FOR FUTURE WORK-----	181
9.1 CONCLUSIONS.....	182
9.2 RECOMMENDATIONS FOR FUTURE WORK.....	185
APPENDIX A RAMONA MODEL DESCRIPTIONS -----	189
A.1 NEUTRON KINETICS.....	189
A.2 FUEL THERMODYNAMICS.....	190
A.3 THERMAL-HYDRAULICS.....	191
A.4 RAMONA-5 VERSION.....	194
APPENDIX B BASIC CONCEPTS OF NONLINEAR DYNAMICS-----	195
B.1 FIXED POINTS.....	195
B.2 LIMIT CYCLE.....	196
B.3 STABLE, UNSTABLE AND CENTER MANIFOLDS.....	197
B.4 FLOQUET THEORY.....	198
B.5 SECONDARY HOPF BIFURCATION (NEIMARK BIFURCATION).....	200
APPENDIX C DIMENSIONLESS PARAMETERS-----	201
APPENDIX D INTERMEDIATE EXPRESSIONS -----	203
APPENDIX E FEEDBACK REACTIVITY CALCULATIONS -----	215

<i>E.1 VOID FEEDBACK REACTIVITY</i>	216
<i>E.2 DOPPLER FEEDBACK REACTIVITY</i>	222
<i>E.3 TOTAL FEEDBACK REACTIVITIES</i>	226
APPENDIX F TYPICAL BWR DESIGN AND OPERATING PARAMETERS-	231
APPENDIX G DESIGN AND OPERATING PARAMETERS FOR THE NOMINAL LEIBSTADT NPP OPERATIONAL POINT -----	233
NOMENCLATURE -----	235
ACKNOWLEDGEMENTS -----	239
CURRICULUM VITAE-----	241

1 INTRODUCTION

Nuclear power currently accounts for 17% of the electricity generation worldwide (see Fig. 1-1). There are currently approximately 437 nuclear power reactors in operation in over 30 countries around the world, with a total output of some 350,000 MWe. An additional 36 reactors (27,000 MWe) are currently under construction. Over 80% of the nuclear generated electricity in the world comes from reactors classified as light water reactors (LWRs). In these reactors the neutrons are slowed down, or moderated, by ordinary (or light) water and the heat is removed by the same water.

In some designs of LWRs, the water is allowed to boil in the reactor core and the steam is directly used to drive a turbine generator to create electricity (Fig. 1-2). These are called boiling water reactors (BWRs). In the other designs, the water in the core is under higher pressure (150 bar) and does not boil. This water goes to a steam generator where the steam is produced in another water loop (Fig.1-3). Such a system is called a pressurized water reactor (PWR).

The fuel used in LWRs is either UO_2 with uranium enriched to 3-5 wt% (low enrichment) or mixed oxide (MOX), a mixture of UO_2 and PuO_2 ¹.

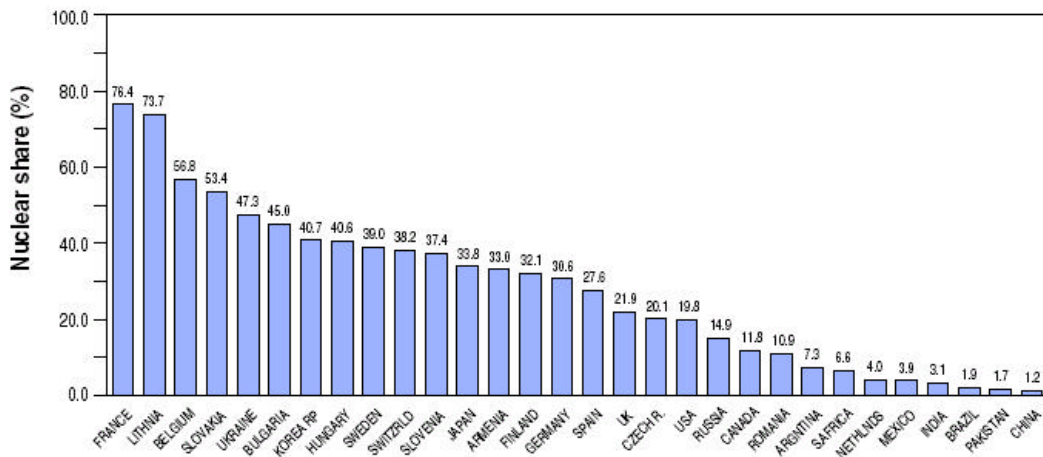


Figure 1-1. The percentage of electricity generated by nuclear power in 30 countries in 2000 [1].

¹ PuO_2 obtained from the reprocessing of spent UO_2 fuel

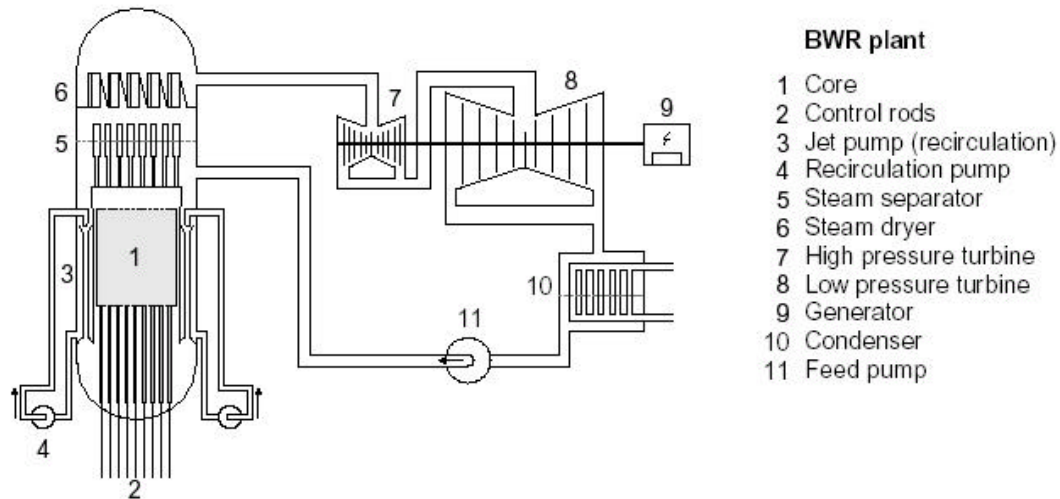


Figure 1-2. Schematic view of a BWR plant

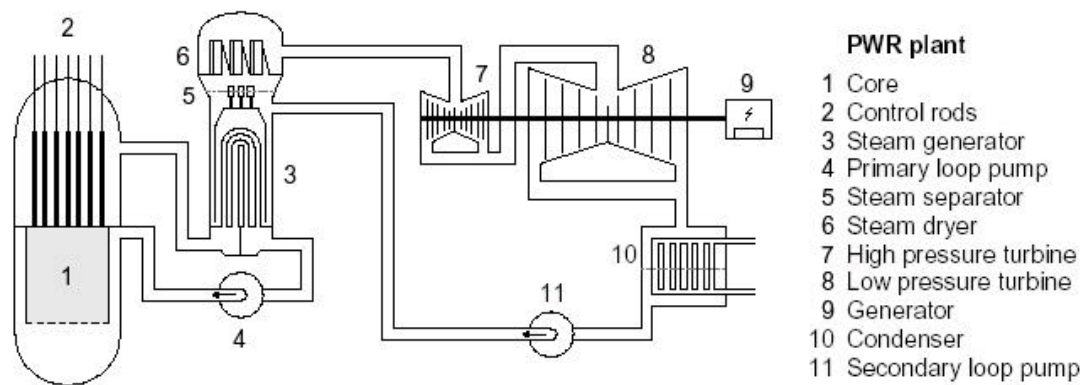


Figure 1-3. Schematic view of a PWR plant

BWRs are found to behave as linear systems under normal operating conditions. However, several stability tests have shown that, under certain conditions, BWRs are susceptible to instabilities in which limit cycle power oscillations are observed. This clearly indicates the transition from a linear regime to a nonlinear operating regime. Thus, although not a serious safety issue, BWR stability behaviour is a very complex phenomenon from the physical point of view. Even though extensive research has been carried out in recent years, the phenomenon is not yet completely understood.

Mainly two kinds of power oscillations have been observed in BWR plants, in which a strong nonlinear coupling exists via void reactivity between the neutronic and thermal-

hydraulic processes. These two types of instability are: (a) global, or in-phase power oscillations, where the power in fuel bundles across the whole core oscillates in phase, and (b) regional, *e.g.* out-of-phase first azimuthal mode oscillations, where half the core behaves out-of-phase with respect to the other half, *i.e.* when the power rises in one half of the core, it falls in the other half so that the average power remains essentially constant.

A BWR stability analysis methodology has been established at the Paul Scherrer Institute (PSI, Switzerland) [2, 3] based on the Studsvik/Scandpower system code RAMONA-3, which simulates the coupled thermal-hydraulics and three-dimensional reactor kinetics behaviour of the reactor core. The nuclear parameters, *i.e.* the cross-sections, are calculated by the assembly code CASMO and converted to RAMONA format using the codes CONVERT and POLGEN, which generate the cross-section polynomial fits. The main goal in such studies is to analyse the behaviour (type of instability) of the reactor core when it is operating in the so-called exclusion area of the power-flow map shown in Fig. 2-3. From the experimental or predicted time series, the decay ratio (DR), which is a linear stability characteristic, is calculated. By applying an appropriate DR-based criterion, the domains to be excluded or monitored in the BWR power-flow map can be identified.

Because of the large computational effort required, system codes cannot in practice be employed for a detailed investigation of the complete manifold of solutions of the nonlinear differential equations describing a BWR system, and so-called reduced order models become necessary. Such models contain a minimum number of system equations describing the physical phenomena of interest with adequate sophistication, but the geometrical complexity is reduced by modelling a limited number of channels only (usually just one or two). The foreseen application for such models is to provide new, deeper insight into the physical mechanisms underlying the neutronics/thermal-hydraulic induced power oscillations in BWRs. The main advantage of employing reduced order models is the possibility of using *semi-analytical* (see Chapter 3) methods for performing bifurcation analysis. In such an analysis, the stability properties of a fixed point, or a limit cycle, are investigated analytically without the need for solving the system of differential equations explicitly.

The present doctoral research, conducted in the framework of a collaboration between PSI and EPFL in the field of reactor physics and systems behaviour, contributes to the in-

depth understanding of the physical mechanisms of neutronic/thermal-hydraulic instabilities, in particular from the nonlinear point of view using modern bifurcation analysis. Thus the research serves to clarify the conditions under which such instabilities can occur in BWRs. For this purpose, a complex analytical model has been developed employing an appropriate set of nonlinear differential equations, the solution manifold for which is examined thoroughly. In parallel, if for a certain parameter set the possibility of a sub- or supercritical bifurcation is identified using the system code RAMONA, the stability behaviour in the neighbourhood of this operational point is examined in greater detail. Thus, one of the main objectives of the present research is to understand system code solutions of BWR stability problems on the basis of the physical mechanisms identified in the course of sophisticated reduced-order model analysis.

1.1 *PREVIOUS WORK*

Benefiting from the development of nonlinear dynamics theory, significant advances have been made in the nonlinear stability analysis of heated channels and BWRs during the last two decades. Moreover, additional efforts have been concentrated recently on bifurcation analyses in which the effects of different reactor design and operating parameters on bifurcation characteristics are analysed. Such analyses give important information that should be taken into account in the development of the next generation of nuclear reactors.

In the following, the most important earlier work relevant to the present research is reviewed and discussed.

1.1.1 Heated Channel Problems

Since the thermal-hydraulic model determines the main feedback gain and the associated time delay, appropriate modelling of the fluid dynamics is of paramount importance in considering modelling of the dynamic behaviour of BWRs. One of the most common types of instability encountered in two-phase flow is so-called density wave oscillations (DWOs). These instabilities are excited through the feedback and interaction among the flow rate, the vapour generation rate and the pressure drop in the heated channel. Details concerning DWOs are given in the introduction of Chapter 5, in which a detailed nonlinear analysis of a heated channel is performed.

Using nonlinear analysis, Achard *et al.* [4,5] carried out an analytical bifurcation study of DWOs on the basis of a homogeneous equilibrium model (HEM). In this work, under certain specific assumptions, the conservation equations were integrated to analytically obtain two functional differential equations (FDEs) for the inlet velocity and the two-phase residence time, respectively. Rizwan-uddin and Dorning [6] extended this work using a drift flux model (DFM) and obtained very complicated nonlinear, functional, delay, integro-differential equations for the inlet velocity and two-phase residence time. They carried out stability and bifurcation analyses and showed that the stability boundary (SB) is sensitive to the value of C_0 (void distribution parameter). The effect of V_{gj} (drift velocity) on the SB appeared to be small. The nature of Hopf bifurcation along the entire SB was found to be supercritical. However, the impact of C_0 and V_{gj} on the nature of Hopf bifurcation was not reported.

Later, again starting from a homogeneous equilibrium model, Clause and Lahey [7] developed a simple model for DWOs by introducing other simplifying assumptions, such as simple linear approximations for the space dependence of the enthalpies of the single phase and two-phase regions.

In the spirit of these developments, Karve *et al.* [8] developed a model, based on HEM, and based on the assumptions that the single-phase enthalpy and the two-phase quality have time-dependent spatially quadratic profiles. This model is simple in that the dynamical system that results is comprised of a set of nonlinear ODEs rather than complicated FDEs.

It should be emphasized that all the previous studies mentioned above applied either pure analytical, or pure numerical², bifurcation analysis. Pure analytical bifurcation needs extensive mathematical manipulation and become almost impossible to carry out for higher order models. Moreover, this type of bifurcation analysis can be carried out only for one specific bifurcation parameter at a time, and must be repeated if the impact of different parameters is to be studied. On the other hand, numerical bifurcation can only be performed for a limited number of operational points. Hence, due to the limitations of these two approaches, the scope of these previous analyses was limited to a small region of the rather large parameter space, in spite of the simplicity of the models used.

² numerical integration

1.1.2 Nuclear-Coupled Thermal-hydraulic Instabilities

A wide range of models has been developed to study and analyse nuclear-coupled thermal-hydraulic instabilities in BWRs, *i.e.* both in-phase and out-of-phase oscillations. In a pioneering work, March-Leuba *et al.* [10], in order to qualitatively and quantitatively simulate the dynamic behaviour of BWRs, proposed a simple phenomenological model based on a point reactor model for the neutron kinetics and a greatly simplified thermal-hydraulic model. In order to keep their model very simple, they assumed that the coolant enters the core at saturation temperature and that the entire recirculation loop can be treated as a single path of fluid of variable cross-sectional area but with constant mass flow rate. Under these assumptions, March-Leuba *et al.* were able to predict limit cycle oscillations in BWRs, with the amplitude of these oscillations found to be very sensitive to the reactor's operating conditions. Their analysis showed that these BWR limit cycles can become unstable and undergo period-doubling bifurcations leading to an aperiodic oscillating behaviour. In a later work [11], they proposed a mechanism for the out-of-phase instabilities observed in BWRs, in which numerical simulations showed that there is a region in the operating power flow map where out-of-phase instabilities are possible even if the fundamental mode is stable.

Using the above model, Muñoz-Cobo and Verdú carried out a purely analytical bifurcation analysis [12]. In effect, this is the first work in which bifurcation analysis is performed analytically in the framework of BWR model analysis. Later, Muñoz-Cobo *et al.* extended the above models in order to study in-phase and out-of-phase instability phenomena [13,14] employing a *I*-modes modal modelling of the neutron kinetics and a homogenous equilibrium model for the thermal-hydraulics. They showed that in-phase oscillations only appear when the first harmonic mode does not have enough thermal-hydraulic feedback to overcome eigenvalue separation. In addition, they demonstrated, using numerical integration, the excitation of limit-cycle out-of-phase oscillations when the reactivity feedback of the first azimuthal mode is increased.

Karve *et al.* [15,16] developed a more detailed model in which they used *w*-modes for the neutron kinetics, and a homogeneous equilibrium model for the thermal-hydraulic treatment of the two-phase flow. After performing stability analysis for the stability boundary, they carry out bifurcation analysis entirely numerically.

With the aim of obtaining a better understanding of BWR instabilities, especially out-of-phase oscillation phenomena, Zhou and Rizwan-uddin [17] carried out *semi-analytical*

stability and bifurcation analyses with the Karve *et al.* model using the bifurcation code BIFDD [9]. They analysed the role of the pairs of complex conjugate eigenvalues with the largest and second largest real parts in determining the in-phase and out-of-phase modes of oscillations. Numerical simulations were then carried out to further confirm the results of the stability and bifurcation analyses.

1.1.3 BWR Stability Analysis Using Complex System Codes

As in the studies with reduced order models, stable nonlinear oscillations (limit cycles) have also been observed and reported in analyses performed using large system codes [18-20] (as also observed experimentally during certain tests performed at nuclear power plants like Leibstadt and Ringhals³ [21,22]). However, unstable limit cycles have never previously been reported using large system codes [23]. In the author's opinion, the reason is that the unstable limit cycle solution has always been confused with the unstable fixed point solution, *i.e.* when growing amplitude oscillations were observed at a specific operational point, the conclusion was always that the system is unstable at this operational point, without any further details being considered concerning the exact type of the solution. This is mainly because system code users usually have limited (or no) experience in nonlinear stability and bifurcation analysis using reduced order models. Effectively, in the context of BWR stability analysis using complex system codes, the question of the bifurcation type responsible for the generation of stable or unstable limit cycle solutions have never been raised. Hence, one of the primary focus points in this thesis (see Chapter 7) is to answer this question by proposing the so-called *correspondence hypothesis* based on the accumulated experience using reduced order models. This hypothesis proposes the correspondence between the stable (unstable) limit cycle solution and the occurrence of supercritical (subcritical) Hopf bifurcation.

1.2 PRESENT OBJECTIVES

The principal goals of the present research can be divided in four main categories:

1. *Heated channel model (without neutron kinetics):*

- a. Employ a thermal-hydraulic model, developed on the basis of a drift flux representation for two-phase flow rather than on a HEM, to perform stability and semi-analytical bifurcation analyses using the bifurcation analysis code

³ a nuclear power plant in Sweden

BIFDD. Such a model is more appropriate for the analysis of a heated channel, since it takes into account: (a) the difference between the two phases velocities, which is particularly important in low-flow regimes, and (b) the radially non-uniform void distribution inside the channel. Moreover, the drift flux model is more general than a HEM or a slip model, *i.e.* HEM and slip models are special cases of the DFM.

- b. Analyse the effects of the drift flux model parameters on the SB and the nature of Hopf bifurcation.
- c. Study the effects of different design and operating parameters on the SB and the nature of Hopf bifurcation.
- d. Perform standard numerical integration to validate the stability and the *semi-analytical* bifurcation analysis, and provide more global information.

2. Two-channel nuclear coupled thermal-hydraulic model:

- a. Develop a two-parallel-channel, nuclear-coupled thermal-hydraulic model (with drift flux representation of the two-phase flow) to simulate BWR instabilities and carry out stability and semi-analytical bifurcation analysis using the bifurcation code BIFDD.
- b. Get a deeper insight into in-phase and out-of-phase oscillation mode excitations and their connection to the excitation of the fundamental and first azimuthal modes based on a detailed examination of the eigenvector properties.
- c. Analyse the effects of the drift flux model parameters on the SB, the nature of Hopf bifurcation, and the excitation of the oscillation modes.
- d. Carry out numerical simulation to verify the findings of the semi-analytical bifurcation analysis and evaluate the system behaviour beyond the region where the bifurcation analysis is valid.
- e. Assess the range of applicability and limitations of the reduced order model for quantitative studies.

3. System code analysis:

- a. Carry out of detailed local bifurcation analysis using a complex system code (RAMONA) at representative operational points for two actual nuclear power plants (Leibstadt and Ringhals-1).

4. Bridge between reduced order model and system code analysis:

- a. Build a bridge between the reduced order model and the system code through, for instance, understanding the system code solutions on the basis of the physical mechanisms identified in the course of applying the sophisticated reduced order model. A much more challenging goal would be to identify the stability properties of certain “interesting” operational points in the power-flow map using the reduced order model (applying semi-analytical bifurcation analysis), and then use the system code to perform a detailed analysis in the neighbourhood of these operational points.
- b. Compare the results of the reduced order model and the system code for a specific operational point for one of the nuclear power plants studied.

1.3 ORIGINAL CONTRIBUTIONS

Following the objectives outlined in the previous section, the following original contributions have been made in the course of the present work:

- Study of the effects of the drift flux model parameters (C_0 and V_{gi}) on the nature of Hopf bifurcation for a heated channel problem, and their effects on the system stability boundary and the nature of Hopf bifurcation for a two-parallel-channel nuclear-coupled thermal-hydraulic model.
- Proposition of a new mathematical interpretation of in-phase and out-of-phase oscillation modes based on their corresponding eigenvectors properties. This has allowed the explanation of the excitation of the fundamental (first azimuthal) mode although the in-phase (out-of-phase) oscillation mode is not excited.
- Proposition and demonstration of the *correspondence hypothesis* that underlines the unique correspondence between a stable (unstable) limit cycle solution and the occurrence of a supercritical (subcritical) Hopf bifurcation
- Performance of a detailed bifurcation analysis using the system code RAMONA. This has allowed the identification, for the first time, of a subcritical Hopf bifurcation using a complex system code.
- Building a qualitative bridge between the reduced order model and the system code RAMONA, with the results obtained by the latter being analysed and explained on the basis of the results from the reduced order model.

1.4 *THESIS OUTLINE*

The two principal aspects of the present research are: (i) development of, as well as stability and bifurcation analysis using, the novel BWR reduced order model (Chapters 4, 5, 6 and 8), and (ii) stability and bifurcation analysis using the system code RAMONA (Chapter 7).

An introductory description of the basic phenomena and concepts that are encountered in the field of BWR stability analysis is provided in Chapter 2. These include linear and nonlinear analyses and the codes used for these purposes, the concept of power-flow map, exclusion area, monitoring system, and various other tools relevant to the power plant operator for experimental analysis. In addition, spatial mode instability phenomena and the corresponding hydraulic boundary conditions are discussed.

Chapter 3 is devoted to certain basic concepts of nonlinear dynamics and bifurcation theory, in particular Hopf bifurcation. In addition, the *semi-analytical* bifurcation method is explained along with the bifurcation analysis code BIFDD.

In Chapter 4, the development of the ODEs of the different components of the newly developed, BWR reduced order model, *i.e.* neutron kinetics, fuel heat conduction, and thermal-hydraulics, are presented.

In Chapter 5, stability and semi-analytical bifurcation analysis is carried out for a heated channel in order to study two-phase flow DWO phenomena using the bifurcation code BIFDD. First, the current thermal-hydraulic model is validated against experimental data and compared to several other analytical models. Then, a comparison is performed between the use of DFM and HEM using both semi-analytical bifurcation analysis and standard numerical integration. Furthermore, a sensitivity study is carried out in order to assess the effect of different parameters on stability, as well as on bifurcation characteristics.

An in-depth study employing the complete, currently developed BWR reduced order model is carried out in Chapter 6. On the basis of this study, a rigorous quantitative explanation of the excitation of in-phase and out-of-phase oscillation modes is proposed, bringing out the exact connection to the excitation of the fundamental and first harmonic modes of the neutron flux. In addition to analysing the effects of the DFM parameters on the stability boundary and the nature of Hopf bifurcation, the effect of these parameters on the type of oscillation mode is investigated. Furthermore, numerical simulations are

carried out at certain operating points to validate the findings of the semi-analytical bifurcation analyses.

Chapter 7 is devoted to a study in which a detailed local bifurcation analysis is performed using the system code RAMONA at two representative NPP operational points. The so-called *correspondence hypothesis* is proposed to underline the unique correspondence between a stable (unstable) limit cycle solution and the occurrence of a supercritical (subcritical) Hopf bifurcation. The detailed investigation has resulted in the identification, for the first time, of a subcritical Hopf bifurcation using a complex system code.

In Chapter 8, the reduced order model is implemented for a particular NPP (Leibstadt) operational point (OP), and a sensitivity analysis is performed to study the effect of uncertainties of different design and operating parameters on the stability boundary and the nature of Hopf bifurcation. The results of the reduced model are then compared to those of the RAMONA model at the same OP. This allows an overall assessment of the performance of the new reduced order model, *i.e.* of its applicability and limitations.

Finally, conclusions from the present research and certain recommendations for future work are presented in the last chapter, Chapter 9.

REFERENCES

- [1] "IAEA (International Atomic Energy Agency) Annual Report for 2001," available via http://www.iaea.org/worldatom/Documents/Anrep/Anrep2001/nuclear_power.pdf.
- [2] D. Hennig, "A Study of Boiling Water Reactor Stability Behaviour," *Nucl. Technology*, **125**, p.10-31, 1999.
- [3] R. Miro, D. Ginestar, D. Hennig, G. Verdú, "On the Regional Oscillation Phenomenon in BWRs," *Prog. Nucl. Energy*, **36**, 2, 189-229, 2000.
- [4] J. L. Achard, D. A. Drew, R. T. Lahey, Jr. "The Analysis of Linear and Nonlinear Instabilities Phenomena in Heated Channels," Tech. Report No. NUREG/CR-1718, Nuclear Regulatory Commission, 1980.
- [5] J. L. Achard, D. A. Drew, R. T. Lahey, Jr. "The Analysis of Nonlinear Density-Wave Oscillations in Boiling Channels," *J. Fluid Mech.*, **15**, 213-232, 1985.
- [6] Rizwan-uddin, J. J. Dorning "Some Nonlinear Dynamics of a Heated Channel," *Nucl. Eng. Des.*, **93**, 1-14, 1986.

- [7] A. Clause, R. T. Lahey, Jr. "The Analysis of Periodic and Strange Attractors During Density-Wave Oscillations in Boiling Flows," *Chaos, Solitons, and Fractals*, **1**, 2, 167-178, 1991.
- [8] A. A. Karve, Rizwan-uddin, J. J. Dorning, "On Spatial Approximations for Liquid Enthalpy and Two-phase Quality During Density Wave Oscillations," *Trans. Am. Nucl. Soc.*, **71**, 533, 1994
- [9] B. D. Hassard, "A Code for Hopf Bifurcation Analysis of Autonomous Delay-Differential Equations," *Proc. Oscillations, Bifurcation and Chaos*, Canadian Mathematical Society, pp.447-463, 1987.
- [10] J. March-Leuba, D. G. Cacuci, R. B. Perez, "Nonlinear Dynamics and Stability of Boiling Water Reactors: Part 1- Qualitative Analysis", *Nucl. Sci. Eng.*, **93**, 111-123, 1986 and "Nonlinear Dynamics and Stability of Boiling Water Reactors: Part 2- Quantitative Analysis", *Nucl. Sci. Eng.*, **93**, 124-136, 1986.
- [11] J. March-Leuba, E. D. Blakeman, "A Mechanism for Out-of-phase Power Instabilities in Boiling Water Reactors", *Nucl. Eng. Des.*, **107**, 173-179, 1991.
- [12] J. L. Muñoz-Cobo, & G. Verdú, "Application of Hopf Bifurcation Theory and Variational Methods to the Study of Limit Cycles in Boiling Water Reactors," *Ann. Nucl. Energy*, **18**, 5, 269, 1991.
- [13] J. L. Muñoz-Cobo, R. B. Pérez, D. Ginestar, A. Escrivá, G. Verdú, "Nonlinear Analysis of Out of Phase Oscillations in Boiling Water Reactors", *Ann. Nucl. Energy*, **23**, 16, 1301-1335, 1996.
- [14] J. L. Muñoz-Cobo, O. Rosello, R. Miró, A. Escrivá, D. Ginestar, G. Verdú, "Coupling of Density Wave Oscillations in Parallel Channels with High Order Modal Kinetics: Application to BWR Out-of-phase Oscillations", *Ann. Nucl. Energy*, **17**, 1345-1371, 2000.
- [15] A. A. Karve, Rizwan-uddin, J. J. Dorning, "Out-of-phase Oscillations in Boiling Water Reactors", *Proc. of the Joint Int. Conf. on Mathematical Methods and Supercomputing*, Saratoga Springs, NY, Oct. 5-9, pp. 1633-1647, 1997.
- [16] A. A. Karve, "Nuclear-Coupled Thermal-Hydraulic Stability Analysis of Boiling Water Reactors", Ph.D. Dissertation, Virginia University, 1999.
- [17] Quan Zhou, Rizwan-uddin, "Bifurcation Analyses of In-phase and Out-of-phase Oscillations in BWRs", *Proc. of International Conference on the New Frontiers of Nuclear Technology, Reactor Physics, Safety and High Performance Computing (PHYSOR-2002)*, Seoul, Korea, Oct. 7-10, 2002, CD-ROM.

- [18] T. Lefvert, "Ringhals-1, Stability Benchmark," NEA/NSC/DOC (96) 22, Nuclear Energy Agency, 1996.
- [19] D. Hennig, "A Study of BWR Stability Behaviour", *Nucl. Technology*, **126**, 10-31, 1999.
- [20] R. Miró, D. Ginestar, D. Hennig, G. Verdú, "On the Regional Oscillation Phenomenon in BWRs", *Prog. Nucl. Energy*, **36**, 2, 189-229, 2000.
- [21] D. Blomstrand, "The KKL Core Stability Test, Conducted on September 6, 1990," Internal ABB report BR91-245, ABB Atom, 1992.
- [22] M. Johansson "Data for Stability Benchmark Calculation, Ringhals Unit 1, Cycles 14, 15, 16 and 17," Internal Vattenfall report 0120/94, Vattenfall AB, 1994.
- [23] R. T. Lahey, Jr. "Applications of Fractals and Chaos Theory in the Field of Multiphase Flow & Heat Transfer," in *Boiling Heat Transfer*, pp. 317-387, edited by R.T. Lahey, Jr., Elsevier Science Publishers, 1992.

2 BWR STABILITY ANALYSIS

This chapter provides an introductory description of the basic phenomena and concepts encountered in the field of BWR stability analysis. The general concept of stability is introduced in the first section. A short description of linear stability analysis and the codes used for this purpose is provided in Section 2.2, while nonlinear analysis is described in Section 2.3. The concepts of power-flow map, exclusion area, monitoring system, time series analysis, and various other tools available to the NPP operator for experimental analysis are explained in Section 2.4. In Sections 2.5 and 2.6, respectively, spatial mode instability phenomena and the corresponding hydraulic boundary conditions are discussed. The last section is devoted to the codes used in this thesis, *viz.* the system code RAMONA, the bifurcation analysis code BIFDD, the main Fortran program *bwr.f* corresponding to the currently developed BWR reduced order model, and finally the Matlab program *integration.m* developed to carry out the numerical integration.

2.1 CONCEPT OF STABILITY

In a general sense, stability is a term that deals with the temporal behaviour of a dynamical system following an internal (noise) or external parameter disturbance during its operation. After such a disturbance, the system may behave in a stable or unstable manner. In a stable case, the dynamical variables of the system return to their steady-state values. In geometrical terms, this means that, in phase space, the system state returns to the stable fixed point or, at least, the system state remains in the neighbourhood of the stable fixed point. In an unstable case, all or some of the variables diverge in an exponential or oscillatory manner. Loosely speaking, the boundary that separates the stable fixed points from the unstable fixed points is called the *stability boundary*.

2.2 LINEAR STABILITY ANALYSIS

Boiling water reactors (BWRs) are complex systems governed by nonlinear equations. Therefore, a rigorous stability analysis of a BWR is only possible if some simplifying assumptions are made. In particular, if the stability boundary is of interest, linearized models are often used. Such models are based on linear analysis that implies perturbing the system equations linearized around a given steady-state operating point. The mathematical background behind the treatment of nonlinear systems by linear analysis is

due to the Hartman-Großman theorem [1], which states that a nonlinear system behaves like a linear one in a sufficiently close neighbourhood of a hyperbolic fixed point (steady-state). This is the justification for using linear stability analysis indicators, *e.g.* the decay ratio (DR) or Nyquist diagram, in the framework of BWR stability analysis. It should be emphasized that, while linear stability analysis can provide exact solutions, much lower computer time requirements, and stability limit predictions at least as accurate as within a nonlinear analysis, this approach does not provide information concerning certain characteristics of nonlinear systems, such as the magnitude and frequency of any limit cycle oscillations.

The linearized system equations around the steady-state are Laplace transformed and the transfer function between two variables can be obtained as the ratio of two polynomials in s , the Laplace transform variable. The roots of the numerator polynomial are called the poles of the transfer function and those of the denominator are the zeros. Once the transfer function $T(s)$ is known, the system output $Y(s)$, for any input $X(s)$, is given in the Laplace domain by the product of the input and the transfer function:

$$Y(s) = T(s)X(s) \quad (2.1)$$

By back transformation in the time domain, the output, $y(t)$, can be obtained using the convolution theorem [2]

$$y(t) = \int_0^t x(t)h(t-t)dt \quad (2.2)$$

where $h(t-t)$ is the inverse Laplace transform of the transfer function. It can be shown that $h(t)$ is also the response of a system to a Dirac delta function input and is, therefore, usually called the impulse response of the system. Using the residue theorem of the theory of complex functions, the impulse response can be calculated as a function of the poles of the transfer function

$$h(t) = \sum_{i=1}^N R_i e^{p_i t} \quad (2.3)$$

where R_i is the residue of the pole p_i and N is the number of existing poles.

Equation (2.3) shows clearly that, if at least one of the poles has a positive real part, the impulse response will grow exponentially and the system will be unstable. If all the poles have negative real parts, the system will be stable. In this case, the asymptotic system behaviour is driven by the pole with the largest real part⁴. Thus, the pole with the largest real part determines the stability of the system.

2.2.1 Linear Stability Criteria

In the previous section, it has been seen that the knowledge of the system transfer function is the basis for discussing linear reactor stability at any operational point. Different techniques exist for defining the criteria for stability as a function of independent parameters, *e.g.* the Nyquist locus method, the root locus method [3], and decay ratio calculation. The decay ratio (DR) is a fundamental quantity in BWR linear stability analysis that measures how rapidly or slowly a disturbance is damped. It can be shown that, if a system has only a single pair of complex conjugate poles, the impulse response is $h(t) = e^{\mathbf{s}t} \cos(\mathbf{w}_d t + \mathbf{f})$, where \mathbf{s} is the real part and \mathbf{w}_d is the imaginary part of the pole. By definition, the decay ratio is the ratio of two consecutive peaks in the impulse response and equal to $DR = e^{2ps / w_d}$.

For this example, we see that the decay ratio is directly related to the position of the pole in the imaginary plane and is a good measure of the system stability. In a more general case, the impulse response is determined by contributions from all the poles. However, it can be shown that the series of values of the decay ratio for every two consecutive oscillations converges to a value equal to the decay ratio of a system with just a single pair of complex poles at the same position as the least stable pair of poles in the original system. This value is called the *asymptotic decay ratio*. In conclusion, the asymptotic value of the DR is computed from the least-damped oscillation, *i.e.* one searches for the complex pole lying nearest to the unit circle.

⁴ or the smallest real part in absolute value

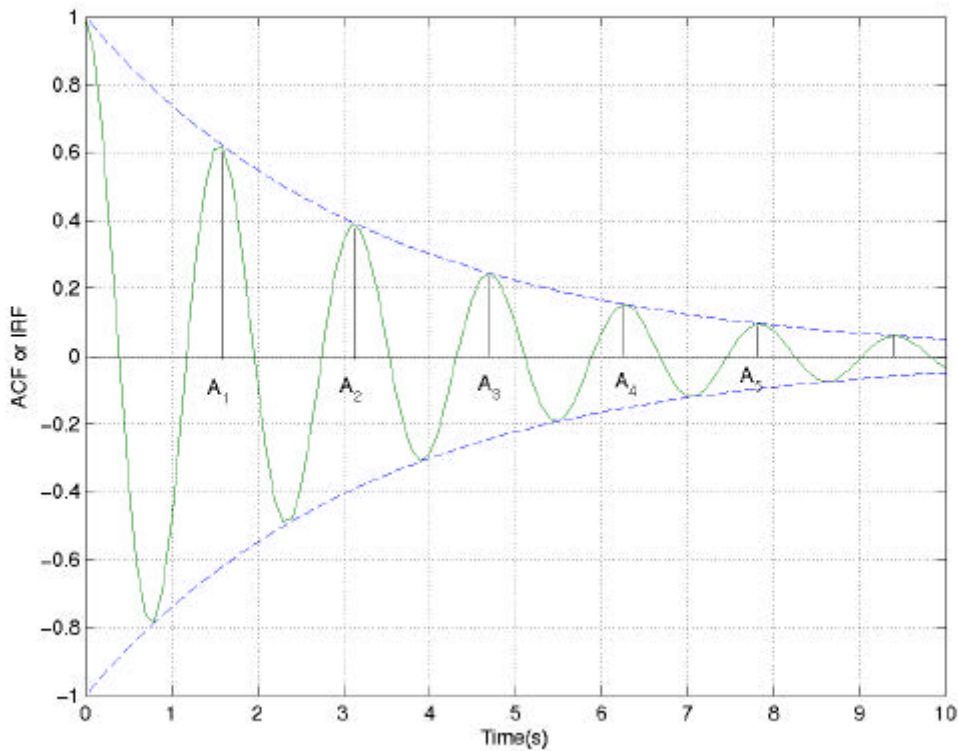


Figure 2-1. DR definition based on successive maxima of the ACF or IRF.

In practice, many methods have been proposed for the calculation of the DR [4], the standard procedure being to use one of the following two methods. The first is based on calculation of the autocorrelation function (ACF), and the second one is based on the impulse response function (IRF) calculated using either an autoregressive moving-average model (ARMA) or an autoregressive model (AR) to fit the behaviour of the system. Once the ACF or the IRF is calculated, for a second order system, the DR is defined as the ratio between two consecutive maxima A_i and A_{i+1} of the ACF or IRF, respectively, *i.e.*

$$DR = \frac{A_{i+1}}{A_i}, \forall i \quad (2.4)$$

These methods are illustrated in Fig. 2-1 above.

2.2.2 BWR Models for Linear Stability Analysis

Models for BWRs based on linear stability analysis are called frequency-domain models. Two classes of frequency-domain models exist: simplified models with low

dimensions that capture only the most significant physical processes determining the dynamics of a BWR, and linear system codes set up with the purpose of a complete description of BWR plant dynamics. Among the frequency domain system codes, one finds STAIF [5], ODYSY [6], MATSTAB [7], LAPUR [8], and NUFREQ [9]. These codes are used for the calculation of stability boundaries because they are fast running and extensively validated. In particular, MATSTAB includes a 3D reactor core model, and hence, this code is applicable for the analysis of both core-wide and regional oscillations.

2.3 *NONLINEAR ANALYSIS*

The response of a perturbed nonlinear system can depend strongly on the magnitude of the initial (external) perturbation. In particular, while for a sufficiently small perturbation the system may return to its original steady-state operational point, an increase in the perturbation's magnitude may lead to a divergent response. When linear system theory is applied to nonlinear BWR systems, it can be used to describe the behaviour of these systems around their steady-state operational points only as long as the perturbation remains sufficiently small. However, this approach is unable to predict other important properties, such as the magnitude of perturbations beyond which stability of the system cannot be maintained, as also the amplitude and the frequency of oscillations if a limit cycle solution is found.

2.3.1 *Stability Boundary in Mathematical Sense*

Suppose a set of nonlinear differential equations for an autonomous⁵ system

$$\frac{d\bar{x}(t)}{dt} = f(\bar{x}(t)) \quad (2.5)$$

The steady-state solutions (fixed points) of this system of ODEs are obtained by solving

$$\frac{d\bar{x}(t)}{dt} = 0 \quad (2.6)$$

⁵*f* does not depend explicitly on time *t*.

Consider $J = D_{\bar{x}}f(\bar{x}(t))$, the Jacobian matrix of the linearized system around the equilibrium point. The system is stable if all the eigenvalues of the Jacobian have strictly negative real part values (Fig. 2-2(a)), while it is unstable if at least one eigenvalue has a positive real part (Fig. 2-2(b)). Hence, the stability boundary, that separates the stable fixed points from the unstable ones, is obtained when the real part of an eigenvalue, or of a pair of complex eigenvalues with the largest real part, becomes equal to zero. In effect, if the set of differential equations for a dynamical system is known, knowledge of the eigenvalues of the Jacobian matrix allows the determination of the stability boundary. Mathematically, the SB is determined by solving the following system of equations:

$$\begin{cases} \frac{d\bar{x}(t)}{dt} = 0 \\ \text{Re}(\det(J - i\omega I)) = 0 \\ \text{Im}(\det(J - i\omega I)) = 0 \end{cases} \quad (2.7)$$

where i is the complex number ($i^2 = -1$), ω is the frequency of the oscillation, Re and Im stand for real and imaginary parts, respectively, and det stands for the determinant.

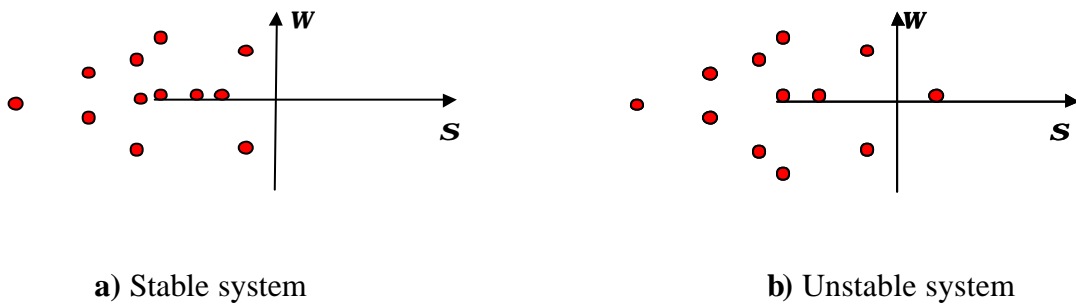


Figure 2-2. Complex plane of Jacobian matrix eigenvalues: a) stable case, all the eigenvalues have negative real part values, b) unstable case, one eigenvalue has a positive real part and the remaining eigenvalues have strictly negative real parts.

2.3.2 BWR Models for Nonlinear Stability Analysis

As is the case of linear stability analysis, two classes of models exist for the description of the nonlinear behaviour of BWRs, *viz.* complex system codes and so-called reduced order models. These two approaches are discussed in more detail in the following paragraphs.

2.3.2.1 Complex system codes

Computer programs developed for the modelling and simulation of a complete nuclear power plant with a high degree of detail are called system codes. Different choices are adopted for neutron kinetics and two-phase flow modelling. Thus, for the neutron kinetics, both 1D and 3D models have been developed and can be used. Clearly, if the analysis of regional oscillation phenomena is of interest, a 3D neutron kinetics model is necessary. For the two-phase flow modelling, a homogenous equilibrium model, a drift flux model, and even a six-equation two-fluid model can be used. Such complex system codes are generally based on the solution of the partial differential equation (PDF) systems representing the thermal-hydraulic, the neutronics, and the heat conduction characteristics of the plant components.

Space and time discretization of the thermal-hydraulic balance equations is performed by suitable numerical methods. Commonly, nodal methods are used. The type of space discretization chosen for the thermal-hydraulic balance equations contributes to determining the effect of truncation errors on the calculated results. In fact, numerical methods, also depending on whether explicit or implicit time discretization is applied, bring in a certain amount of numerical diffusion, which may quantitatively and qualitatively change the behaviour of the predicted phenomena in comparison with the exact solution. Such numerical diffusion is sometimes responsible for damping the amplitude of the physical oscillations and may lead to the prediction of a stable state, whereas unstable ones might be expected. However, it should be noted that some minimal numerical diffusion is necessary to prevent the growth of numerically induced oscillations. Among complex LWR system codes, one finds RAMONA [11], TRAC-G [12], TRAC-B [13], RETRAN [14], and RELAP [15].

In using system codes with a free nodalization structure, *e.g.* TRAC-B or RELAP, strong damping effects due to numerical diffusion can be expected and, therefore, such codes are not suitable for stability analysis unless the solution algorithm is modified, in

particular the discretization schemes. On the other hand, the integration, for example, of the momentum equation along a closed recirculation loop, as featured in RAMONA, reduces numerical diffusion effects significantly. For such reason, RAMONA is one of the most suitable codes for BWR stability analysis and is, therefore, the code used in this thesis, in Chapter 7, to carry out numerical bifurcation analysis at two representative operational points, *viz.* for the Leibstadt (KKL) and Ringhals-1 nuclear power plants, respectively.

2.3.2.2 *Reduced order models*

Because of the large computational effort required, it is not possible in practice to employ system codes for detailed investigations of the complete solution manifold of the nonlinear equations describing BWR stability behaviour. In this context, reduced order analytical models become necessary. Such models contain a minimum number of system equations describing the physical phenomena⁶ of interest with adequate sophistication, but the geometrical complexity is reduced to a few-channel model. The objective of such models is generally to provide understanding of the basic physical mechanisms involved in BWR behaviour beyond the stability boundary, making use of nonlinear dynamics and bifurcation theory. Usually these models are formulated as systems of partial or ordinary differential equations to be solved by appropriate numerical methods. A wide range of analytical nonlinear reduced order models has been developed.

A relevant example is the pioneering work, mentioned earlier, of March-Leuba *et al.* [16] who proposed a simple phenomenological model to qualitatively simulate the behaviour of BWRs. In order to keep their model very simple, they assumed that the coolant enters the core at saturation temperature and that the entire recirculation loop can be treated as a single path of fluid with variable area but with constant mass flow rate. This model consists of two first order differential equation for neutron kinetics with a single delayed neutron group, one first order differential equation for fuel temperature behaviour and one second-order differential equation for feedback reactivity. March-Leuba *et al.* were able to predict limit cycle oscillations in BWRs, with the amplitude of these oscillations found to be very sensitive to the reactor's operating conditions. Their analysis showed that these BWR limit cycles can become unstable and undergo period-doubling bifurcations leading to an aperiodic oscillating behaviour. This model has subsequently

⁶ That is why reduced order models are sometimes called simplified phenomenological models [4].

been adopted by many researchers (*e.g.* [17], [18]) to demonstrate interesting trends in the overall behaviour of BWRs during instabilities, including the prediction of limit cycles, Hopf bifurcation, period-doubling cascades, and even chaotic behaviour.

Benefiting from the development of nonlinear dynamics theory, significant advances have been made in the nonlinear stability analysis of heated channels as well as BWRs. Moreover, additional efforts have been concentrated recently on bifurcation analyses in which the effects of different design, as well as operational, parameters on bifurcation characteristics are analysed. Such bifurcation analyses give important information that should be taken into account in the design and operational analysis of the next generation of nuclear reactors. Hence, more detailed models have been developed during the last decade in order to simulate more complicated BWR behaviour, such as space-time dependent instability, *i.e.* global and regional oscillations as well as sub- and supercritical Hopf bifurcation phenomena [19-22]. A more detailed description of bifurcation analysis is provided in the next chapter.

2.4 EXPERIMENTAL ANALYSIS (TIME SERIES ANALYSIS)

For an operator in a BWR power plant, the stability boundary defines the limits between normal operational points at which the plant can be operated and the exclusion area shown in the so-called power-flow map (Fig. 2-3). The power-flow map is clearly an important BWR operational characteristic. It represents the strong dependence of the thermal reactor power on the core mass flow rate because of the void reactivity feedback. Power oscillations can start if the BWR is operated within the exclusion area. In general, this region is defined over the range of 40-70 % of rated power and 30-45 % of the rated mass flow. It should be noted that the boundary of the exclusion area is conservatively defined. Therefore, both stable and unstable operational points are found inside the exclusion area. Quantitatively, the exclusion area is defined on the basis of measured and calculated values of the decay ratio for the least damped power oscillation. The limiting value of the DR for defining the exclusion area depends on the uncertainty which is assumed for the measured or predicted DR⁷.

⁷ In general, all operational points outside the exclusion area must have a decay ratio less than 0.8.

KKL POWER FLOW MAP

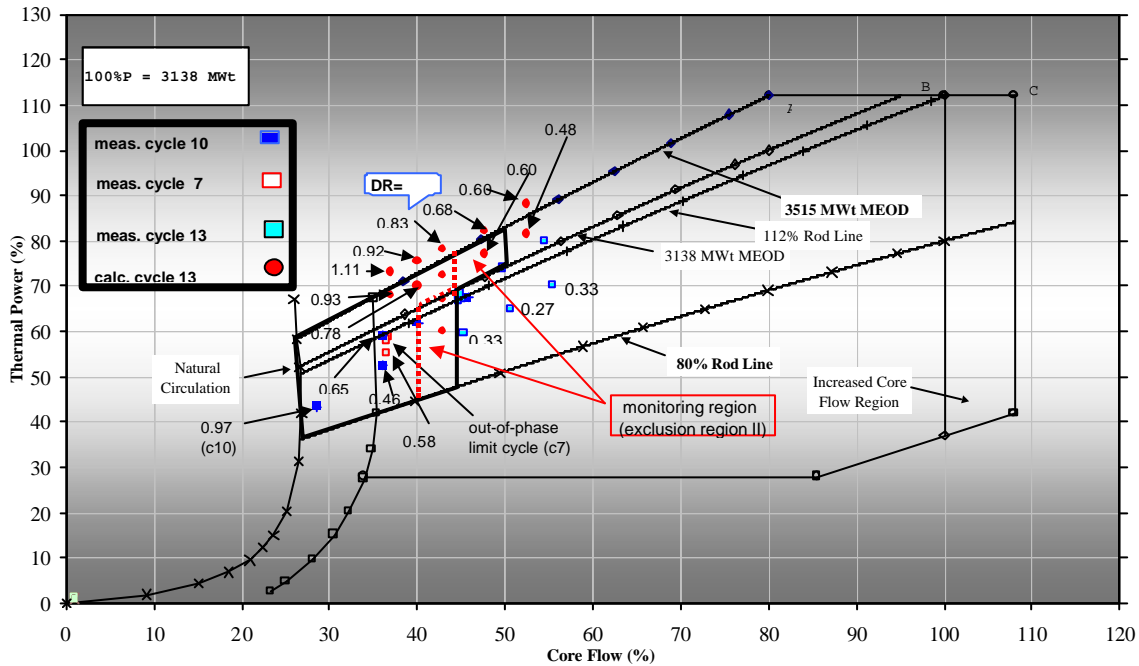


Figure 2-3. Leibstadt nuclear power plant (KKL) power-flow map.

It should be emphasized that, although the decay ratio is a quantity that arises from linear analysis, it is widely used in nonlinear analysis as an indicator of the stability of the system (see 2.2.1). However, the DR is not a measure of the stability margin [10], *i.e.* from a given DR value, the operator is not able to know as to how far the operational point is from the stability boundary. The uncertainty on the DR is given by the experimental error in stability experiments.

2.4.1 Monitoring System

Modern BWRs are equipped with in-core instrumentation consisting of Local Power Range Monitor (LPRM) and Average Power Range Monitor (APRM) detectors. The LPRM detectors are fission-chamber type detectors distributed over the core (Fig. 2-4), and some selected LPRM detectors are connected to APRMs to measure the core average power. For instance, the Leibstadt LPRM system consists of 35 detector strings, each having 4 detectors at 4 different core axial levels⁸. If the BWR is operated at an unstable operational point, the power oscillations are detected by all LPRM and APRM-group detectors.

⁸ Note that level 1 corresponds to the lowest axial level, while level 4 corresponds to the highest axial position (largest void content).

The power oscillations are excited by the naturally occurring reactor parameter noise and, for a plant stability test, one has to select time series records of 8 to 10 minutes length. Since the natural frequency of the power oscillation is determined by the velocity of the kinematic wave propagation in the hydraulic channels, oscillation frequencies of about 0.4 to 0.6 Hz can be expected for a BWR-type like KKL. This means that the sampling frequency of a discrete signal should not be less than 8 to 10 Hz. The task is to extract an indicator that characterizes the stability behaviour from the measured noise time series records (Fig. 2-4) or, in other words, the analysis involves calculation of the DR and the natural frequency (NF) from the LPRM or APRM time series.

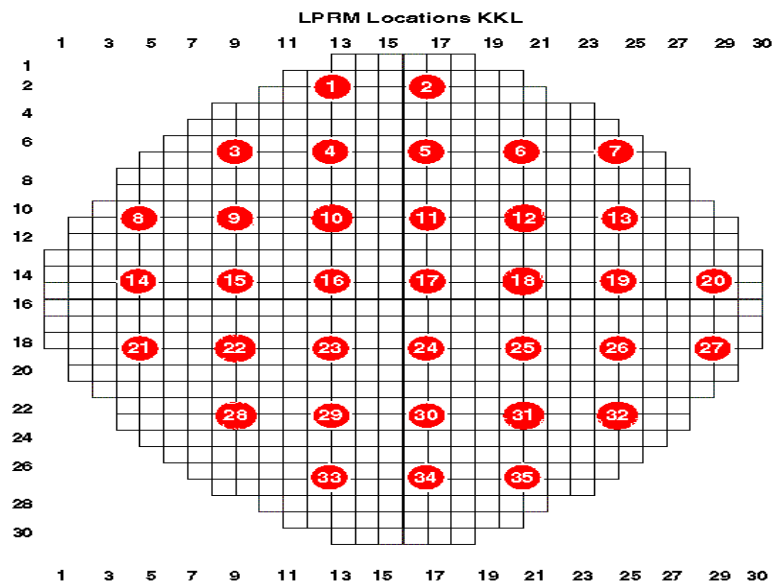


Figure 2-4. Leibstadt LPRM locations at a particular axial level

2.4.2 Time Series Analysis

Time series analysis for the determination of stability indicators is described in many papers, *e.g.* [23, 24]. In particular, the methodology employed at PSI is discussed in [25, 26] and is briefly summarized in this subsection.

A dynamical system is described by a system of nonlinear differential equations. After linearization of this system and time discretization, one can transform the system equations into a linear difference equation system. If one adds parametric noise and solves this equation system, a noise time history of the appropriate parameters is obtained. If the system equations are unknown and one only has the system output as an analysed power time series (or other quantity), the system parameters can be reconstructed by a system identification procedure [27].

Assuming that the system is described by a system of linear difference equations and the dynamics is driven by noise, the system output at discrete times kT , *i.e.* the measured time series, may be written as:

$$y(kT) = a_1 y((k-1)T) - a_2 y((k-2)T) - \dots - a_{n_a} y((k-n_a)T) + e(kT) + c_1 e((k-1)T) + c_2 e((k-2)T) + \dots + c_{n_c} e((k-n_c)T) \quad (2.8)$$

where T is the sampling interval. The time series in (2.8) is assumed generated by the stochastic process called coloured noise,

$$C(q)e(kT) = \sum_{n=0}^{n_c} c_n q^{-n} e(kT) \quad (2.9)$$

where q is the time shift operator, $q^{-1}e(kT) = e((k-1)T)$. $e(kT)$ is the white noise Gaussian process. Eq. (2.8) characterizes an autoregressive moving average (ARMA) model, and the task at hand is to determine the coefficients a_i and c_i by a suitable approximation algorithm [28]. It should be emphasized here that the experimental uncertainty of a stability indicator (*e.g.* DR) is given by the uncertainties of the time series analysis results.

2.5 SPATIAL MODE INSTABILITIES

Although BWR core dynamics is a nonlinear space-time dependent problem, the neutron flux or the power can be expressed as a spatial expansion with time dependent amplitudes⁹. A detailed mode analysis shows that, for normal operational points, all modes except the fundamental mode have eigenvalues smaller than one, so that they decay with time¹⁰ and do not significantly affect the reactor dynamics. However, this situation need not be the case under certain other conditions. For instance, if the reactor, for any reason, is operated in the exclusion area (Fig. 2-3), the reactor core may experience instabilities.

As mentioned earlier, there are two kinds of instabilities: global or in-phase oscillations, and regional oscillations. In the in-phase mode, the whole core behaves as one (Fig. 2-5). This is due to oscillation of the fundamental mode. However, in the regional mode, *e.g.* out-of-phase oscillations, half of the core behaves out-of-phase from the other half (Fig. 2-6), *i.e.* when the power or flow rises in one half of the core, it decreases in the other half. Such out-of-phase oscillations are related to the excitation of the first azimuthal mode. The out-of-phase oscillation mode does not require changes in the total mass flow because the two oscillating core regions adjust their flows to maintain the pressure drop across the core constant in time and in space.

To the author's best knowledge, it was March-Leuba *et al.* who, in their pioneering work [16], first gave an explanation of the out-of-phase power oscillations observed in certain stability tests on the basis of the above spatial mode superposition picture. Miró *et al.* studied the phenomenon in more detail [29]. They found a mode coupling mechanism based on dynamic feedback reactivities. However, it needs to be stated that radial and axial power distributions play a very important role in exciting such instabilities [29]. Thus, a strongly bottom-peaked axial power shape makes the core more unstable, and a bowl shape for the radial power distribution makes the core more susceptible to out-of-phase oscillations. Hence, the spatial power distribution is an additional indicator for the excitation of higher mode oscillations. In this thesis, in Chapter 6, a more rigorous and quantitative explanation is proposed for in-phase and out-of-phase oscillations based on an in-depth investigation of the properties of the elements of the eigenvectors associated with these oscillation modes.

⁹ Note that the superposition principle is valid for linear systems.

¹⁰ This is the reason why they are sometimes called subcritical modes.

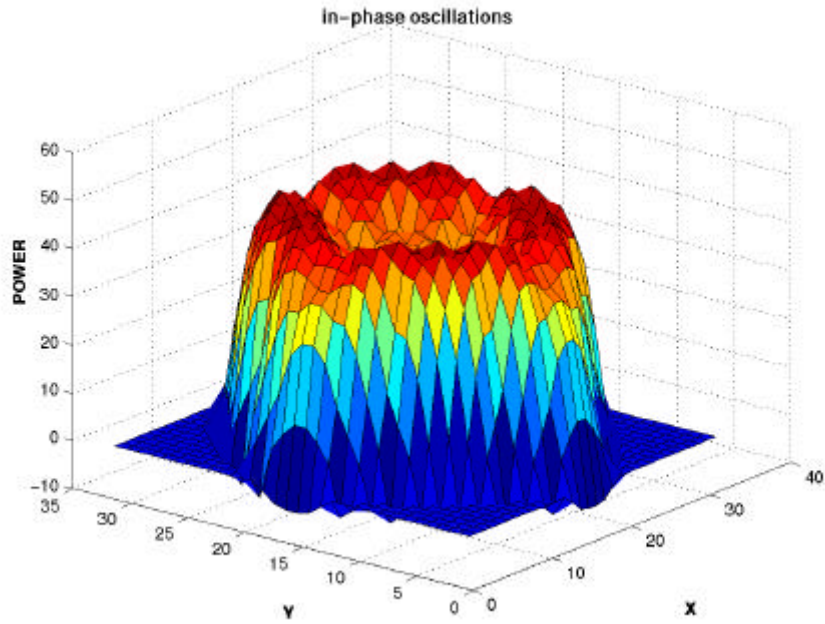


Figure 2-5. A schematic view of in-phase power oscillations.

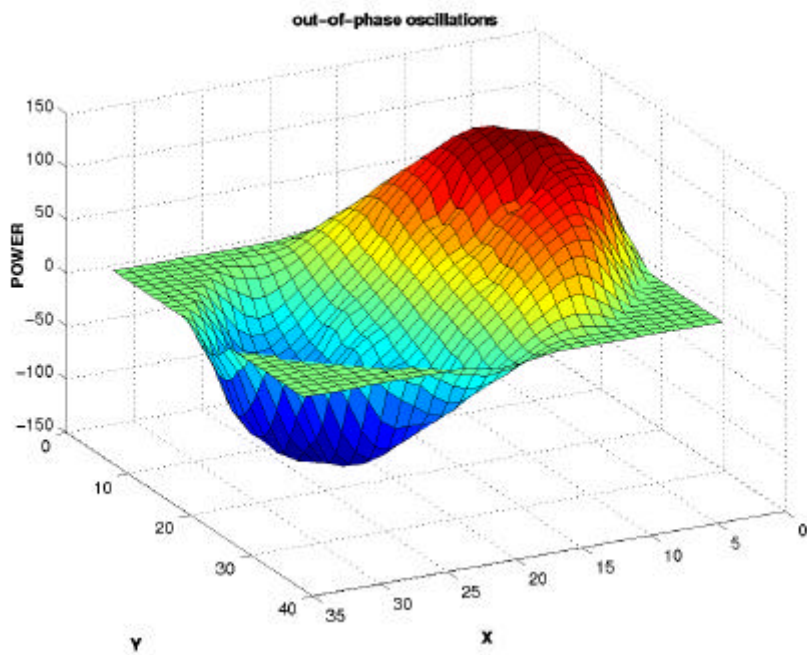


Figure 2-6. A schematic view of out-of-phase power oscillations.

2.6 **HYDRAULIC BOUNDARY CONDITIONS ISSUE**

In general, the effects of the outer loop are considered to be very important in the stability analysis of BWRs. Thus, in the case of global oscillations, the outer loop may amplify or damp the core oscillations. However, loop effects can be neglected in the case of out-of-phase oscillations, *i.e.* the reactor core can be considered decoupled from the outer loop in this case. In effect, the assumption of a constant pressure drop across the reactor core can replace the outer loop model. For instance, Grandi *et al.* [30] illustrated that almost identical results are obtained in out-of-phase oscillation calculations using either (i) a vessel model, *i.e.* a core model plus a model for the peripheral system (outer loop), or (ii) a core model in which constant core inlet flow and constant core pressure drop hydraulic boundary conditions are imposed. They showed that not only the qualitative behaviour of the two solutions is the same, but the quantitative behaviour as well.

It was in a reduced order model study of the boundary conditions for a system formed by two parallel channels coupled to multimodal neutron kinetics that Muñoz-Cobo *et al.* [31] suggested that, in the out-of-phase oscillations case, two hydraulic boundary conditions have to be imposed, *viz.* (i) constant pressure drop across the core and (ii) constant total inlet mass flow rate. On the other hand, the boundary conditions in the in-phase oscillations case were pointed out to be (i) constant pressure drop across the two channels and (ii) no restrictions on the incoming mass flow rate to both channels. In a later paper, Muñoz-Cobo *et al.* [32] went through the boundary conditions issue again and argued that, during out-of-phase oscillations, the total pressure drop cannot be imposed to be constant because imposing, at the same time, a constant pressure drop boundary condition and a constant mass flow rate through the entire core leads to a system of differential equations that is overdetermined and allows only small variations in the inlet flow rate.

The results of numerical investigations carried out for two different operational points with the RAMONA system code (see next section) are presented here. In the first case, one has a small in-phase oscillation amplitude (1%). Fig. 2-7 shows the time evolution of the pressure drop across the core, which can clearly be considered to be constant. Hence, we can assume that, for small in-phase oscillation amplitudes, a constant pressure drop assumption across the core, in a given BWR model, can replace explicit consideration of the outer loop.

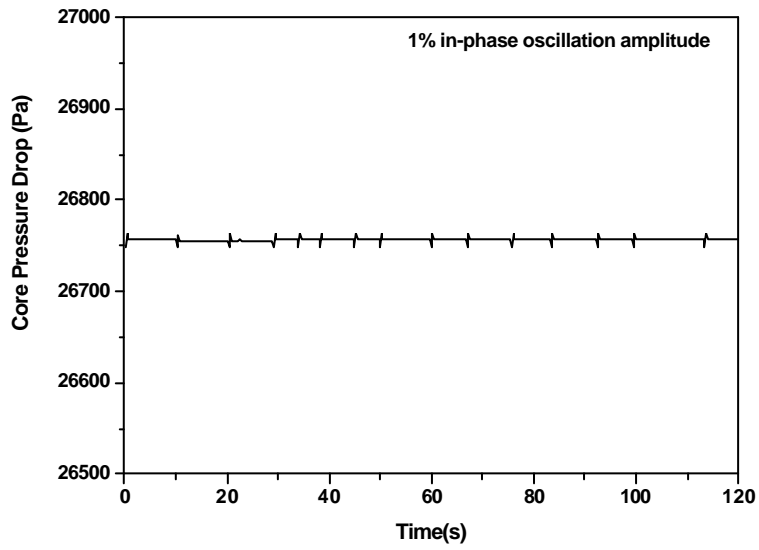


Figure 2-7. Pressure drop across the core for a 1% power in-phase oscillation amplitude (RAMONA results).

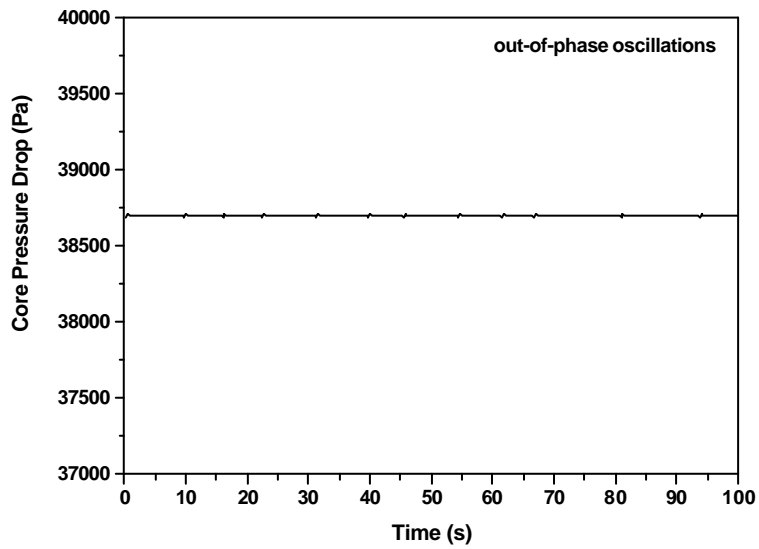


Figure 2-8. Pressure drop across the core for an out-of-phase oscillation case (RAMONA results).

The second operational point considered with RAMONA is an out-of-phase oscillation case. It is clear from the time evolution shown in Fig. 2-8 that, once again, the pressure drop is constant. In the BWR reduced order model analysis carried out throughout this research, a constant pressure drop across the core is the unique hydraulic boundary condition applied. As illustrated with the above two RAMONA cases, such a boundary condition is clearly valid for both out-of-phase oscillations and small in-phase oscillation amplitudes.¹¹

2.7 CODES USED IN THIS THESIS

As mentioned in Subsections 2.2.2 and 2.3.2, many different codes have been used in the past to carry out BWR stability analysis. In this section, a description is given of the specific codes used in the various types of analysis conducted within this thesis. First of all, a short description is provided of RAMONA, the complex system code used to carry out bifurcation analysis numerically for the Leibstadt and Ringhals-1 NPPs (operational points in cycle 7 and cycle 14, respectively). Then, BIFDD, a code for performing the so-called *semi-analytical* bifurcation analysis (see Section 3.2), is mentioned briefly, further details being provided after the discussion of Hopf bifurcation in Chapter 3. Next, a short description is given of the main Fortran program *bwr.f* that provides the right hand side of the set of nonlinear ODEs, as well as the Jacobian matrix, of the currently developed reduced order model (see Chapter 4). It is this code which is used in conjunction with BIFDD for the stability and bifurcation analyses carried out in Chapter 5¹², 6 and 8. Finally, a short description is given of the MATLAB code *integration.m*, used for numerical integration of the system of ODEs of the reduced order model.

¹¹ As regards the condition of a constant mass flow rate, this cannot be imposed in the currently developed reduced order model (see Chapter 4) since the mass flow rate is a state variable. It will be shown later (Chapter 6) that, in the out-of-phase oscillation case, although the total mass flow is not imposed as fixed, the system adjusts itself in such a way as to yield a near-to-constant total mass flow.

¹² For the heated channel analyses described in Chapter 5, the sub-program *drift.f*, corresponding to the thermal-hydraulic part of the complete reduced order model, is used.

Cross Section Calculation

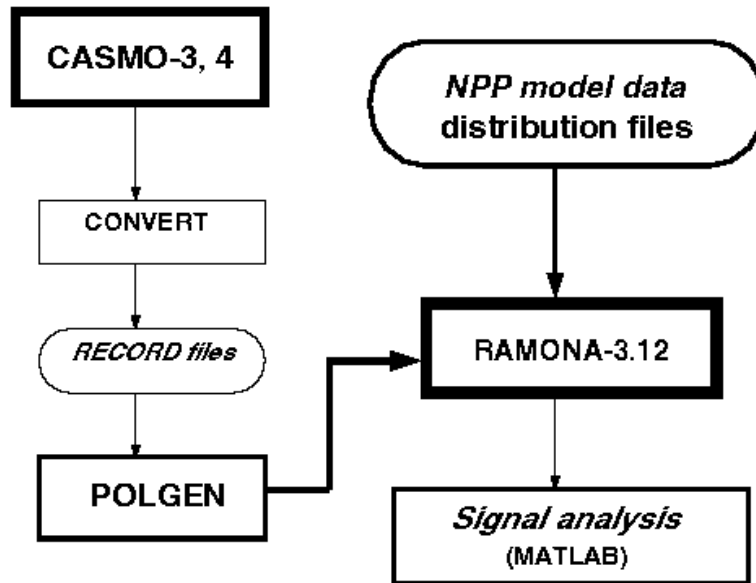


Figure 2-9. PSI methodology for BWR stability analysis.

2.7.1 System Code RAMONA

2.7.1.1 PSI methodology [33]

The PSI stability analysis methodology is based on use of the Scandpower system code RAMONA-3¹³, which provides a three-dimensional core model. The nuclear parameters, the cross-sections, are calculated by the lattice code CASMO (version 3 or 4) [36] and converted to the RAMONA format using the Scandpower codes CONVERT and POLGEN. Effectively, a POLGEN cross-section file and a POLGEN kinetic parameter file are generated, both these serving as input to the RAMONA-3 model (Fig. 2-9).

The cross-sections are functions of the reactor history parameters (such as burnup and void history) and instantaneous reactor parameters (such as void and fuel temperature). The so-called PRESTO Core Master distribution file, that contains the nodal distributions

¹³ Recently, a new version called RAMONA-5 is in use at PSI [34, 35].

for burnup, void history and (optionally) power and Xenon concentrations, represents the third set of input data (apart from the two POLGEN files) for RAMONA-3.

With an initial core perturbation, usually corresponding to a specific sinusoidal control rod perturbation amplitude, the neutronic-thermal-hydraulic coupled system code calculates the time evolution of the LPRM and APRM power detectors that are modelled in RAMONA. The predicted (as in the case of measured) time series are analysed in order to determine stability indicators, such as the DR and the natural frequency, that are calculated based on an ARMA model [33].

2.7.1.2 RAMONA Model

RAMONA is a well-known system code with a broad validation basis for stability analysis [37]. The code simulates the coupled thermal-hydraulics and three-dimensional reactor kinetics behaviour. In the RAMONA-3 versions, the space-time dependent neutron diffusion equation is solved in the so-called $1\frac{1}{2}$ energy-group approximation (see Appendix A), while for RAMONA-5 (PRESTO2 option), there is a full PRESTO2-two-group model [39].

The thermal-hydraulic model in RAMONA-3 is based on a 4-equation, non-equilibrium two-phase flow model. The 4 equations are the vapour and liquid mass balances, the mixture energy balance and the mixture momentum balance. The model has two main assumptions. Firstly, the local variation of system pressure is ignored, *i.e.* acoustic effects are neglected. The second assumption is that the vapour is assumed to be at saturation but the liquid in the two-phase mixture is allowed to depart from saturation conditions. Based on the first assumption, the momentum equation is integrated along closed contours, each one comprising a hydraulic channel as well as the other six RAMONA plant model components: lower plenum (LP) 1 and 2, upper plenum, riser, and downcomer (DC) 1 and 2 (Figs. 2-10 and 2-11). For instance, this results in 648 closed integration paths for the Leibstadt nuclear power plant.

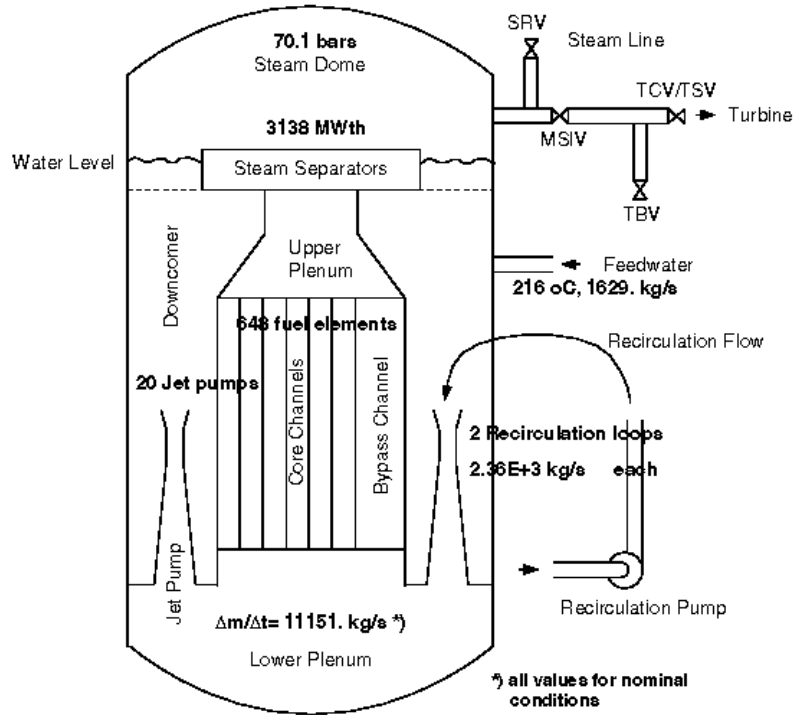


Figure 2-10. Schematic view of a BWR plant.

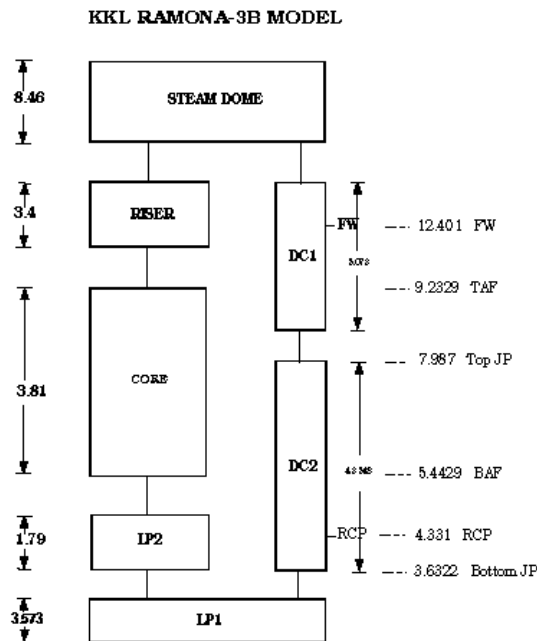


Figure 2-11. RAMONA BWR model.

The fuel model calculates the temperature distribution within the fuel pin and the transport of heat from the fuel into the coolant. The numerical time-integration is performed using an implicit predictor-corrector scheme for the neutronics and fuel model. The hydraulics is integrated using explicit methods for all equations except the momentum equations, which have the option to be integrated implicitly. The steam line model employs a higher order Runge-Kutta explicit method. More details on the RAMONA mathematical models are presented in Appendix A. Preparing a RAMONA input deck signifies mapping the components of a given BWR (Fig. 2-10) onto the RAMONA model (Fig. 2-11).

2.7.2 Bifurcation code BIFDD

The bifurcation code BIFDD has been used in conjunction with the currently developed *bwr.f* code to perform the semi-analytical bifurcation analysis of the set of ODEs of the new reduced order model. Details on BIFDD are presented in Chapter 3, Section 3.3.

2.7.3 Reduced order model Fortran code (*bwr.f*)

A main Fortran program called *bwr.f* has been written corresponding to the currently developed, BWR reduced order model (see Chapter 4). This program comprises subroutines that numerically evaluate the right hand side of the set of nonlinear ODES as well as the Jacobian matrix, which, in turn, have been obtained using the Maple symbolic toolbox. *bwr.f* allows any one of the system parameters to be selected as the bifurcation parameter, along with a second parameter which can be incremented in small steps. Variation of the second chosen parameter allows, in turn, evaluation of critical values of the bifurcation parameter and the associated bifurcation characteristics. Thus, the entire stability boundary (SB) in two-dimensional parameter space can be determined.

2.7.4 Matlab program for numerical integration (*integration.m*)

For independent confirmation of the results of the bifurcation analyses carried out by BIFDD and *bwr.f*, and to evaluate the system behaviour in regions away from the stability boundary, Matlab programs have currently been developed to numerically integrate the sets of ODEs of the analysed models: a heated channel model (two-phase flow instabilities) with 5 ODEs, a single channel nuclear-coupled thermal-hydraulic model with 11 ODEs, and a two channel nuclear-coupled thermal-hydraulic model with 22 ODEs.

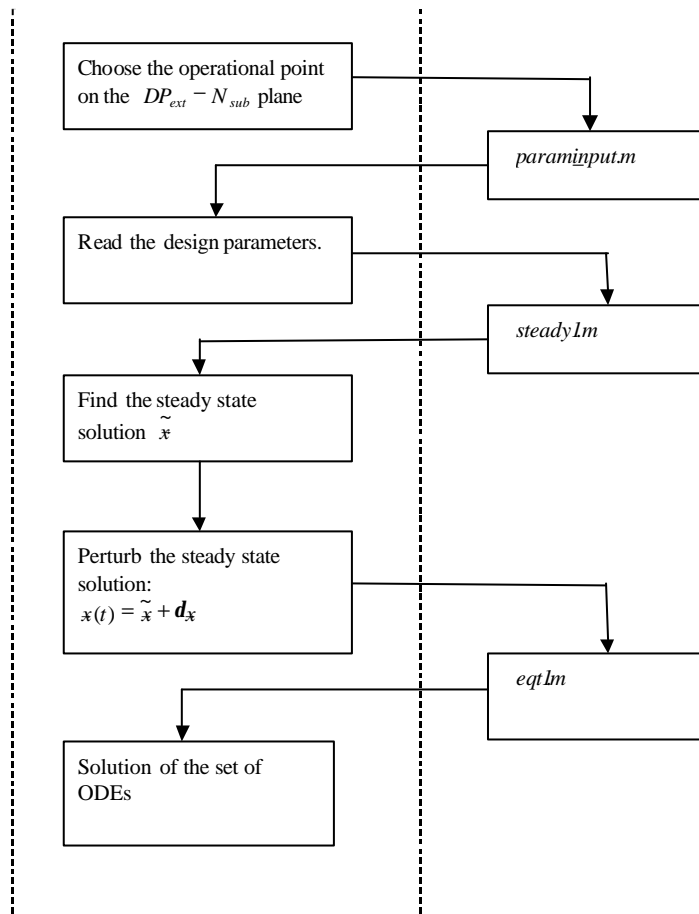


Figure 2-12. Diagram showing the different steps to carry out numerical integration using the Matlab code *integration.m*.

Mainly, two solvers have been used, viz. a 5th order Runge-Kutta method for integrating the 5 ODE model¹⁴, and the Gear's method for numerically integrating the 11 and 22 ODE models¹⁵.

In a main program called *integration.m*, the operational point to be analysed is first chosen. For instance, in the 22 ODE model, values of the parameters N_{sub} and DP_{ext} ¹⁶ are first selected. The main program then calls a subroutine *param_input.m* to read the numerical values of the various design and operating parameters of the system. After that, the main program calls a subroutine *steadylm* in order to find the steady-state solution of the system. Then, the steady-state vector solution is perturbed, and the main program calls

¹⁴ model that simulates thermal-hydraulic instabilities

¹⁵ stands for the single- and two-channel nuclear-coupled thermal-hydraulic models, respectively

¹⁶ subcooling number and the total pressure drop across the core, respectively

a subroutine *eqt1.m* to integrate the set of ODEs of the analysed system. Finally, the code gives the solution vector as a time series. Fig. 2-12 illustrates the different steps performed during the numerical integration.

REFERENCES

- [1] J. Guckenheimer, P. Holmes, “Nonlinear Oscillations, Dynamical Systems, and Bifurcation of Vector Fields”, Applied Mathematical Sciences 42, Springer Verlag, 1984.
- [2] J. March-Leuba, “Dynamic Behaviour of Boiling Water Reactors”, Ph.D. Dissertation, University of Tennessee, USA, 1984.
- [3] K. Ogata, “Modern Control Engineering,” Prentice-Hall, Englewood Cliffs, New Jersey, 1970.
- [4] F. D’Auria, “State-of-the-art Report on Boiling Water Reactor Stability,” NEA report NEA/CSNI/R (96) 21, OECD/GD (97) 13, 1997.
- [5] E. Pollman, J. Schulze, D. Kreuter, “Stability Measurements in German Nuclear Power Plant Würgassen during Cycle 14,” *Nucl. Technology*, **108**, 350, 1994.
- [6] General Electric, “ODYSY01/ODYSY02, Qualification Report”, NEDE-30227, 1983.
- [7] T. Smed, P. Lansakar, “RAMONA in 10-Minutes-Frequency Domain Analysis”, Studsvik-Scandpower European User Group Meeting, Sep 1999, Lake Windermere, England.
- [8] P. Otaduy, J. March-Leuba, “LAPUR User Guide”, NUREG/CR-5421, 1989.
- [9] S. J. Peng, M. Z. Podowski, R. T. Lahey, Jr. M. Becker, “NUFREQ-NP: A Computer Code for Stability Analysis of BWRs”, *Nucl. Sci. Eng.*, **88**, 404-411, 1984.
- [10] T. H. J. J. Van der Hagen, R. Zboray, W. d’Kruijff, “Questioning the Use of Decay Ratio in BWR Stability Monitoring”, *Ann. Nucl. Energy*, **27**, 727-732, 2000.
- [11] W. Wulff, H. S. Chen, D. J. Diamond, and M. Khatib-Rahbar, “A Description and Assessment of RAMONA-3B Mod0, Cycle4: A Computer Code with Three-Dimensional Neutron Kinetics for BWR System Transients,” NUREG/CR-3664, 1984.
- [12] J. C. Shaug et al., “TRAC-G Analysis of BWR Plants Stability Data,” *Proc. Int. Workshop on BWR Stability*, OECD/NEA CSNI Report 178, 354-369, 1990.
- [13] K. Valtonen, “RAMONA-3B and TRAC-B Assessment Using Oscillation Data from TVO-I,” *Proc. Int. Workshop on BWR Stability*, OECD/NEA CSNI Report 178, 205-231, 1990.

- [14] P. J. Jensen, R. R. Galer, "Analysis of Water Level Reduction During ATWS/Instability Events," *Proc. Int. Workshop on BWR Stability*, OECD/NEA CSNI Report 178, 446-456, 1990.
- [15] K. E. Ransom et al., "RELAP5/Mod2 Code Manual, Vol.I: Code Structure, System Models, and Solution Methods," EG&G Idaho, Inc., NUREG/CR- 5535, EGG-2596, June 1990.
- [16] J. March-Leuba, D. G. Cacuci, R. B. Perez, "Nonlinear Dynamics and Stability of Boiling Water Reactors: Part I- Qualitative Analysis," *Nucl. Sci. Eng.*, **93**, 111-123, 1986.
- [17] J.L. Muñoz-Cobo, G. Verdú, "Application of Hopf Bifurcation Theory and Variational Methods to the Study of Limit Cycles Boiling Water Reactors," *Ann. Nucl. Energy*, **18**, 5, 269-302, 1991.
- [18] Rizwan-uddin, "Sub- and Supercritical Bifurcations and Turning Points in a Simple BWR Model," *Proc. Int. Top. Mtg. Advances in Reactor Physics and Mathematics (PHYSOR-2000)*. Pittsburgh, Pennsylvania, May 7-11, 2000.
- [19] J. L. Muñoz-Cobo, R. B. Pérez, D. Ginestar, A. Escrivá, G. Verdú, "Nonlinear Analysis of out of Phase Oscillations in Boiling Water Reactors," *Ann. Nucl. Energy*, **23**, 16, 1301-1335, 1996.
- [20] A. A. Karve, "Nuclear-Coupled Thermal-hydraulic Stability Analysis of Boiling Water Reactors," Ph.D. Dissertation, Virginia University, USA, 1998.
- [21] J. L. Muñoz-Cobo, O. Rosello, R. Miró, A. Escrivá, D. Ginestar, G. Verdú, "Coupling of Density Wave Oscillations in Parallel Channels with High Order Modal Kinetics: Application to BWR out of Phase Oscillations," *Ann. Nucl. Energy*, **17**, 1345-1371, 2000.
- [22] A. Dokhane, D. Hennig, Rizwan-uddin, R. Chawla, "Nuclear-Coupled Thermal-Hydraulic Nonlinear Stability Analysis Using a Novel BWR Reduced Order Model: Part 1 – The Effect of Using Drift Flux Versus Homogeneous Equilibrium Models, Part2 – Stability Limits for In-phase and Out-of-phase Oscillations," *Proc. 11th International Conference on Nuclear Engineering (ICONE11)*, Tokyo, Japan, April 20-23, 2003.
- [23] B. R. Upadhyaya, M. Kitamura, "Stability Monitoring of BWRs by Time Series Analysis of Neutron Noise," *Nucl. Sci. Eng.*, **77**, 480-492, 1981.
- [24] R. Oguma, "Investigation of Power Oscillation Mechanisms Based on Noise Analysis at Forsmark-1 BWR," *Ann. Nucl. Energy*, **23**, 6, 469-485, 1996.
- [25] D. Hennig, "Time Series Analysis for BWR Stability Studies," Internal PSI report, TM-41-97, 1997.

- [26] B. Askari, D. Hennig, "High Performance Time Series Analysis (HPTSAC 2000)," Internal PSI- report, 2001.
- [27] L. Ljung, System Identification: Theory for Users, Prentice-Hall, Englewood Cliffs, New Jersey, 1987.
- [28] T. Söderström, P. Stoica, System Identification, Prentice-Hall, 1989.
- [29] M. Miró, D. Ginestar, D. Hennig, G. Verdú, "On the Regional Oscillation Phenomenon in BWRs," *Progress in Nuclear Energy*, **36**, 2, 189-229, 2000.
- [30] G. M. Grandi, K. S. Smith, "BWR Stability Analysis with SIMULATE-3K," *Proc. of International Conference on the New Frontiers of Nuclear Technology Reactor Physics, Safety and High Performance Computing (PHYSOR-2002)*, Seoul, Korea, Oct. 7-10, 2002, CD-ROM.
- [31] J. L. Muñoz-Cobo, O. Rosello, R. Miró, A. Escrivá, D. Ginestar, G. Verdú, "Coupling of Density Wave Oscillations with High Order Modal Kinetics: Application to BWR Out-of-phase Oscillations", *Annals of Nucl. Energy*, **27**, 1345-1371, 2000.
- [32] J. L. Muñoz-Cobo, M. Z. Podowski, S. Chiva, "Parallel Channel Instabilities in Boiling Water Reactor Systems: Boundary Conditions for Out-of-phase Oscillations", *Annals of Nucl. Energy*, **29**, 16, 1891-1917, 2002.
- [33] D. Hennig, "A Study of BWR Stability Behaviour," *Nuclear Technology*, **126**, 10-31, 1999.
- [34] H. Ferroukhi, D. Hennig, C. Aguirre, "Comparative Study between RAMONA-5 and RAMONA-3 for the Analysis of the KKL C19 Stability Measurements," Internal PSI report TM-41-03-09, May 2003.
- [35] D. Hennig, C. Aguirre, "Post-calculations of the Stability Measurement Records #4 and #5 at NPP Leibstadt (Cycle 7), 1990," Internal PSI report TM-41-03-15, June 2003.
- [36] B. H. Forssen, "CASMO-3, a Fuel Assembly Burnup Program, User's Manual (Version 4.7)," Studsvik/NFA-89/3, Studsvik Energiteknik AB, 1992.
- [37] A. Noel, A. Stepniewski, "NEA BWR Stability Benchmark: RAMONA-3 Results" OECD/NEA NRC Specialist Meeting on Light Water Reactors, Paris, May, 1995.
- [38] W. Wulff, H. S. Cheng, D. J. Diamond, M. Khatib-Rahbar, "A Description and Assessment of RAMONA-3B Mod. 0, Cycle 4: A Computer Code with 3D Neutron Kinetics for BWR System Transients," NUREG/CR-3664, BNL-NUREG-51746, Brookhaven National Laboratory, 1984.
- [39] N. Patino, "PRESTO-2 Topical Report," Scandpower report No. TR1/41.72.54, 1998.

3 BIFURCATION ANALYSIS

This chapter presents the concept of bifurcation analysis, in particular Hopf bifurcation theory and its relation to the existence of periodic solutions. Bifurcation, a French word introduced into nonlinear dynamics by Poincaré, is used to indicate a qualitative change in the features of a system, such as the number and type of solutions, under the variation of one or more parameters on which the considered system depends [1]. The existence of stable or unstable periodic solutions to a set of nonlinear ordinary differential equations was proven by Hopf [2]. Recognizing earlier contributions by Poincaré and Andronov, the theorem is sometimes called the Poincaré-Andronov-Hopf (PAH) bifurcation theorem. This theorem guarantees the existence of periodic (stable or unstable) solutions to nonlinear differential equations if certain conditions are satisfied. Details of this theorem are presented in the next section. Section 3.2 outlines the *semi-analytical* bifurcation methodology used in the current work, while Section 3.3 gives details of the code BIFDD mentioned earlier. Appendix B defines some of the nonlinear dynamics concepts used in this chapter.

3.1 HOPF BIFURCATION THEORY

Hopf bifurcation has been reported by many researchers [3-9] to be the most important type of bifurcation observed during BWR stability analysis. Moreover, it is the only type of bifurcation that has been encountered during the loss of system stability¹⁷. In general terms, Hopf bifurcation theory states that stable or unstable periodic solutions to a set of nonlinear differential equations exist under certain conditions. Consider the following system of ODEs

$$\frac{d\bar{x}(t)}{dt} = F(\bar{x}, \mathbf{I}) \quad (3.1)$$

where $\bar{x}(t)$ is the state vector, F is an analytical vector function, and \mathbf{I} is the so-called bifurcation parameter. $\tilde{\bar{x}}$ is the steady state solution, or the fixed point, of Eq. (3.1), *i.e.* $F(\tilde{\bar{x}}, \mathbf{I}) = 0$ for all \mathbf{I} .

The Hopf bifurcation theorem states that:

¹⁷ In crossing the first stability boundary, only Hopf bifurcation has been encountered. However, deep in the unstable region, a cascade of period-doubling bifurcations may exist as reported for instance in [6].

If

- 1) a pair of complex conjugate eigenvalues $\mathbf{s}(I) \pm i\mathbf{w}(I)$ of the Jacobian matrix crosses the imaginary axis for a critical value of $I = I_c$ in such a way that $\mathbf{w}(I_c) > 0$, $\mathbf{s}(I_c) = 0$, and
- 2) $\frac{\partial \mathbf{s}(I = I_c)}{\partial I} \neq 0$, and
- 3) all the other eigenvalues have strictly negative real parts (see Figure 3-1),

then:

periodic solutions of Eq. (3.1) bifurcate from a branch of the steady-state solution x_{eq} at $I = I_c$.

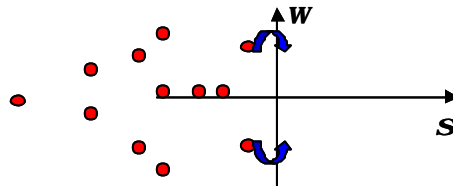


Figure 3-1. Schematic illustration of the occurrence of Hopf bifurcation in the complex plane of Jacobian matrix eigenvalues.

In simpler terms, the theorem implies that periodic solutions to the nonlinear differential equations exist for parameter values I if at $I = I_c$ a pair of complex conjugate eigenvalues of the Jacobian matrix has zero real part while all others are away from, and to the left of, the imaginary axis, and the derivative of the real part of the pair of eigenvalues on the imaginary axis with respect to I is non-zero. These periodic solutions only exist either on the stable side or on the unstable side. If the periodic solutions exist on the unstable side of the SB, they are stable, and the PAH bifurcation is called supercritical. On the other hand, if the periodic solutions exist on the stable side of the SB, they are unstable and the PAH bifurcation is called subcritical.

The stability of the periodic solution is determined by applying the Floquet theory of differential equations with periodic coefficients [1], in which two Floquet exponents appear to give more nonlinear information regarding the system stability behaviour. The first exponent is always zero and the other exponent, \mathbf{b} , determines the stability of the

periodic oscillation. More details can be found in Appendix B. If $\mathbf{b} < 0$, the periodic solution is stable (supercritical bifurcation), while if $\mathbf{b} > 0$ the periodic solution is unstable (subcritical bifurcation). Since Floquet theory is based on linear analysis, the obtained information on the periodic solutions is valid only close to the stability boundary.

Transition from a stable (unstable) fixed point solution to an unstable (stable) fixed point and a stable (unstable) periodic solution (limit cycle) is shown schematically in Fig. 3-2. The case of subcritical PAH bifurcation, shown in Fig. 3-2(a), has an unstable periodic solution (repeller limit cycle) for $I > I_c$. Hence, for $I > I_c$, perturbations of amplitude less than the amplitude of the parabola will decay to zero (stable fixed point solution). Perturbations of amplitude greater than the limit cycle amplitude will be repelled and hence will move away from the stable fixed point as well as from the unstable limit cycle. On the other hand, in the supercritical PAH bifurcation case, shown in Fig. 3-2(b), there exist stable limit cycles in the unstable region, and hence small perturbations grow and stabilize at the limit cycle, while perturbations with amplitude larger than the limit cycle radius (amplitude) can decay onto the limit cycle, depending upon the size of the perturbation and the basin of attraction of the stable limit cycle.

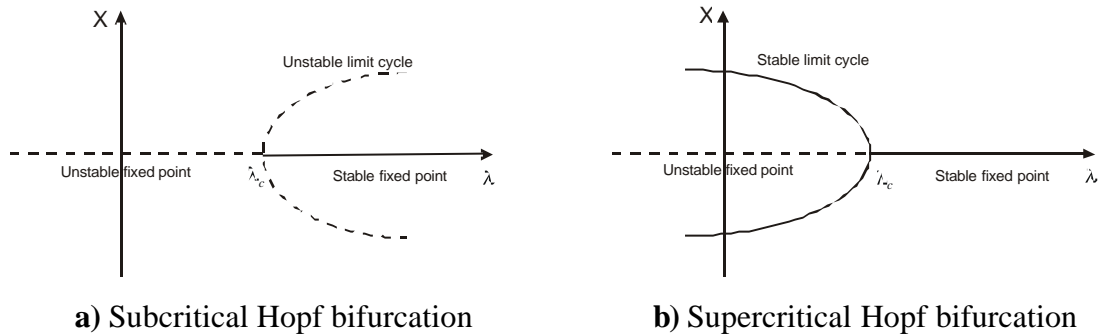


Figure 3-2. Sub- and supercritical PAH bifurcations, unstable limit cycle for subcritical PAH bifurcation, and stable limit cycle for supercritical PAH bifurcation.

In summary, crossing a stability boundary between a region with no eigenvalues with positive real parts and a region with one pair of complex conjugate eigenvalues with positive real parts implies PAH bifurcation. Such a stability boundary can be easily determined via a linear analysis. However, to determine the nature of bifurcation (sub- vs. supercritical) and to determine the oscillation amplitude close to the stability boundary,

additional (bifurcation) analyses are necessary. Such bifurcation studies are usually performed in one of two ways, *viz.* either by numerically integrating the set of governing equations or analytically.

3.1.1 Center Manifold Reduction

In studies of dynamical systems, simplification methods are often used to reduce the order of the system of equations. Center manifold reduction is one of these methods and has been used as a basis for the current bifurcation analysis with the code BIFDD. Recalling the concept of the center manifold of a fixed point, we note that there is a center manifold (see Appendix B) associated with a fixed point undergoing a bifurcation. This manifold is a curved m -dimensional surface that is tangential at the bifurcation point to the subspace spanned by the m eigenvectors $\vec{p}_1, \vec{p}_2, \dots, \vec{p}_m$ corresponding to the m eigenvalues I_1, I_2, \dots, I_m with zero real parts. The dimension m is less than the dimension n of the full system. In a physical sense, this reduction means that the physics of the system of order n , at the bifurcation point, can be described by just a subsystem with dimension m . For a Hopf bifurcation, at the bifurcation point, the number of eigenvalues with zero real parts is two. Therefore, the center manifold dimension for this type of bifurcation is two, *i.e.* the dynamical system of order n is reduced to a system of order 2.

3.1.2 Poincaré Normal Form

Commonly, in bifurcation analysis, a center manifold reduction is used to reduce the order of the dynamical system first, and then the method of normal forms [1] is used to simplify the general structure of the reduced system to the so-called Poincaré normal form. The Poincaré normal form for a Hopf bifurcation is a two-dimensional autonomous system

$$\dot{x}_1 = \mathbf{a}x_1 - \mathbf{w}x_2 + [\text{Re}(c_1)x_1 - \text{Im}(c_1)x_2] \cdot (x_1^2 + x_2^2) \quad (3.2)$$

$$\dot{x}_2 = \mathbf{w}x_1 + \mathbf{a}x_2 + [\text{Re}(c_1)x_2 - \text{Im}(c_1)x_1] \cdot (x_1^2 + x_2^2) \quad (3.3)$$

where \mathbf{a} and \mathbf{w} are the real and imaginary parts of the pair of complex eigenvalues of the Jacobian matrix of the 2×2 system.

The coefficient c_1 is a complicated term that results from the reduction of the general structure of the reduced order of the dynamical system equations to a bidimensional system of equations, using center manifold reduction, and the transformation of the latter

to Poincaré normal form via the so-called near identity transformation. This coefficient comprises first, second, and even third partial derivatives of the vector function [10]. It is the key parameter to be determined in order to evaluate the bifurcation parameters \mathbf{m}_2 , \mathbf{t}_2 and \mathbf{b}_2 , defined in the next section. Once c_1 is evaluated, only $\mathbf{a}'(\mathbf{I}_c)$ and $\mathbf{w}'(\mathbf{I}_c)$ are needed to evaluate \mathbf{m}_2 , \mathbf{t}_2 and \mathbf{b}_2 . It can be demonstrated that these bifurcation parameters are related to c_1 as follows:

$$\mathbf{b}_2 = 2 \cdot \text{Re}(c_1(\mathbf{I}_c)) \quad (3.4)$$

$$\mathbf{m}_2 = -\text{Re}(c_1(\mathbf{I}_c)) / \mathbf{a}'(\mathbf{I}_c) \quad (3.5)$$

$$\mathbf{t}_2 = -(\text{Im}(c_1(\mathbf{I}_c)) + \mathbf{m}_2 \mathbf{w}'(\mathbf{I}_c)) / \mathbf{w}_0 \quad (3.6)$$

where $c_1(\mathbf{I}_c)$ is the value of c_1 at the critical bifurcation point, and $\mathbf{a}'(\mathbf{I}_c)$ and $\mathbf{w}'(\mathbf{I}_c)$ are the first derivatives of, respectively, the real and imaginary parts of the pair of complex eigenvalues at the critical bifurcation point.

3.2 SEMI-ANALYTICAL BIFURCATION METHOD

As reported in the previous section, if Hopf bifurcation conditions are fulfilled, a family of periodic solutions, with small amplitude¹⁸ \mathbf{e} , exists in a neighbourhood of the stability boundary:

$$\bar{\mathbf{x}}(t, \mathbf{I}) = \tilde{\mathbf{x}}(\mathbf{I}_c) + \mathbf{e} \text{Re}(e^{2\pi i t / T(\mathbf{e})} \vec{V}_1) + o(\mathbf{e}^2) \quad (3.7)$$

where $\bar{\mathbf{x}}(t, \mathbf{I})$ is the vector of the state variables of the system, $\tilde{\mathbf{x}}(\mathbf{I}_c)$ is the steady-state vector solution at the critical value (on the stability boundary) of the bifurcation parameter \mathbf{I} , and \vec{V}_1 is the eigenvector associated with the pair of complex eigenvalues responsible for the bifurcation. In order to determine the nature of Hopf bifurcation along the SB, Lindstedt-Poincaré asymptotic expansion [1,10] is applied to expand, in terms of the small amplitude \mathbf{e} , the state variable vector $\bar{\mathbf{x}}(t, \mathbf{I})$, the oscillation frequency \mathbf{w} , the bifurcation parameter \mathbf{I} , and the Floquet exponent \mathbf{b} :

¹⁸ Because bifurcation analysis is based on linear Floquet theory, the analysis should be close to the SB, which is equivalent to a small amplitude.

$$\bar{x} = \tilde{x} + \mathbf{e}\bar{x}_1 + \mathbf{e}^2\bar{x}_2 + \dots \quad (3.8)$$

$$1/\mathbf{w} = 1/\mathbf{w}_0 + \mathbf{e}\mathbf{t}_1 + \mathbf{e}^2\mathbf{t}_2 + \dots \quad (3.9)$$

$$\mathbf{l} = \mathbf{l}_c + \mathbf{e}\mathbf{m}_1 + \mathbf{e}^2\mathbf{m}_2 + \dots \quad (3.10)$$

$$\mathbf{b} = \mathbf{e}\mathbf{b}_1 + \mathbf{e}^2\mathbf{b}_2 + \dots \quad (3.11)$$

The Lindstedt-Poincaré asymptotic expansion analysis shows that the values of \mathbf{t}_1 , \mathbf{m}_1 and \mathbf{b}_1 are zero [10]. Hence, \mathbf{m}_2 , \mathbf{t}_2 and \mathbf{b}_2 are evaluated to determine the nature of the bifurcation. It should be emphasized that the analytical evaluation of \mathbf{m}_2 , \mathbf{t}_2 and \mathbf{b}_2 needs extensive mathematical manipulations and becomes almost impossible with increasing order of the model equations. Another drawback of analytical bifurcation studies is that each is specific to a specific bifurcation parameter and must be repeated if the impact of a different parameter is to be studied.

Due to the limitations of both the numerical integration and analytical bifurcation approaches, there has been limited investigation of the large parameter space even in simple models of BWRs. Therefore, currently an alternative approach to the two approaches described above has been adopted, in which analytical bifurcation is carried out numerically. In this approach, the governing set of nonlinear equations is neither integrated numerically in time nor treated entirely analytically. Rather, the analytical reduction to the Poincaré normal form via the center manifold theorem is carried out numerically [11]. This approach, which henceforth is called the *analytic-numeric* approach or the *semi-analytical* method [13], allows accurate and efficient evaluation of the entire parameter space of interest.

3.3 CODE BIFDD

The bifurcation code BIFDD (Bifurcation Formulae for Delay-Differential system) was developed by Hassard [12] to perform *semi-analytical* bifurcation analysis of sets of ODEs and ODEs with delays. This code has been used in conjunction with the novel reduced order model developed currently to analyse BWR stability characteristics in design and operating parameter space. For a given set of nonlinear ODEs or ODEs with delays and the corresponding Jacobian matrix, the code determines the critical value of the bifurcation

parameter I_c , the frequency and amplitude of the oscillation, and parameters m_2 , t_2 and b_2 . A negative (positive) value of b_2 indicates a supercritical (subcritical) PAH bifurcation. t_2 is a correction factor for the oscillation frequency, and m_2 relates the oscillation amplitude to the value of the bifurcation parameter through

$$e = \sqrt{\frac{I - I_c}{m_2}} \quad (3.12)$$

By incrementally varying a second parameter and repeating the calculations for the critical value of the bifurcation parameter, one can easily generate stability boundaries and determine the nature of the bifurcation along such boundaries in two-dimensional parameter spaces.

As mentioned in Subsection 2.7.3, the main Fortran program *bwr.f*, which calls BIFDD, has been written to provide the right hand side of the set of nonlinear ODEs, as well as the Jacobian matrix, of the currently developed BWR reduced order model (see next chapter). The main program assigns initial estimates (guesses) of I_c , w_0 and $\tilde{x}(t, I_c)$, before calling BIFDD to carry out the bifurcation analysis as depicted in Figure 3-3.

3.3.1 Numerical Evaluation of Hopf Bifurcation Parameters

One can summarize the analysis performed by BIFDD to evaluate the Hopf bifurcation parameters in six different steps:

1. Determination of the critical value of the bifurcation parameter I_c .
2. Computation of the derivatives of the real and imaginary parts of the pair of complex eigenvalues responsible for bifurcation, *i.e.* $\mathbf{a}'(I_c)$ and $\mathbf{w}'(I_c)$.
3. Application of the center manifold reduction from an $n \times n$ system to a 2×2 system.
4. Reduction of the general 2×2 system to Poincaré normal form; as a consequence, the parameter $c_1(I_c)$ can be evaluated.

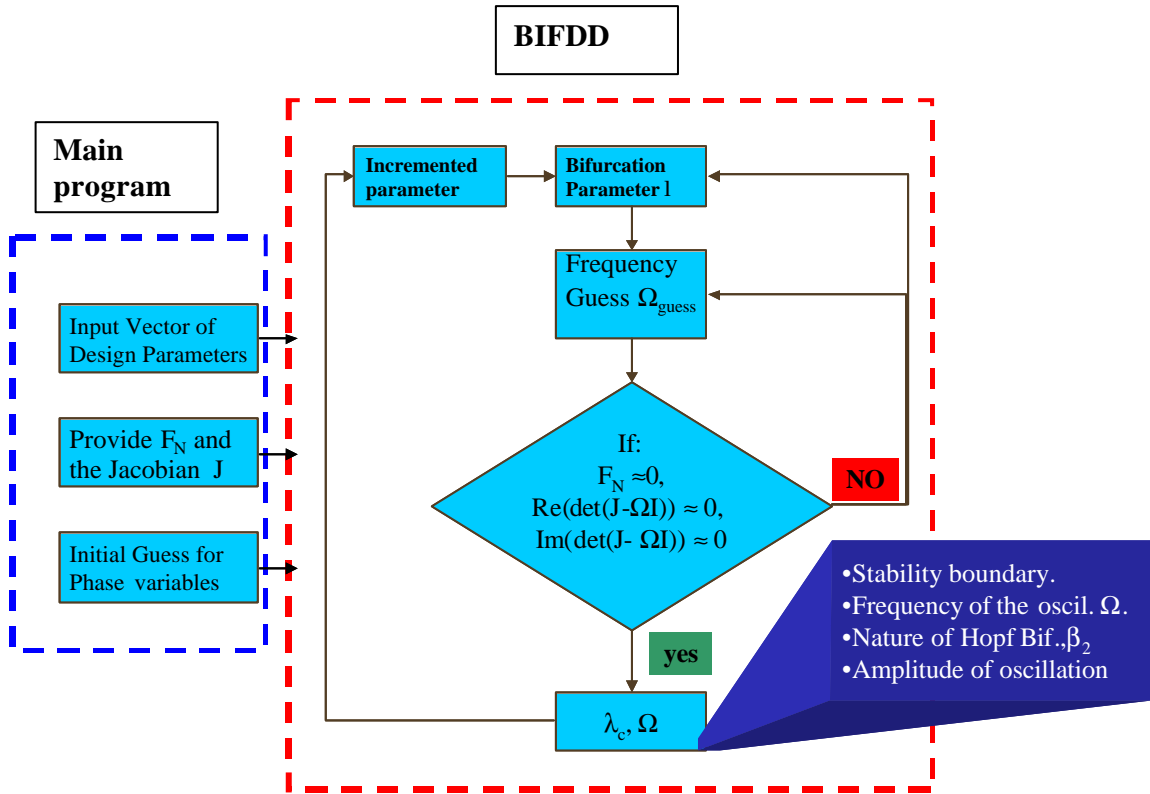


Figure 3-3. Diagram summarizing the bifurcation analysis using BIFDD.

5. Computation of \mathbf{m}_2 , \mathbf{t}_2 , and \mathbf{b}_2 on the basis of the relationships between these parameters and $c_1(I_c)$ (Eqs. (3.4), (3.5), and (3.6)).
6. Verification of the hypothesis that, at $I = I_c$, all the eigenvalues other than $\pm i\omega_0$ fulfil the condition $\text{Re}(I) < 0$.

3.3.2 BIFDD Modification

It must be stated here that, while the BIFDD code was found to work perfectly in the case of the 5-ODE model used to study thermal-hydraulic instabilities (Chapter 5), it became very difficult and even impossible to run it for evaluation of the steady-state solution in the case of the 22-ODE BWR model used for investigating two-channel nuclear-coupled thermal-hydraulic instabilities. This is because the standard version of the code uses the simple Newton method for the purpose. Accordingly, the subroutine responsible for the steady-state solution calculation has currently been replaced by a more efficient subroutine called *dnsqe.f* which employs a modified Powell hybrid method.

REFERENCES

- [1] Ali H. Nayfeh, B. Balachandran, Applied Nonlinear Dynamics, John Wiley & Sons, Inc., New York, 1995.
- [2] E. Hopf, "Abzweigung einer periodischen Lösung von einer stationären Lösung eines differential Systems," *Ber. Math.-Phys. Kl. Sachs. Acad. Wiss. Leipzig*, **94**, 1-22, and *Ber. Verh. Sachs. Acad. Wiss. Leipzig Math. Nat. Kl.*, **95** (1), 3-22, 1942. A translation by L. Howard and N. Koeppel appeared in *The Hopf Bifurcation and its Applications*, Eds. J. E. Marsden and M. McCracken, Springer-Verlag, Berlin, 1976.
- [3] J. L. Muñoz-Cobo and G. Verdú, "Application of Hopf Bifurcation Theory and Variational Methods to the Study of Limit Cycles in Boiling Water Reactors", *Ann. Nucl. Energy*, **18**, 5, 269, 1991.
- [4] M. Tsuji, K. Nishio, and M. Narita, "Stability Analysis of BWRs Using Bifurcation Theory", *J. Nucl. Sci. and Tech.*, **30**, 11, 1107-1119, 1993.
- [5] A. A. Karve, Rizwan-uddin, J. J. Dorning, "Stability Analysis of BWR Nuclear Coupled Thermal-Hydraulics Using a Simple Model", *Nucl. Eng. and Design*, **177**, 155-177, 1997.
- [6] D. D. B. van der Bragt, Rizwan-uddin, and T. H. J. J. van der Hagen, "Nonlinear Analysis of a Natural Circulation Boiling Water Reactor", *Nucl. Sci. Eng.*, **131**, 23-44, 1999.
- [7] R. Zboray, D. D. B. van der Bragt, Rizwan-uddin, T. H. J. J. van der Hagen and H. van Dam, "Influence of Asymmetrical Axial Power Distributions on Nonlinear BWR Dynamics", *Proc. of 9th Int. Topical Mtg. On Nuclear Thermal Hydraulics (NURETH-9)*, San Francisco, USA, October 3-8, 1999.
- [8] D. D. B. van der Bragt, Rizwan-uddin, and T. H. J. J. van der Hagen, "Effect of Void Distribution Parameter and Axial Power Profile on Boiling Water Reactor Bifurcation Characteristics", *Nucl. Sci. Eng.*, **134**, 227-235, 2000.
- [9] A. Dokhane, D. Hennig, Rizwan-uddin, R. Chawla, "Nuclear-Coupled Thermal-Hydraulic Nonlinear Stability Analysis Using a Novel BWR Reduced Order Model: Part I – The Effect of Using Drift Flux Versus Homogeneous Equilibrium Models", *Proc. Of 11th Int. Conf. of Nuclear Engineering (ICONE11)*, Tokyo, Japan, April 20-23, 2003.
- [10] B. D. Hassard, N. D. Kazarinoff, Y. H. Wan, *Theory and Application of Hopf Bifurcation*, Cambridge University Press, New York, 1981.

- [11] B. D. Hassard, "Numerical Evaluation of Hopf Bifurcation Formulas," Chapter 9 in *Dynamics of Nonlinear Systems*, V. Hlavacek, Editor, Gordon and Breach, 1986.
- [12] B. D. Hassard, "A Code for Hopf Bifurcation Analysis of Autonomous Delay-Differential Equations," *Proc. Oscillations, Bifurcation and Chaos*, Canadian Mathematical Society, pp. 447-463, 1987.
- [13] Rizwan-uddin, "Sub- and Supercritical Bifurcation and Turning Points in a Simple BWR Model," *Proc. Int. Top. Mtg. on Advances in Reactor Physics and Mathematics (PHYSOR-2000)*, Pittsburgh, May 7-11, 2000.

4 DEVELOPMENT OF THE NOVEL REDUCED ORDER MODEL

In this chapter, the development of the ODEs of different components of the new BWR reduced order model is presented. Following the introduction, Section 4.2 is devoted to the development of the ODEs of the neutron kinetic model obtained from the neutron diffusion equation and the equations for the neutron precursor concentrations. In Section 4.3, the fuel heat conduction model developed by Karve [7], and used in the present reduced order model, is briefly reviewed. Development of the thermal-hydraulic model is described in Section 4.4, with two of the correlations used being presented in Section 4.5. This is finally followed by a summary of the reduced order model system of ODEs in an explicit form.

4.1 INTRODUCTION

The new reduced order model for nonlinear stability analysis developed currently, describes all significant physical processes determining the dynamics of a BWR system. The strategy followed in the model construction is the following: firstly, to develop a model as simple as possible from the mathematical point of view (simple geometry; ordinary (O), instead of partial differential equations (PDEs)) while preserving the most important physical phenomena; secondly, to have a model as close to the system code RAMONA as possible [1]. For the latter purpose, several of the correlations and assumptions in RAMONA have been used in the reduced order model. The new model has the following components:

- The neutron power dynamics of the fundamental and higher neutron flux modes, determined by the feedback reactivities and the time delays given by the void and fuel temperature dynamics.
- The fuel heat conduction dynamics, determined by the fuel geometry and the material properties of the fuel such as thermal conductivity and specific heat capacity (represented by the heat conduction equation).
- The heat transfer from fuel to coolant (represented by two different heat transfer correlations which depend on the thermodynamic state).

- The two-phase flow dynamics represented by the hydraulic equations, *i.e.* the mass, momentum and energy balance equations and certain hydraulic correlations, *e.g.* single and two-phase friction factors.
- Use of appropriate boundary conditions, as illustrated in Section 2.6, for replacement of the recirculation loop.

Application of the new reduced order model in the present research has been carried out in two stages. The first involves stability and bifurcation analysis for a single heated channel without neutron kinetics, described by 5 of the 22 equations of the full model. This first stage is described in Chapter 5. The second stage of application is that of the complete two-channel nuclear-coupled thermal-hydraulic model with all 22 ODEs (Chapters 6 and 8). The latter essentially represents a reduction of the geometric complexity of a BWR. In effect, each half of the core is replaced by a single representative channel. As indicated earlier, the effects of the outer loop are simulated by specifying the external pressure boundary condition across the core.

4.2 NEUTRON KINETICS

To solve the diffusion equation for the space and time dependent neutron flux, there are many different approaches. A frequently used method is the so-called modal expansion method, where the neutron flux is expanded on stationary eigenvectors of a spatial form for the stationary diffusion equation. The most useful eigenvector types are the so-called \mathbf{w} - and \mathbf{I} -modes. Karve *et al.* [2] used the \mathbf{w} -modes in their reduced order model, while the modal expansion method in terms of \mathbf{I} -modes has been used earlier by Hashimoto [3], Muñoz-Cobo *et al.* [4], and Miró *et al.* [5]. It is the latter approach which has currently been adopted for obtaining the modal kinetic equations for the neutronics model. Thus, the present neutron kinetic model is based on the following assumptions:

- Two neutron energy groups (thermal and fast neutrons). From the physical point of view, it is more realistic to consider at least two energy groups due to the strong dependence of the cross-sections on the energy [6, 5].
- Modal expansion of the neutron flux in terms of \mathbf{I} -modes. This choice of modal expansion is mainly due to the fact that previous experience at PSI was based on the use \mathbf{I} -modes in the framework of a collaboration with the reactor physics group of the Technical University of Valencia [5].

With the above assumptions, the neutron kinetic equations can be written as

$$\mathbf{u}^{-1} \frac{\partial}{\partial t} \mathbf{f}(\vec{r}, t) + L(\vec{r}, t) \mathbf{f}(\vec{r}, t) = (1 - \mathbf{b}) M(\vec{r}, t) \mathbf{f}(\vec{r}, t) + \sum_{k=1}^K \mathbf{I}_k U_k(\vec{r}, t) X \quad (4.1)$$

$$\frac{\partial}{\partial t} U_k(\vec{r}, t) = \mathbf{b}_k F^T \mathbf{f}(\vec{r}, t) - \mathbf{I}_k U_k(\vec{r}, t) \quad (4.2)$$

where $\mathbf{f}(\vec{r}, t) = \begin{bmatrix} \mathbf{f}_1(\vec{r}, t) \\ \mathbf{f}_2(\vec{r}, t) \end{bmatrix}$ is the neutron flux vector consisting of the fast (subscript 1) and thermal (subscript 2) neutron fluxes respectively, $X = \begin{pmatrix} 1 \\ 0 \end{pmatrix}$, \mathbf{u}^{-1} is the neutron inverse velocity matrix, and U_k is the concentration of delayed neutron precursors in precursor group k .

L is the net-loss operator accounting for losses by leakage, scattering and absorption

$$L(\vec{r}, t) = \begin{bmatrix} -\vec{\nabla}(D_1(\vec{r}, t)\vec{\nabla}) + \Sigma_{a1}(\vec{r}, t) + \Sigma_{12}(\vec{r}, t) & 0 \\ -\Sigma_{12}(\vec{r}, t) & -\vec{\nabla}(D_2(\vec{r}, t)\vec{\nabla}) + \Sigma_{a2}(\vec{r}, t) \end{bmatrix}.$$

M is the fission production operator

$$M(\vec{r}, t) = \begin{bmatrix} \mathbf{n}\Sigma_{f1}(\vec{r}, t) & \mathbf{n}\Sigma_{f2}(\vec{r}, t) \\ 0 & 0 \end{bmatrix}, \text{ and } F^T = \begin{bmatrix} \mathbf{n}\Sigma_{f1} & \mathbf{n}\Sigma_{f2} \end{bmatrix}.$$

where \mathbf{S}_{fj} and \mathbf{S}_{aj} are the macroscopic fission and absorption cross-sections for the j -th neutron energy group. \mathbf{n} is the number of neutrons per fission. \mathbf{I}_k and \mathbf{b}_k are the decay constant and the delayed neutron fraction, respectively, for the k^{th} group of delayed neutron precursors.

One may now look to the solution of the following steady-state eigenvalue problem

$$L_0(\vec{r}) \mathbf{f}_n(\vec{r}) = \frac{1}{k_n} M_0(\vec{r}) \mathbf{f}_n(\vec{r}) \quad (4.3)$$

The eigenvectors satisfy the biorthogonality relation

$$\langle \mathbf{f}_m^+, M_0 \mathbf{f}_n \rangle = \langle \mathbf{f}_n^+, M_0 \mathbf{f}_n \rangle \mathbf{d}_{m,n} = N_n \mathbf{d}_{m,n} \quad (4.4)$$

where $\langle \mathbf{a}, \mathbf{b} \rangle = \int_R \mathbf{a}^T(\bar{r}) \mathbf{b}(\bar{r}) d\bar{r}$, \mathbf{f}_n^+ is the adjoint neutron flux, satisfying the adjoint equation

$$L_0^+ \mathbf{f}_n^+ = \frac{1}{k_n^*} M_0^+ \mathbf{f}_n^+ \quad (4.5)$$

The $\mathbf{f}_n(\bar{r})$ are the so-called \mathbf{I} -modes.

Expanding the neutron flux and the delayed neutron concentration in terms of the \mathbf{I} -modes, one can derive the kinetic modal expansion equations

$$\mathbf{f}(\bar{r}, t) = \sum_{l=0}^{\infty} n_l(t) \mathbf{f}_l(\bar{r}) \quad (4.6)$$

$$U_k(\bar{r}, t) X = \sum_{l=0}^{\infty} U_{lk}(t) M_0 \mathbf{f}_l(\bar{r}) \mathbf{L}_l \quad (4.7)$$

where $\mathbf{f}_l(\bar{r})$ are the \mathbf{I} -modes. $n_l(t)$ and $U_{lk}(t)$ are the time dependent expansion coefficients for the neutron flux and the delayed neutron precursor concentration, respectively.

The operators L and M can be written as a steady-state plus an oscillating term, *i.e.*

$$L(\bar{r}, t) = L_0(\bar{r}) + \mathbf{d}L(\bar{r}, t) \quad (4.8)$$

$$M(\bar{r}, t) = M_0(\bar{r}) + \mathbf{d}M(\bar{r}, t) \quad (4.9)$$

It should be noted that $X F^T = M$.

Substituting Eqs. (4.6), (4.7), (4.8), and (4.9) in Eqs. (4.1) and (4.2), multiplying the resulting equations by \mathbf{f}_m^+ , and then integrating over the whole reactor core volume, one gets the ODEs for the modal expansion equations (obtained from the neutron diffusion equation) and the neutron precursor concentration equations, *viz.*

$$\sum_{l=0}^{\infty} \Lambda_{ml} \frac{dn_l(t)}{dt} = (\mathbf{r}_m^s - \mathbf{b}) \cdot n_m(t) - \sum_{l=0}^{\infty} \mathbf{r}_{ml}^D n_l(t) + \sum_{l=0}^{\infty} \mathbf{r}_{ml}^F n_l(t) + \sum_{k=1}^K \mathbf{I}_k U_{mk}(t) \Lambda_m \quad (4.10)$$

$$\frac{dU_{mk}(t)}{dt} = \frac{1}{\Lambda_m} \mathbf{b}_k n_m(t) + \frac{1}{\Lambda_m} \sum_{l=0}^{\infty} \mathbf{r}_{ml}^{D_k} n_l(t) - \mathbf{I}_k U_{mk}(t) \quad (4.11)$$

where $\Lambda_{ml} = \frac{1}{N_m} \langle \mathbf{f}_m^+, \mathbf{u}^{-1} \mathbf{f}_l \rangle$, $\mathbf{r}_{ml}^s = 1 - \frac{1}{k_m}$ is the static reactivity,

$\mathbf{r}_{ml}^F = \frac{1}{N_m} \langle \mathbf{f}_m^+, (\mathbf{dM} - \mathbf{dL}) \mathbf{f}_l \rangle$ are the dynamical feedback reactivities, and

$\mathbf{r}_{ml}^{D_k} = \mathbf{b}_k \frac{1}{N_m} \langle \mathbf{f}_m^+, \mathbf{dM} \mathbf{f}_l \rangle$, $\mathbf{r}_{ml}^D = \mathbf{b} \frac{1}{N_m} \langle \mathbf{f}_m^+, \mathbf{dM} \mathbf{f}_l \rangle$ are the delayed feedback reactivities.

The matrix Λ_{ml} can be considered diagonal due to the dominance of the diagonal elements as reported in [5]. To illustrate this fact the matrix Λ_{ml} has been computed for the first three \mathbf{I} -modes at two representative operational points. The first operational point is cycle 7 record 4 (*klc7_rec4*) of the Leibstadt NPP, and the second one is cycle 14 record 9 of the Ringhals-1 NPP (see Table 4-1). Referring to Table 4-1, $\Lambda_{ml} = \Lambda_{mm} \mathbf{d}_{m,l} = \Lambda_m \mathbf{d}_{m,l}$.

Table 4-1. Matrix Λ_{mn} for the first three \mathbf{I} -modes calculated for Leibstadt and Ringhals-1.

	<i>Leibstadt cycle 7 rec 4</i>	<i>Ringhals-1 cycle14 rec9</i>
Λ_{11}	1.061 10 ⁻⁸	1.100 10 ⁻⁸
Λ_{12}	5.761 10 ⁻¹³	-1.444 10 ⁻¹⁴
Λ_{13}	-7.544 10 ⁻¹⁴	-3.546 10 ⁻¹⁰
Λ_{21}	2.229 10 ⁻¹³	3.588 10 ⁻¹³
Λ_{22}	1.096 10 ⁻⁸	1.104 10 ⁻⁸
Λ_{23}	-9.229 10 ⁻¹²	-8.345 10 ⁻¹³
Λ_{31}	-1.707 10 ⁻¹³	-3.184 10 ⁻¹⁰
Λ_{32}	9.621 10 ⁻¹³	-8.558 10 ⁻¹³
Λ_{33}	1.096 10 ⁻⁸	1.062 10 ⁻⁸

If one restricts the calculation to the first two modes ($l = 0, 1$), the neutron kinetics ODEs can be obtained from Eqs. (4.10) and (4.11) as

$$\frac{d}{dt}n_m(t) = \frac{1}{\Lambda_{mm}} \left[(\mathbf{r}_m^s - \mathbf{b})n_m(t) + \sum_{l=0}^1 \mathbf{r}_{ml}^F n_l(t) - \sum_{l=0}^1 \mathbf{r}_{ml}^D n_l(t) \right] + \sum_{k=1}^K \mathbf{I}_k U_{mk}(t) \quad (4.12)$$

$$\frac{d}{dt}U_{mk}(t) = \frac{1}{\Lambda_m} \left[\mathbf{b}_k n_m(t) + \sum_{l=0}^1 \mathbf{r}_{ml}^{D_k} n_l(t) \right] - \mathbf{I}_k U_{mk}(t) \quad (4.13)$$

For simplicity, an effective single group of delayed neutron precursors is considered ($K = 1$, *i.e.* $\mathbf{I}_k = \mathbf{I}$, $U_k = U$, and $\mathbf{b}_k = \mathbf{b}$). It can be shown that contributions of the delayed neutron precursors to the reactivity feedback can be neglected ($\mathbf{r}_{ml}^D = 0$)¹⁹. Taking into account only the fundamental and first azimuthal modes, Eqs. (4.12) and (4.13) give the four modal kinetic equations, *viz.*

$$\frac{dn_0(t)}{dt} = \frac{1}{\Lambda_0} [(\mathbf{r}_{00}(t) - \mathbf{b})n_0(t) + \mathbf{r}_{01}(t)n_1(t)] + \mathbf{I}U_0(t) \quad (4.14)$$

$$\frac{dn_1(t)}{dt} = \frac{1}{\Lambda_0} [\mathbf{r}_{10}(t)n_0(t) + (\mathbf{r}_{11}(t) + \mathbf{r}_1^s - \mathbf{b})n_1(t)] + \mathbf{I}U_1(t) \quad (4.15)$$

$$\frac{dU_0(t)}{dt} = \frac{\mathbf{b}}{\Lambda_0} n_0(t) - \mathbf{I}U_0(t) \quad (4.16)$$

$$\frac{dU_1(t)}{dt} = \frac{\mathbf{b}}{\Lambda_0} n_1(t) - \mathbf{I}U_1(t) \quad (4.17)$$

where $\mathbf{L}_0 = \mathbf{L}_{00} = \mathbf{L}_{11}$ ²⁰, $U_0(t) = U_{00}(t)$, $U_1(t) = U_{11}(t)$. $\mathbf{r}_{ml}(t) = \mathbf{r}_{ml}^F$ is the total feedback reactivity for the coupling between the m^{th} -mode and the l^{th} -mode. The governing neutron kinetics equations are coupled with the equations of the heat conduction and the

¹⁹ because the delayed neutrons represent a very small fraction of the total fission neutrons (<1%)

²⁰ We consider that $\mathbf{L}_{00} = \mathbf{L}_{11}$.

thermal-hydraulic via the feedback reactivity terms in Eqs. (4.14) and (4.15). In this thesis, the void and Doppler feedback reactivities are considered to be the only relevant ones.

The models for the void and Doppler feedback reactivities are described in detail in Appendix E. They are based on the assumption of linear reactivity profiles in terms of the void fraction and fuel temperature, respectively. Eq. (E.31) is rewritten here

$$\mathbf{r}_{mn}(t) = fact_{mn} \cdot \sum_{l=1}^2 c_{1mn,l}(\mathbf{a}_l(t) - \mathbf{a}_{0,l}) + c_{2mn,l}(T_{avg,l}(t) - T_{avg,0,l}) \quad (4.18)$$

where the index l stands for the channel number. As mentioned earlier, only two channels, each representing one half of the reactor core, are considered currently. The quantities $\mathbf{a}_{0,l}$ and $T_{avg,0,l}$ are the reference steady-state void fraction and the average fuel temperature in the channel l , respectively²¹. The quantities $T_{avg,l}(t)$ and $T_{avg,0,l}(t)$ are equivalent to $T_{f,l}(t)$ and $T_{f,0,l}(t)$ in Eq. (E.31), respectively. The terms $c_{1mk,l}$ and $c_{2mk,l}$ are the void and Doppler feedback reactivity coefficients, respectively. The calculation method for these coefficients is also presented in detail in Appendix E. Finally, as discussed in this appendix, $fact_{mn}$ is a bifurcation (or feedback gain) parameter, introduced as a multiplier of the corresponding feedback reactivity, in order to increase the feedback gain coupling between the first and fundamental modes and thus enable the excitation of out-of-phase oscillation phenomena in specific cases.

4.3 FUEL ROD HEAT CONDUCTION

In this section, the fuel rod heat conduction model is reviewed. This model was originally developed and validated by Karve [7]. Since it has currently been adopted without any further modifications, the detailed algebra involved in developing the model is not presented here. It should be stressed, however, that although the original fuel heat conduction model was not modified, new calculations were necessary to obtain the corresponding ODEs using the symbolic toolbox of Maple.

The fuel rod is modelled separately in the two axial regions corresponding to the single and two-phase regions of the boiling channel. In each of these regions, it is modelled with

²¹ These quantities are dimensionless quantities (see following sections, as also Appendix C).

three distinct radial regions, the fuel pellet ($0 < r < r_p$), the gap ($r_p < r < r_g$), and the clad ($r_g < r < r_c$) (Fig. 4-1). The ODEs are developed by reducing the one-dimensional (radial) time dependent PDE of the heat conduction equation for the fuel rod, assuming a two-piecewise quadratic spatial approximation for the fuel rod temperature. The heat conduction model is based on the following assumptions;

- Azimuthal symmetry for heat conduction in the radial direction.
- Neglected heat conduction in the z-direction.
- Time-dependent, spatially uniform volumetric heat generation.

A variational principle approach is used to derive the final ODEs, which represent the BWR fuel rod heat conduction dynamics. For each channel, four ODEs are obtained for the two coefficients of each of the two spatially-piecewise quadratic function representations of the fuel pellet temperature (in the single and two-phase regions, respectively). In this section, we omit the channel index on all quantities. Furthermore, an asterisk on a variable or parameter indicates the original dimensional quantity, and any quantity without an asterisk is dimensionless. The various dimensionless variables and parameters used are presented in Appendix C.

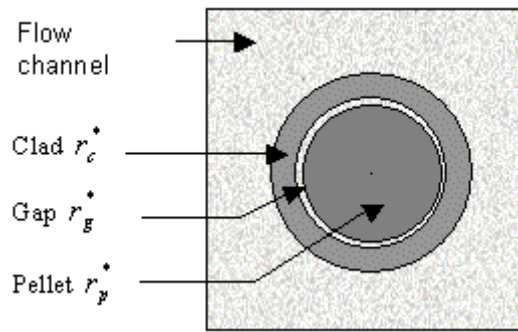


Figure 4-1. Fuel-centred boiling flow channel.

The heat conduction equations for the fuel rod, with the above assumptions, are

$$\mathbf{r}_p^* c_p^* \frac{\partial T_{p,jf}^*(r^*, t^*)}{\partial t^*} = k_p^* \left[\frac{\partial^2 T_{p,jf}^*(r^*, t^*)}{\partial r^{*2}} + \frac{1}{r^*} \frac{\partial T_{p,jf}^*(r^*, t^*)}{\partial r^*} \right] + q'''(t^*), \quad 0 \leq r^* \leq r_p^* \quad (4.19)$$

$$\mathbf{r}_c^* c_c^* \frac{\partial T_{c,jf}^*(r^*, t^*)}{\partial t^*} = k_c^* \left[\frac{\partial^2 T_{c,jf}^*(r^*, t^*)}{\partial r^{*2}} + \frac{1}{r^*} \frac{\partial T_{c,jf}^*(r^*, t^*)}{\partial r^*} \right], \quad r_g^* \leq r^* \leq r_c^* \quad (4.20)$$

with the boundary conditions

$$\frac{\partial T_{p,jf}^*(0, t^*)}{\partial r^*} = 0 \quad (4.21)$$

$$-k_p^* \frac{\partial T_{p,jf}^*(r_p^*, t^*)}{\partial r^*} = \frac{r_g^*}{r_p^*} h_g^* [T_{p,jf}^*(r_p^*, t^*) - T_{c,jf}^*(r_g^*, t^*)] \quad (4.22)$$

$$-k_c^* \frac{\partial T_{c,jf}^*(r_g^*, t^*)}{\partial r^*} = h_g^* [T_{p,jf}^*(r_p^*, t^*) - T_{c,jf}^*(r_g^*, t^*)] \quad (4.23)$$

$$-k_c^* \frac{\partial T_{c,jf}^*(r_c^*, t^*)}{\partial r^*} = h_{\infty,jf}^* [T_{c,jf}^*(r_c^*, t^*) - T_{bulk,jf}^*] \quad (4.24)$$

where $T_{p,jf}^*(r^*, t^*)$ and $T_{c,jf}^*(r^*, t^*)$ are the pellet and clad temperature in the j^{th} region, respectively. $j = 1$ corresponds to the single-phase (1f) region, while $j = 2$ corresponds to the two-phase (2f) region (see next section). $q^{m*}(t^*)$ is the spatially uniform volumetric heat generation rate which is proportional to the neutron density

$$q^{m*}(t^*) = c_q^* n_0(t^*) + c_q^* \mathbf{x} n_1(t^*) \quad (4.25)$$

where \mathbf{r}_p^* , c_p^* and k_p^* are the UO_2 fuel pellet density, specific heat, and thermal conductivity respectively. \mathbf{r}_c^* , c_c^* and k_c^* are the Zircaloy clad density, specific heat, and thermal conductivity respectively. $h_{\infty,jf}^*$ is the convective heat transfer coefficient estimated by the Dittus-Boelter correlation in the single-phase and the Jens-Lottes correlation in the two-phase region. These two correlations are given in Section 4.5, along with all the other correlations used in this work.

Equations (4.19) and (4.20) can be written in the dimensionless form as follows:

$$\frac{1}{\mathbf{a}_p} \frac{\partial T_p(r, t)}{\partial t} = \frac{\partial^2 T_p(r, t)}{\partial r^2} + \frac{1}{r} \frac{\partial T_p(r, t)}{\partial r} + q^m(t), \quad 0 \leq r \leq r_p \quad (4.26)$$

$$\frac{1}{\mathbf{a}_c} \frac{\partial T_c(r,t)}{\partial t} = \frac{\partial^2 T_c(r,t)}{\partial r^2} + \frac{1}{r} \frac{\partial T_c(r,t)}{\partial r}, \quad r_g \leq r \leq r_c \quad (4.27)$$

The boundary conditions become

$$\frac{\partial T_p(0,t)}{\partial r} = 0 \quad (4.28)$$

$$-\frac{\partial T_p(r_p,t)}{\partial r} = \frac{Bi_p}{r_p} [T_p(r_p,t) - T_c(r_g,t)] \quad (4.29)$$

$$-\frac{\partial T_c(r_g,t)}{\partial r} = \frac{Bi_g}{r_g} [T_p(r_p,t) - T_c(r_g,t)] \quad (4.30)$$

$$-\frac{\partial T_c(r_c,t)}{\partial r} = \frac{Bi_c}{r_c} [T_c(r_c,t) - T_{bulk}] \quad (4.31)$$

where $\mathbf{a}_p, T_p, c_p, \mathbf{a}_c, T_c, Bi_p, Bi_g$ and $Bi_{c,jf}$ are dimensionless quantities defined in Appendix C. It should be noted that, from now on, the subscript jf is omitted with the understanding that the analysis applies to both the single-phase ($j=1$) and two-phase ($j=2$) regions.

A change of variables is now made by introducing the temperature deviations from their steady-state values:

$$\mathbf{q}_p(r,t) = T_p(r,t) - \tilde{T}(r), \quad 0 \leq r \leq r_p \quad (4.32)$$

$$\mathbf{q}_c(r,t) = T_c(r,t) - \tilde{T}(r), \quad r_g \leq r \leq r_c \quad (4.33)$$

the tilde over a quantity indicating the steady-state solution, obtained by solving the heat conduction equation at steady-state. It can be shown that the solutions are:

$$\tilde{T}_p(r) = -c_q \tilde{n}_0 \frac{r^2}{4} + \tilde{b}_1, \quad 0 \leq r \leq r_p \quad (4.34)$$

$$\tilde{T}_c(r) = \tilde{b}_2 \log(r) + \tilde{b}_3, \quad r_g \leq r \leq r_c \quad (4.35)$$

Then the heat conduction equations can be written as:

$$\frac{1}{\mathbf{a}_p} \frac{\partial \mathbf{q}_p(r,t)}{\partial t} = \frac{\partial^2 \mathbf{q}_p(r,t)}{\partial r^2} + \frac{1}{r} \frac{\partial \mathbf{q}_p(r,t)}{\partial r} + \mathbf{q}'''(t), \quad 0 \leq r \leq r_p \quad (4.36)$$

$$\frac{1}{\mathbf{a}_c} \frac{\partial \mathbf{q}_c(r,t)}{\partial t} = \frac{\partial^2 \mathbf{q}_c(r,t)}{\partial r^2} + \frac{1}{r} \frac{\partial \mathbf{q}_c(r,t)}{\partial r}, \quad r_g \leq r \leq r_c \quad (4.37)$$

These equations have to be supplemented with the corresponding boundary conditions.

Two assumptions are now made for the solutions of \mathbf{q}_c and \mathbf{q}_p .

Assumption 1

The clad heat conduction dynamics can be modelled without solving the transient heat conduction equation.

The idea behind this is that there is no significant change in the clad temperature profile from its initial steady-state distribution, due to the large clad thermal diffusivity \mathbf{a}_c , which is about ten times larger than that of the pellet \mathbf{a}_p . Based on the logarithmic spatial distribution of the steady-state clad temperature, the space and time dependence for $\mathbf{q}_c(r,t)$ can be written as

$$\mathbf{q}_c(r,t) = b_2(t) \log r + b_3(t) \quad (4.38)$$

The coefficients $b_2(t)$ and $b_3(t)$ are simply deduced from the two boundary conditions (4.23) and (4.24).

The task now is to solve the heat conduction equation in the fuel pellet. For this, a method based on a variational principle approach is used to deduce the ODEs of the fuel pellet in the single and two-phase regions. The main steps to be applied are:

- Choose a functional that accommodates all the trial functions.

- Each time choose a trial function that satisfies Eq. (4.36) and the boundary conditions, and see if it minimizes the functional.
- Choose among these minimizing functions the one that corresponds to the global minimum for the functional. This is the best solution of the heat conduction equation.

Consider a general functional $F(\mathbf{j}(r,t))$ ²² that accommodates discontinuous trial functions $\mathbf{j}(r,t)$, which do not need to satisfy the boundary conditions.

$$\begin{aligned}
F(\mathbf{j}) = & (\mathbf{j}, H\mathbf{j}) - 2(\mathbf{j}, f) + \left[\frac{r_p^2}{2Bi_p^+} \left(\frac{\partial \mathbf{j}}{\partial r} \right)^2 - \frac{Bi_p^+}{2} \mathbf{j}^2 \right]_{r=r_p} - \left[\frac{r_p^2}{2} \left(\frac{\partial \mathbf{j}}{\partial r} \right)^2 \right]_{r=r_p} \\
& + r_d \left[\mathbf{j}_l \frac{\partial \mathbf{j}_r}{\partial r} - \mathbf{j}_r \frac{\partial \mathbf{j}_l}{\partial r} \right]_{r=r_d}
\end{aligned} \tag{4.39}$$

where the notation (\mathbf{a}, \mathbf{b}) denotes $(\mathbf{a}, \mathbf{b}) = \int_0^{r_p} \mathbf{a}(t) \mathbf{b}(t) dr$. The radius r_d is the point of discontinuity between $r=0$ and $r=r_p$ of the trial function $\mathbf{j}(r,t)$. r_d ($r_d = 0.83 \cdot r_p$) was determined empirically in [7]. This value leads to a stability boundary that best matches the reference stability boundary. The subscripts l and r in Eq. (4.39) stand for the limits of the functions from the left and the right of the discontinuity, respectively.

The function that minimises the functional $F(\mathbf{j}(r,t))$ is $\mathbf{j} = \mathbf{q}_p$. It satisfies (4.36) subject to the boundary conditions.

Assumption 2

For the pellet temperature, a two-piecewise quadratic form can be considered for the solution [7]:

$$\begin{aligned}
\mathbf{q}_p(r,t) = & T_1(t) + \mathbf{a}_1(t)r + \mathbf{a}_2(t)r^2, \quad 0 < r < r_d \\
= & T_2(t) + \mathbf{b}_1(t)r + \mathbf{b}_2(t)r^2, \quad r_d < r < r_p
\end{aligned} \tag{4.40}$$

²² The procedure for constructing this functional can be found in references [8,9].

where $\mathbf{q}_p(r_d, t)$ and $\frac{\partial \mathbf{q}_p(r_d, t)}{\partial r}$ should be continuous at $r = r_d$ and $\frac{\partial^2 \mathbf{q}_p(r_d, t)}{\partial r^2}$ is a discontinuous function at this point.

By following the Rayleigh-Ritz procedure [9,10], $\mathbf{q}_p(r, t)$ is substituted in the functional F , and $T_1(t)$ and $T_2(t)$ are adjusted in order to minimize F . This is achieved by setting, using the Maple symbolic toolbox:

$$\begin{cases} \frac{\partial F}{\partial T_1} = 0 \\ \frac{\partial F}{\partial T_2} = 0 \end{cases} \quad (4.41)$$

Finally the ODEs for $T_1(t)$ and $T_2(t)$, which represent the BWR fuel rod heat conduction dynamics, are obtained as

$$\frac{dT_1(t)}{dt} = ll_{1,1}T_1(t) + ll_{2,1}T_2(t) + ll_{3,1}[c_q(n_0(t) - \tilde{n}_0) + c_q \mathbf{x}n_1(t)] \quad (4.42)$$

$$\frac{dT_2(t)}{dt} = ll_{1,2}T_1(t) + ll_{2,2}T_2(t) + ll_{3,2}[c_q(n_0(t) - \tilde{n}_0) + c_q \mathbf{x}n_1(t)] \quad (4.43)$$

where $ll_{1,s}$, $ll_{2,s}$, and $ll_{3,s}$ are somewhat complicated constants which depend on the design parameters $r_d, r_p, r_g, r_c, Bi_p, Bi_c$ and Bi_g , defined in Appendix C.

In summary, for each channel, four ODEs are developed from the heat conduction PDE. These ODEs are for the two coefficients of each of the two spatially piecewise quadratic representations of the fuel pellet temperature in the single and two-phase regions of the channel. In an explicit index form, these ODEs can be written as

$$\frac{dT_{1,jf,l}(t)}{dt} = ll_{1,1,jf,l}T_{1,jf,l}(t) + ll_{2,1,jf,l}T_{2,jf,l}(t) + ll_{3,1,jf,l}[c_q(n_0(t) - \tilde{n}_0) + c_q \mathbf{x}n_1(t)] \quad (4.44)$$

$$\frac{dT_{2,jf,l}(t)}{dt} = ll_{1,2,jf,l}T_{1,jf,l}(t) + ll_{2,2,jf,l}T_{2,jf,l}(t) + ll_{3,2,jf,l} [c_q(n_0(t) - \tilde{n}_0) + c_q \mathbf{x}n_1(t)] \quad (4.45)$$

where jf stands for single ($1f$) or two-phase ($2f$) region and l stands for channel number (1 or 2).

Important Intermediate Variables

The most important variable that depends on the heat conduction phase variables is the fuel rod average temperature, which is of relevance in determining the feedback between the neutronics and the thermal-hydraulics. The average temperature of the fuel rod, used in Eq. (4.18), is defined as the weighted average of the single and two-phase region average temperatures

$$T_{avg}(t) = \mathbf{m}(t)T_{avg,1f}(t) + [1 - \mathbf{m}(t)]T_{avg,2f}(t) \quad (4.46)$$

where $\mathbf{m}(t)$ is the boiling boundary (see next section) and $T_{avg,jf}(t)$ is the average fuel rod temperature in the j^{th} phase region defined as

$$T_{avg,jf}(t) = \frac{2}{r_p^2} \int_0^{r_p} T_{p,jf}(r, t) r dr \quad j = 1, 2 \quad (4.47)$$

Other intermediate variables used can be found in [7]. All the intermediate variables have been determined currently using the symbolic toolbox of Maple and directly included in the *bwr.f* code (see Subsection 2.7.3) used in conjunction with BIFDD for stability and bifurcation analysis.

4.4 THERMAL-HYDRAULICS

The heat generated in the fuel rod is conducted and convected to the coolant in the flow channel. The single-phase coolant enters the bottom of the channel with a velocity $v_{inlet}^*(t^*)$ and temperature T_{inlet}^* , and then starts boiling at a certain level—called the boiling boundary $\mathbf{m}^*(t^*)$ —in the flow channel where the coolant reaches the saturation

temperature T_{sat}^* . Above the boiling boundary, the coolant is a mixture of two phases, *i.e.* water and steam. The flow channel is accordingly divided into two regions, the single-phase and two-phase regions.

The three-dimensional mass, energy, and momentum equations in the single-phase and two-phase regions, that describe the fluid mechanics in the channel, are averaged over the cross-section of the flow channel to arrive at equations that depend only on a single spatial variable (axial position z) and time. Then, for each representative flow channel²³, ODEs are developed from the one-dimensional time dependent PDEs by carrying out symbolic integration using a weighted residual method in which spatial approximations for the single-phase enthalpy and two-phase quality are used [11]. This symbolic integration is performed employing the symbolic toolbox of Maple.

The following are the assumptions on which the thermal-hydraulic model is based:

- The core system pressure is assumed constant.
- In the single-phase region, the fluid density is assumed to be constant and equal to the density of the liquid phase.
- As already mentioned, the heated channel is divided into two axial regions, the single and two-phase regions.
- Energy terms due to the pressure gradient, friction dissipation, kinetic energy and potential energy are neglected in the energy equation.
- The two phases are considered to be incompressible.
- The two phases are assumed to be in thermodynamic equilibrium.
- A drift flux model is used to represent the two-phase flow, rather than a homogeneous equilibrium model; such a model is more appropriate since it takes into account (a) the difference between the two phase velocities (the drift velocity V_{gj}), particularly important in the case of low flow rates, and (b) the radially non-uniform void distribution (the void distribution parameter C_0) inside the channel.
- The time-dependent single-phase enthalpy and two-phase quality have spatially quadratic profiles. These two assumptions have been successfully validated and used earlier [11] with the homogeneous equilibrium model for two-phase flow.

For each channel, five ODEs result from the integration of the one-dimensional time-dependent continuity, energy and momentum equations in the single and two-phase regions. As in the previous section, an asterisk on a variable or parameter indicates the

²³ In this thesis, a model of up to two channels has been considered.

original dimensional quantity, while any quantity without an asterisk is dimensionless. The various dimensionless variables and parameters used, as mentioned earlier, are presented in Appendix C.

Single-Phase Region

The single-phase region extends from the channel inlet to the boiling boundary $m(t)$, *i.e.* the location where bulk boiling starts. Since, in the single-phase region, the liquid density is taken as constant (equal to the density of the liquid). The velocity along the single-phase region is constant and equal to the channel inlet velocity v_{inlet}^* .

The energy equation can be written as follow:

$$\mathbf{r}_f^* \frac{\partial h^*(z^*, t^*)}{\partial t^*} + \mathbf{r}_f^* v_{inlet}^*(t^*) \frac{\partial h^*(z^*, t^*)}{\partial z^*} = \frac{q_{1f}''^*(t^*) \mathbf{x}_h^*}{A^*} \quad (4.48)$$

where \mathbf{r}_f^* is the liquid density; $h^*(z^*, t^*)$ is the single-phase enthalpy and $q_{1f}''^*(t^*)$ is the wall heat flux in the single-phase region related to the single-phase convective heat transfer coefficient $h_{\infty,1f}^*$ by $q_{1f}''^*(t^*) = h_{\infty,1f}^* \cdot (T_{s,1f}^*(t^*) - T_{bulk,1f}^*)$. $h_{\infty,1f}^*$ is estimated by the Dittus-Boelter correlation presented in Section 4.5.

The single-phase momentum equation is

$$-\frac{\partial P_{1f}^*}{\partial z^*} = \mathbf{r}_f^* \frac{dv_{inlet}^*(t^*)}{dt^*} + \mathbf{r}_f^* \frac{f_{1f}^*}{2D_h^*} v_{inlet}^2(t^*) + \mathbf{r}_f^* g^* \quad (4.49)$$

Eqs. (4.48) and (4.49) can be written in dimensionless form:

$$\frac{\partial h(z, t)}{\partial t} + v_{inlet}(t) \frac{\partial h(z, t)}{\partial z} = N_r N_r N_{pch,1f}(t) \quad (4.50)$$

$$-\frac{\partial P_{1f}}{\partial z} = \frac{dv_{inlet}(t)}{dt} + N_{f,1f} v_{inlet}^2(t) + Fr^{-1} \quad (4.51)$$

where $N_{pch,1f}(t)$ is the time-dependent phase change number in the single-phase region, which is proportional to the wall heat flux in the single-phase region;

$N_{pch,1f}(t) = N_{cov,1f}(T_{s,1f}(t) - T_{bulk,1f})$. The dimensionless numbers Fr , N_r , N_r and $N_{cov,1f}$ are defined in Appendix C.

A time-dependent, spatially quadratic distribution for the enthalpy, as originally proposed and validated by Karve *et al.* [11], is now introduced.

$$h(z, t) \approx h_{inlet} + a_1(t)z + a_2(t)z^2 \quad (4.52)$$

Substituting this expression in the single-phase energy equation (4.50), using a weighted residual procedure with the weight functions 1 and z [7], and integrating from the inlet of the channel $z = 0$ to the boiling boundary $z = \mathbf{m}(t)$, we arrive at the ODEs for the phase variables $a_1(t)$ and $a_2(t)$ for the single-phase region:

$$\frac{da_1(t)}{dt} = \frac{6}{\mathbf{m}(t)} [N_r N_r N_{pch,1f}(t) - v_{inlet}(t)a_1(t)] - 2v_{inlet}(t)a_2(t) \quad (4.53)$$

$$\frac{da_2(t)}{dt} = \frac{6}{\mathbf{m}^2(t)} [N_r N_r N_{pch,1f}(t) - v_{inlet}(t)a_1(t)] \quad (4.54)$$

The boiling boundary $\mathbf{m}(t)$ is the level at which the enthalpy is equal to the saturation enthalpy h_{sat} . Hence the expression for the boiling boundary can be obtained by applying the boundary conditions: $h(0, t) = h_{inlet}$, and $h(\mathbf{m}(t), t) = h_{sat}$ on Eq. (4.52)

$$\mathbf{m}(t) = \frac{2N_r N_r N_{sub}}{a_1(t) + \sqrt{a_1^2(t) + 4a_2(t)N_r N_r N_{sub}}} \quad (4.55)$$

Two-Phase Region

The two-phase region extends from the boiling boundary to the channel exit. The drift flux model is characterized by the vapour drift velocity V_{gj}^* and the void distribution parameter C_0 . This model is described by four fundamental equations [12]:

Continuity equations for liquid and vapour,

$$\frac{\partial(1-\mathbf{a}^*)\mathbf{r}_f^*}{\partial t^*} + \frac{\partial(1-\mathbf{a}^*)\mathbf{r}_f^*\mathbf{u}_f^*}{\partial z^*} = \Gamma_f^* \quad (4.56)$$

$$\frac{\partial\mathbf{a}^*\mathbf{r}_g^*}{\partial t^*} + \frac{\partial\mathbf{a}^*\mathbf{r}_g^*\mathbf{u}_g^*}{\partial z^*} = \Gamma_g^* \quad (4.57)$$

where Γ_f^* , and Γ_g^* are the liquid and void generation rates.

Energy equation of the mixture

$$\Gamma_g^*\Delta h_{fg}^* = q_{2f}^* \left(\frac{\mathbf{X}^*}{A^*} \right) \quad (4.58)$$

where $\Delta h_{fg}^* = h_g^* - h_f^*$. The wall heat flux in the two-phase region q_{2f}^* can be expressed in terms of the fuel rod surface temperature in the two-phase region $T_{s,2f}^*(t^*)$ by the Jens-Lottes correlation (see Section 4.5).

Momentum equation of the mixture [13],

$$\frac{\partial P_{2f}^*}{\partial z^*} = \mathbf{r}_m^* \left(\frac{\partial v_m^*}{\partial t^*} + v_m^* \frac{\partial v_m^*}{\partial z^*} \right) + g^* \mathbf{r}_m^* + \frac{f_{2f}^*}{2D^*} \mathbf{r}_m^* v_m^{*2} + \frac{\partial}{\partial z^*} \left(\frac{\mathbf{a}^*}{1-\mathbf{a}^*} \frac{\mathbf{r}_g^* \mathbf{r}_f^*}{\mathbf{r}_m^*} \bar{v}_{gj}^{*2} \right) \quad (4.59)$$

with the different quantities defined as follows:

$\bar{v}_{gj}^* = V_{gj}^* + (C_0 - 1)j^*(z^*, t^*)$, where $V_{gj}^* = \frac{\langle \mathbf{a}^* V_{gj}^* \rangle}{\langle \mathbf{a}^* \rangle}$ is the drift velocity, and

$C_0 = \frac{\langle \mathbf{a}^* j^* \rangle}{\langle \mathbf{a}^* \rangle \langle j^* \rangle}$ is the void distribution parameter.

$v_m^*(z^*, t^*) = j^*(z^*, t^*) + [V_{gj}^* + (C_0 - 1)j^*(z^*, t^*)] \left(1 - \frac{\mathbf{r}_f^*}{\mathbf{r}_m^*(z^*, t^*)} \right)$ is the mixture velocity.

Here, it needs to be pointed out that, in the present work, particular attention has been given to the role of the parameters C_0 and V_{gj}^* . Thus, the impact of these two parameters

on stability characteristics has been studied by varying their values in a realistic interval based on several different correlations including the RAMONA model, see Chapters 5, and 6.

By combining equations (4.56), (4.57) and (4.58), we obtain the so-called Void Propagation Equation [12],

$$\frac{\partial \mathbf{a}^*(z^*, t^*)}{\partial t^*} + C_k^* \frac{\partial \mathbf{a}^*(z^*, t^*)}{\partial z^*} = \mathbf{v}^* \quad (4.60)$$

where,

$$C_k^* = j^* + \frac{\partial(\mathbf{a}^* V_{gj}^*)}{\partial \mathbf{a}^*}, \quad (4.61)$$

$$\mathbf{v}^* = \frac{\mathbf{r}_m^* \Gamma_g^*}{\mathbf{r}_f^* \mathbf{r}_g^*} \quad (4.62)$$

We can rewrite Eqs. (4.56)-(4.58), (4.60) and (4.59) in a dimensionless form as

$$\frac{\partial j(z, t)}{\partial t} = N_{pch, 2f} \quad (4.63)$$

$$\frac{\partial \mathbf{a}(z, t)}{\partial t} + (C_0 j(z, t) + V_{gj}) \frac{\partial \mathbf{a}(z, t)}{\partial z} = N_{pch, 2f}(t) [N_r - C_0 \mathbf{a}(z, t)] \quad (4.64)$$

$$\begin{aligned} -\frac{\partial P_{2f}}{\partial z} = & \mathbf{r}_m(z, t) [Fr^{-1} + \frac{\partial v_m(z, t)}{\partial t} + v_m(z, t) \frac{\partial v_m(z, t)}{\partial z} + N_{f, 2f} v_m^2(z, t)] \\ & + N_r \frac{\partial}{\partial z} \left(\frac{\mathbf{a}}{1 - \mathbf{a}} \frac{\bar{V}_{gj}^2}{\mathbf{r}_m(z, t)} \right) \end{aligned} \quad (4.65)$$

where $\bar{V}_{gj} = V_{gj} + (C_0 - 1) \cdot j(z, t)$, and $j(z, t) = v_{inlet}(t) + N_{pch, 2f}(t)(z - \mathbf{m}(t))$.

The mixture density is $\mathbf{r}_m(z, t) = 1 - \mathbf{a}(z, t) / N_r$.

The mixture velocity is $v_m(z, t) = j(z, t) + (V_{gj} + (C_0 - 1)j(z, t)) \cdot \left(1 - \frac{1}{\mathbf{r}_m(z, t)} \right)$.

The drift flux relation between the void fraction and the equilibrium quality $x(z, t)$ can be written as a sum of the void fraction due to the homogenous equilibrium model and a correction term:

$$\mathbf{a}(z, t) = \frac{1}{C_0} (\mathbf{a}_{homo}(z, t) - V_{gj} \cdot \mathbf{a}_{corr}(z, t)) \quad (4.66)$$

where

$$\mathbf{a}_{homo}(z, t) = \frac{x(z, t)N_r}{(x(z, t) + N_r N_r)} \text{ and } \mathbf{a}_{corr}(z, t) = \frac{x(z, t)N_r}{(x(z, t) + N_r N_r)(C_0 j(z, t) + V_{gj})}.$$

Taking into account the quadratic dependence of the quality in the axial direction [11],

$$x(z, t) \approx N_r N_r [s_1(t)(z - \mathbf{m}(t)) + s_2(t)(z - \mathbf{m}(t))^2] \quad (4.67)$$

we substitute the values of $x(z, t)$ and $j(z, t)$ in Eq. (4.66), substitute the resulting equation (4.66) in the void propagation equation (4.64) and finally, using the weighted residuals method with weight functions 1 and z , we obtain the ODEs for the phase variables in the two-phase region, $s_1(t)$ and $s_2(t)$, by integrating from the boiling boundary $z = \mathbf{m}(t)$ to the channel exit $z = 1$:

$$\frac{ds_1(t)}{dt} = \frac{1}{ff_5(t)} \left[ff_1(t) \frac{d\mathbf{m}(t)}{dt} + ff_2(t) \frac{dv_{inlet}(t)}{dt} + ff_3(t) \frac{dN_{pch,2f}(t)}{dt} + ff_4(t) \right] \quad (4.68)$$

$$\frac{ds_2(t)}{dt} = \frac{1}{ff_{10}(t)} \left[ff_6(t) \frac{d\mathbf{m}(t)}{dt} + ff_7(t) \frac{dv_{inlet}(t)}{dt} + ff_8(t) \frac{dN_{pch,2f}(t)}{dt} + ff_9(t) \right] \quad (4.69)$$

where $s_1(t)$ and $s_2(t)$ are the coefficients of the linear and quadratic terms in the quality profile expression, and $ff_n(t), n = 1, \dots, 9$ are complicated intermediate quantities, which depend on the phase variables, the operating parameters and the design parameters. Since these expressions are very long, their forms are presented in Appendix D.

Finally, using the fixed total pressure drop with respect to time as a boundary condition, the single-phase and two-phase momentum equations are used to derive the

ODE for the inlet liquid velocity $v_{inlet}(t)$, which is one of the state variables. Integrating the momentum equation for the single and two-phase regions, we get the equations for the single and two-phase pressure drops in terms of $v_{inlet}(t)$. Finally, these pressure drops are summed along with the inlet and exit pressure drops, and the result set equal to the external pressure drop DP_{ext} :

$$\Delta P_{1f}(t) + \Delta P_{2f}(t) + \Delta P_{inlet}(t) + \Delta P_{exit}(t) = DP_{ext} \quad (4.70)$$

where ΔP_{inlet} , ΔP_{exit} are the inlet and exit channel pressure drops respectively, defined as

$$DP_{inlet} = K_{inlet} \cdot v_{inlet}^2(t) \quad (4.71)$$

$$DP_{exit} = K_{exit} \cdot \mathbf{r}_m(z=1,t) \cdot v_m^2(z=1,t) \quad (4.72)$$

where k_{inlet} and k_{exit} are the inlet and outlet pressure loss coefficients, respectively.

Rearranging Eq. (4.70) leads to the equation for the inlet velocity

$$\frac{dv_{inlet}(t)}{dt} = \frac{1}{ff_{14}(t)} \left(ff_{11}(t) \frac{d\mathbf{m}(t)}{dt} + ff_{12}(t) \frac{dN_{pch2f}}{dt} + ff_{13}(t) \right) \quad (4.73)$$

where $ff_n(t)$, $n = 11, \dots, 14$ are again complicated intermediate quantities, which depend on the phase variables, and the operating and design parameters. The expressions for these quantities are presented in Appendix D.

It should be noted that, as illustrated in Section 2.6, the assumption of a constant pressure drop across the core serves as an accurate replacement of the outer loop for the out-of-phase oscillation case. However, in the case of in-phase (global) oscillations, this boundary condition is only valid for small oscillation amplitudes. In all the studies carried out in this thesis, constant pressure drop is the only boundary condition. Therefore, it is understood that these studies are restricted to out-of-phase oscillations and to small amplitude in-phase oscillations. For future studies, it is strongly recommended that an outer loop model be included with the core model in order to avoid the boundary condition issue.

4.5 CORRELATIONS USED

1) The single-phase heat transfer coefficient $h_{\infty,1f}^*$ is estimated using the Dittus-Boelter correlation

$$h_{\infty,1f}^* = 0.023 \cdot \frac{k_f}{D_h} \cdot (\text{Re})^{0.8} \cdot (\text{Pr})^{0.4} \quad (4.74)$$

for $0.7 < Pr < 100$, and $Re > 10000$, where Pr and Re are the Prandtl and Reynolds numbers, respectively. k_f is the thermal conductivity, D_h is the heated diameter, L is the channel length, and D is the channel diameter.

2) The two-phase heat transfer coefficient $h_{\infty,2f}^*$ is estimated using the Jens-Lottes correlation

$$h_{\infty,2f}^* = \frac{\text{EXP}\left(\frac{4 \cdot p \cdot 10^{-6}}{6.2}\right)}{25^4 \cdot 10^{-6}} \left(T_{s,2f}^*(t^*) - T_{sat}^*\right)^3 \quad (4.75)$$

where p is the system pressure, $T_{s,2f}^*(t)$ is the fuel surface temperature in the two-phase region, which is equivalent to $T_{c,2f}^*(r_c^*, t^*)$, and T_{sat}^* is the saturation temperature. The wall heat flux in the two-phase region is

$$q_{2f}^{**}(t^*) = h_{\infty,2f}^* (T_{s,2f}^*(t^*) - T_{sat}^*) \quad (4.76)$$

It should be pointed out that several other correlations have been used in the current model, such as: the fuel heat capacity, the fuel thermal conductivity, the gap conductance, the single and the two-phase friction factors, etc. These correlations are also used in the RAMONA model (see Eqs. (A.7), (A.8), (A.9), (A.15), and (A.16), respectively).

4.6 SUMMARY OF THE NEW REDUCED ORDER MODEL

In this section, we present the system of ODEs in an explicit form that depends on the channel index (l). For a two-parallel-channel model, four ODEs result from the neutron kinetic model

$$\frac{dn_0(t)}{dt} = \frac{1}{\mathbf{L}_0} [(\mathbf{r}_{00}(t) - \mathbf{b}) \cdot n_0(t) + \mathbf{r}_{01}(t) n_1(t)] + \mathbf{I}U_0(t) \quad (4.77)$$

$$\frac{dn_1(t)}{dt} = \frac{1}{\mathbf{L}_0} [\mathbf{r}_{10}(t) n_0(t) + (\mathbf{r}_{11}(t) + \mathbf{r}_1^s - \mathbf{b}) \cdot n_1(t)] + \mathbf{I}U_1(t) \quad (4.78)$$

$$\frac{dU_0(t)}{dt} = \frac{\mathbf{b}}{\Lambda_0} n_0(t) - \mathbf{I}U_0(t) \quad (4.79)$$

$$\frac{dU_1(t)}{dt} = \frac{\mathbf{b}}{\Lambda_0} n_1(t) - \mathbf{I}U_1(t). \quad (4.80)$$

For each channel, four ODEs are derived from the fuel rod heat conduction PDE.

$$\frac{dT_{1,1,l}(t)}{dt} = ll_{1,1,1,l} T_{1,1,l}(t) + ll_{2,1,1,l} T_{2,1,l}(t) + ll_{3,1,1,l} \cdot [c_q(n_0(t) - \tilde{n}_0) + c_q \mathbf{x} n_1(t)] \quad (4.81)$$

$$\frac{dT_{2,1,l}(t)}{dt} = ll_{1,2,1,l} T_{1,1,l}(t) + ll_{2,2,1,l} T_{2,1,l}(t) + ll_{3,2,1,l} \cdot [c_q(n_0(t) - \tilde{n}_0) + c_q \mathbf{x} n_1(t)] \quad (4.82)$$

$$\frac{dT_{1,2,l}(t)}{dt} = ll_{1,1,2,l} T_{1,2,l}(t) + ll_{2,1,2,l} T_{2,2,l}(t) + ll_{3,1,2,l} \cdot [c_q(n_0(t) - \tilde{n}_0) + c_q \mathbf{x} n_1(t)] \quad (4.83)$$

$$\frac{dT_{2,2,l}(t)}{dt} = ll_{1,2,2,l} T_{1,2,l}(t) + ll_{2,2,2,l} T_{2,2,l}(t) + ll_{3,2,2,l} \cdot [c_q(n_0(t) - \tilde{n}_0) + c_q \mathbf{x} n_1(t)]. \quad (4.84)$$

For each channel, there are five ODEs that describe the thermal-hydraulic model.

$$\frac{da_{1,l}(t)}{dt} = \frac{6}{\mathbf{m}_l^2(t)} [N_r N_r N_{pch,1f,l}(t) - v_{inlet,l}(t) a_{1,l}(t)] - 2v_{inlet,l}(t) a_{2,l}(t) \quad (4.85)$$

$$\frac{da_{2,l}(t)}{dt} = \frac{6}{\mathbf{m}_l^2(t)} [N_r N_r N_{pch,1f,l}(t) - v_{inlet,l}(t) a_{1,l}(t)] \quad (4.86)$$

$$\frac{ds_{1,l}(t)}{dt} = \frac{1}{ff_{5,l}(t)} \left[ff_{1,l}(t) \frac{d\mathbf{m}(t)}{dt} + ff_{2,l}(t) \frac{dv_{inlet,l}(t)}{dt} + ff_{3,l}(t) \frac{dN_{pch,2f,l}(t)}{dt} + ff_{4,l}(t) \right] \quad (4.87)$$

$$\frac{ds_{2,l}(t)}{dt} = \frac{1}{ff_{10,l}(t)} \left[ff_{6,l}(t) \frac{d\mathbf{m}(t)}{dt} + ff_{7,l}(t) \frac{dv_{inlet,l}(t)}{dt} + ff_{8,l}(t) \frac{dN_{pch,2f,l}(t)}{dt} + ff_{9,l}(t) \right] \quad (4.88)$$

$$\frac{dv_{inlet,l}(t)}{dt} = \frac{1}{ff_{14,l}(t)} \left(ff_{11,l}(t) \frac{d\mathbf{m}(t)}{dt} + ff_{12,l}(t) \frac{dN_{pch,2f,l}}{dt} + ff_{13,l}(t) \right) \quad (4.89)$$

It should be noted that Eqs. (4.81) through (4.89) have been obtained by integrating and manipulating the corresponding fundamental PDEs using again the Maple symbolic toolbox. These equations have been then incorporated, along with Eqs. (4.77) through (4.80), in the main Fortran program called *bwrf* (see Subsection 2.7.3) used in conjunction with BIFDD to perform semi-analytical bifurcation analysis.

REFERENCES

- [1] W. Wulff, H.S. Cheng, D. J. Diamond, M. Khatib-Rahbar, "A Description and Assessment of RAMONA-3B Mod. 0, Cycle 4: A Computer Code with 3D Neutron Kinetics for BWR System Transients", NUREG/CR-3664, BNL-NUREG-51746, Brookhaven National Laboratory, 1984.
- [2] A. A. Karve, Rizwan-uddin, J. J. Dorning, "Stability Analysis of BWR Nuclear-Coupled Thermal-hydraulics using a Simple Model," *Nucl. Eng. Des.* **177**, 155-177, 1997.
- [3] K. Hashimoto, "Linear Modal-Analysis of Out-of-phase Instability in Boiling Water Reactors Cores," *Ann. Nucl. Energy*, **12**, 789-797, 1993.
- [4] J. L. Muñoz-Cobo, R. B. Perez, D. Ginestar, A. Escrivá, G. Verdú, "Nonlinear Analysis of Out-of-phase Oscillations in BWRs", *Ann. Nucl. Energy*, **23**, 16, 1301-1335, 1996.
- [5] R. Miró, D. Ginestar, D. Hennig, G. Verdú, "On the Regional Oscillation Phenomenon in BWRs," *Prog. Nucl. Energy*, **36**, 2, 189-229, 2000.

- [6] J. L. Muñoz-Cobo, O. Rosello, R. Miró, A. Escrivá, D. Ginestar, G. Verdú, "Coupling of Density Wave Oscillations with High Order Modal Kinetics: Application to BWR Out-of-phase Oscillations," *Ann. Nucl. Energy*, **27**, 1345-1371, 2000.
- [7] A. A Karve, "Nuclear-Coupled Thermal-hydraulic Stability Analysis of BWRs", Ph.D. Dissertation, Virginia University, USA, 1998.
- [8] L. V. Kantorovich, V. I. Krylov, *Approximate Methods of Higher Analysis*, Interscience, New York, 1964.
- [9] I. Stackgold, *Boundary Value Problems of Mathematical Physics-II*, Macmillan, New York, 1968.
- [10] M. J. Powell, "A Fast Algorithm for Nonlinear Constrained Optimisation Calculations," *Numerical Analysis Proceedings*, **630**, 144, 1978.
- [11] A. A. Karve, Rizwan-uddin, and J. J. Dorning, "On Spatial Approximations for Liquid Enthalpy and Two-phase Quality during Density Wave Oscillations," *Trans. Am. Nucl. Soc.*, **71**, 533, 1994.
- [12] N. Zuber, F. W. Staub, "An Analytical Investigation of the Transient Response of the Volumetric Concentration in a Boiling Forced-Flow System", *Nucl. Sci. Eng.*, **30**, 268-278, 1967.
- [13] Rizwan-uddin, "Linear and Nonlinear Stability Analyses of Density-Wave Oscillations in Heated Channels", Ph.D. Dissertation of University of Illinois, USA, 1981.

5 STABILITY AND BIFURCATION ANALYSIS OF A HEATED CHANNEL

5.1 INTRODUCTION

Since the thermal-hydraulic model determines the main feedback gain and the associated time delay (void feedback reactivity), the modelling of the fluid dynamics is of paramount importance for the reduced order model analysis of BWRs. For a certain set of hydraulic parameter values, the system of nonlinear differential equations describing the fluid dynamics generates so-called self-sustained density wave oscillations (DWOs). Such oscillations represent probably the most common type of instability encountered in two-phase flow systems and are due to the feedback and interaction among the flow rate, the vapour generation rate and the pressure drop in a boiling channel. The physical mechanisms leading to DWOs are now clearly understood and can be described in a number of equivalent ways [1]. The following description reflects the essence of the physical phenomena involved.

Consider a heated channel with a fixed imposed pressure drop across its length and a steady-state inlet flow rate. The bulk of the fluid starts boiling at a certain level called the boiling boundary. Consider a small perturbation in the inlet velocity. This small perturbation creates a propagating enthalpy perturbation in the single-phase region. The boiling boundary oscillates due to this enthalpy perturbation. The change in the inlet velocity and in the length of the single-phase region combine to create a change in the single-phase region pressure drop. At the boiling boundary, the enthalpy perturbation is converted into a void (quality) perturbation that travels up through the two-phase region. The combined effects of the changes in the flow rate, void fraction and the two-phase region length create a two-phase pressure drop perturbation. Since the total pressure drop across the boiling channel is fixed, the two-phase pressure drop perturbation produces a feedback perturbation of the opposite sign in the single-phase region. In case the pressure drop in the two-phase region is delayed 180 degrees with respect to the inlet flow rate, self-sustained oscillations are excited.

The study of the nonlinear behaviour of density wave instabilities has attracted considerable interest in the last two decades. Benefiting from the development of nonlinear dynamics theory, significant advances have been made in the nonlinear stability

analysis of heated channels as well as BWRs. Moreover, additional efforts have been concentrated recently on bifurcation analyses in which the effects of different design, as well as operating, parameters on bifurcation characteristics are analysed. Such bifurcation analyses give important information that should be taken into account in the design and operational analysis of the next generation of BWRs. As stated in Chapter 3, supercritical Hopf bifurcation implies existence of stable periodic solutions close to the SB in the unstable region, and subcritical Hopf bifurcation implies unstable periodic solutions close to the SB in the *stable* region. Hence, in the case of subcritical Hopf bifurcation, the oscillation amplitude may grow—even on the stable side of the SB—if the perturbation is large enough.

Achard *et al.* [2] carried out an analytical bifurcation study of DWO phenomena on the basis of a homogeneous equilibrium model. This led to two functional differential equations (FDEs). Rizwan-uddin and Dorning [3] extended that model using a drift flux model and obtained very complicated nonlinear, functional, delay, integro-differential equations for the inlet velocity and two-phase residence time. They carried out stability and bifurcation analyses and showed that the stability boundary is sensitive to the value of C_0 (void distribution parameter). The effect of V_{gj} (drift velocity) on the SB appeared to be small. The nature of Hopf bifurcation along the entire SB was found to be supercritical. However, the impact of C_0 and V_{gj} on the nature of Hopf bifurcation was not reported.

Later, starting from the homogeneous equilibrium model, Clause and Lahey [4] developed a simple model for DWOs by introducing some simplifying assumptions, such as simple linear approximations of the space dependence of the enthalpies of the single-phase and two-phase regions. In the spirit of these developments, Karve *et al.* [5] developed a model (using the homogeneous equilibrium model) based on the assumption that the time-dependent single-phase enthalpy and two-phase quality have spatially quadratic profiles. This model is simple in that the dynamical system that results is comprised of a set of nonlinear ODEs rather than complicated FDEs. After stability analysis for the stability boundary, they carried out bifurcation analysis entirely numerically [6].

In the present chapter, the thermal-hydraulic drift flux model developed in Section 4.4 is applied. As mentioned earlier, such a model is more appropriate since it takes into account: (a) the difference between the two-phase velocities, which is particularly important in low-flow regimes, and (b) the radially non-uniform void distribution inside

the channel. Moreover, the drift flux model is more general than the HEM and the slip model, *i.e.* the latter are special cases of the DFM. Furthermore, stability and semi-analytical bifurcation analyses (see Chapter 3) have been performed using the bifurcation analysis code BIFDD [7]. In effect, this is the first analysis that systematically shows the effects of the drift flux model parameters, C_0 and V_{gj} , on the nature of Hopf bifurcation in a heated channel problem.

This chapter is organized in the following way. The next section presents a short description of the heated channel model, which is effectively a 5-equation subset of the complete BWR reduced order model derived in Chapter 4. In Section 3, this model is validated against appropriate experimental data, and compared to several other analytical models developed to simulate density wave oscillations. Section 4 is devoted to the comparison between the use of drift flux and homogeneous equilibrium models, using both semi-analytical bifurcation analysis and standard numerical integration of the set of ODEs. In Section 5, a sensitivity study is carried out in order to assess the effects of different parameters on the stability and bifurcation characteristics. Finally, a summary and conclusions section completes the chapter.

5.2 THE HEATED CHANNEL MODEL

Using drift flux model representation of the two-phase flow, the current mathematical model for the heated channel is based on the assumption that the time-dependent single-phase enthalpy and two-phase quality have spatially quadratic profiles. As mentioned previously, this assumption was used earlier [5] with the homogeneous equilibrium model for two-phase flow. The current dynamical system that describes the heated channel essentially corresponds to that developed and presented in Section 4.4. It consists of five ODEs, *viz.* Eqs. (4.53), (4.54), (4.68), (4.69) and (4.73), which can be written in compact form as:

$$\dot{X}(t) = F(X; \mathbf{k}) \quad (5.1)$$

where $X(t)$ is the vector of phase variables

$$X(t) = (a_1(t), a_2(t), s_1(t), s_2(t), v_{inlet}(t))^T \quad (5.2)$$

Here $a_1(t)$ and $a_2(t)$ are the coefficients of the linear and quadratic terms for the liquid enthalpy profile, $s_1(t)$ and $s_2(t)$ are the coefficients of the linear and quadratic terms for the quality profile, $v_{inlet}(t)$ is the liquid velocity at the channel inlet, and \mathbf{k} is the vector of parameters that includes both operating and design parameters as defined in Appendix C.

$$\mathbf{k} = (N_r, N_r, N_{pch,1f}, N_{pch,2f}, N_{sub}, K_{inlet}, K_{exit}, N_{f,1f}, N_{f,2f}, Fr, \Delta P_{ext}, C_0, V_{gj}) \quad (5.3)$$

5.3 VALIDATION OF THE THERMAL-HYDRAULIC MODEL

Since the phenomenon of thermally induced two-phase flow instability is of basic interest for the design and operation of BWRs, the aim in this section is to validate the current thermal-hydraulic model against appropriate experimental data and to compare its performance with the results obtained using several earlier models that were developed to simulate density wave oscillations.

Saha *et al.* [8] carried out an experimental study on the onset of self-sustained thermal-hydraulic two-phase density wave oscillations. The experimental facility used consists of a uniformly heated boiling channel with Freon-113 as the operating fluid. Freon-113 was chosen because of the low operating costs. Figure 5-1 shows a simplified schematic sketch of this facility. The experimental data sets were generated by changing the inlet velocity v_0 . For each experiment, the system pressure, the inlet and exit restrictions, and the inlet velocity (v_0) were kept constant. The inlet subcooling was established by adjusting the preheating system, and the power was then increased in small steps until sustained flow oscillations were observed, thus identifying points on the stability boundary. Consequently, such points were plotted on the subcooling-number versus the equilibrium-phase-change-number plane ($N_{sub} - N_{pch}$). The operating conditions for different set of experiments are given in Table 5-1.

It should be emphasized that, although these experiments were performed for a heated channel, they are very relevant to BWR stability analysis since the thermal-hydraulic phenomena investigated are of paramount importance in its context. Figures 5-2 to 5-5

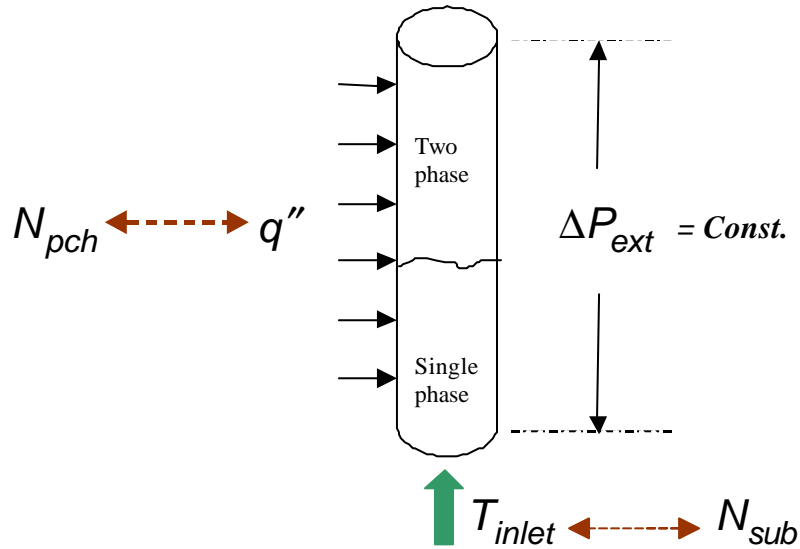


Figure 5-1. Simplified schematic sketch of the Saha *et al.* test facility

Table 5-1. Operating conditions for Sets I, III, V and VI of the Saha *et al.* experiments

	Set I	Set III	Set V	Set VI
Pressure (bar)	12.1	10.3	12.1	12.1
v_0 (m/s)	0.98	1.02	0.72	1.49
K_{inlet}	2.85	2.85	6.55	6.55
K_{exit}	2.03	2.03	2.03	2.03

show the comparison of the stability boundaries calculated from the current thermal-hydraulic model²⁴ with the experimental data (Sets I, III, V, VI) as re-evaluated by Rizwan-uddin and Dorning²⁵ [9]. Also compared in the figures are the stability boundaries calculated from various models that were developed earlier to study two-phase flow instabilities. These models are: (i) the two-fluid (6 equations) model developed by Dykhuizen *et al.* [10] that, naturally, includes subcooled boiling, (ii) the non-equilibrium slip model of Saha and Zuber [11] that also includes subcooled boiling, but with a flat void profile ($C_0 = 1$), (iii) the Ishii and Zuber slip model based on a simplified stability

²⁴ In this study, all the points on a SB have the same coolant inlet velocity value.

²⁵ Rizwan-uddin and Dorning found some errors in the evaluation of the dimensionless numbers N_{sub} and N_{pch} for the experimental data. These resulted from errors in the thermodynamic properties that were used to calculate the dimensionless numbers [9].

criterion with a flat void profile [12], (iv) the drift flux model developed by Rizwan-uddin and Dorning [13], and (v) the homogeneous equilibrium model of Karve *et al.* [5].

Figure 5-2 shows the current model benchmarked against the experimental data for Set I with $v_0 = 0.98 \text{ m/s}$, as well as against the two-fluid model, the Rizwan and Dorning DFM model, and the Karve *et al.* HEM. For large values of the inlet subcooling, all models are in good agreement with the experimental data. However, for lower values of N_{sub} , the current model produces the second best predictions of the experimental data, after the two-fluid model that includes subcooled boiling effects. This suggests that inclusion of a subcooled boiling model may be important for low values of inlet subcooling.

Stability boundaries calculated by the current model, the Saha and Zuber thermal non-equilibrium model, the Rizwan-uddin and Dorning DFM, and the Karve *et al.* HEM are compared with the Set III experimental data in Fig. 5-3. This experiment corresponds to $v_0 = 1.02 \text{ m/s}$. For large value of N_{sub} , the SBs calculated by the current model and the Rizwan-uddin and Dorning model provide the best predictions. This is because these two models take into account the radially non-uniform void distribution. However, for lower values of N_{sub} , the current model gives the second best results for predicting the experimental data, after the Saha and Zuber model that includes a subcooled boiling model. This shows again that including subcooled boiling has a significant effect, especially for low values of N_{sub} .

The Set V experimental data are shown in Fig. 5-4, comparison being made with results obtained using the models presented previously in Fig. 5-3, as well as the Ishii and Zuber model based on a simplified stability criterion. Except for the Saha and Zuber model that shows a large discrepancy, all the models including the ones based on $C_0 = 1$ are in good agreement with the experimental data. This is due to the low value of the inlet velocity ($v_0 = 0.72 \text{ m/s}$), which corresponds to a void distribution parameter C_0 very close to 1.

The importance of a radially non-uniform void distribution is clearly shown in Fig. 5-5 for the Set VI experimental data with $v_0 = 1.49 \text{ m/s}$. It should be emphasized that this value of inlet velocity is in the range of values representative of an actual BWR²⁶, so that

²⁶ For KKL, the maximum inlet velocity is 2.67 m/s .

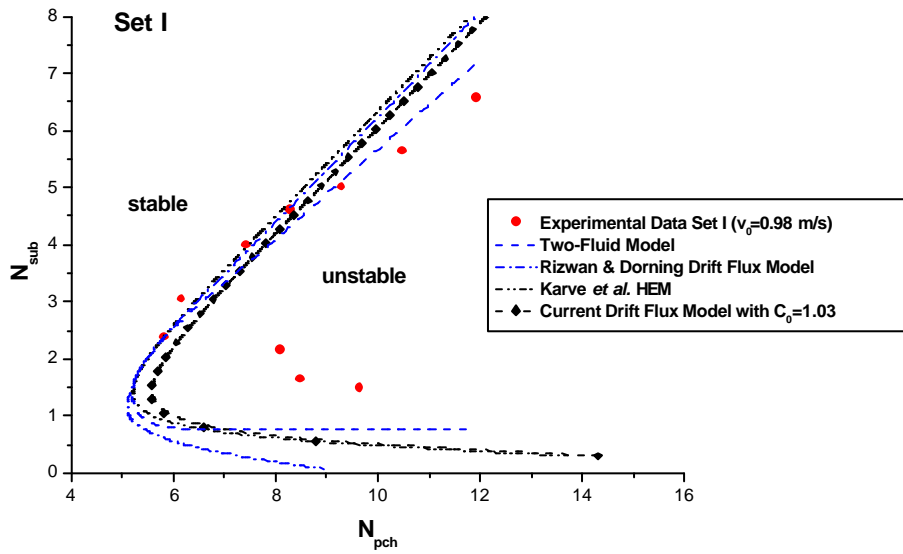


Figure 5-2. Comparison of calculated stability boundaries with Set I experimental data ($v_0 = 0.98$ m/s).

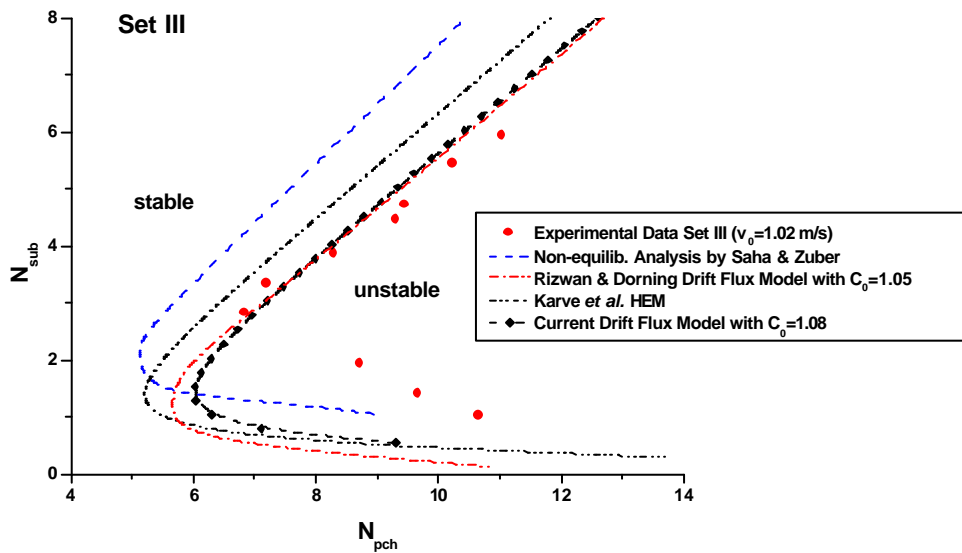


Figure 5-3. Comparison of calculated stability boundaries with Set III experimental data ($v_0 = 1.02$ m/s).

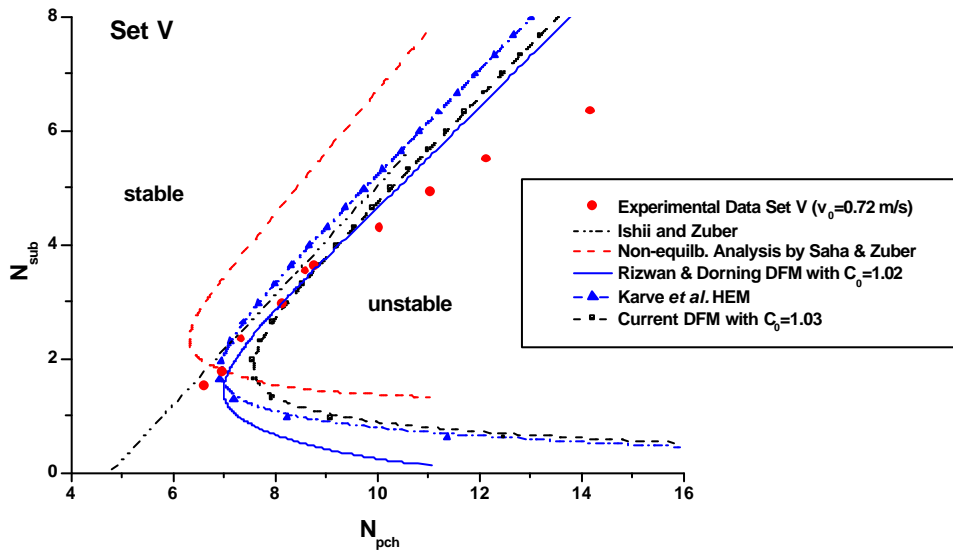


Figure 5-4. Comparison of calculated stability boundaries with Set V experimental data ($v_0 = 0.72$ m/s).

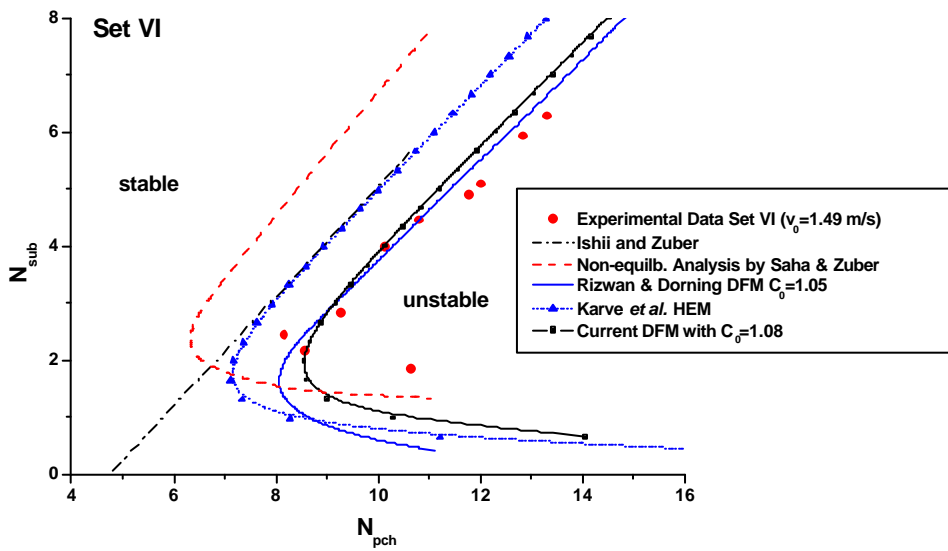


Figure 5-5. Comparison of calculated stability boundaries with Set VI experimental data ($v_0 = 1.49$ m/s).

these data are particularly relevant as validation base. The SBs predicted by the current model ($C_0 = 1.08$) and the Rizwan-uddin and Dorning model ($C_0 = 1.05$) are seen to agree very well with the experiment results. This is because for large values of v_0 , C_0 is larger than 1 and, therefore, the models based on $C_0 = 1$ (HEM or slip models) are likely to be inadequate. For lower values of N_{sub} , the Saha and Zuber model fits the data best, followed by the current model. It should be pointed out that, although the current model and the Rizwan-uddin and Dorning model are based on the same drift flux approach, they are constructed differently. The Rizwan-uddin and Dorning model is an exact model, *i.e.*, involves a direct integration of the first order, nonlinear, functional, ordinary differential equations. However, the authors ignored the higher terms of $(C_0 - 1)$ that were assumed to be small quantities. The present DFM is based on two assumptions implying an approximate spatial treatment, *viz.* that the single-phase enthalpy and the two-phase quality have a quadratic dependence on the spatial z direction (see Section 4.4). Higher order terms, such as that of $(C_0 - 1)$, however, have not been neglected. This could explain why the current model fits the data better than the Rizwan-uddin and Dorning model for low values of N_{sub} .

To summarize, the current thermal-hydraulic model has been found to be in good agreement with the Saha *et al.* experimental data for large N_{sub} , as is the case for several, earlier developed models. For lower values of N_{sub} , the current model agrees better than most of the others, so that its validation against the experimental data can be considered quite satisfactory. Moreover, an advantage of the current model is that it is represented by a system of ODE that allows a very easy coupling to the neutron kinetic and heat conduction models, as seen in Chapter 4 where the complete, novel reduced order model for carrying out BWR stability analysis was presented. More important is that this ODE system can be handled in a straightforward fashion for carrying out semi-analytical bifurcation analysis using the bifurcation code BIFDD, as presented in the following section.

5.4 DRIFT FLUX VS. HOMOGENEOUS EQUILIBRIUM MODEL

5.4.1 Semi-Analytical Bifurcation Analysis

The aim in this section is to carry out a comparative analysis between the use of DFM vs. HEM for the semi-analytical bifurcation analysis with the Code BIFDD. For this, use has been made of the sub-program *drift.f* of the *bwr.f* code (see Subsection 2.7.3), comprising the set of 5 nonlinear ODEs of the thermal-hydraulic model as well as the corresponding Jacobian matrix. As mentioned earlier, the program allows any one of the design or operational parameters to be selected as the bifurcation parameter. Then, by incrementally varying a second parameter, the critical value of the bifurcation parameter can be repeatedly calculated, leading to the generation of a SB in two-dimensional parameter space.

Results of stability boundaries are presented here in the $N_{sub} - N_{pch}$ operational parameter plane, *i.e.* the same as that used for validation against experimental data (Section 5.3). It should be noted that, the steady-state inlet flow velocity at each point of the SB is constant ($\tilde{v}_{inlet} = 1$). Typical numerical values for the design and operating parameters in dimensionless form are given in Table 5-2.

The validation of the current thermal-hydraulic model against experimental data and other analytical models, as reported in the previous section, showed that a value of the void distribution parameter C_0 between 1 and 1.08, depending on the inlet flow, can fit the experimental data satisfactorily. Accordingly, in the numerical study reported here, the value of C_0 has been varied within this “realistic” interval. On the other hand, the choice of the values of the drift velocity used in this comparative study have been estimated from several different sources such as the RAMONA model, Inoue *et al.* [14], and Meier and Coddington correlations [15], which show that the chosen variation of V_{gj} in an interval between 0 and 0.15 is well justified.

It should be noted that, by setting $C_0 = 1$ and $V_{gj} = 0$, the present model reduces to the homogeneous equilibrium model, exactly as used in [5].

Table 5-2. Design and operating parameter values used in Sections 5.4 and 5.5.

N_r	N_r	K_{inlet}	K_{exit}	N_{fl}	N_{j2}	Fr
1.05397	0.05120	6.0	2.0	2.8	5.6	0.0333

Shown in Fig. 5-6 are the stability and bifurcation results for the HEM ($C_0 = 1$ and $V_{gj} = 0$) and for the DFM with $C_0 = 1.03$ and $V_{gj} = 0.1$. The stability boundaries in the $N_{sub} - N_{pch}$ plane are shown in Fig. 5-6(a). This figure clearly shows that the SB is sensitive to the model used. The corresponding bifurcation diagram in the $N_{sub} - \mathbf{b}_2$ plane (Fig. 5-6(b)) shows that both sub- and supercritical Hopf bifurcations are encountered (as discussed in Chapter 3, \mathbf{b}_2 is a parameter in the bifurcation analysis [7]. $\mathbf{b}_2 < 0$ implies supercritical Hopf-B, while $\mathbf{b}_2 > 0$ indicates subcritical Hopf-B). In this case, Hopf bifurcation is subcritical ($\mathbf{b}_2 > 0$) for $N_{sub} < 3.15$, and supercritical ($\mathbf{b}_2 < 0$) for higher values of N_{sub} (see Fig. 5-6(b)). Referring to Fig. 5-6(b), the operational points A, B and C shown in Fig. 5-6(a) are located in the region where supercritical bifurcation is predicted when crossing the SB, while the operational points D, E and F are located in the region where subcritical bifurcation is expected.

In references [2] and [3], however, it was reported that only supercritical Hopf bifurcation is encountered in the above parameter range. This disagreement in the bifurcation results may be ascribed to differences in the assumptions made in the individual models. It would seem, therefore, that further investigations are needed to clarify this discrepancy. For instance, a study that evaluates the effects of using other simplifying assumptions (e.g. those made in models [4] and [5]) on the nature of Hopf bifurcation would help considerably to understand this disagreement.

The effects of the drift flux model parameters (C_0 and V_{gj}) on the stability, as well as on the bifurcation characteristics, are investigated next. While the stability boundary is sensitive to the value of C_0 ($V_{gj} = 0$) as seen in Fig. 5-7(a), the nature of Hopf bifurcation is less affected. Only a small shift of the transition point between the sub- and supercritical regions is observed as C_0 is changed from 1.0 to 1.03 (Fig. 5-7(b)). For example, the transition occurs at $N_{sub} = 3.15$ for HEM, at $N_{sub} = 3.4$ for DFM with $C_0 = 1.03$ and $V_{gj} = 0$, and at $N_{sub} = 3.65$ for $C_0 = 1.05$ and $V_{gj} = 0$.

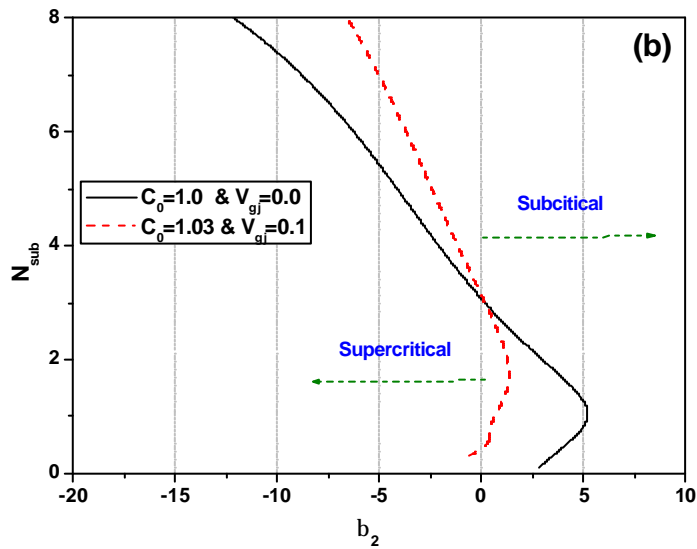
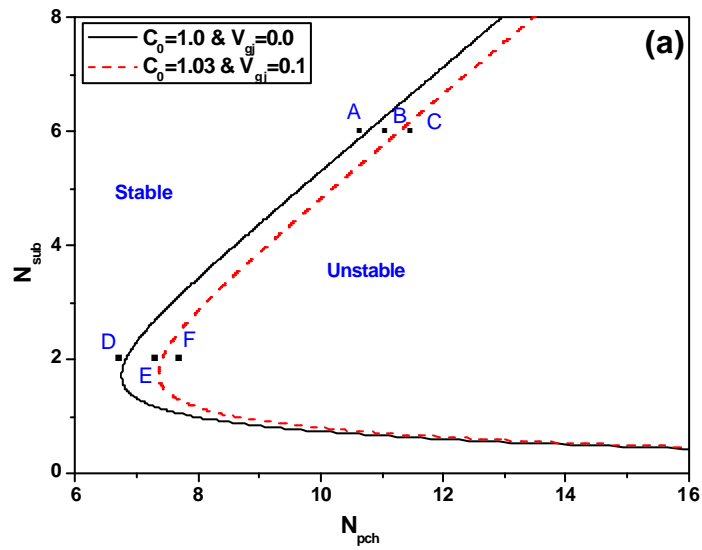


Figure 5-6. **a)** Stability boundaries in $N_{sub} - N_{pch}$ plane for Homogeneous Equilibrium Model (HEM) and Drift Flux Model (DFM). **b)** Nature of Hopf bifurcation in $N_{sub} - b_2$ plane for HEM and DFM. Bifurcation is supercritical for $b_2 < 0$, and subcritical for $b_2 > 0$.

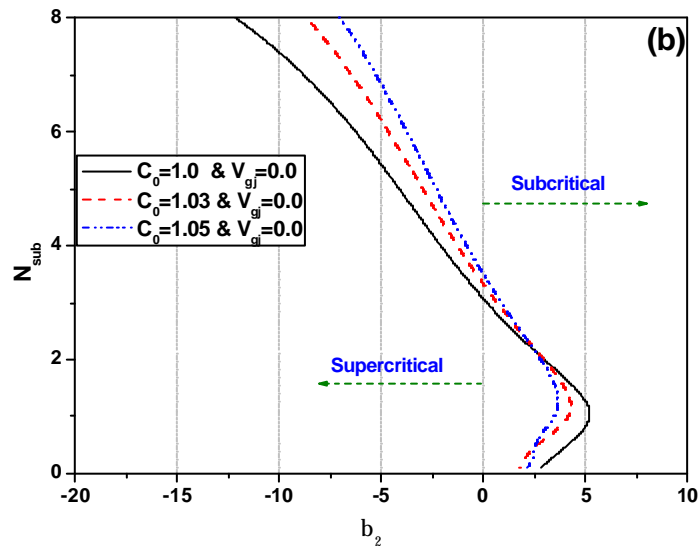
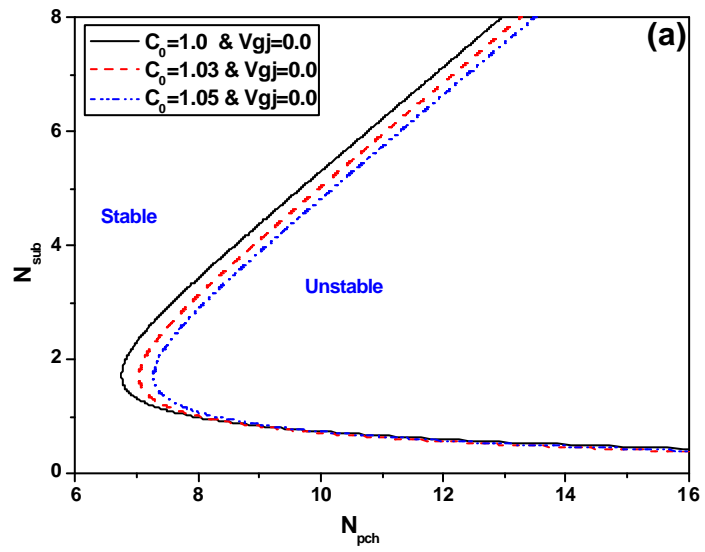


Figure 5-7. **a)** Stability boundaries in $N_{sub} - N_{pch}$ plane. **b)** Nature of Hopf bifurcation in $N_{sub} - b_2$ plane. Bifurcation is supercritical for $b_2 < 0$, and subcritical for $b_2 > 0$.

As was reported earlier by Rizwan-uddin and Dorning [3], C_0 is seen to have a stabilizing effect (Fig. 5-7(a)). This can be explained qualitatively by the following: for $C_0 > 1$, the concentration of bubbles at the periphery of the heated channel is lower than that for HEM. This causes less friction in the two-phase region, which means a lower two-phase region pressure drop; thus, the heated channel is more stable.

Results for the effects of the drift velocity V_{gj} are presented in Fig. 5-8. The SB is a little less sensitive to the value of V_{gj} (Fig. 5-8(a)) than it is to typical values of C_0 (Fig. 5-7(a)). Like C_0 , V_{gj} also has a stabilizing effect. The reason is that, for $V_{gj} > 0$, the velocity of the liquid is less than the mixture velocity in the HEM. This results in a decrease of the two-phase pressure drop that stabilizes the system. Although there is a partly compensating effect due to the steam velocity being higher than the mixture velocity in the HEM, the contribution of the liquid phase to the pressure drop is greater than that of the gas phase. The nature of Hopf bifurcation for lower values of N_{sub} is significantly more sensitive to V_{gj} than to C_0 . For example, for $V_{gj} = 0.12$ ($C_0 = 1$), the branch of the SB which was subcritical in the HEM disappears and the entire SB becomes supercritical (Fig. 5-8(b)). It should be noted that, although the stabilizing effects of C_0 and V_{gj} are well understood, understanding the effects of these two parameters on the bifurcation characteristics remains a challenge.

5.4.2 Numerical Simulation

It needs to be pointed out that bifurcation analyses of the above type are only valid in the vicinity of the SB. Hence, numerical integration of the set of 5 ODEs has been carried out—in the MATLAB environment—to confirm the predictions of the semi-analytical bifurcation analyses close to the SB. This also serves to provide global information beyond the local bifurcation findings, *i.e.* to evaluate the system behaviour in regions away from the SB. For the numerical integration of the ODEs, a 5th order Runge-Kutta method has been used. Figures 5-9, 5-10 and 5-11 show, respectively, the time evolution of the inlet velocity with parameter values corresponding to points A, B and C—in the supercritical region—shown in Fig. 5-6(a) for the HEM and DFM. As expected, the point A is stable for both models (Fig. 5-6(a)). Hence, the oscillation amplitude decays to the fixed point (Fig. 5-9(a-b)).

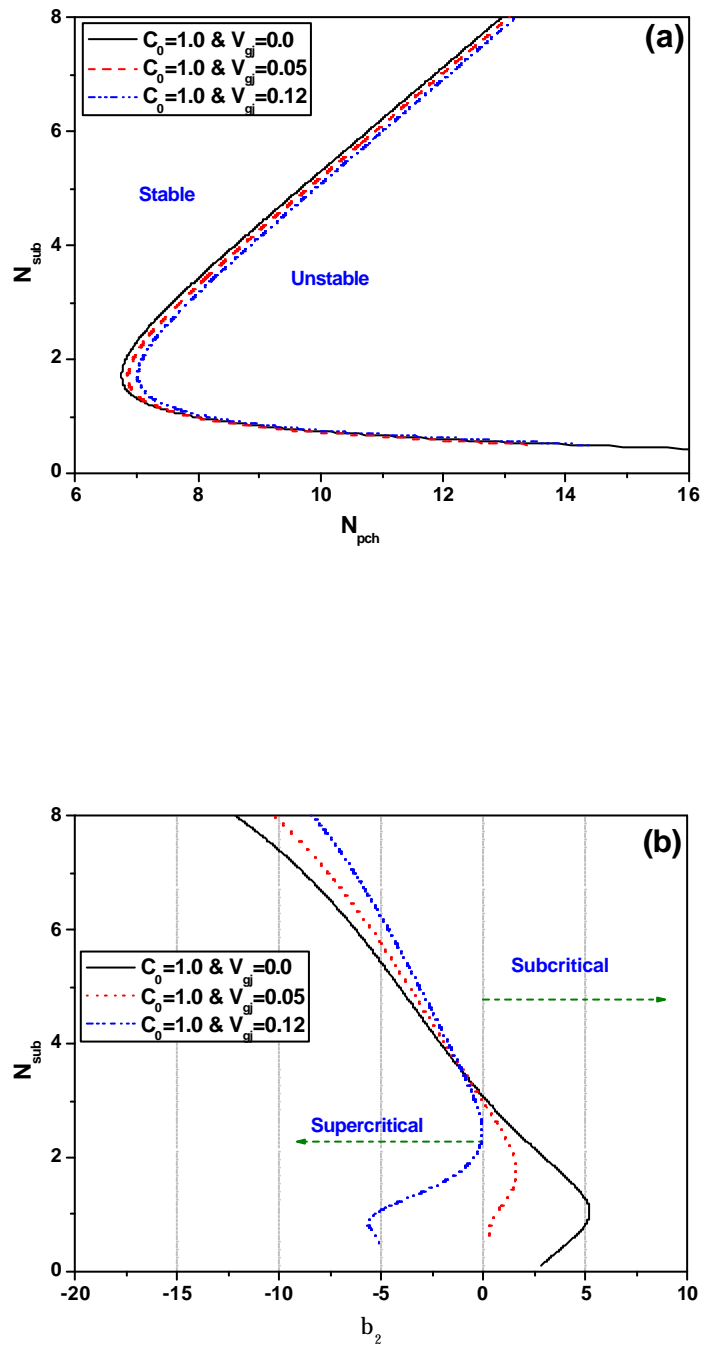


Figure 5-8. **a)** Stability boundaries in $N_{sub} - N_{pch}$ plane. **b)** Nature of Hopf bifurcation in $N_{sub} - b_2$ plane. Bifurcation is supercritical for $b_2 < 0$, and subcritical for $b_2 > 0$.

Point B shown in Fig. 5-6(a) is in the unstable region for the HEM. It is close to the stability boundary and the nature of Hopf bifurcation is supercritical. Therefore, as predicted by the bifurcation analysis, this leads to stable limit cycle oscillations as shown in Fig. 5-10(a). However, point B is stable for the DFM, and consequently the oscillation amplitude decays to the fixed point (Fig. 5-10(b)). Finally, point C is in the unstable region and it is far from the SB for the HEM (Fig. 5-6(a)). Therefore, the oscillation amplitude grows away from the fixed point (Fig. 5-11(a)). However, for the DFM case, point C is in the unstable region but close to the SB. Hence, this leads to a stable limit cycle as shown in Fig. 5-11(b).

Figures 5-12, 5-13 and 5-14 show, respectively, the system dynamics at points D, E and F shown in Fig. 5-6(a). Point D is in the stable region for both models. In addition, it is close to the SB for the HEM and the type of Hopf-B is subcritical. Therefore, besides the stable fixed point, an unstable limit cycle is predicted. Numerical simulations confirm these findings, as shown in Figures 5-12(a) and 5-12(b). The small amplitude perturbation ($ds_2 = 0.1$) decays to the fixed point (Fig. 5-12(a)), and the large amplitude perturbation ($ds_2 = 5.0$) leads to growing amplitude oscillations (Fig. 5-12(b)). For the DFM (Fig. 5-12(c)), however, point D is far enough from the SB so that only decaying oscillations are encountered, *i.e.* only a fixed-point attractor exists.

Numerical integration results with parameter values corresponding to point E are shown in Fig. 5-13. This operational point is on the unstable side for the HEM, so that the system evolves with growing amplitude oscillations (Fig. 5-13(a)). However, for the DFM, since point E is on the stable side and close to the SB, and the nature of Hopf bifurcation is subcritical, a fixed point attractor for small amplitude perturbations around the fixed point and an unstable limit cycle for large perturbation amplitude are predicted by the bifurcation analysis. Again, numerical simulations confirm these predictions (Fig. 5-13(b-c)). Finally, point F is a trivial unstable fixed point for both models, and Fig. 5-14(a, b) shows its dynamics.

It should be noted that, in the case of subcritical Hopf bifurcation, the strip close to the SB where unstable limit cycles exist is very narrow. However, for the supercritical case, the strip that comprises stable limit cycles is quite wide. This means that it is much easier to identify a stable limit cycle than an unstable limit cycle.

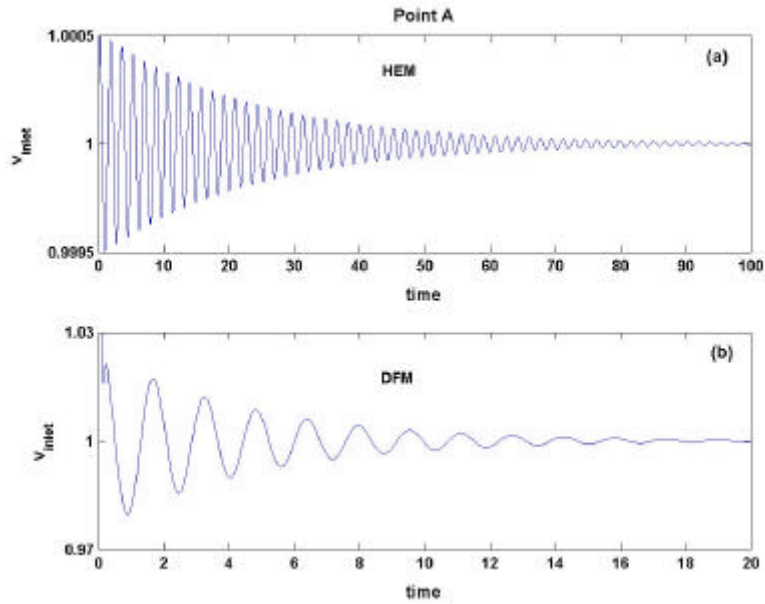


Figure 5-9. Time evolution of liquid inlet velocity $v_{inlet}(t)$ for parameter values corresponding to point A: a) for Homogenous Equilibrium Model (HEM), b) for Drift Flux Model (DFM).

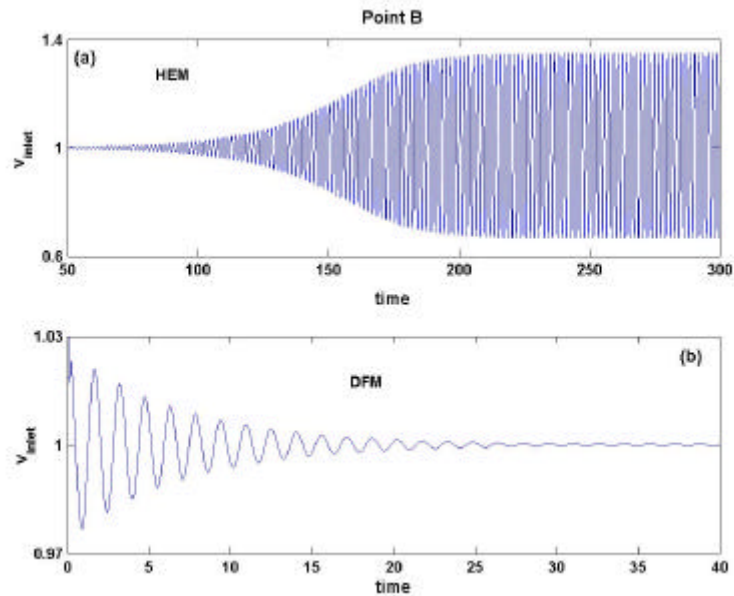


Figure 5-10. Time evolution of liquid inlet velocity $v_{inlet}(t)$ for parameter values corresponding to point B: a) for Homogenous Equilibrium Model (HEM), b) for Drift Flux Model (DFM).

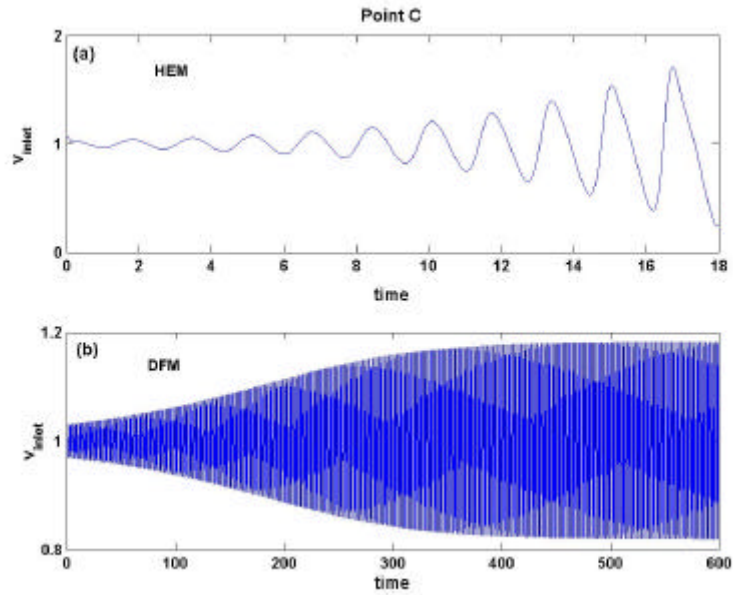


Figure 5-11. Time evolution of liquid inlet velocity $v_{inlet}(t)$ for parameter values corresponding to point C: a) for Homogenous Equilibrium Model (HEM), b) for Drift Flux Model (DFM).

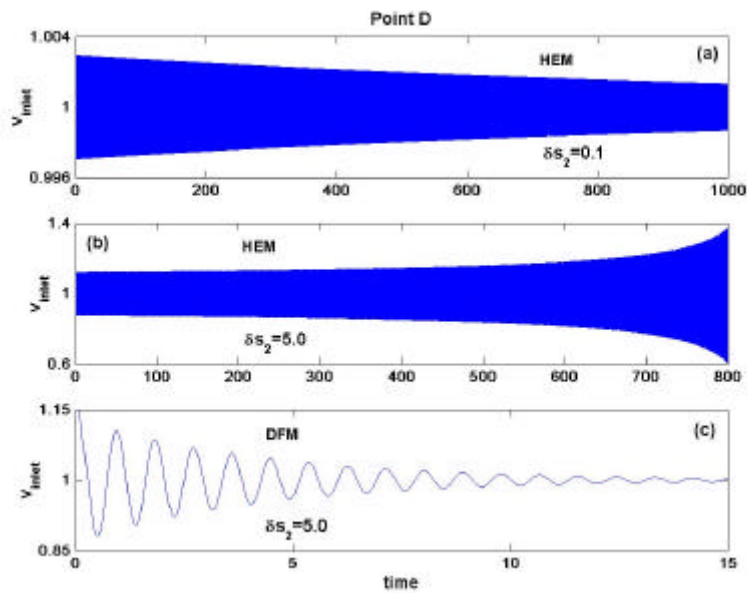


Figure 5-12. Time evolution of liquid inlet velocity $v_{inlet}(t)$ for parameter values corresponding to point D: a-b) for Homogenous Equilibrium Model (HEM) with, respectively, small and large perturbation amplitudes, c) for Drift Flux Model (DFM).

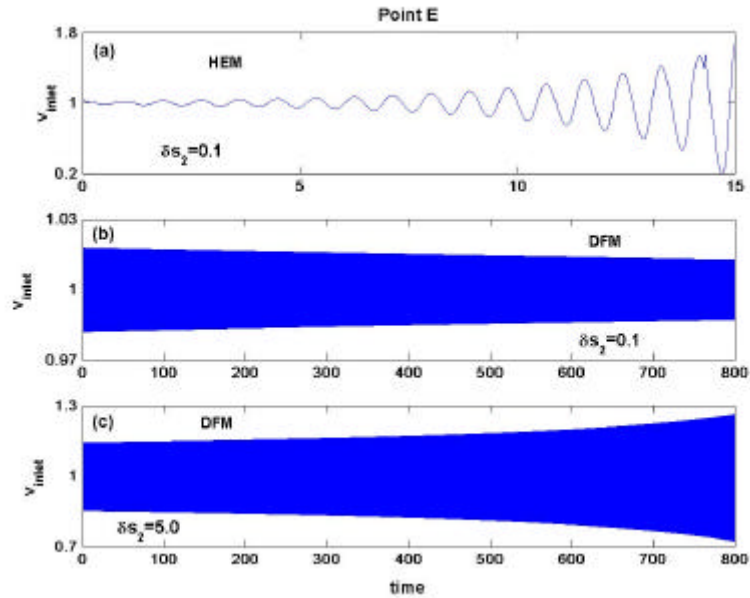


Figure 5-13. Time evolution of liquid inlet velocity $v_{inlet}(t)$ for parameter values corresponding to point E: a) for Homogenous Equilibrium Model (HEM), b-c) for Drift Flux Model (DFM) with small and large perturbation amplitudes, respectively.

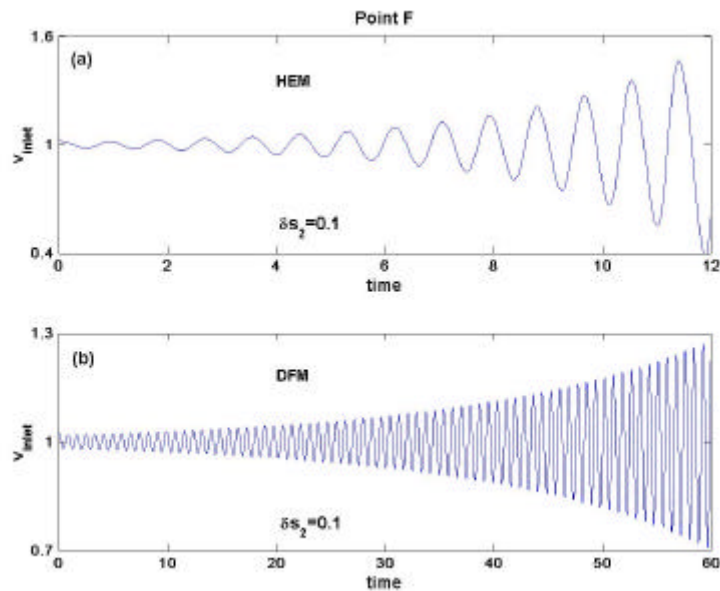


Figure 5-14. Time evolution of liquid inlet velocity $v_{inlet}(t)$ for parameter values corresponding to point F: a) for Homogenous Equilibrium Model (HEM), b) for Drift Flux Model (DFM).

5.5 SENSITIVITY ANALYSIS

5.5.1 Semi-Analytical Bifurcation Analysis

Sensitivity of the stability boundary to design and operational parameters for heated channels with two-phase flow has been studied extensively [13,16,17]. In practice, it is found that the oscillation amplitude for some parameter values continues to grow, while under other conditions the oscillation amplitude saturates. Clearly, the choice of parameter values can lead to stable amplitude oscillations or to growing amplitude oscillations. Nonlinear dynamics, and specifically Hopf bifurcation theory explains these experimental facts. Hence, this section is devoted to a design and operational parameter sensitivity analysis conducted with the current model with $C_0 = 1.0$ and $V_{gj} = 0.0$. The results obtained in terms of stability boundaries in the $N_{sub} - N_{pch}$ plane confirm that the inlet loss coefficient (K_{inlet}), the Froude number²⁷ (Fr) and the single-phase friction factor (N_{f1}) have stabilizing effects (Fig. 5-15(a), Fig. 5-17(a) and Fig. 5-18(a), respectively), and that the two-phase friction factor (N_{f2}) and the exit loss coefficient (K_{exit}) have destabilizing effects (Fig. 5-19(a) and Fig. 5-16(a), respectively).

Much more significant than the effects, studied extensively earlier, of these parameters on the SB are their effects on the nature of Hopf bifurcation. Thus, for example, Fig. 5-15(b) indicates that K_{inlet} can significantly affect the type of bifurcation that occurs as the SB is crossed. It is seen that, for lower values of K_{inlet} (say 4.0), the nature of Hopf bifurcation along the SB in the $N_{sub} - N_{pch}$ plane is subcritical for $N_{sub} < 1.9$ and supercritical for higher values of N_{sub} . For higher values of K_{inlet} (say 20.0), the nature of HB along the entire SB becomes subcritical, which means that growing oscillations are expected, for a large enough perturbation, everywhere in the stable region close to the SB.

In addition, the Fr number also shows considerable impact on the nature of Hopf bifurcation. Thus, Fig. 5-17(b) shows that at higher values of Fr number²⁸ (say around 0.033), the nature of Hopf bifurcation along the SB in the $N_{sub} - N_{pch}$ plane is subcritical for $N_{sub} < 3.15$ and supercritical for higher values of N_{sub} . At a lower Fr number (say 0.015), the supercritical region shrinks, and the Hopf bifurcation is subcritical along the

²⁷ Froude number is inversely proportional to the channel length.

²⁸ smaller channel length.

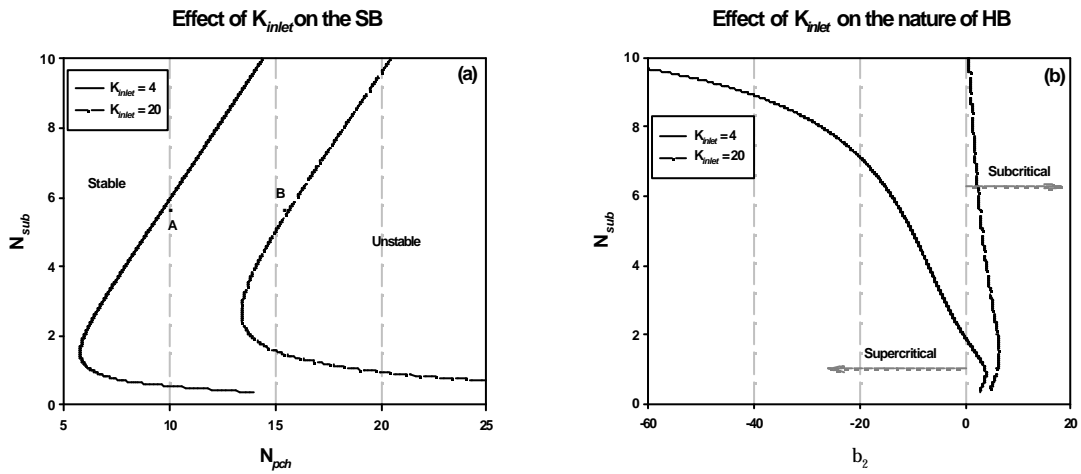


Figure 5-15. Variation of K_{inlet} : a) Stability boundaries in $N_{sub} - N_{pch}$ plane, b) nature of Hopf bifurcation in $N_{sub} - b_2$ plane.

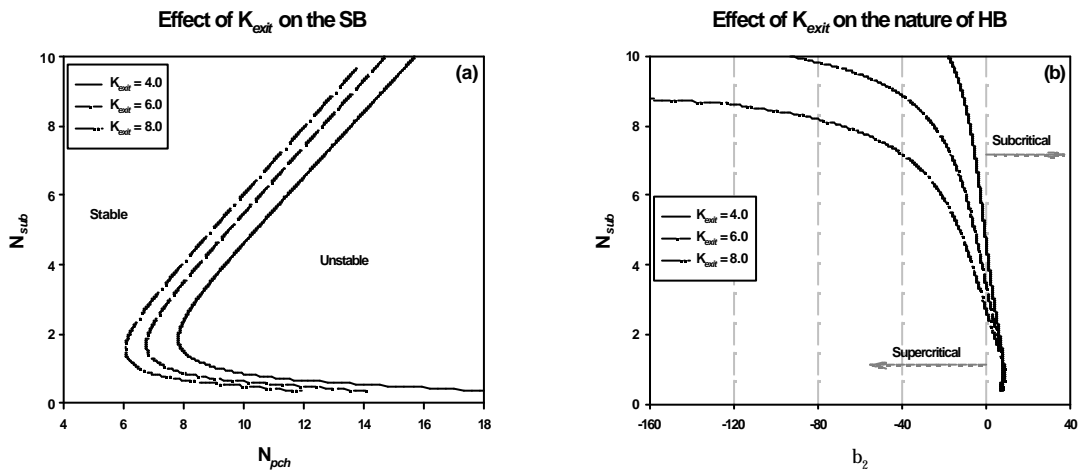


Figure 5-16. Variation of K_{exit} : a) Stability boundaries in $N_{sub} - N_{pch}$ plane, b) nature of Hopf bifurcation in $N_{sub} - b_2$ plane.

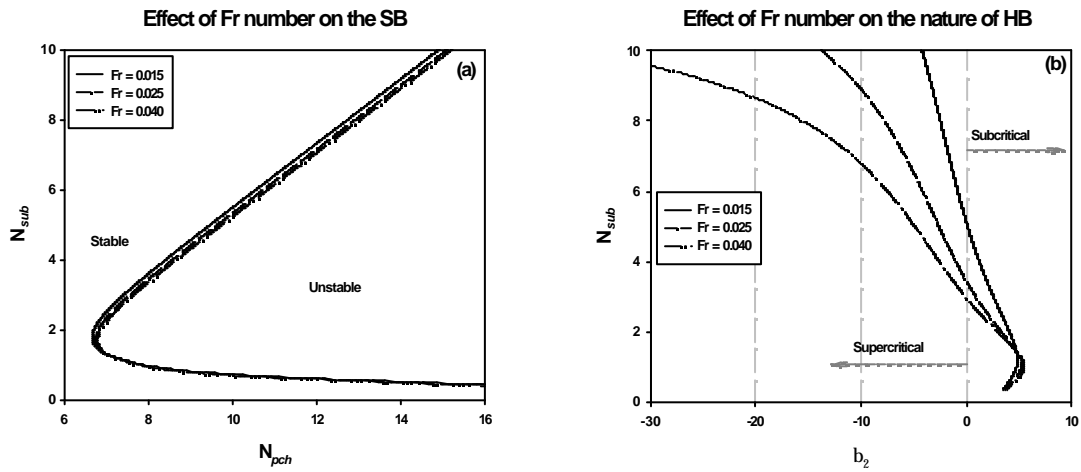


Figure 5-17. Variation of Fr number: a) Stability boundaries in $N_{sub} - N_{pch}$ plane, b) nature of Hopf bifurcation in $N_{sub} - b_2$ plane.

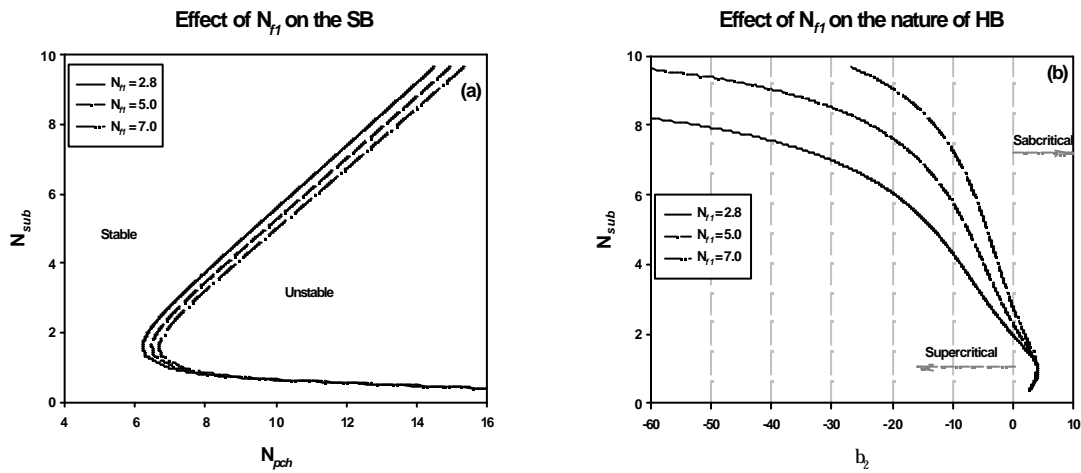


Figure 5-18. Variation of N_{f1} : a) Stability boundaries in $N_{sub} - N_{pch}$ plane, b) nature of Hopf bifurcation in $N_{sub} - b_2$ plane.

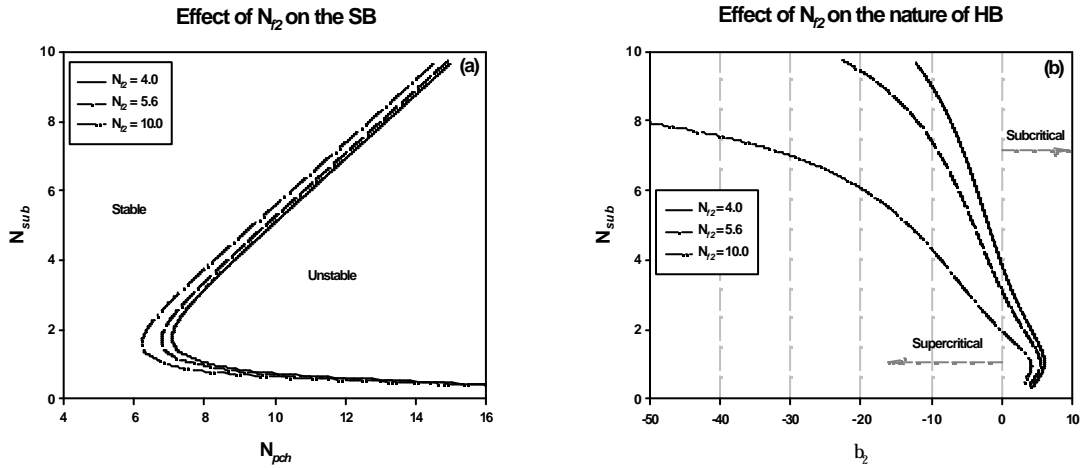


Figure 5-19. Variation of N_{f2} : a) Stability boundaries in $N_{sub} - N_{pch}$ plane, b) nature of Hopf bifurcation in $N_{sub} - b_2$ plane.

SB for $N_{sub} < 5.0$ and supercritical for higher values (Fig. 5-17(b)). This finding may be of considerable importance in design considerations for natural circulation reactors. In the ranges analysed, the other design parameters were found to have relatively small effects on the nature of Hopf bifurcation (Fig. 5-16(b), Fig. 5-18(b) and Fig. 5-19(b)). Overall, the present study has clearly underlined the parametric dependence of the nature of bifurcation, thus indicating the need for its being taken into account more explicitly in the design and operational analyses of future BWR systems.

5.5.2 Numerical Simulation

Additional numerical integrations have been carried out to illustrate the findings of the sensitivity analyses conducted using the bifurcation approach. Examples of three typical simulations are shown in Figs. 5-20 and 5-21. Numerical integrations with parameter values corresponding to point A in Fig. 5-15(a) ($K_{inlet} = 4.0, N_{sub} = 4.04, N_{pch} = 8.0$), as expected, lead to stable limit cycle oscillations (see Fig. 5-20). Two different numerical simulations were carried out with parameter values corresponding to point B in Fig. 5-15(a) ($K_{inlet} = 20.0, N_{sub} = 4.04, N_{pch} = 14.0$). Starting from an initial condition close

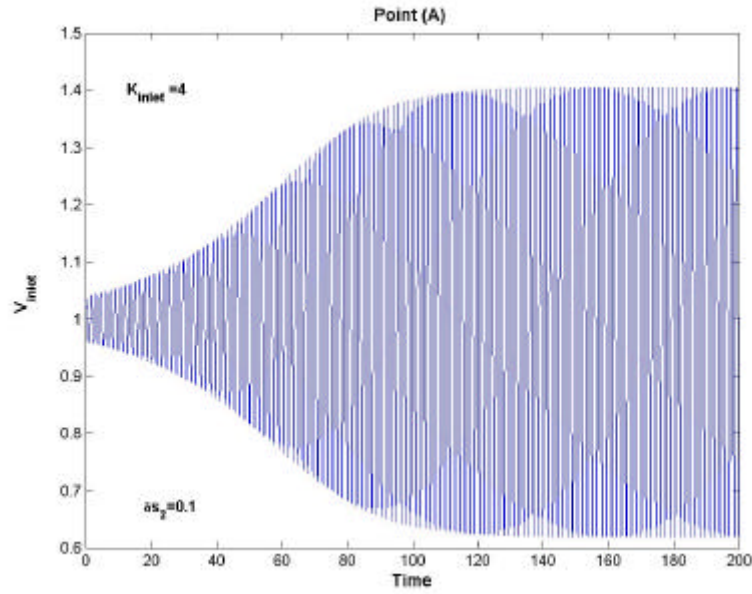


Figure 5-20. Results of numerical simulations for a supercritical Hopf bifurcation leading to a stable limit cycle oscillation at point A in the unstable region shown in Fig. 5-15(a).

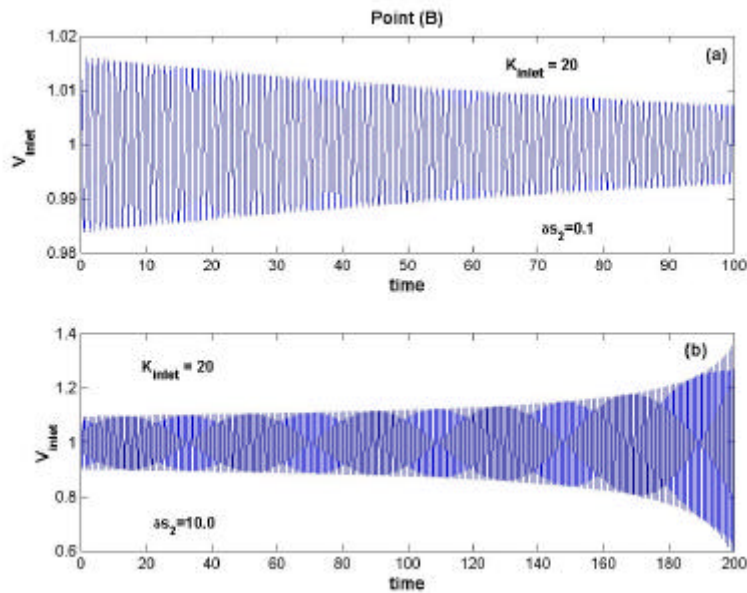


Figure 5-21. Results of numerical simulation for a subcritical Hopf bifurcation at point B in the stable region shown in Fig. 5-15(a): (a) small amplitude perturbation ($d s_2 = 0.1$) decays to the stable fixed point, (b) large amplitude perturbation ($d s_2 = 10.0$) leads to growing amplitude oscillations.

to the fixed point (small perturbation), the oscillations are found to decay to the fixed point (Fig. 5-21(a)). However, oscillations grow in amplitude for the same set of parameter values when the initial conditions are far from the stable fixed point (Fig. 5-21(b)).

5.6 SUMMARY AND CONCLUSIONS

The new model developed for a heated channel using drift flux representation for the two-phase flow has been validated against appropriate experimental data and its performance has been compared with that of several other models that were developed earlier to simulate density wave oscillations. It has been found that the current thermal-hydraulic model is in good agreement with the experimental data for large N_{sub} , and for lower values of N_{sub} , agrees with these better than do most of the other models.

Stability and bifurcation analyses have been performed using the bifurcation analysis code BIFDD, stability boundaries and bifurcation characteristics being determined in the $N_{sub} - N_{pch}$ and $N_{sub} - \mathbf{b}_2$ plane, respectively. Results of the bifurcation analysis along these stability boundaries clearly show that both sub- and supercritical Hopf bifurcations can be expected. The impact of the parameters of the drift flux model (C_0 and V_{gj}) has been investigated in this context. While the SB is found to be sensitive to values of both C_0 and V_{gj} , the nature of Hopf bifurcation for lower values of N_{sub} is found to be considerably more sensitive to the value of V_{gj} . The above results have been confirmed by numerical integration of the set of ODEs.

The sensitivity analysis study carried out shows that the nature of Hopf bifurcation can vary significantly with the values of certain design and operating parameters, *e.g.* K_{inlet} . Clearly, design studies for next generation BWRs stand to benefit from tools such as the bifurcation analysis code BIFDD used in conjunction with appropriate reduced order models. Knowledge acquired, in this context, of the nature of bifurcation in different regions of the design parameter space could help assure adequate safety margins.

REFERENCES

- [1] R. T. Lahey, F. J. Moody, *The Thermal Hydraulics of a Boiling Water Nuclear Reactor*, American Nuclear Society, La Grange Park, IL, 1977.
- [2] J. L. Achard, L. A. Drew, R. T. Lahey, "The Analysis of Nonlinear Density Wave Oscillations in Boiling Channels," *J. Fluid Mech.*, **155**, 213-232, 1985.

- [3] Rizwan-uddin, J. J. Dorning, "Some Nonlinear Dynamics of a Heated Channel," *Nucl. Eng. Des.*, **93**, 1-14, 1986.
- [4] A. Clause, R. T. Lahey, "The Analysis of Periodic and Strange Attractors During Density Wave Oscillations in Boiling Flows," *Chaos, Solitons, and Fractals*, **1, 2**, 167-178, 1991.
- [5] A. A. Karve, Rizwan-uddin, J. J. Dorning, "On Spatial Approximations for Liquid Enthalpy and Two-Phase Quality During Density Wave Oscillations," *Trans. Am. Nucl. Soc.*, **71**, 533, 1994.
- [6] A. A. Karve, Rizwan-uddin, J. J. Dorning, "Stability Analysis of BWR Nuclear-Coupled Thermal-Hydraulics using a Simple Model," *Nucl. Eng. Des.*, **177**, 155-177, 1997.
- [7] B. D. Hassard, "A Code for Hopf Bifurcation Analysis of Autonomous Delay-Differential Equations," *Proc. Oscillations, Bifurcation and Chaos*, Canadian Mathematical Society, pp.447-463, 1987.
- [8] P. Saha, M. Ishii, N. Zuber, "An Experimental Investigation of Thermally Induced Flow Oscillations in Two-Phase Systems," *J. Heat Transfer*, **98**, 616-622, 1976.
- [9] Rizwan-uddin, J. J. Dorning, "Linear and Nonlinear Stability Analyses of Density Wave Oscillation Using the Drift Flux Model," *ANS Proceedings of the 23rd ASME/AIChE/ANS National Heat Transfer Conference*, Am. Nucl. Soc, LaGrange Park, IL, pp.48-61, 1985.
- [10] R.C. Dykhuizen, R. P. Roy, S. P. Kalra, "A Linear Time-Domain Two-Fluid Model Analysis of Dynamic Instability in Boiling Flow Systems," *J. Heat Transfer*, **108**, 222, 1986.
- [11] P. Saha, N. Zuber, "An Analytical Study of the Thermally Induced Two-Phase Flow Instabilities Including the Effect of Thermal Non-Equilibrium," *Int. J. Heat and Mass Transfer*, **21**, 415-426, 1978.
- [12] M. Ishii, N. Zuber, "Thermally Induced Flow Instabilities in Two-Phase Mixtures," *Heat Transfer 1970*, Vol V, pp. B11, Elsevier Publishing Co. (1970).
- [13] Rizwan-uddin, J. J. Dorning, "Some Nonlinear Dynamics of a Heated Channel", *Nucl. Eng. Des.*, **93**, 1-14, 1986.
- [14] A. Inoue, T. Kurosu, M. Yagi, S. Morooka, A. Hoshide, T. Ishizuka, K. Yoshimura, "In-Bundle Void Measurement of a BWR Fuel Assembly by X-ray CT Scanner:

Assessment of BWR Design Void Correlation and Development of a new Void Correlation,” *Proc. ASME/JSME Nuclear Engineering Conference*, Vol. 1, pp. 39-45.

[15] D. Meier, P. Coddington, “Review of Wide Void Correlations against an Extensive Database of Rod Bundle Void Measurements,” *5th International Conference on Nuclear Engineering, ICONE5*, May 26-30, Nice, France, 1997.

[16] J. A. Bouré, A. E. Bergles, L. S. Tong, "Review of Two-Phase Flow Instability," *Nucl. Eng. Des.*, **25**, 165-192, 1973.

[17] G. Yadigaroglu, “Two-Phase Flow Instabilities and Propagation Phenomena,” in *Thermohydraulics of Two-Phase Systems for Industrial Design and Nuclear Engineering*, edited by J. M. Delhaye, M. Giot, M. L. Riethmuller, Hemisphere Publishing Corporation, 1981.

6 NONLINEAR BWR STABILITY ANALYSIS USING THE CURRENT TWO-CHANNEL REDUCED ORDER MODEL

6.1 INTRODUCTION

Various instability events have been observed in different BWRs during the last two decades [1-4]. As mentioned earlier, there are mainly two kinds of BWR instabilities: global or in-phase oscillations, and regional or out-of-phase oscillations. In the in-phase mode, the whole core behaves as one, *i.e.* the local power in each fuel bundle oscillates with the same phase. However, in the case of out-of-phase oscillations, one half of the core behaves out-of-phase from the other half, *i.e.* when the power or flow rises in one half of the core, it decreases in the other half in such a way that the total mass flow remains almost constant. Because of the strong coupling between the neutronics and the thermal-hydraulics via the void and Doppler feedback reactivities, BWR instabilities are also called nuclear-coupled-thermal-hydraulic instabilities.

A wide range of analytical reduced order models have been developed for BWR stability analysis, both in the linear and nonlinear domain as reported in Chapter 2. The most important developments that have formed the basis for the current reduced order model (described in Chapter 4) are reviewed once again here.

Thus, in their pioneering work, March-Leuba *et al.* [5] proposed a simple phenomenological model to qualitatively and quantitatively simulate the behaviour of BWRs based on a point reactor model for the neutron kinetics and a greatly simplified thermal-hydraulic model. In order to keep their model very simple, they assumed that the coolant enters the core at saturation temperature and that the entire recirculation loop can be treated as a single path of fluid with variable cross-sectional area but with constant mass flow rate. This physical model was implemented in a computer code, called LAPUR, using which the authors were able to predict limit cycle oscillations in BWRs with the amplitude of the oscillations being found to be very sensitive to the reactor's operating conditions. Furthermore, their analysis showed that the limit cycles can become unstable and undergo period-doubling bifurcations leading to an aperiodic oscillating behaviour. In a later work [6], they proposed a mechanism for the out-of-phase instabilities observed in BWRs. This mechanism was modelled by upgrading the LAPUR code, numerical

simulations then showing the existence of a region in the operating power-flow map where out-of-phase instabilities are possible even if the fundamental mode is stable.

Using the above model, Muñoz-Cobo and Verdú carried out a purely analytical bifurcation analysis [7]. In effect, this is the first reported work in which bifurcation analysis is performed analytically in the framework of BWR model analysis. Later, Muñoz-Cobo *et al.* extended the work of March-Leuba *et al.* in order to study in-phase and out-of-phase instability phenomena in greater detail [8,9]. This extension based on a *I*-modes model for the neutron kinetics and a thermal-hydraulic treatment based on a homogenous equilibrium model. They showed that in-phase oscillations only appear when the first harmonic mode does not have enough thermal-hydraulic feedback to overcome eigenvalues separation. In addition, they demonstrated the excitation of out-of-phase limit cycle oscillations using numerical integration when the reactivity feedback of the first azimuthal mode is increased.

Karve *et al.* [10,11] developed a more detailed model in which they used *w*-modes for the neutron kinetics, and a homogeneous equilibrium model for the thermal-hydraulic treatment of the two-phase flow. Their model is based on the assumption that the single-phase enthalpy and two-phase quality have time-dependent spatially quadratic profiles. After performing stability analyses for the stability boundary, they carried out bifurcation analyses entirely numerically.

With the aim of better understanding the instabilities in BWRs, especially out-of-phase oscillation phenomena, Zhou and Rizwan-uddin [12] carried out semi-analytical stability and bifurcation analyses with the Karve *et al.* model using the bifurcation code BIFDD. They analysed the role of the pairs of complex conjugate eigenvalues with the largest and second largest real parts in determining the in-phase and out-of-phase modes of oscillations. Numerical simulations were carried out to confirm the results of the stability and bifurcation analyses.

In Chapter 5, the currently developed model, based on a drift flux treatment of the two-phase flow, was used for studying thermal-hydraulic instabilities in a heated channel. By adding to this model a simple point reactor treatment of the neutron kinetics and a model for the fuel heat conduction dynamics, an initial study was conducted in [13] of the single-channel, nuclear-coupled thermal-hydraulic dynamics in a BWR. This investigation, however, was preliminary and, in order to achieve a clearer understanding of both in-phase and out-of-phase mode excitations by investigating their stability limits, it has been

necessary to develop the complete, current reduced order model (see Chapter 4) in which two parallel channels are coupled via spatial modal kinetics to the fundamental and the first azimuthal modes of the neutron flux.

Application of the complete BWR model for achieving the above goal is the subject of the present chapter. Section 6.2 first briefly summarizes the current model. In Section 6.3, it is shown how the properties of the eigenvectors corresponding to the pairs of complex conjugate eigenvalues with the largest and second largest real parts give important information that determines the type of oscillation mode without the need to solve the system of ODEs explicitly. The exact connection to the excitation of the fundamental and first azimuthal modes is established, so that a rigorous quantitative explanation of in-phase and out-of-phase mode excitation results. In addition to analysing the effects of the DFM parameters on the stability boundaries and the nature of Hopf bifurcation, Section 6.4 considers the effects of these parameters on the type of oscillation mode encountered. Furthermore, numerical simulations are carried out at certain operating points to validate the findings of the bifurcation analyses. Finally, a summary and conclusions of this study are presented in the last section.

6.2 SUMMARY OF THE BWR MODEL

The dynamical system that results from the two-channel nuclear-coupled thermal-hydraulic model consists of twenty-two ODEs (see Chapter 4), four from the neutron kinetic model (Eqs. (4.77) to (4.80)), ten that describe the thermal-hydraulic model (five for each channel (Eqs. (4.85) to (4.89))), and eight ODEs that describe the fuel rod heat conduction (two equations for each phase, in each channel (Eqs. (4.81) to (4.84))). The set of 22 ODEs can be written in a compact form as:

$$\dot{X}(t) = F(X; \mathbf{k}) \quad (6.1)$$

where $X(t)$ is the vector of 22 phase variables

$$\begin{aligned} X(t) = & (a_{1,1}(t), a_{2,1}(t), s_{1,1}(t), s_{2,1}(t), v_{inlet,1}(t), T_{1,1,1}(t), T_{2,1,1}(t), T_{1,2,1}(t), T_{2,2,1}(t), n_0(t), \\ & U_0(t), a_{1,2}(t), a_{2,2}(t), s_{1,2}(t), s_{2,2}(t), v_{inlet,2}(t), T_{1,1,2}(t), T_{2,1,2}(t), T_{1,2,2}(t), T_{2,2,2}(t), \\ & n_1(t), U_1(t))^T, \end{aligned} \quad (6.2)$$

and \mathbf{k} is the vector of parameters that includes both the operating and design parameters defined in Appendix C.

$$\mathbf{k} = (N_r, N_r, N_{pch,1f}, N_{pch,2f}, K_{inlet}, K_{exit}, N_{f,1f}, N_{f,2f}, Fr, C_0, V_{gj}) \quad (6.3)$$

The two principal operating parameters chosen for the current stability analysis are N_{sub} and DP_{ext} , the channel inlet subcooling number, and the external pressure drop across the two channels, respectively.

6.3 STABILITY LIMITS FOR IN-PHASE AND OUT-OF-PHASE MODES

Typical numerical values for the design and operating parameters of a General Electric Company (GE) BWR-6, with an approximate power of 1100 Mwe, have been used in this context and are given in Appendix F. Stability and bifurcation analyses are reported in this section using the current 22-equation reduced order model with the drift flux parameters set to correspond to a HEM, *i.e.* $C_0 = 1$ and $V_{gj} = 0.0$.

As mentioned, the stability boundaries are presented here in the $N_{sub} - DP_{ext}$ parameter space. Detailed investigations of the effects of the DFM on the SB, the bifurcation characteristics, and the type of oscillation mode are presented in Section 6.4.

In this study, we consider the gain of the feedback reactivities for different coupling modes (introduced in Appendix E, Section E.3) as follows:

$$fact_{11} = fact_{00} = 1 \quad (6.4)$$

and

$$fact_{01} = fact_{10} = fact \quad (6.5)$$

with $fact > 1$. This means that the feedback reactivities of the coupling between the fundamental and the first modes ($\mathbf{r}_{10}, \mathbf{r}_{01}$) are “artificially” amplified by an amount equal to $fact$. This is due, as shown in Appendix E, to the inability of the linear approximation of

the feedback reactivity model to accurately simulate the values of the feedback reactivities for the coupling between the fundamental and first modes. This assumption is physically consistent since it is well known that $\mathbf{r}_{10}(t) = \mathbf{r}_{01}(t)$. In the author's opinion, the assumption introduced in [9, 12] that considers $\mathbf{r}_{10}(t) \neq \mathbf{r}_{01}(t)$ is not correct from the physical viewpoint. However, since the linear approximation model of the feedback reactivity gives accurate values for the fundamental and first modes themselves, artificial amplification is not needed in these cases ($fact_{11} = fact_{00} = 1$).

6.3.1 Semi-analytical Bifurcation Analysis

A modified version of the code BIFDD that allows the evaluation of all the 22 eigenvalues and their corresponding eigenvectors at each point on the stability boundary has been used for the present study. It turns out that there are two relevant pairs of complex eigenvalues which correspond to the in-phase and out-of-phase oscillation modes. In this subsection, the first and the second stability boundaries are presented for different values of the reactivity feedback for the coupling between the fundamental and first modes, *i.e.* while increasing the bifurcation parameter $fact$, in order to simulate the excitation of the out-of-phase oscillation mode. The first SB corresponds to points in the parameter space at which the real part of the first largest pair of complex eigenvalues is equal to zero, while the second SB corresponds to points in the parameter space at which the real part of the second largest pair of eigenvalues is equal to zero. In other words, the first SB corresponds to the occurrence of a Hopf bifurcation while the second SB is associated with the occurrence of a secondary Hopf bifurcation, or a so-called Neimark bifurcation (see Appendix B). Actually, the second SB has little relevance for the stability of the system, since the system is already unstable once the first SB has been crossed. However, it is crucial for understanding the switch between the in-phase and out-of-phase oscillation modes.

A detailed investigation has been carried out to see as to which oscillation mode is excited during the loss of stability related to the crossing of the first and second SBs. The question to be answered is whether the crossing pair of eigenvalues corresponds to an in-phase or an out-of-phase mode. Zhou and Rizwan-uddin [12] reported that the excitation of out-of-phase oscillations can be explained by the second largest pair of complex eigenvalues whose real part gets closer and closer to zero as the feedback reactivity of the first mode is increased. They looked at the magnitude of the elements corresponding to the

fundamental and first modes in the eigenvectors in order to define the associated mode of oscillation. In the current analysis, it has been found that looking at other elements of the eigenvectors helps in extracting additional information on the type of oscillation mode. More specifically, in the in-phase mode, the corresponding eigenvector (\vec{V}_{in}) has the following properties:

- in-1.* The element corresponding to the fundamental mode, V_{in,n_0} , is much larger than the element corresponding to the first mode, V_{in,n_1} . This was also reported by Zhou and Rizwan-uddin [12].
- in-2.* The elements corresponding to the thermal-hydraulic/heat conduction variables in the first channel have the same sign and the same absolute value as the corresponding elements of the second channel.

On the other hand, the eigenvector (\vec{V}_{out}) corresponding to the out-of-phase mode is characterized by:

- out-1.* The element corresponding to the first mode, V_{out,n_1} , is much larger than the element corresponding to the fundamental mode, V_{out,n_0} . This was also reported by Zhou and Rizwan-uddin [12].
- out-2.* The elements corresponding to the thermal-hydraulic/heat conduction variables in the first channel are of opposite sign and have the same absolute value as the corresponding elements of the second channel.

It is also to be noted that the element corresponding to the fundamental (first) mode in the in-phase mode eigenvector, V_{in,n_0} (V_{in,n_1}), is much larger (smaller) than the corresponding element in the out-of-phase eigenvector, V_{out,n_0} (V_{out,n_1}). However, the elements of the thermal-hydraulic and heat conduction components in the eigenvector associated with the in-phase mode have the same absolute values as the corresponding elements in the eigenvector associated with the out-of-phase mode.

Using some algebra based on linear analysis, a detailed study is now made of the consequences of the eigenvector element properties for both oscillation modes on the behaviour of the system, *i.e.* the evolution of the system variables with time, close to the steady-state solutions. More importantly, a rigorous quantitative explanation will be given

of in-phase and out-of-phase mode excitations and their exact connection to the excitation of the fundamental and first modes of the neutron flux.

Suppose the linearized system of the set of nonlinear ODEs (6.1) is

$$\frac{d\vec{X}(t)}{dt} = A \cdot \vec{X}(t), \quad (6.6)$$

where A is the Jacobian matrix and $\vec{X}(t)$ is the vector variable. To solve this system of equations, suppose the matrix A can be diagonalized. For this, the eigenvalues $\mathbf{I}_i = \mathbf{s}_i + i\mathbf{w}_i$ and their corresponding eigenvectors \vec{V}_i are evaluated. Then the solution of the linearized system can be written as:

$$\vec{X}(t) = \vec{X} + \sum_{i=1}^{22} c_i \vec{V}_i e^{I_i t}, \quad (6.7)$$

where \vec{X} is the steady-state variable vector and c_i is a constant that can be evaluated from initial condition problem.

Generally speaking, it is well known that the dynamical system is asymptotically stable only if real parts of all the eigenvalues of the Jacobian are negative, *i.e.* the oscillation amplitudes of all the variables asymptotically decay with time. On the other hand, the system is asymptotically unstable if the real part of at least one eigenvalue is positive, *i.e.* the oscillation amplitudes of at least some of the variables asymptotically²⁹ grow with time. Suppose that the in-phase oscillation mode is excited, *i.e.* the real part of the eigenvalue associated with the in-phase mode is positive and all the other eigenvalues have negative real parts. The asymptotic solution can then be approximated by:

$$\vec{X}(t) \cong \vec{X} + c_{in} \vec{V}_{in} e^{I_{in} t}, \quad (6.8)$$

where the subscript *in* stands for in-phase. The terms I_{in} and \vec{V}_{in} are, respectively, the eigenvalue and the corresponding eigenvector associated with the in-phase oscillation

²⁹ It could happen that the oscillation amplitudes of certain variables decay initially, and then grow later.

mode. The quantity c_{in} is a constant that can be evaluated from initial conditions. It should be noted that the oscillation amplitude of the solution is directly proportional to the eigenvector, *i.e.* the eigenvector is relevant in determining the oscillation amplitude of the solution.

The fundamental and the first mode solutions can be approximated by:

$$n_0(t) \cong \tilde{n}_0 + c_{in} V_{in,n_0} e^{I_{in} t} \quad (6.9)$$

$$n_1(t) \cong \tilde{n}_1 + c_{in} V_{in,n_1} e^{I_{in} t} \quad (6.10)$$

where $I_{in} = s_{in} + i w_{in}$, $s_{in} > 0$ and $s_i < 0$ for $\forall i = 1, n$ and $i \neq in$. The terms V_{in,n_0} and V_{in,n_1} are the eigenvector elements corresponding to phase variables $n_0(t)$ and $n_1(t)$. As stated above (in-phase eigenvector property *in-1*), the element corresponding to the fundamental mode (V_{in,n_0}) is found to be much larger than the element corresponding to the first mode (V_{in,n_1}), in the eigenvector corresponding to the in-phase mode. Therefore, the oscillation amplitude of the fundamental mode is much larger than the oscillation amplitude of the first mode.

The liquid inlet velocities in channels 1 and 2 can then be written as:

$$v_{inlet,1}(t) \cong \tilde{v}_{inlet,1} + c_{in} V_{in,v_{inlet,1}} e^{I_{in} t} \quad (6.11)$$

$$v_{inlet,2}(t) \cong \tilde{v}_{inlet,2} + c_{in} V_{in,v_{inlet,2}} e^{I_{in} t} \quad (6.12)$$

where $V_{in,v_{inlet,1}}$ and $V_{in,v_{inlet,2}}$ are the eigenvector elements corresponding to phase variables $v_{inlet,1}(t)$ and $v_{inlet,2}(t)$. It should be noted that $\tilde{v}_{inlet,1} = \tilde{v}_{inlet,2}$ because the two channels are similar from the thermal-hydraulic point of view. As stated earlier, the elements corresponding to the inlet velocity variable in channel 1 ($V_{in,v_{inlet,1}}$) and channel 2 ($V_{in,v_{inlet,2}}$), in the eigenvector corresponding to in-phase oscillations, are found to have the same sign and the same absolute value (in-phase eigenvector property *in-2*). Therefore, referring to Eqs. (6.11) and (6.12), the inlet velocities in the two channels oscillate in an in-phase mode.

It needs to be stressed that, even if the out-of-phase mode is not excited in this case, the oscillation amplitude of the first mode grows with time asymptotically. It may actually decay initially³⁰, but then should grow asymptotically. A possible initial decay of the first mode amplitude oscillation can be explained by the contribution of the term associated with the second pair of complex eigenvalues that has a negative real part. In this case, Eq. (6.10) can be written as:

$$n_1(t) \cong \tilde{n}_1 + c_{out} V_{out,n_1} e^{I_{out}t} + c_{in} V_{in,n_1} e^{I_{in}t} \quad (6.13)$$

with $Re(I_{in}) > 0$ and $Re(I_{out}) < 0$. In the initial transient time interval, the term of the second pair of complex eigenvalues ($c_{out} V_{out,n_1} e^{I_{out}t}$) may be dominant because, as reported earlier, V_{out,n_1} is found to be much larger than V_{in,n_1} (about 100 times) and, consequently, decaying oscillations of the first mode are observed. The time evolution of the thermal-hydraulic and heat conduction variables, however, is always growing because here the term of the second pair of complex eigenvalue is almost negligible even in the initial time interval.

In case the out-of-phase mode eigenvalue is dominant, the asymptotic solution will be:

$$\bar{X}(t) \cong \bar{X} + c_{out} \bar{V}_{out} e^{I_{out}t}, \quad (6.14)$$

where the subscript *out* stands for out-of-phase mode. I_{out} and \bar{V}_{out} are, respectively, the eigenvalue and the corresponding eigenvector associated with the out-of-phase oscillation mode. The term c_{out} is a constant that can be evaluated using the initial conditions. As in the in-phase case, the fundamental and the first mode solution can be approximated as:

$$n_0(t) \cong \tilde{n}_0 + c_{out} V_{out,n_0} e^{I_{out}t} \quad (6.15)$$

$$n_1(t) \cong \tilde{n}_1 + c_{out} V_{out,n_1} e^{I_{out}t}, \quad (6.16)$$

³⁰ It may happen that the asymptotic time is very large, which could make the “initial” interval very long.

where $\mathbf{I}_{out} = \mathbf{s}_{out} + i\mathbf{w}_{out}$, $\mathbf{s}_{out} > 0$ and $\mathbf{s}_i < 0$ for $\forall i = 1, n$ and $i \neq out$. The terms V_{out, n_0} and V_{out, n_1} are the eigenvector elements corresponding to phase variables $n_0(t)$ and $n_1(t)$, respectively. As stated earlier (out-of-phase eigenvector property *out-1*), the element corresponding to the first mode (V_{out, n_1}) is found to be much larger than the element corresponding to the fundamental mode (V_{out, n_0}), in the eigenvector corresponding to the out-of-phase mode. Therefore, the oscillation amplitude of the first mode is much larger than the oscillation amplitude of the fundamental mode.

The inlet velocity in both channels can be written as follows:

$$v_{inlet,1}(t) \cong \tilde{v}_{inlet,1} + c_{out} V_{out, v_{inlet,1}} e^{I_{out} t} \quad (6.17)$$

$$v_{inlet,2}(t) \cong \tilde{v}_{inlet,2} + c_{out} V_{out, v_{inlet,2}} e^{I_{out} t} \quad (6.18)$$

In the out-of-phase case, the elements $V_{out, v_{inlet,1}}$ and $V_{out, v_{inlet,2}}$ of the eigenvector are found to have opposite signs and almost the same absolute value (out-of-phase eigenvector property *out-2*). Therefore, referring to Eqs. (6.17) and (6.18), the inlet velocities in both channels oscillate in an out-of-phase mode.

Again it needs to be emphasized that, even if the in-phase mode is not excited in this case, the oscillation amplitude of the fundamental mode grows with time asymptotically, *i.e.* it may decay initially but should grow asymptotically. A possible decay of the fundamental mode amplitude oscillation in the initial time interval can be explained by the contribution of the term associated with the second pair of complex eigenvalues that has a negative real part. In this case, Eq. (6.15) can be written as:

$$n_0(t) \cong \tilde{n}_0 + c_{out} V_{out, n_0} e^{I_{out} t} + c_{in} V_{in, n_0} e^{I_{in} t} \quad (6.19)$$

with $Re(\mathbf{I}_{out}) > 0$ and $Re(\mathbf{I}_{in}) < 0$. In the initial transient time interval, the term of the second pair of complex eigenvalues ($c_{in} V_{in, n_0} e^{I_{in} t}$) may be dominant because, as mentioned above, V_{in, n_0} is found to be much larger than V_{out, n_0} (about 100 times) and, consequently, decaying oscillations of the fundamental mode are observed. However, this is not the case for the time evolution of the other thermal-hydraulic and heat conduction variables, *i.e.*

there are no decaying oscillations in the first time interval because here the term of the second pair of complex eigenvalues is almost negligible even initially.

Shown in Fig. 6-1 are the first and the second SBs in the $N_{sub} - DP_{ext}$ plane, parts (a) and (b) of the figure illustrating their correspondence to the in-phase and out-of-phase oscillation modes as the bifurcation parameter $fact$ is increased from 1 to 2.5. Fig. 6-1(a) shows that, for $fact = 1$, the entire first stability boundary is associated with the in-phase mode, while the entire second stability boundary is associated with the out-of-phase mode. The two SBs are very close for $N_{sub} > 4$, and they become far from each other for lower values of N_{sub} . In Fig. 6-1(b), it is seen that increasing the value of $fact$ to 2.5 makes the SB corresponding to the out-of-phase mode become closer and closer to the SB corresponding to the in-phase mode in the lower branch.

Figure 6-2 shows the case of higher feedback reactivity for the coupling between the fundamental and first modes ($fact = 3.5$), in which the two SBs intersect at point $T(DP_{ext}, N_{sub}) = T(7.38, 1.44)$. In this case, the first SB corresponds to the in-phase oscillation mode for $N_{sub} > 1.40$, and to the out-of-phase mode for $N_{sub} < 1.40$. In other words, if the system loses its stability in the region where $N_{sub} < 1.40$, the first type of instability that will be excited is the out-of-phase oscillation mode. On the other hand, for $N_{sub} > 1.40$, the first type of instability that will be encountered is the in-phase oscillation mode.

Figure 6-3 displays the first stability boundary corresponding to different gains of the feedback reactivity for the coupling between the fundamental and the first modes. The stability boundaries and the bifurcation curve for $fact$ equalling 1 and 2.5 cannot be distinguished. As seen earlier, further increasing the feedback for the coupling between the fundamental and first modes ($fact = 3.5$) causes the out-of-phase mode to be excited. Consequently, the lower branch of the SB that was associated with the in-phase mode becomes associated with the out-of-phase mode.

Points A and B are two operational points that will be investigated, in Subsection 6.3.2, using numerical integration of the set of system equations. As shown in Fig. 6-3(a), point A is stable for $fact$ equal to 1 or 2.5. However, it is out-of-phase unstable³¹ for $fact = 3.5$. In addition, point A is in the region where a supercritical Hopf bifurcation is expected (see

³¹ This means that the out-of-phase mode is excited at the operational point A.

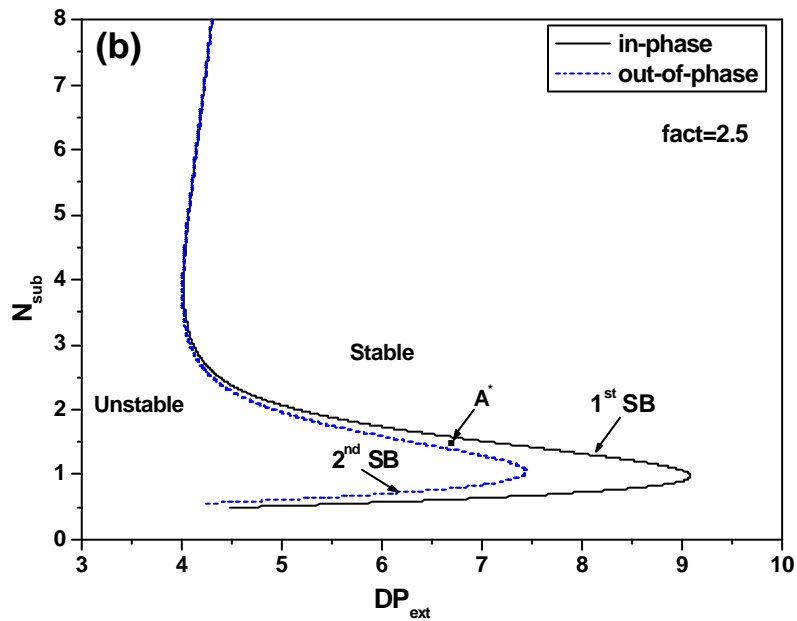
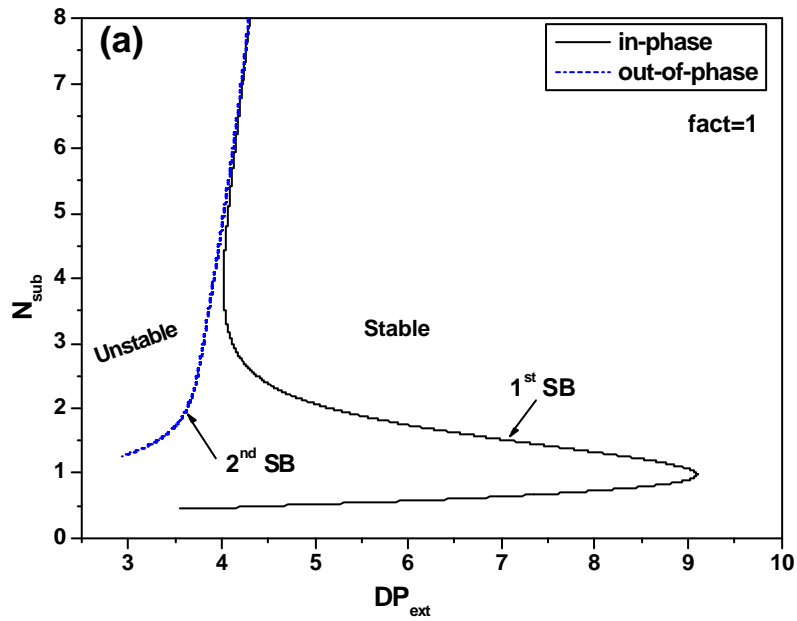


Figure 6-1. First and second stability boundaries, and their correspondence to the in-phase and out-of-phase modes. In both parts of the figure, the first stability boundary corresponds to the in-phase mode of oscillation and the second stability boundary corresponds entirely to the out-of-phase oscillation mode.

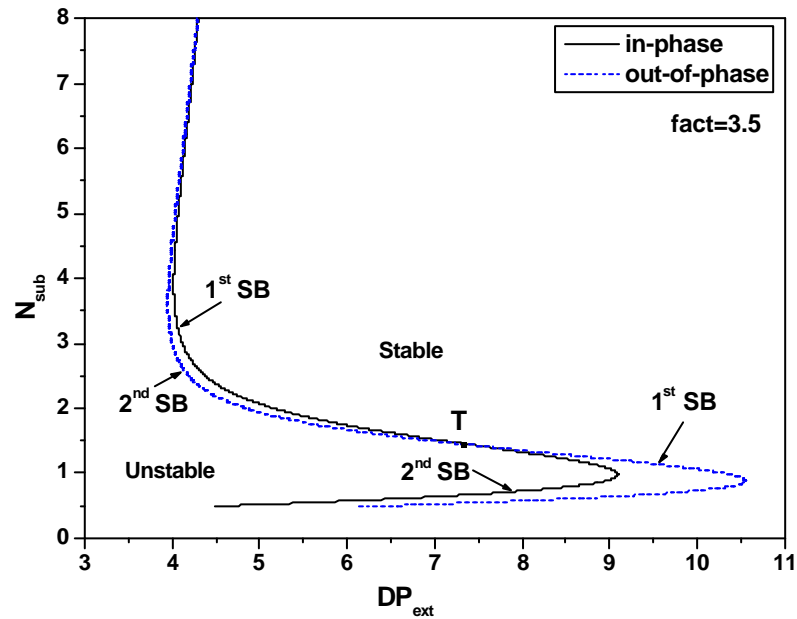


Figure 6-2. First and second stability boundaries, and their correspondence to the in-phase and out-of-phase modes. For $fact = 3.5$, the first stability boundary corresponds to the in-phase mode for $N_{sub} > 1.40$ and to the out-of-phase mode for $N_{sub} < 1.40$.

Fig. 6-4). Therefore, an out-of-phase stable limit cycle oscillation is expected here. Point B, for all $fact$ -value cases, is located in a stable region where subcritical bifurcation is expected.

The SBs shown in Fig. 6-3(b) are the transformed SBs from $N_{sub} - DP_{ext}$ to the steady-state values of neutron number density vs. total inlet velocity (power-flow) plane $n_{0s} - v_{inlet,s}$. It is clear from Figs. 6-3(a) and 3(b) that underestimating the feedback reactivity for the coupling between the fundamental and first modes leads to non-conservative results. For instance, point C, which is predicted to be a completely stable operational point under $fact = 1$ conditions, becomes an out-of-phase unstable operating point if the gain of the feedback reactivity coupling between the fundamental and first modes is increased sufficiently to represent realistic conditions corresponding, for instance, to a bowl-shaped radial power distribution³² [3].

³² resulting, for example, from a certain control rod configuration

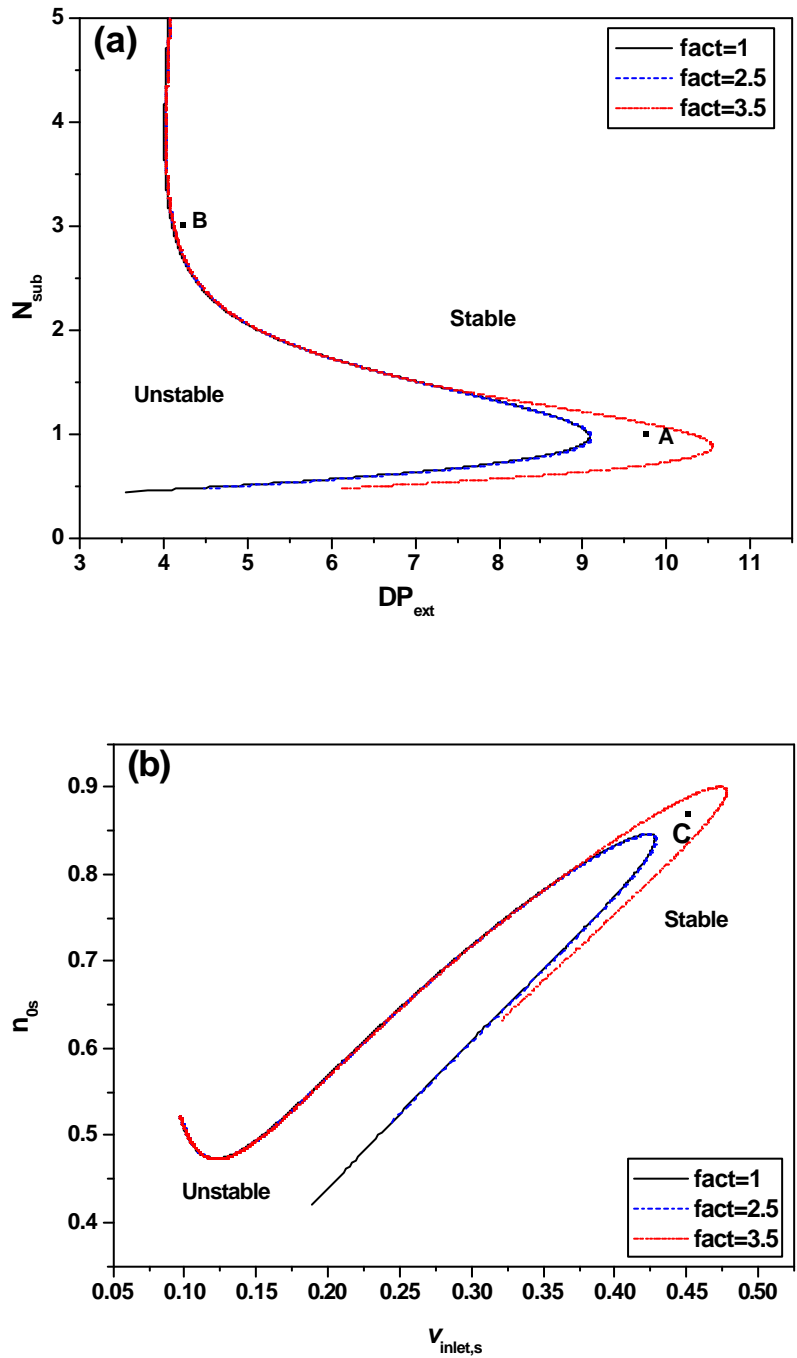


Figure 6-3. a) The first stability boundaries for different feedback reactivities for the first mode in the $N_{sub} - DP_{ext}$ plane. b) Transformed stability boundaries in the power-flow map (n_{0s} and $v_{inlet,s}$ are the steady-state values of the neutron density of the fundamental mode and the total inlet velocity, respectively).

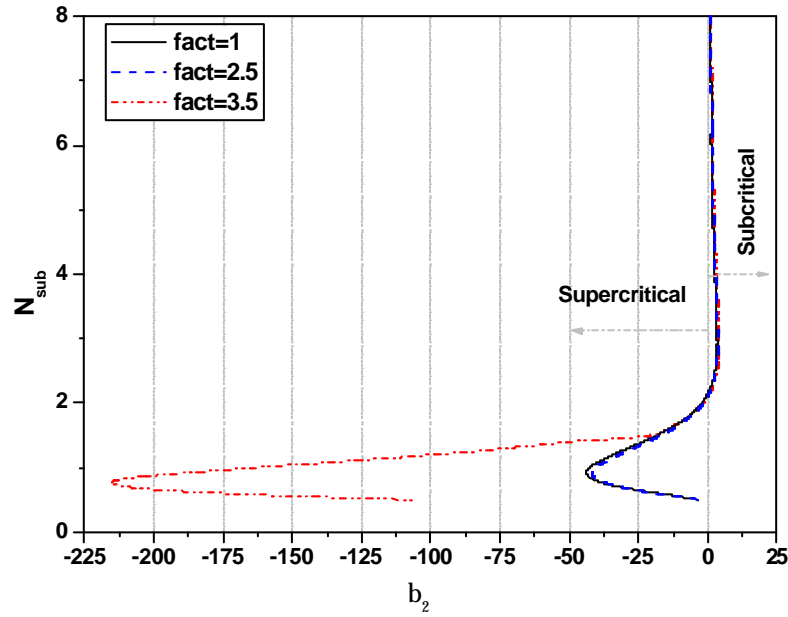


Figure 6-4. Nature of Hopf bifurcation in the $N_{sub} - b_2$ plane. Bifurcation is supercritical for $b_2 < 0$, and subcritical for $b_2 > 0$.

It should be pointed out that the typical value of the subcooling number N_{sub} for normal operational conditions for a BWR cannot exceed 2.0, which corresponds to 30 degrees of temperature difference between the inlet liquid temperature and the saturation temperature. In the current study, higher values of N_{sub} were also investigated in order to try to understand the physical mechanisms behind the transition between the in-phase and out-of-phase modes as a given parameter is changed, especially in a region where the two SBs are very close to each other.

6.3.2 Numerical Simulation

For independent confirmation of the results of the bifurcation analyses, and to evaluate the system behaviour in regions away from the SB, a MATLAB code has been developed to numerically integrate the set of the 22 ODEs using the Gear's algorithm (see Subsection 2.7.3). Results are presented here for parameter values corresponding to the operational points A and B shown in Fig. 6-3(a) with $fact = 3.5$. Figure 6-5 shows the time evolution of normalized components of the fundamental ($n_0(t)$) and the first modes ($n_1(t)$), the inlet liquid velocity in both channels ($v_{inlet,1}$ and $v_{inlet,2}$), and the total liquid inlet velocity v_{inlet} ,

with parameter values corresponding to point A. As expected, at point A, the system is out-of-phase unstable but in-phase stable, *i.e.* the out-of-phase mode is dominant. Moreover, point A is in the supercritical Hopf bifurcation region. Hence, the oscillation amplitude for each of the variables grows to a stable limit cycle. The oscillation amplitude of the first mode is larger than that of the fundamental mode (Fig. 6-5(a)).

Fig. 6-5(b) clearly shows the out-of-phase mode oscillation between the inlet liquid velocities of the two channels. The total mass flow (v_{inlet}) is oscillating with very small amplitude (1%) and can, as such, be considered constant (Fig. 6-5(c)). This agrees with previous findings that state that in an out-of-phase oscillation mode the total mass flow remains almost constant, although the individual mass flows are oscillating. This is because the two oscillating core regions adjust their flows to maintain the pressure drop across the core constant in time and in space. In fact, the 1% oscillation amplitude of the total flow rate is related to the fundamental mode that shows a very small stable limit cycle oscillation amplitude. It should be pointed out that, although the in-phase mode is not excited³³ at point A, the oscillation amplitude of the fundamental mode is increasing but with very small amplitude compared to the first mode.

Fig. 6-6 shows the results of numerical integration for the operational point A* in Fig. 6-1(b). It is clearly seen that, although the out-of-phase mode is not excited³⁴ (only the in-phase is), the first mode amplitude grows asymptotically (time > 170 s) but with an amplitude much smaller than that of the fundamental mode. This can only be explained by the argumentation presented earlier, *viz.* that in the initial time interval [0, 170s] the first mode amplitude is decaying because of the dominance of the term of the second pair of complex eigenvalues with negative real part (associated in this case with the out-of-phase mode, $c_{out} V_{out,n_1} e^{I_{out}t}$), and that later the first mode amplitude grows with time because of the dominance of the term of the first pair of complex eigenvalues with positive real part (associated in this case with the in-phase mode, $c_{in} V_{in,n_1} e^{I_{in}t}$). This leads to the following important statement: if the in-phase (out-of-phase) mode is excited, this does not mean that

³³ This means that the real part of the pair of complex eigenvalues associated with the in-phase mode is negative.

³⁴ This means that the real part of the pair of complex eigenvalues associated with the out-of-phase mode is negative.

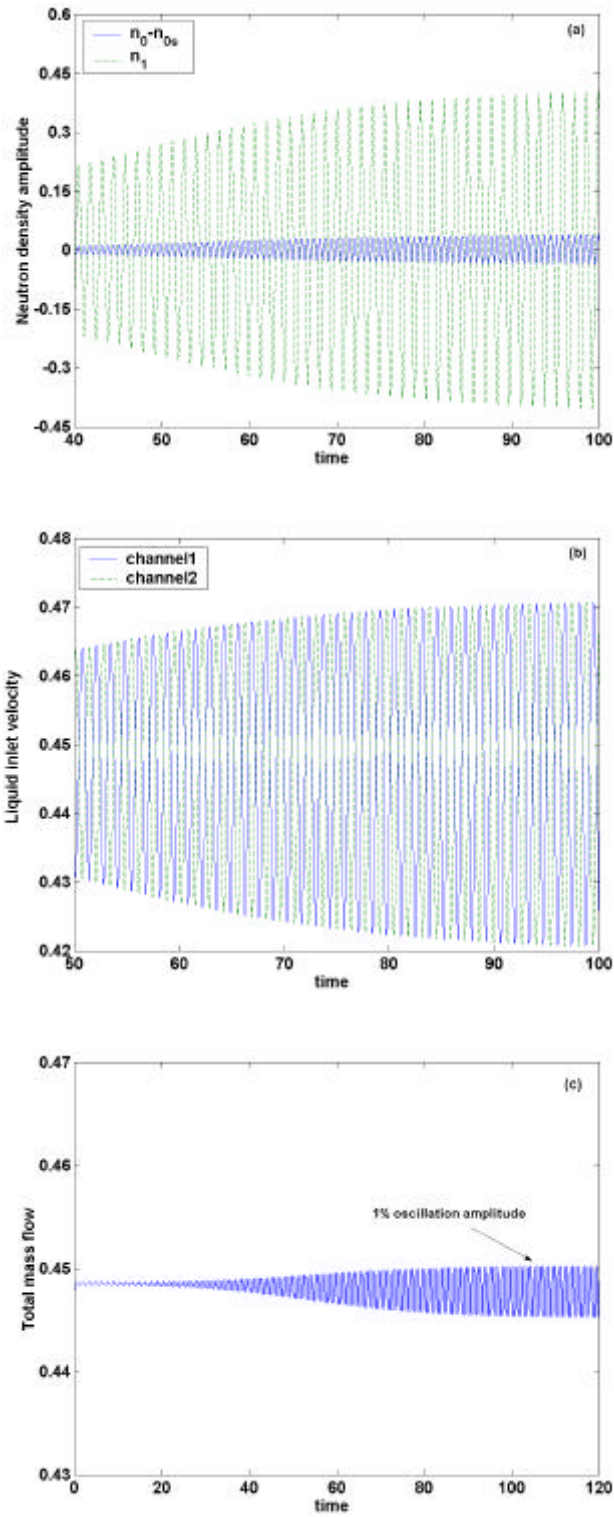


Figure 6-5. a) Time evolution of $n_0(t) - n_{0s}$ and $n_1(t)$ at point A. b) Time evolution of inlet flow velocity in the two channels. c) Time evolution of the total inlet flow velocity.

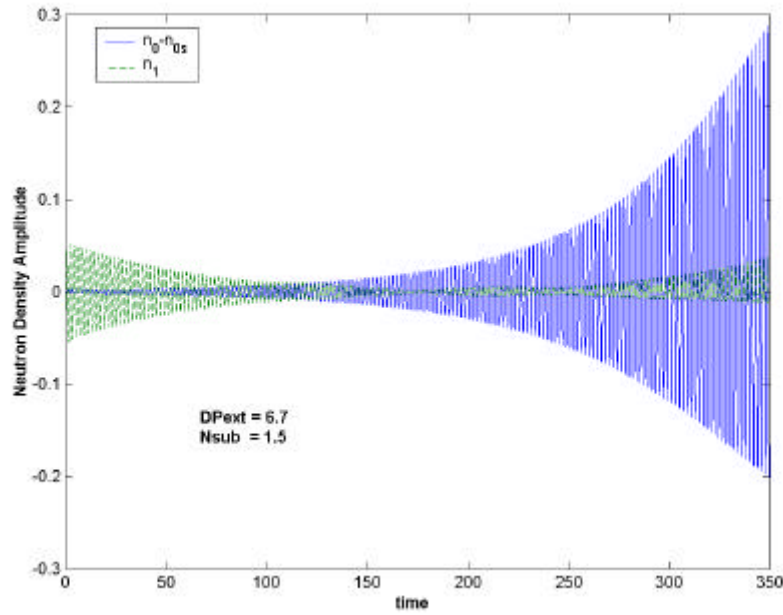


Figure 6-6. Time evolution of $n_0(t) - n_{0s}$ and $n_1(t)$ at point A^* in Fig. 6-1(b). The first mode amplitude is decaying from 0 to 170s, then starts to grow but with much smaller amplitude than that of the fundamental mode.

the first mode $n_1(t)$ (fundamental mode $n_0(t)$) is not excited—as many researchers suppose—but rather, it only means that the oscillation amplitude of the fundamental (first) mode is larger than that of the first (fundamental) mode.

As regards point B in Fig. 6-3(a), it is clear that here the first SB corresponds to the in-phase mode, the second SB being associated with the out-of-phase mode (see Fig. 6-2) and the two being very close. Point B is in the stable region and close to the SB, and the type of Hopf bifurcation to be expected is subcritical. Therefore, beside the stable fixed point, an unstable limit cycle is predicted. Numerical simulations confirm these findings, as shown in Figs. 6-7 and 6-8. The small amplitude perturbation in Fig. 6-7 ($\mathbf{d}v_{inlet,1} = 0.05$) decays to the fixed point, and the large amplitude perturbation ($\mathbf{d}v_{inlet,1} = 0.7$) in Fig. 6-8 leads to growing amplitude oscillations for $n_0(t)$ and $v_{inlet,1}(t)$. However, in both cases, the first mode decreases rapidly. As discussed above, this is because of the dominance of the term of the second pair of complex eigenvalues, $c_{out} V_{out,n_1} e^{l_{out} t}$, with $\mathbf{l}_{out} < 0$.

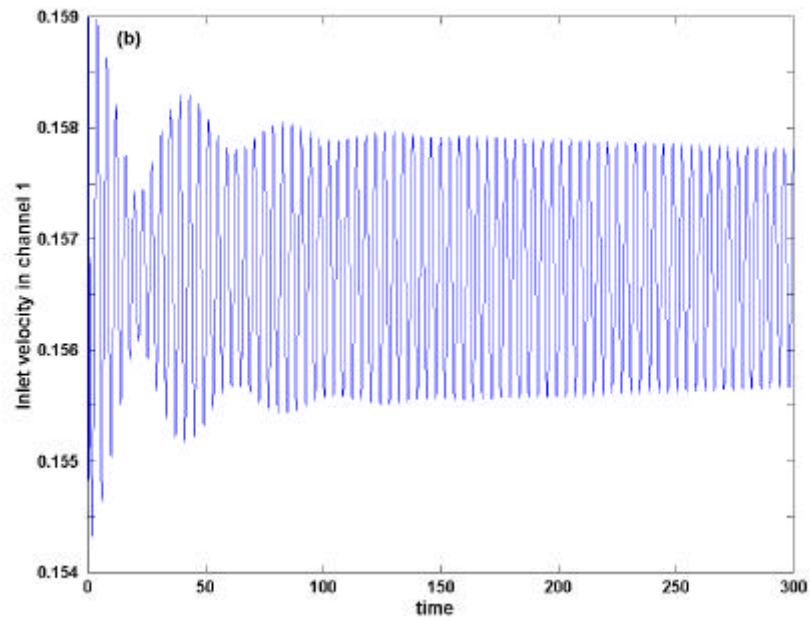
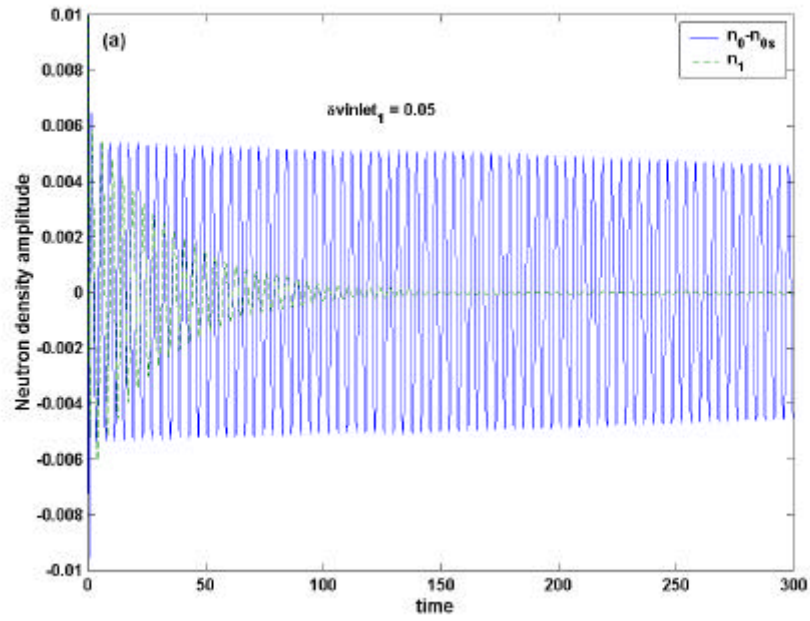


Figure 6-7. a) Time evolution of $n_0(t) - n_{0s}$ and $n_1(t)$ at point B for small perturbation amplitude. b) Corresponding time evolution of inlet flow velocity in channel 1.

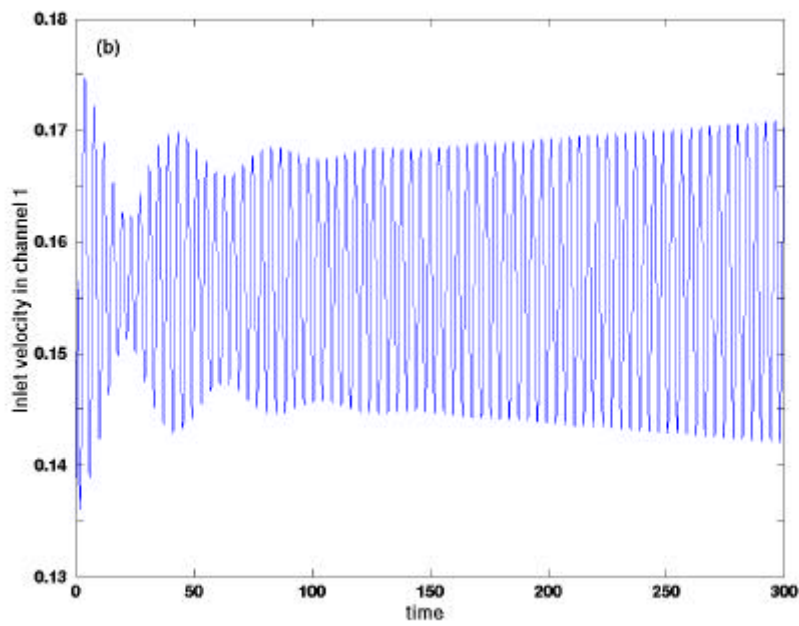
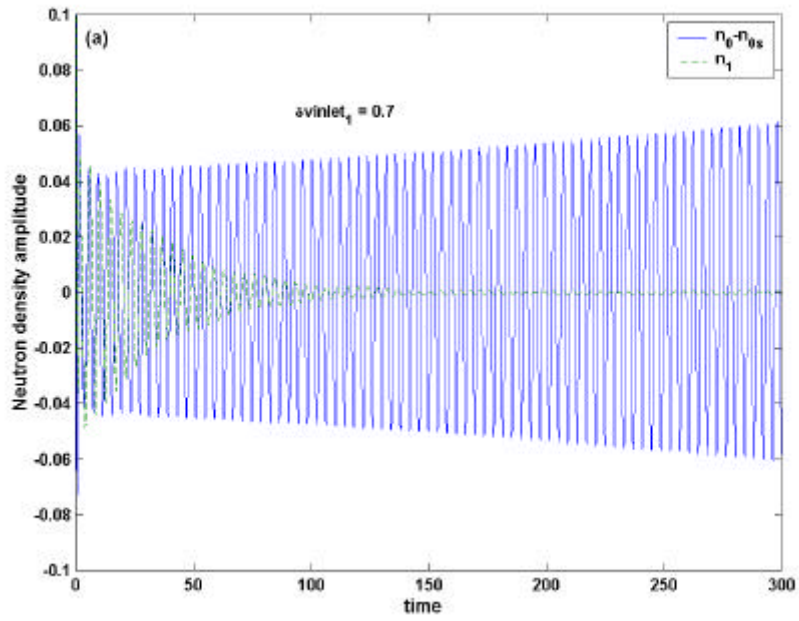


Figure 6-8. a) Time evolution of $n_0(t) - n_{0s}$ and $n_1(t)$ at point B for large perturbation amplitude. b) Corresponding time evolution of inlet flow velocity in channel 1.

The evolution of flow inlet velocity in channel 1 is seen to experience the beating phenomenon³⁵ in the first 80 seconds (Fig. 6-7(b) and 6-8(b)), because during this time interval the term of the pair of complex eigenvalues associated with out-of-phase mode ($c_{out} V_{out, v_{inlet,1}} e^{I_{out} t}$) has a comparable value to that associated to the in-phase mode ($c_{in} V_{in, v_{inlet,1}} e^{I_{in} t}$). This leads to a combined impact of the two different natural frequencies associated with the two modes.

6.3.3 Conclusions

The eigenvector properties presented in Subsection 6.3.1 (*in-1*, *in-2*, *out-1*, and *out-2*), *i.e.* the properties of the elements of the eigenvectors associated with the in-phase and out-of-phase oscillation modes, provide clear evidence that these instabilities involve not only the fundamental and first modes of the neutron flux, but rather all the system components (*viz.* variables of the neutron kinetics, the thermal-hydraulics, and the heat conduction). Therefore, *a statement like: “Excitation of the fundamental (first) mode implies that the in-phase (out-of-phase) oscillation mode is excited” is not completely correct. It is also necessary that the amplitude of the fundamental (first) mode is much larger than that of the first (fundamental) mode.* Thus, it is seen from the system behaviour observed at operational point A (A*), as shown in Fig. 6-5 (Fig. 6-6), that the fundamental (first) mode may be unstable even though in-phase (out-of-phase) oscillations are not excited. Moreover, as mentioned, the thermal-hydraulic and heat conduction variables (components) are also involved in the definition of the state (eigenvector properties).

In the author’s opinion, this can be understood in the frame of the center manifold theorem (see Chapter 3), in which the full system of 22 ODEs is reduced and lumped at the bifurcation point into just two ODEs (Poincaré normal form, see Subsection 3.1.2) which represent a combination of all the original system variables (22 variables). Consequently, this lumping is translated into eigenvector properties which reflect all the system components. *This is a very clear argument for the fact that in-phase and out-of-phase oscillations are whole-system mechanisms and, as such, are not just limited to the excitation of the fundamental and/or the first mode.* Thus, this leads one to reformulate the definition of the in-phase and out-of-phase states based on the properties of the corresponding eigenvectors as follows: *The in-phase (out-of-phase) oscillation mode is an intrinsic state that the reactor can fall into, in which the amplitude of the fundamental*

³⁵ It is well known that the beating phenomenon is observed when two or more frequencies exist.

(first) mode is larger than that of the first (fundamental) mode, and the thermal-hydraulic and heat conduction variables in half of the core have the same (opposite) sign and the same absolute value as the corresponding variables in the other half of the core.

It should be emphasized that, during numerical simulation, it was found to be more difficult to identify an unstable limit cycle than a stable one. As reported in Section 5.4, this is mainly because the strip adjacent to the SB which comprises unstable limit cycles is much narrower than that comprising stable limit cycles.

6.4 THE EFFECTS OF USING A DRIFT FLUX VERSUS HOMOGENEOUS EQUILIBRIUM MODEL

The aim in this section is to perform a comparative study between the use of HEM and DFM for the modelling of the two-phase flow in the current BWR reduced order model. For this, an investigation of the effects of the DFM parameters—the void distribution parameter C_0 and the drift velocity V_{gj} —on the SB, the nature of PAH bifurcation, and on the type of oscillation mode (in-phase or out-of-phase) is carried out.

6.4.1 Effects of the drift flux parameters on the SB and the nature of Hopf bifurcation

Stability boundaries were first generated in the $N_{sub} - DP_{ext}$ operating parameter plane. They were then transformed to the steady-state neutron density vs. steady-state inlet velocity ($n_{0s} - v_{inlet,s}$) plane (power-flow map). For this comparative HEM/DFM study, the numerical values used for the parameters are the same as in the last section, *viz.* those used by Karve (Appendix F). In addition, throughout this study, *fact* is set equal to 1. The DFM parameters C_0 and V_{gj} are varied in the ranges [1.0, 1.03] and [0.0, 0.1], respectively. The justification for this choice is provided by:

- The validation of the thermal-hydraulic model against experimental data and several other analytical models, as carried out in Section 5.3, shows that a value of C_0 between 1 and 1.08, depending on the inlet flow, can adequately fit the experimental results. Considering further that a typical BWR fuel assembly has a rather complex geometry (grid spacers, etc.), one may justifiably lower the maximum value of C_0 to be expected [14].

- BWR modelling with the RAMONA code (Subsection 2.7.1) shows that the slip value can vary from 1.0 to 1.7. This corresponds to a drift velocity between 0.0 and 0.17.

Figures 6-9(a) and 6-9(b) show the sensitivity of the SB to the value of C_0 , which is seen to have a stabilizing effect. Figure 6-10 shows that, except in a small interval, the nature of Hopf bifurcation is not affected much as the value of C_0 is increased. Thus, it is seen that there is only a small shift of the transition point between the sub- and supercritical Hopf bifurcation regions as C_0 is changed from 1.0 to 1.03. For instance, the branch of the SB with $1.8 < N_{sub} < 2.1$ that was associated with supercritical Hopf bifurcation for $C_0 = 1.0$ becomes subcritical for $C_0 = 1.03$. In addition, it is to be noted from Fig. 6-10 that the effect of C_0 on the value of b_2 , the Floquet exponent, in the subcritical bifurcation region, *i.e.* $N_{sub} > 2.1$, is very small, while in the supercritical bifurcation region this effect is much more pronounced with a clear shift of the bifurcation curve. Similar effects of C_0 on bifurcation characteristics were also observed in the context of the heated channel study without neutronics (see Fig. 5-7(b)). This may suggest that increasing C_0 favours the occurrence of a subcritical Hopf bifurcation, relative to that of a supercritical one.

Results for the effects of the drift flux velocity V_{gj} are presented in Figures 6-11 and 6-12. Figure 6-11(a) shows the sensitivity of the SB to the value of V_{gj} , with shifts in the SB comparable to those resulting from the C_0 variations shown in Fig. 6-9(a). This is, however, in slight contrast to the results of the heated channel study without neutronics (Section 5.4), where the SB was found to be somewhat less sensitive to the value of V_{gj} than to that of C_0 . This suggests that effects of the drift flux velocity V_{gj} are more important in the nuclear-coupled thermal-hydraulic system than in the simple heated channel case.

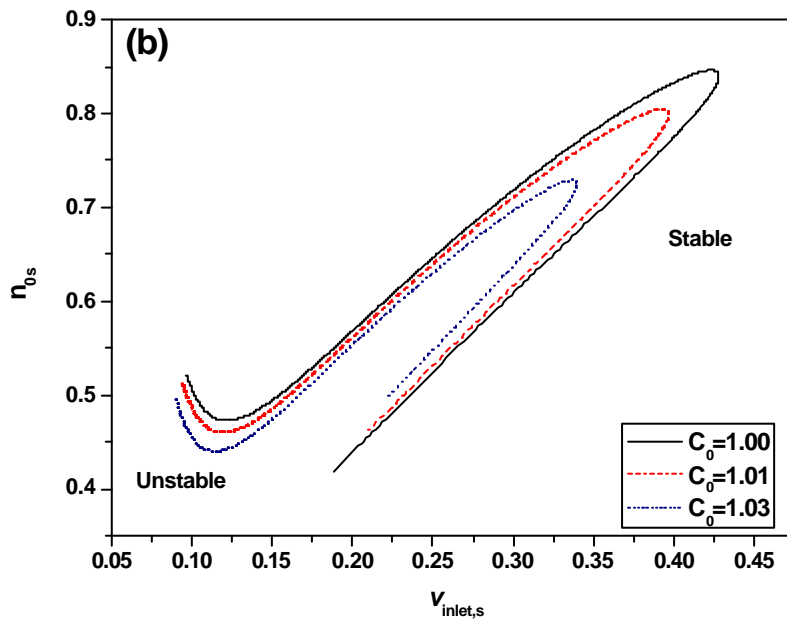
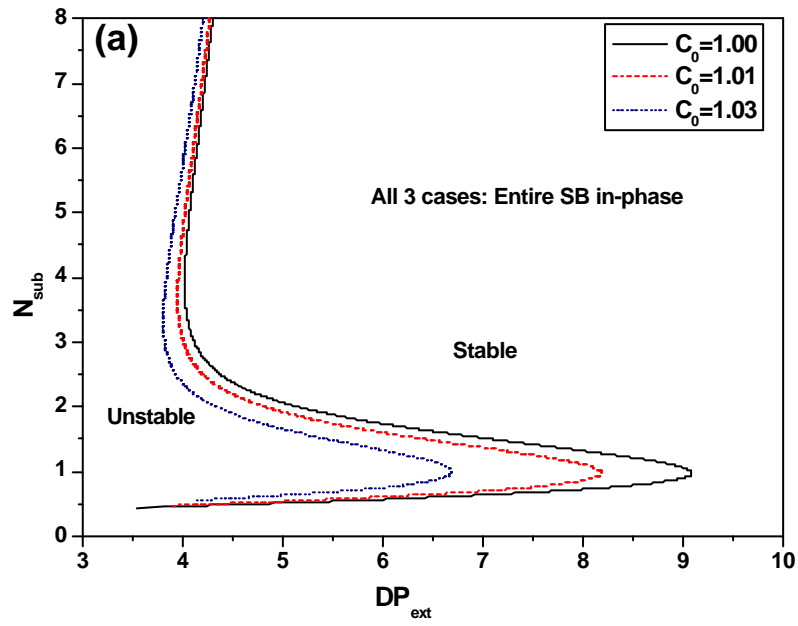


Figure 6-9. Effects of the void distribution parameter C_0 . **a)** Stability boundaries in the $N_{sub} - DP_{ext}$ plane. **b)** Stability boundaries in the power-flow plane.

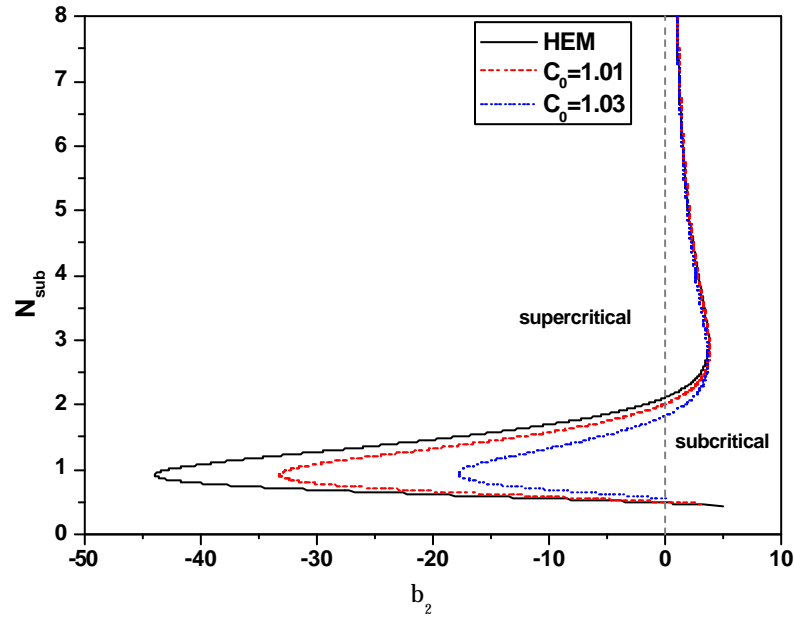


Figure 6-10. Effects of the void distribution parameter C_0 on the nature of Hopf bifurcation presented in the $N_{sub} - \mathbf{b}_2$ plane.

It should be noted that, while V_{gj} has a clearly stabilizing effect in the entire $N_{sub} - DP_{ext}$ plane (Fig. 6-11(a)), there are two conflicting trends to be observed in the power-flow map (Fig. 6-11(b)). The first is a destabilizing one for the system, *viz.* a clear shift of the stability boundary, while the second is stabilizing, *viz.* a significant shrinkage of the unstable region. Some further discussion of this phenomenon is presented in the following paragraphs.

Like C_0 , V_{gj} affects the nature of Hopf bifurcation only in a small interval, as shown in Fig. 6-12. For instance, the SB branch with $1.45 < N_{sub} < 2.10$ that was associated with supercritical Hopf bifurcation for $V_{gj} = 0.0$ become subcritical for $V_{gj} = 0.1$. In addition, Fig. 6-12 shows that increasing the value of V_{gj} causes the absolute value of \mathbf{b}_2 to decrease in both sub- and supercritical branches. This is qualitatively similar to the trend observed in the context of the heated channel study without neutronics (see Fig. 5-8(b)).

Shown in Figures 6-13 and 6-14 are the stability and bifurcation results using the HEM ($C_0 = 1.0, V_{gj} = 0.0$) and two particular cases of the DFM ($C_0 = 1.01, V_{gj} = 0.05$ and $C_0 = 1.03, V_{gj} = 0.08$). The SBs in the $N_{sub} - DP_{ext}$ plane are shown in Fig. 6-13(a). Here

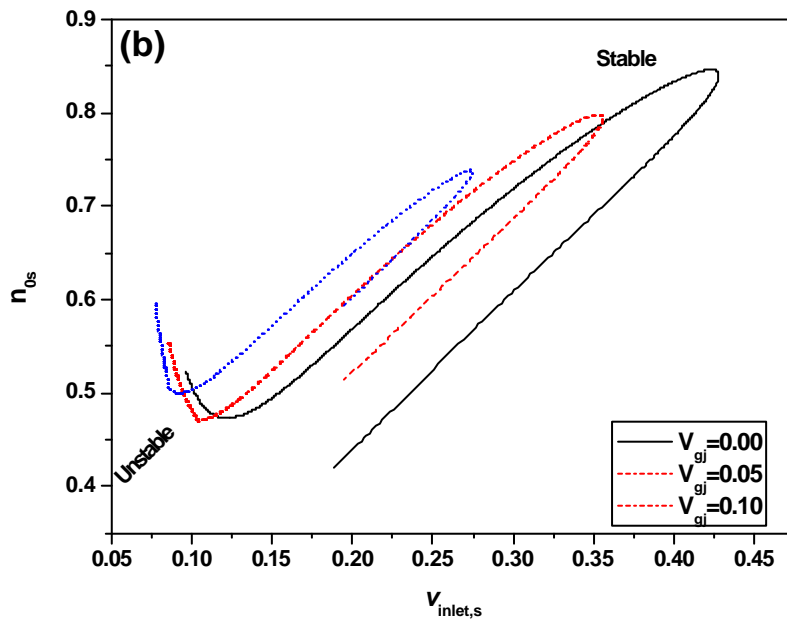
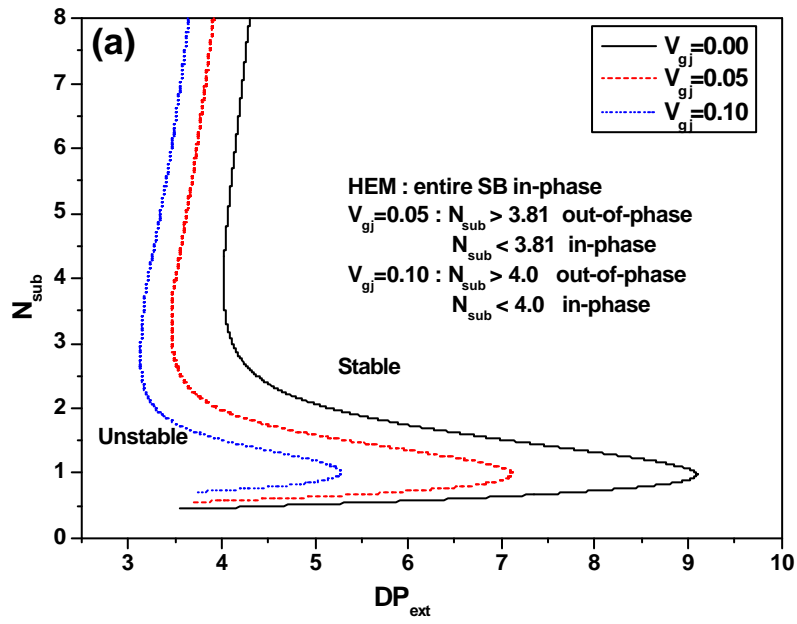


Figure 6-11. Effects of the drift velocity V_{gj} . **a)** Stability boundaries in the $N_{sub} - DP_{ext}$ plane. **b)** Stability boundaries in the power-flow plane.

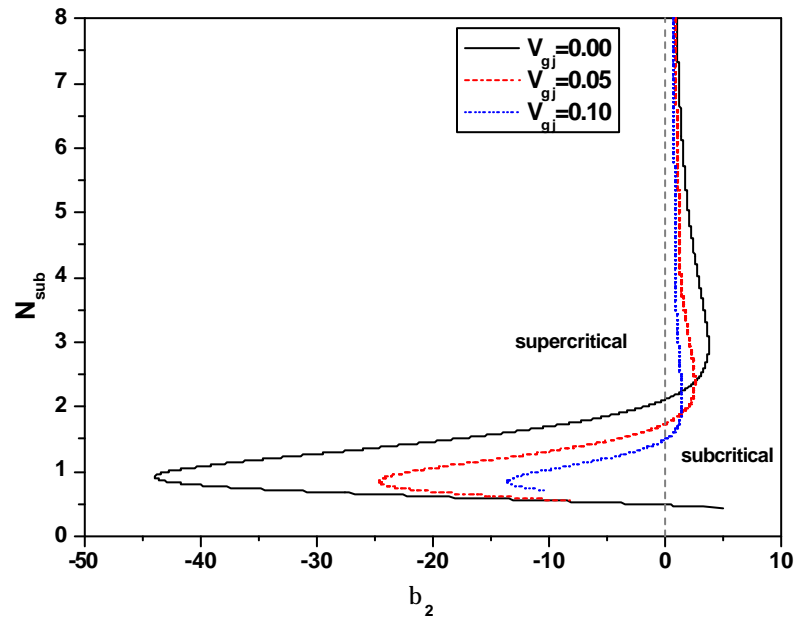


Figure 6-12. Effects of the drift velocity V_{gj} on the nature of Hopf bifurcation presented in the $N_{sub} - b_2$ plane.

it is clearly seen that the SB is sensitive to the model used for two-phase flow: the larger the DFM parameters (C_0 and V_{gj}), the greater the shift of the SB towards the unstable region. The corresponding Hopf bifurcation diagram in the $N_{sub} - b_2$ plane (Fig. 6-14) shows that both sub- and supercritical bifurcation regions are affected. The nature of Hopf bifurcation for lower values of N_{sub} is more sensitive to the values of C_0 and V_{gj} . For instance, for $C_0 = 1.03$ and $V_{gj} = 0.08$, the entire SB becomes subcritical.

Fig. 6-13(b) shows the SBs transformed from the $N_{sub} - DP_{ext}$ to the $n_{0s} - v_{inlet,s}$ plane. Here it is clearly seen that the HEM can be non-conservative in the power-flow plane, although it always remains conservative in the operating-parameter $N_{sub} - DP_{ext}$ plane. This is in contradiction to the generally held viewpoint that the HEM is conservative³⁶ in all situations. Although a clear interpretation of this phenomenon is still needed, it is clear that we are dealing with a totally different complex system where the tight nuclear coupling to the thermal-hydraulics can generate completely new behaviour.

³⁶ This is true in the context of purely thermal-hydraulic phenomena and cannot be generalized for nuclear-coupled thermal-hydraulic systems.

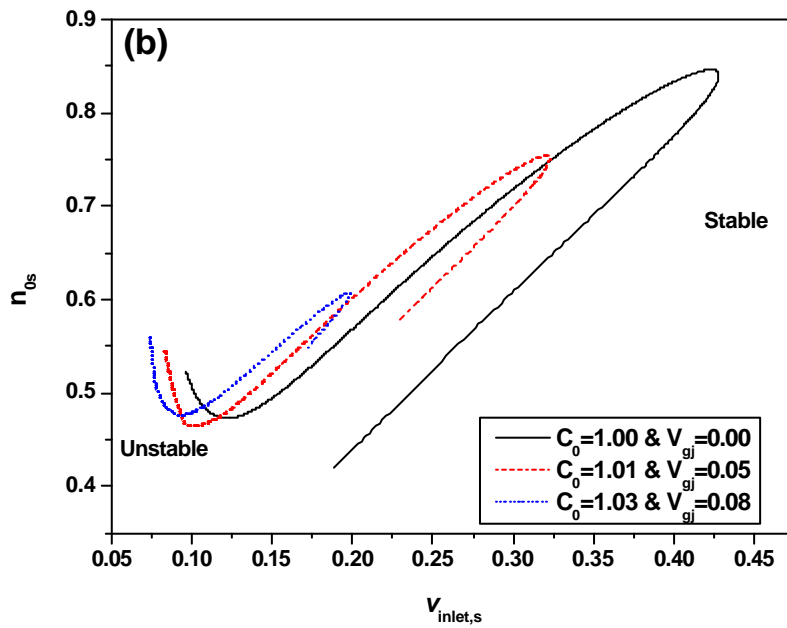
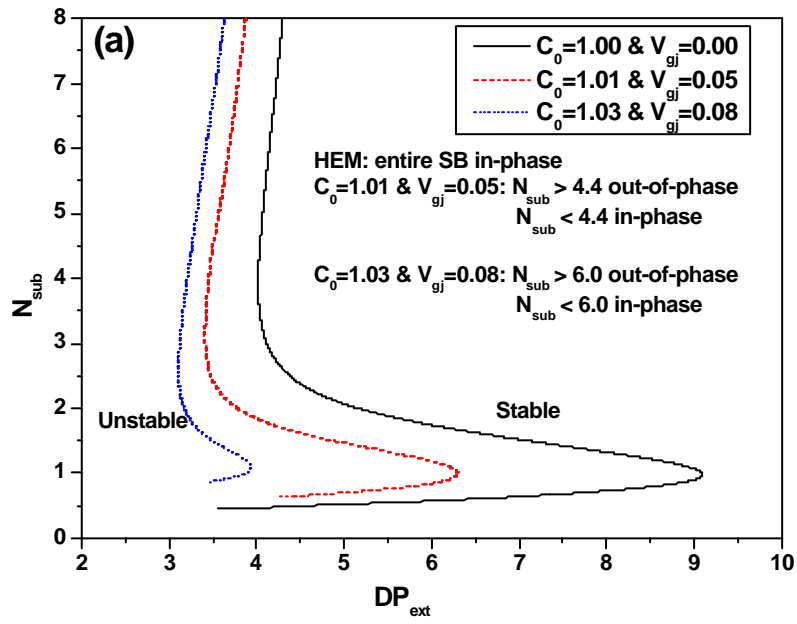


Figure 6-13. Effects of the DFM parameters: **a)** Stability boundaries in the $N_{sub} - DP_{ext}$ plane. **b)** Stability boundaries in the power-flow plane.

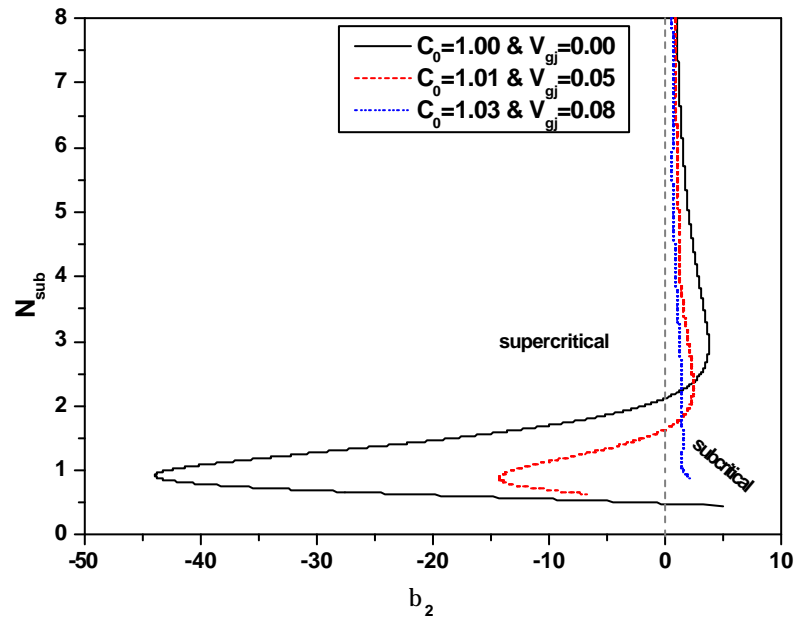


Figure 6-14. Effects of the DFM parameters on the nature of Hopf bifurcation in the $N_{sub} - b_2$ plane.

It should be pointed out that changing the values of the DFM parameters causes a change in the steady-state value of the liquid inlet velocity in both channels. Therefore, the shifts observed in the SBs (Figs. 6-9(a), 6-11(a), and 6-13(a))—that seem to be large—are due to effects of the DFM parameters and the liquid inlet velocity that changes each time the DFM parameters are changed.

6.4.2 Effects of the drift flux parameters on the type of oscillation mode

The effects of the drift flux parameters on the mode of oscillation (in-phase or out-of-phase) are investigated here by tracking the properties of the elements of the eigenvector corresponding to the pair of complex eigenvalues that has the largest real part. Results indicate that the entire SB obtained with the HEM corresponds to the in-phase mode.

Figure 6-9(a) shows that C_0 has no effect on the mode of oscillation and the whole SB remains in-phase. However, V_{gj} shows a significant impact on the SB in the higher N_{sub} region (Fig. 6-11(a)). Thus, the branch for $N_{sub} > 3.81$ with $V_{gj} = 0.05$, that was in-phase in the HEM, becomes out-of-phase. The lower branch ($N_{sub} < 3.81$) remains in-phase. It

should be emphasized that the observed effects of V_{gj} occur for parameter values that are far from the normal operating conditions for a typical BWR³⁷.

In summary, using the DFM instead of the HEM affects the type of oscillation mode in the higher branch of the SB. This is mainly because of the effect of the drift velocity. For instance, for a DFM with $C_0 = 1.01$ and $V_{gj} = 0.05$, the higher branch ($N_{sub} > 4.4$) that was in-phase in the HEM becomes out-of-phase, while the lower branch ($N_{sub} < 4.4$) remains unaffected (Fig. 6-13(a)).

6.5 SUMMARY AND CONCLUSIONS

In this chapter, the complete two-channel nuclear-coupled thermal-hydraulic reduced order model has been applied to simulate global and regional oscillations in a BWR. As detailed in Chapter 4, this model comprises three parts: spatial lambda-mode neutron kinetics with the fundamental and first azimuthal modes, fuel heat conduction dynamics, and a thermal-hydraulic model based on a DFM representation. Stability and bifurcation analyses have been performed using the bifurcation analysis code BIFDD, the stability boundaries and the nature of Hopf bifurcation being determined and visualized in a suitable two-dimensional parameter-state space.

The stability limits for both in-phase and out-of-phase modes have been displayed in parameter space. It has been shown that analysing the properties of the elements of the eigenvectors gives complete information on the type of oscillation mode (in-phase or out-of-phase) *without* even solving the set of ODEs. A clear statement has been proposed: *the in-phase (out-of-phase) mode is excited only if the oscillation amplitude of the fundamental (first) mode is larger than that of the first (fundamental) mode, and the thermal-hydraulic and heat conduction variables in one half of the core oscillate in-phase (out-of-phase) but with the same amplitude as the corresponding variables in the other half.* Numerical integration of the set of 22 ODEs has been carried out to confirm the results of the bifurcation analysis. For that, a Matlab code has been developed based on the Gear's algorithm to solve stiff problems. The numerical results obtained clearly show, for example, that the excitation of the out-of-phase mode indeed corresponds to oscillations of the first mode which are much larger than those of the fundamental.

³⁷ N_{sub} is usually less than 2.0 for normal operational conditions for a BWR. This corresponds to 30 K temperature difference between the inlet and saturation temperatures.

A comparative study between the use of the homogeneous equilibrium model (HEM) and the drift flux model (DFM) has been carried out to investigate the effects of the DFM parameters, *viz.* the void distribution parameter C_0 and the drift velocity V_{gj} , on the SB, the nature of Hopf bifurcation, and on the mode of oscillation. Results clearly show that both sub- and supercritical Hopf bifurcation regions are affected. The SBs have been found to be sensitive to the actual value of C_0 as well as of V_{gj} , separately, the nature of Hopf bifurcation being influenced by both parameters. Using a DFM instead of a HEM thus has a significant effect on stability characteristics.

Contrary to the generally held viewpoint, it has been shown that using the HEM is not always conservative. In addition, it has been seen that using the DFM instead of the HEM affects the type of oscillation mode mostly for higher values of N_{sub} . Although this SB branch is of little importance from the safety viewpoint for normal BWR operation, further investigations in this context may help provide deeper understanding of the mechanisms behind the transition from the in-phase to out-of-phase mode (or *vice versa*) as a given parameter is changed.

REFERENCES

- [1] F. Araya, K. Yoshida, Y. Yabushita, "Analysis of a Neutron Flux Oscillation Event at LaSalle-2", *Nucl. Technology*, **93**, 82, 1991.
- [2] Y. M. Farawila, D. W. Pruitt, P. E. Smith, "Analysis of the Laguna Verdu Instability Event", *Proc. of ANS National Heat Transfer Conf.*, Houston, Texas, **9**, 198, 1992.
- [3] R. Miró, G. Ginestar, D. Hennig, G. Verdú, "On the Regional Oscillation Phenomena in BWRs", *Prog. Nucl. Energy*, **36**, 2, 189-229, 2000.
- [4] G. Th. Analytis, D. Hennig, J. K. H. Karlsson, "The Physical Mechanism of Core-Wide and Local Instabilities at Forsmark-1 BWR", *Nucl. Eng. Des.*, **205**, 91-105, 2001.
- [5] J. March-Leuba, D. G. Cacuci, R. B. Perez, "Nonlinear Dynamics and Stability of Boiling Water Reactors: Part 1- Qualitative Analysis", *Nucl. Sci. Eng.*, **93**, 111-123, 1986, and "Nonlinear Dynamics and Stability of Boiling Water Reactors: Part 2- Quantitative Analysis", *Nucl. Sci. Eng.*, **93**, 124-136, 1986.
- [6] J. March-Leuba, E. D. Blakeman, "A Mechanism for Out-of-phase Power Instabilities in Boiling Water Reactors", *Nucl. Eng. Des.*, **107**, 173-179, 1991.

- [7] J. L. Muñoz-Cobo, G. Verdú, “Application of Hopf Bifurcation Theory and Variational Methods to the Study of Limit Cycles in Boiling Water Reactors,” *Ann. Nucl. Energy*, **18**, 5, 269, 1991.
- [8] J. L. Muñoz-Cobo, R. B. Pérez, D. Ginestar, A. Escrivá, G. Verdú, “Nonlinear Analysis of Out-of-phase Oscillations in Boiling Water Reactors”, *Ann. Nucl. Energy*, **23**, 16, 1301-1335, 1996.
- [9] J. L. Muñoz-Cobo, O. Rosello, R. Miró, A. Escrivá, D. Ginestar, G. Verdú, “Coupling of Density Wave Oscillations in Parallel Channels with High Order Modal Kinetics: Application to BWR Out-of-phase Oscillations”, *Ann. Nucl. Energy*, **17**, 1345-1371, 2000.
- [10] A. A. Karve, Rizwan-uddin, J. J. Dorning, “Out-of-phase Oscillations in Boiling Water Reactors”, *Proc. of the Joint Int. Conf. on Mathematical Methods and Super-Computing*, Saratoga, Springs, NY, Oct. 5-9, **2**, 1633-1647, 1997.
- [11] A. A. Karve, “Nuclear-Coupled Thermal-Hydraulic Stability Analysis of Boiling Water Reactors”, Ph.D. Dissertation, Virginia University, 1999.
- [12] Quan Zhou, Rizwan-uddin, “Bifurcation Analyses of In-phase and Out-of-phase Oscillations in BWRs”, *Proc. of International Conference on the New Frontiers of Nuclear Technology, Reactor Physics, Safety and High Performance Computing (PHYSOR-2002)*, Seoul, Korea, Oct. 7-10, 2002, CD-ROM.
- [13] A. Dokhane, D. Hennig, Rizwan-uddin, R. Chawla, “Nonlinear Stability Analysis with a Novel BWR Reduced Order Model,” *Proc. of International Conference on the New Frontiers of Nuclear Technology, Reactor Physics, Safety and High Performance Computing (PHYSOR-2002)*, Seoul, Korea, Oct. 7-10, 2002, CD-ROM.
- [14] R. T. Lahey, Jr., F. J. Moody, *The Thermal-Hydraulics of a Boiling Water Nuclear Reactor*, American Nuclear Society, La Grange Park, IL, 1977.

7 BIFURCATION ANALYSIS USING RAMONA

7.1 INTRODUCTION

As stated in Chapter 3, sub- and supercritical Hopf bifurcations are the only types of bifurcations that have been encountered during the loss of system stability³⁸ in BWR studies using reduced order models [1-7]. The results reported in Chapter 6 for investigations conducted using the currently developed, 22-equation model confirm these findings.

As with reduced order models, stable nonlinear oscillations (limit cycle) have been observed and reported using large system codes [8-10], and even during some stability experiments performed in commercial reactors like Leibstadt and Ringhals [11,12]. However, unstable limit cycles have never previously been observed or reported using such codes [13]. In the author's opinion, the reason for this is that the unstable limit cycle solution has always been confused with the unstable fixed point solution, *i.e.* when growing amplitude oscillations were observed at a specific operational point, the conclusion was always that the system is unstable at this operational point, without any detailed investigation being made concerning the exact type of solution encountered. This can be explained by the fact that most system code users usually have limited (or no) experience in nonlinear stability analysis using reduced order models.

Within the framework of reduced order model analysis, it is quite easy to distinguish between an unstable fixed point and an unstable limit cycle solution. Thus, for an unstable fixed point, whatever the initially induced perturbation amplitude, oscillations always grow in amplitude. On the other hand, for unstable limit cycles the initial perturbation amplitude plays an important role in determining the behaviour of the system, *viz.* for small perturbation amplitudes the oscillations decay to the fixed point that exists inside the unstable limit cycle, whereas for a large enough perturbation amplitude the oscillations grow in amplitude. The situation has been different for BWR stability analyses carried out using large system codes, the question of the bifurcation type responsible for the generation of a given observed limit cycle solution never having been raised before. The primary focus in this chapter is accordingly to address the use of system codes in the

³⁸ As stated earlier, in crossing the first stability boundary, only Hopf bifurcation has been encountered. However, deep in the unstable region, a cascade of period-doubling bifurcations may exist as reported for instance in [4].

above context, using what is introduced as the *correspondence hypothesis* and is based on the accumulated experience in BWR stability analysis using reduced order models. This hypothesis proposes the correspondence between a stable (unstable) limit cycle solution and the occurrence of a supercritical (subcritical) Hopf bifurcation.

By carrying out detailed bifurcation analysis using the system code RAMONA at various different operational points for the two nuclear power plants (NPPs) Leibstadt and Ringhals-1, the correspondence hypothesis is conclusively confirmed by comparing the results with those found using the current reduced order model. The analysis carried out close to the Leibstadt cycle7 operational point (OP), called record 4 (*kklc7_rec4* OP), leads to the identification of a subcritical Hopf bifurcation. To the author's knowledge, this is the first time that a subcritical Hopf bifurcation is identified using large system codes. Details of this analysis are presented in Section 7.3. This is followed by the RAMONA analysis of the Ringhals-1 cycle 14 operational point, called record 9. Results, in this case, show the occurrence of a supercritical Hopf bifurcation (see Section 7.4).

7.2 THE CORRESPONDENCE HYPOTHESIS: STABLE (UNSTABLE) LIMIT CYCLE VS. SUPERCRITICAL (SUBCRITICAL) HOPF BIFURCATION

For a Hopf bifurcation to occur, three conditions (see Section 3.1) have to be fulfilled, *viz.*

- 1) a pair of complex conjugate eigenvalues $\mathbf{s}(I) \pm i\mathbf{w}(I)$ of the Jacobian matrix crosses the imaginary axis for a critical value of $I = I_c$ in such a way that $\mathbf{w}(I_c) > 0$, $\mathbf{s}(I_c) = 0$,
- 2) $\frac{\partial \mathbf{s}(I = I_c)}{\partial I} \neq 0$, and
- 3) all the other eigenvalues have strictly negative real parts (see Figure 3-1),

These conditions can easily be verified when using models represented by a system of ODEs, as is the case with reduced order models, since analytical bifurcation analysis can then be carried out using a bifurcation code like BIFDD. However, for models based on PDEs, as those used by the system code RAMONA, one does not presently have the

capability to check the fulfilment of the conditions for the occurrence of a Hopf bifurcation. Therefore, for this reason, a new approach has currently been taken based on the following two important facts:

1. *A supercritical Hopf bifurcation is characterized by the appearance of stable limit cycle solutions inside the linear unstable region close to the SB, while a subcritical Hopf bifurcation is characterized by a stable fixed point and an unstable limit cycle solution inside the linear stable region close to the SB.*
2. ***Only** sub- or supercritical **Hopf** bifurcations have been observed and reported so far during the loss of system stability in the context of BWR stability analysis using reduced order models. Therefore, one can confidently assume that these two types of bifurcation are the **only** ones that can be expected to occur when a BWR loses its stability.*

This is equivalent to the setting up of the following hypothesis:

The Correspondence Hypothesis

When a BWR system loses its stability, the observation of a stable limit cycle is indication of the occurrence of a supercritical Hopf bifurcation, while the existence of an unstable limit cycle indicates the occurrence of a subcritical Hopf bifurcation.

7.3 SUBCRITICAL HOPF BIFURCATION USING RAMONA

In this section, the stability behaviour of the Leibstadt NPP is analysed, using the system code RAMONA-5/PRESTO1 option (see Appendix A), around the reference operational point (OP), *klc7_rec4* (referred to here as the nominal OP), located in the plant's exclusion area³⁹ and for which a stability measurement was carried out during cycle 7 reactor start-up in September 1990. The Leibstadt core in cycle 7 contained 8x8 fuel assemblies supplied by General Electric, apart from 4 SVEA-64 fuel assemblies supplied by ABB Atom [11].

³⁹ As mentioned in Chapter 2, this is a conservatively defined region in the power-flow map where the reactor is not allowed to operate during normal operating conditions.

KKL POWER FLOW MAP

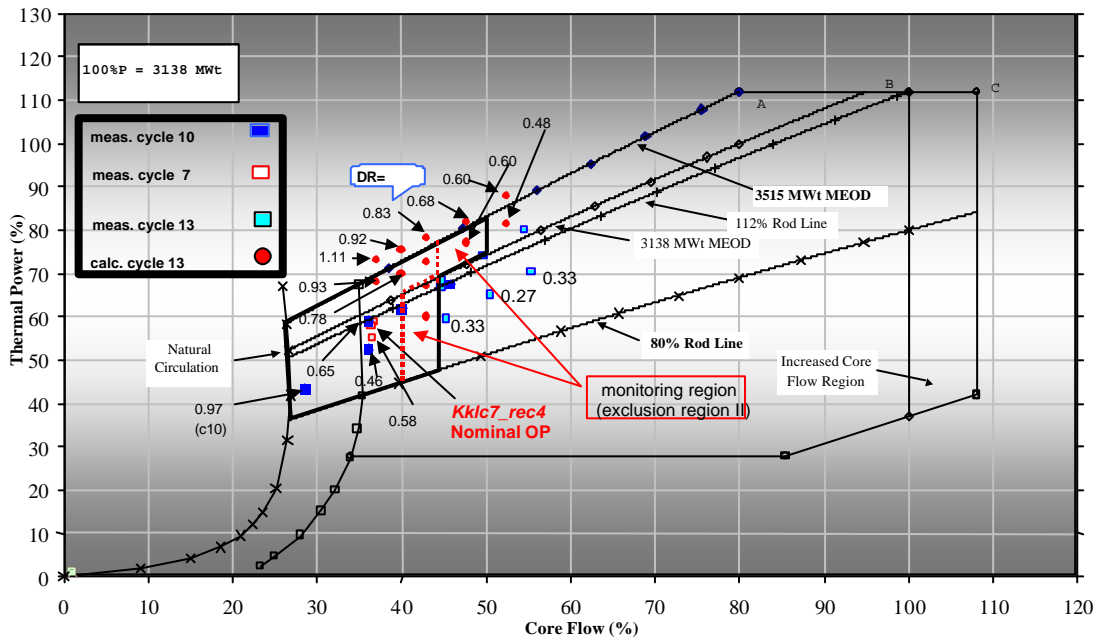


Figure 7-1. Location of the reference case in the Leibstadt NPP power-flow map.

A detailed local investigation is carried out to study how the solution manifold of the system varies as a function of the mass flow, which is here considered as the bifurcation parameter. Then, the results are explained by comparing them with the results found using the currently developed reduced order model. In effect, the stability behaviour is investigated at the following five OPs:

- ❑ 60.5% thermal power and 36.7% mass flow rate (nominal OP, *kklc7_rec4*).
- ❑ 60.5% thermal power and 37.0% mass flow rate (+0.3% F OP⁴⁰).
- ❑ 60.5% thermal power and 37.7% mass flow rate (+1%F OP).
- ❑ 60.5% thermal power and 36.4% mass flow rate (-0.3% F OP⁴¹).
- ❑ 60.5% thermal power and 35.7% mass flow rate (-1%F OP).

At these OPs, the RAMONA analyses are carried out by inducing control rod (CR) perturbations with different amplitudes, the objective being to analyse the stability behaviour for each OP and for each CR perturbation amplitude. For instance, a 2-node amplitude control rod perturbation means that a sinusoidal perturbation movement of a

⁴⁰ means that the mass flow for this OP is higher than that for the nominal OP by 0.3%

⁴¹ means that the mass flow for this OP is less than that for the nominal OP by 0.3%

specific control rod bank is induced with an amplitude of 2 nodes (1 node = 15.24 cm) during 1 second. Figures 7-2 to 7-6 show the RAMONA-calculated LPRM354⁴² time series signals for the nominal OP, +0.3%F OP, +1%F OP, -0.3%F OP and -1%F OP, respectively.

7.3.1 Results for the Different Leibstadt NPP Operational Points

The nominal OP: 60.5% power and 36.7% mass flow

As mentioned previously, this operating point is located in the exclusion area in the power-flow map of the Leibstadt NPP (see Fig. 7-1). For a small amplitude perturbation (0.05-node control rod perturbation⁴³), the power decays to the stable steady-state solution as shown in Fig. 7-2(a), while a perturbation amplitude of 0.1-node of the control rod leads to growing oscillation amplitudes (Fig. 7-2(b)). Increasing the initial perturbation further to 2 nodes also results in growing amplitude oscillations (Fig. 7-2(c)). Mathematically, this means that, beside the stable fixed point solution, an unstable limit cycle solution exists at this operational point. Therefore, referring to the correspondence hypothesis, this indicates the occurrence of a subcritical Hopf bifurcation.

Next, a detailed local investigation close to this OP is carried out to analyse the different solution manifold of the system when the mass flow is changed by very small values. The results are thereafter compared with the ones obtained using the reduced order model.

The +0.3% F OP: 60.5% power and 37.0% mass flow

Figure 7-3 shows clearly that, at this operational point, the system again has two different behaviours depending on the perturbation amplitude. Thus, for 0.05-node and 0.1-node control rod perturbation amplitudes, the power oscillations are seen to decay to the stable steady-state solution (stable fixed point) as shown in Fig. 7-3(a-b), while, for a 2-node control rod perturbation amplitude, oscillations with growing amplitudes are observed. Therefore, an unstable limit cycle solution exists also at this OP.

⁴² LPRM354 stands for Local Power Range Monitor number 35 at the core axial level number 4. In KKL there are 35 LPRM strings, each having 4 detectors at 4 different core axial levels. Note that level 1 corresponds to the lowest axial level, while level 4 corresponds to the highest and most highly voided axial position

⁴³ The Leibstadt core is modelled with 25 axial nodes in RAMONA, where each node equals 15.24 cm.

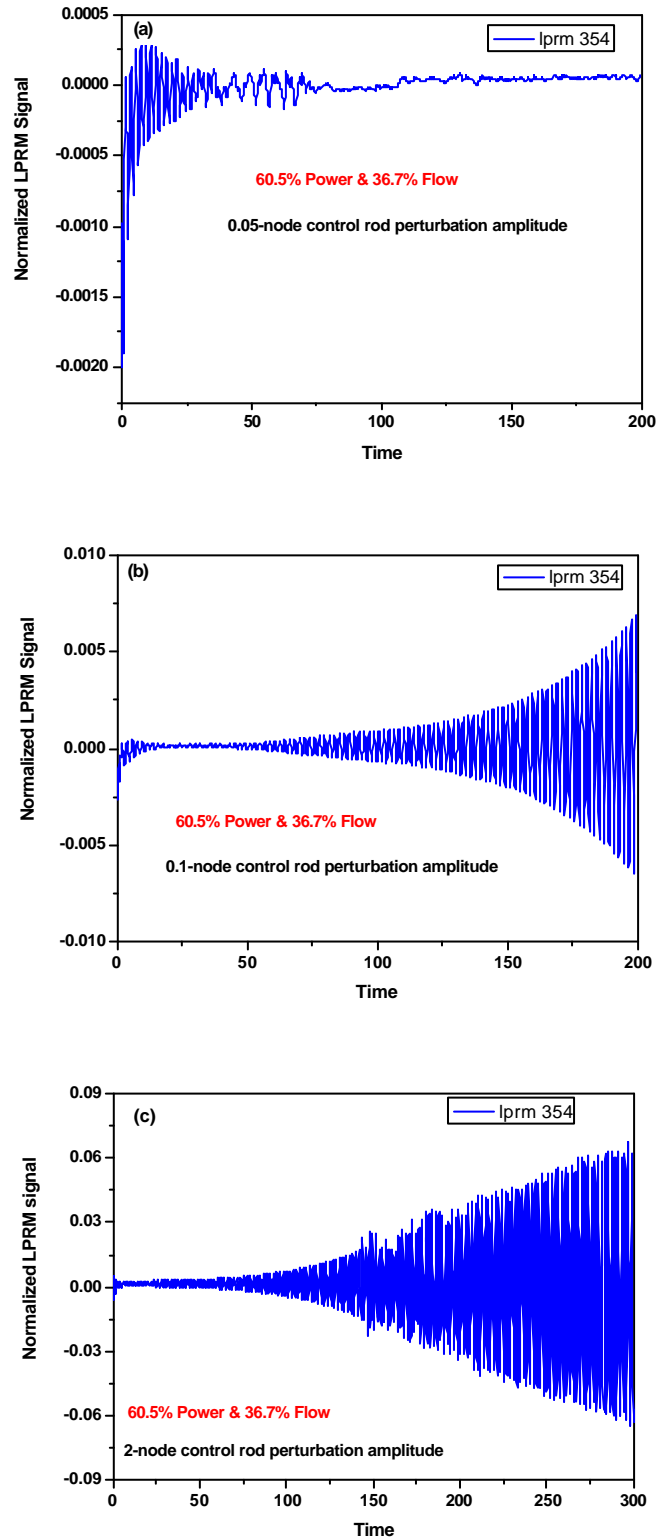


Figure 7-2. Nominal OP time series of KKL LPRM showing the occurrence of a subcritical Hopf bifurcation: **(a)** 0.05-node control rod perturbation amplitude. **(b)** 0.1-node control rod perturbation amplitude. **(c)** 2-node control rod perturbation amplitude.

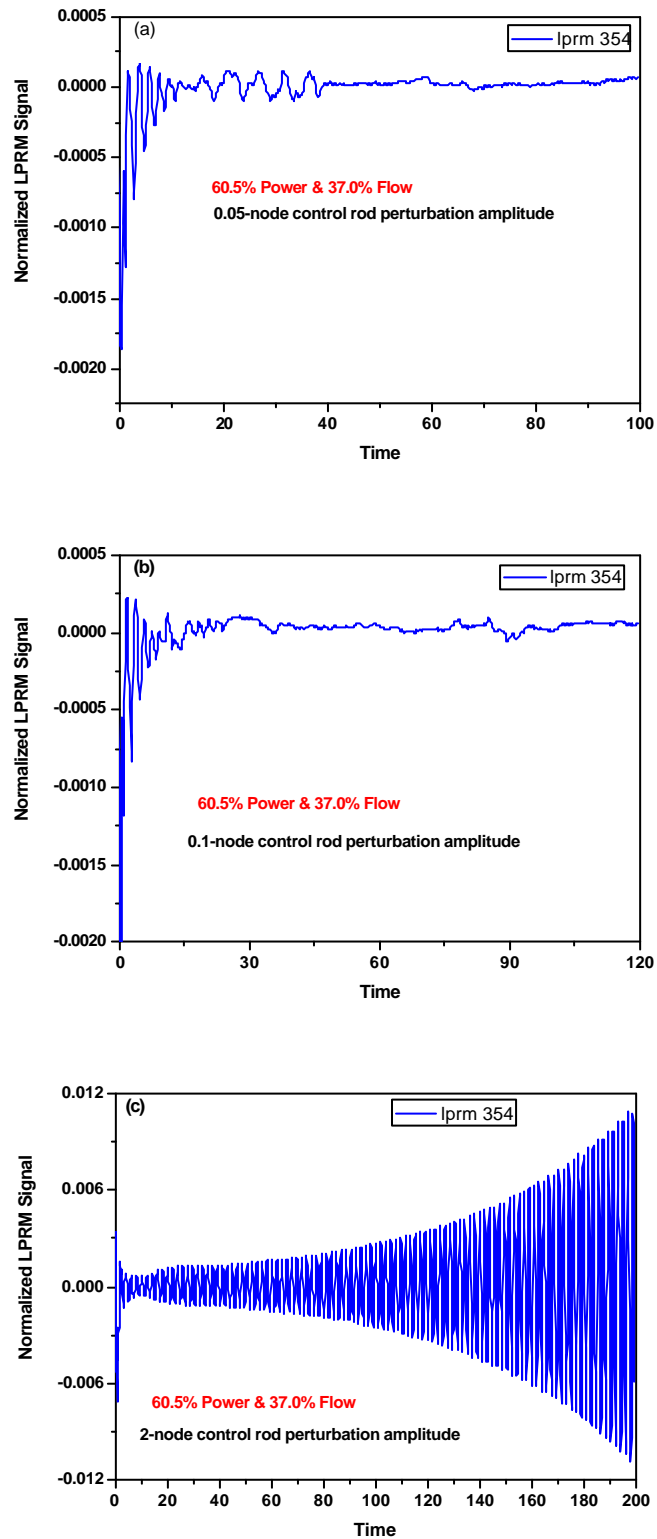


Figure 7-3. +0.3%F OP time series of KKL LPRM showing the occurrence of a subcritical Hopf bifurcation: (a) 0.05-node control rod perturbation amplitude. (b) 0.1-node control rod perturbation amplitude. (c) 2-node control rod perturbation amplitude.

However, there is an important observation to be made here, *viz.* that while at the nominal OP a 0.1-node perturbation is enough to take the system out of the unstable limit cycle (growing oscillations (Fig. 7-2(b))), the same perturbation at +0.3%F OP is not enough to destabilise the system (decaying oscillations (Fig. 7-3(b))). This can be explained by the difference in the amplitude of the unstable limit cycles at the two different OPs (nominal and +0.3%F). Thus, it is seen that, at the nominal OP, the unstable limit cycle amplitude is smaller than the 0.1-node control rod perturbation amplitude. Therefore, inducing a perturbation amplitude that is equal to or larger than 0.1-node brings the system into the unstable region (outside of the limit cycle (Fig. 7-2(b, c))). On the other hand, at the +0.3%F OP, the unstable limit cycle amplitude is larger than the 0.1 node control rod perturbation amplitude. Consequently, for a perturbation amplitude of 0.1 node or less, the system state remains inside the limit cycle and is attracted by the stable fixed point (Fig. 7-3(a, b)).

The +1%F OP: 60.5% power and 37.7% mass flow

The behaviour of the reactor at this operational point is shown in Fig. 7-4. From parts (a) and (b) of this figure, it is clearly seen that the system is stable (stable fixed point solution) for both 0.05- and 2-node control rod perturbation amplitudes. In order to be able to draw a definitive conclusion regarding the solution type encountered at this operational point, the control rod perturbation amplitude was increased to 5 nodes⁴⁴ so as to rule out the existence of a large-amplitude unstable limit cycle solution⁴⁵. Figure 7-4(c) clearly shows that this is not the case and that the analysed OP is indeed a stable fixed point.

The -0.3%F OP: 60.5% power and 36.4% mass flow

Figures 7-5(a), (b) show that, for the -0.3%F OP, the oscillation amplitude grows independently of the perturbation amplitude (0.05- or 2-node control rod perturbation), *i.e.* the system is unstable (unstable fixed point solution). To conclusively answer the question as to whether the system solution at this OP is an unstable fixed point or an unstable limit cycle, a case has been analysed in which there was no induced control rod perturbation at all, *i.e.* only the numerical noise, assumed to be very small, acts as a perturbation.

⁴⁴ A control rod perturbation amplitude of 5 nodes is considered to be a very large perturbation.

⁴⁵ If a large amplitude limit cycle exists, larger perturbation amplitudes are needed to take the system outside the limit cycle.

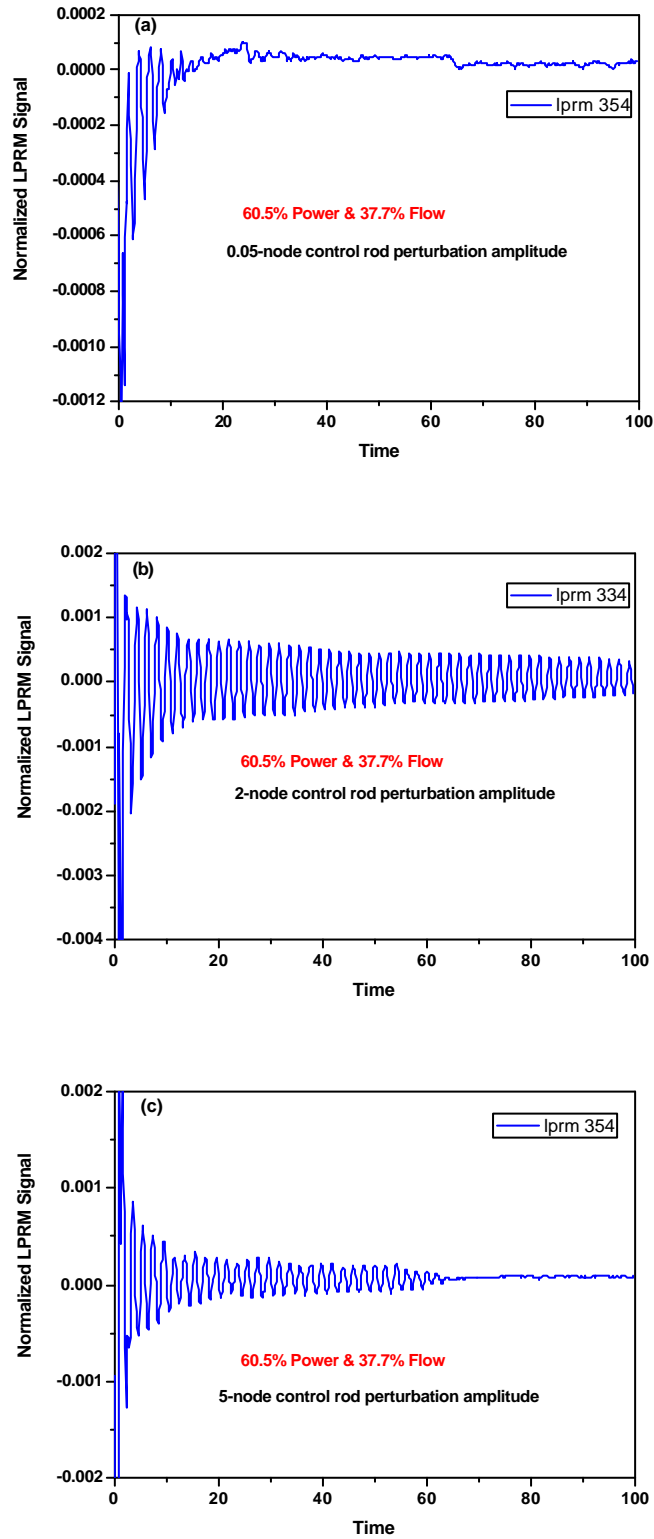


Figure 7-4. +1%F OP time series of KKL LPRM showing a stable fixed point solution: (a) 0.05-node control rod perturbation amplitude. (b) 2-node control rod perturbation amplitude. (c) 5-node control rod perturbation amplitude.

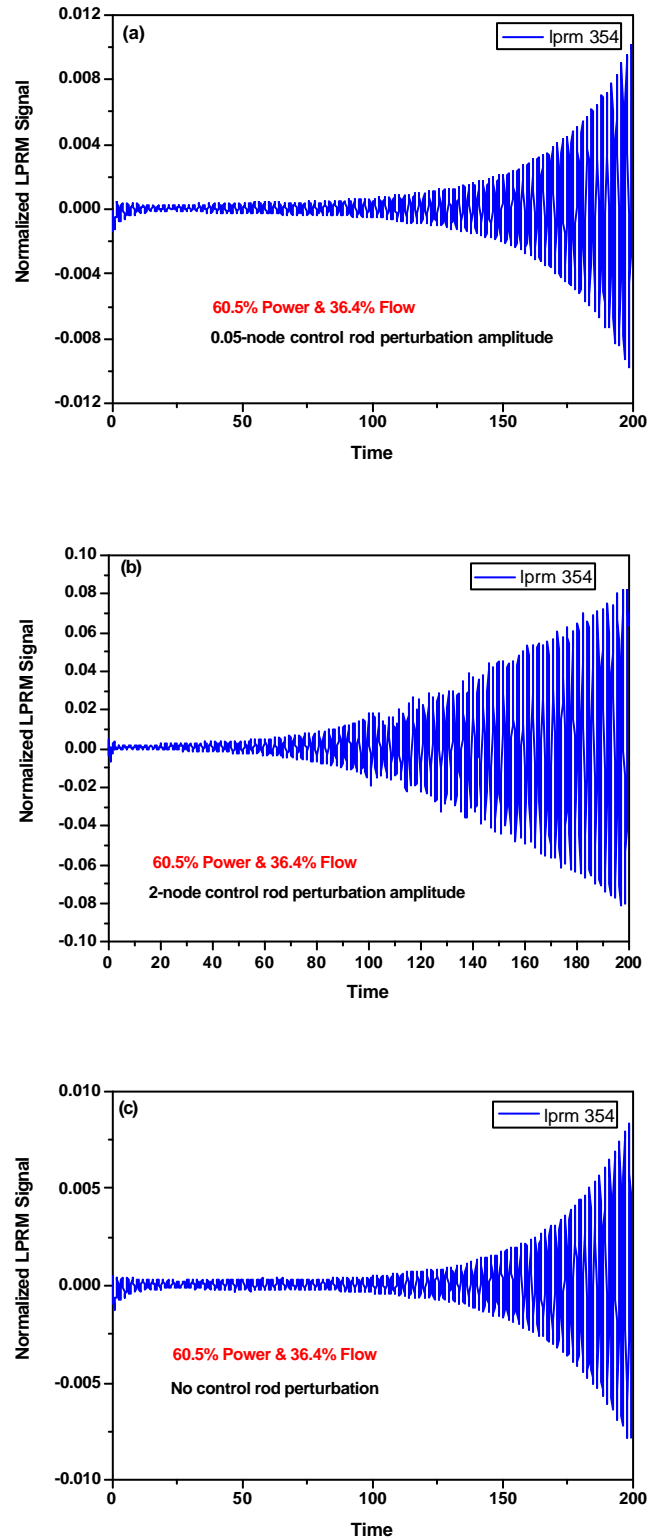


Figure 7-5. $-0.3\%F$ OP time series of KKL LPRM showing an unstable fixed point solution: (a) 0.05-node control rod perturbation amplitude. (b) 2-node control rod perturbation amplitude. (c) No control rod perturbation.

Figure 7-5(c) clearly confirms that the system is linearly unstable in this case, *i.e.* an unstable fixed point is indeed the solution at this OP.

The -1%F OP: 60.5% power and 35.7% mass flow

The behaviour of the system at the $-1\%F$ OP is the same as that for the $-0.3\%F$ OP (see Fig. 7-6(a)-(c)), *i.e.* once again the solution is seen to be an unstable fixed point.

7.3.2 Interpretation and Discussion

At first glance, it may seem quite peculiar that the qualitative behaviour (solution type) of the system changes dramatically within a small variation interval of the mass flow (from 37.7% to 35.7%), *i.e.* from a stable fixed point solution at the $+1\%F$ OP, to stable fixed points with unstable limit cycle solutions at the $+0.3\%F$ and nominal OPs, and then to unstable fixed point solutions at the $-0.3\%F$ and $-1\%F$ OPs. While carrying out bifurcation analysis using the currently developed reduced order model, such a variation of system behaviour has, in qualitative terms, *only* been observed when a subcritical Hopf bifurcation occurs during the loss of system stability. Figure 7-7 shows the different solutions that exist close to the SB when such a bifurcation is expected for the reduced order model, the similarity in the variation of the solution type between the BWR system analysis with RAMONA and the reduced order model analysis being clearly underlined thereby.

Thus points A, B, and C in the figure are located in a region where a subcritical Hopf bifurcation is expected⁴⁶. Because the operational point A is in the stable region and close to the stability boundary, both a stable fixed point and an unstable limit cycle solution are found. Point B is inside the stable region but far from the SB. Therefore, only a stable fixed point solution is observed. Finally, point C is in the unstable region and the unstable fixed point is, therefore, the only solution of the system. Again, it needs to be emphasized that such a change of solution type happens only because of the occurrence of a subcritical Hopf bifurcation. Therefore, based on the current reduced order model findings, two important conclusions can be drawn:

⁴⁶ from analysis using the bifurcation code BIFDD

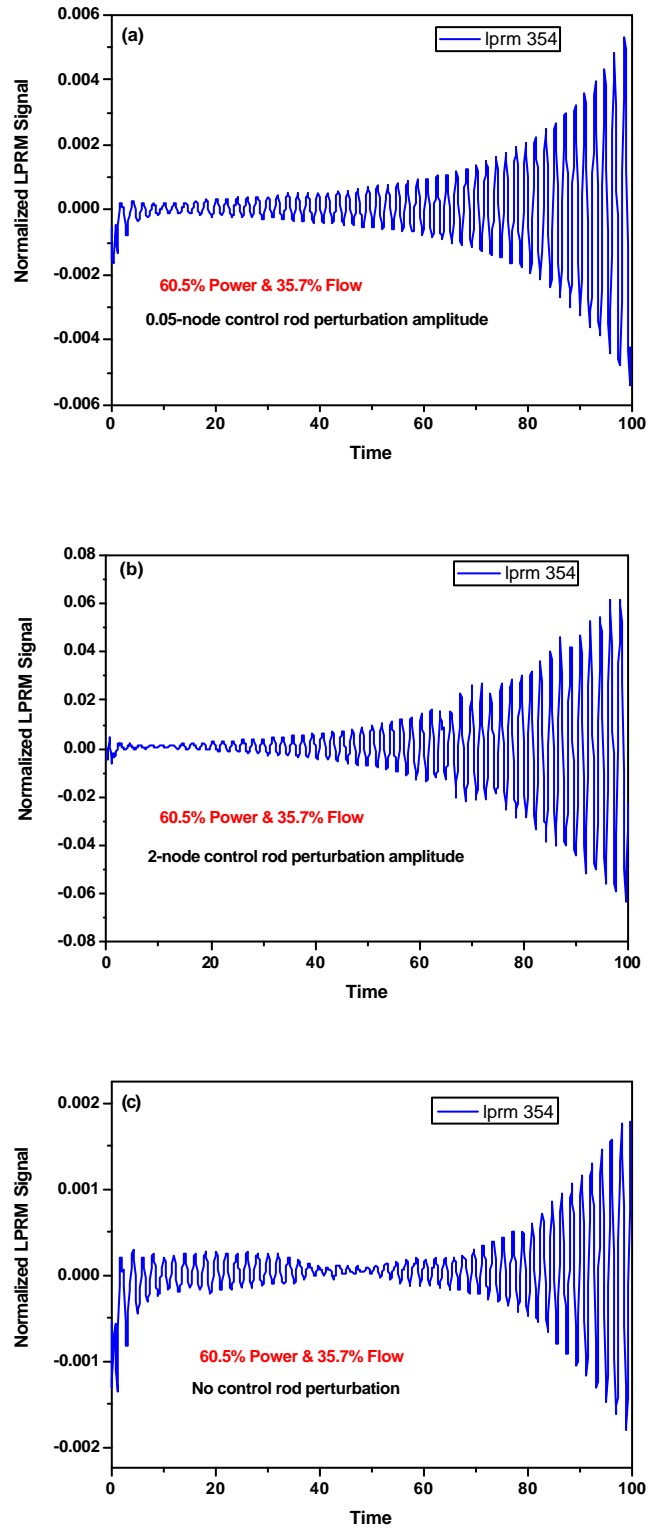


Figure 7-6. -1%F OP time series of KKL LPRM showing an unstable fixed point solution: (a) 0.05-node control rod perturbation amplitude. (b) 2-node control rod perturbation amplitude. (c) No control rod perturbation is induced.

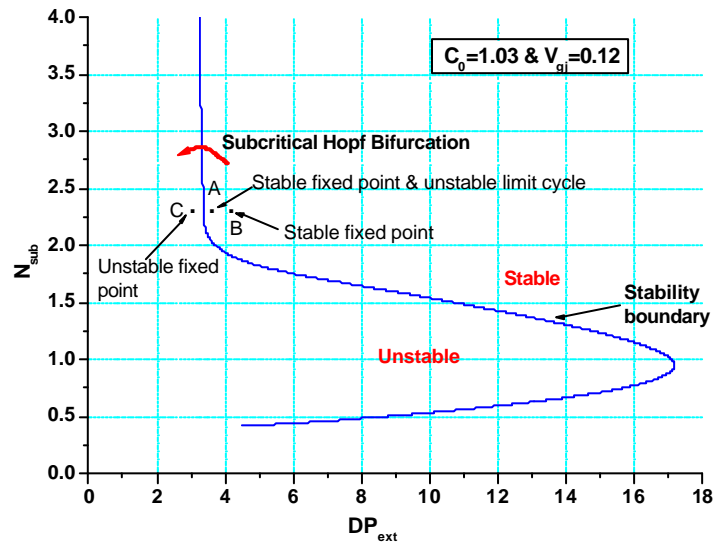


Figure 7-7. Different types of solutions during a subcritical Hopf bifurcation occurrence, as predicted using the current reduced order model.

1. The change of the solution type from +1%F OP to -1%F OP in the RAMONA calculation can be explained only by the occurrence of a subcritical Hopf bifurcation during the loss of system stability. This is in accordance with the proposed correspondence hypothesis.
2. The nominal, +0.3%F, and +1%F OPs are located in the linear stable region, while the -0.3%F and -1%F OPs are located in the linear unstable region. Consequently, a local stability boundary exists between the nominal OP and the -0.3%F OP. The scheme shown in Fig. 7-8 summarizes the results found in this study.

It should be pointed out that the intention here has been to perform a qualitative comparison between the results found using RAMONA and those found using the current reduced order model. In other words, the objective has been to compare how the solution manifold can vary as a function of a certain bifurcation parameter, which is here the mass flow. A detailed quantitative comparison of results for *kklc7_rec4* OP from RAMONA and the reduced order model will be presented in the next chapter.

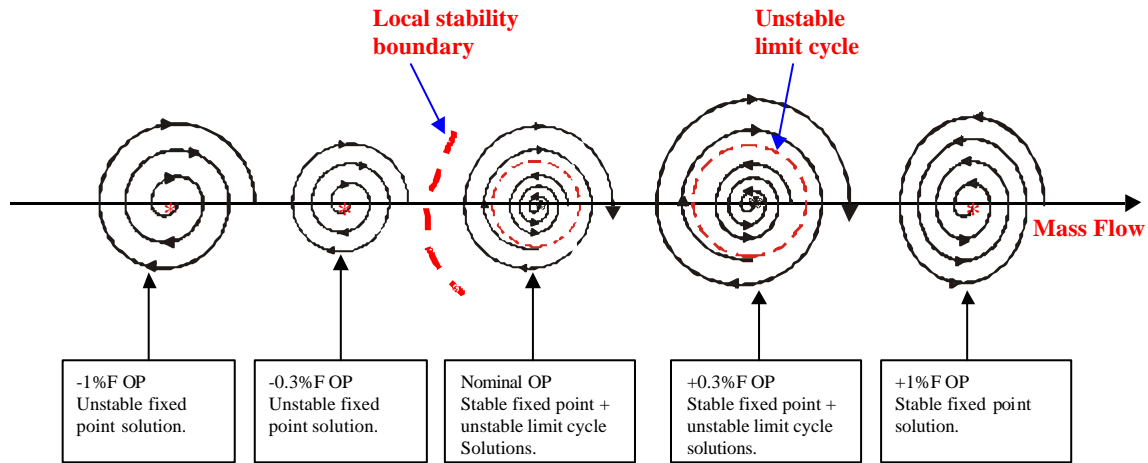


Figure 7-8. Scheme showing the different solution types encountered when the mass flow is varied for the nominal Leibstadt OP.

7.4 SUPERCRITICAL HOPF BIFURCATION USING RAMONA

In this section, RAMONA analyses are carried out to study the stability behaviour of the Ringhals-1 NPP around a reference operational point called record9 of cycle 14, referred to here as the nominal OP, and characterized by 72.5% thermal power and 32.0% mass flow. Historically, this OP, along with several others, was analysed in the framework of an international BWR stability benchmark in which calculated stability characteristics (DR and NF) were compared with experimental results [8].

As in the previous section, a detailed local bifurcation analysis is performed to study how the system solution varies as a function of the mass flow. A qualitative comparison with reduced order model findings is then carried out to explain the RAMONA results.

The following are the Ringhals-1 OPs at which the stability behaviour has currently been investigated:

- ❑ 72.5% thermal power and 32.0% mass flow rate (nominal OP).
- ❑ 72.5% thermal power and 31.0% mass flow rate (-1%F OP).
- ❑ 72.5% thermal power and 33.0% mass flow rate (+1%F OP).
- ❑ 72.5% thermal power and 35.0% mass flow rate (+3%F OP).

At each OP, two cases with different control rod perturbation amplitudes have been studied. Thus, Figs. 7-9(a) to 7-11(a) show the results for cases with 2-node CR

perturbation amplitude, while Figs. 7-9(b) to 7-11(b) show those for zero CR perturbation (*i.e.* with only numerical noise active as perturbation, which is considered to be very small). The results shown are the RAMONA-calculated LPRM354 time series signals for the nominal, -1%F, +1%F and +3%F OPs, respectively.

7.4.1 Results for the Different Ringhals-1 NPP Operational Points

The nominal OP: 72.6% power and 32.0% mass flow

It seen from Fig. 7-9 that the system behaviour at the nominal OP corresponds, for both control rod perturbation amplitudes, to a stable limit cycle oscillation with 6% amplitude. Referring to the correspondence hypothesis, this means that a supercritical Hopf bifurcation occurs as the system loses its stability.

The -1%F OP: 72.6% power and 31.0% mass flow

Decreasing the mass flow of the nominal OP by 1% of the maximum mass flow⁴⁷, the solution of the system becomes an unstable fixed point as illustrated in Fig. 7-10, *i.e.* for both 2-node CR perturbation amplitude and no CR perturbation, the oscillation amplitude grows with time. Note the very high oscillation amplitude that the power can reach, *viz.* after 175 seconds, the power amplitude increases by more than 100% (Fig. 7-10(b)), while at the nominal OP the maximum power oscillation amplitude is only about 6% (Fig. 7-9(a-b)). This happens even though the two OPs are very close to each other and is clearly indicative of the high sensitivity of the system behaviour to parameter changes.

The +1%F OP: 72.6% power and 33.0% mass flow

Figure 7-11 shows the system behaviour at the +1%F OP after the induction of a 2-node amplitude CR perturbation (Fig. 7-11(a)) and without any perturbation induction (Fig. 7-11(b)). In both cases, as for the nominal OP, this leads to a stable limit cycle solution. However, note that the amplitude of this limit cycle is around 2%, while it is 6% for the one observed at the nominal OP (Fig. 7-9). The reason for this will be discussed in Subsection 7.4.2, in which these results are compared qualitatively with those obtained using the reduced order model.

⁴⁷ The maximum mass flow for Ringhals is 11550 kg/s.

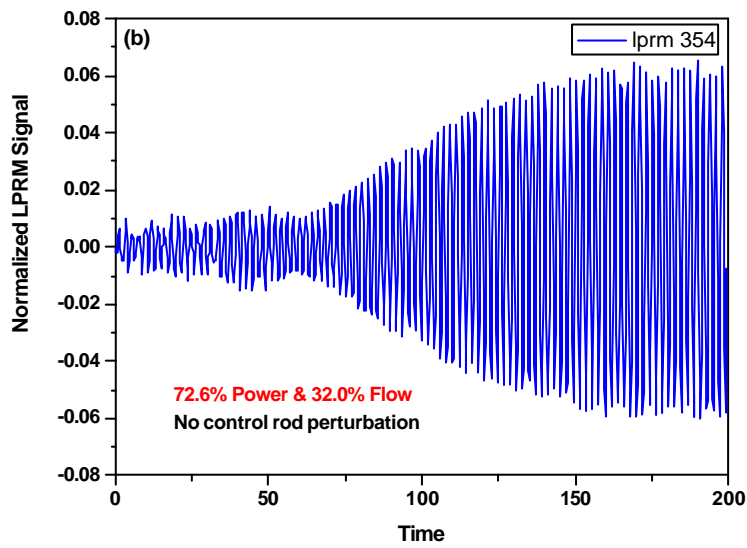
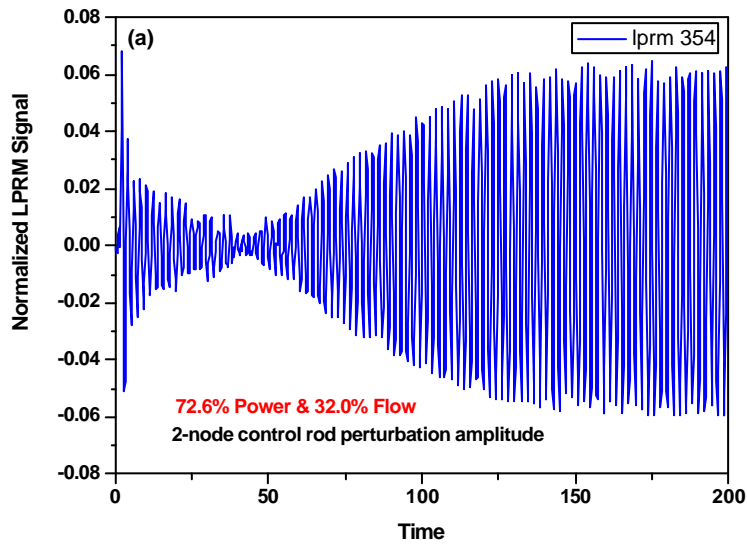


Figure 7-9. Nominal OP time series of Ringhals-1 LPRM showing a stable limit cycle solution with around 6% amplitude: (a) 2-node control rod perturbation amplitude. (b) No control rod perturbation is induced.

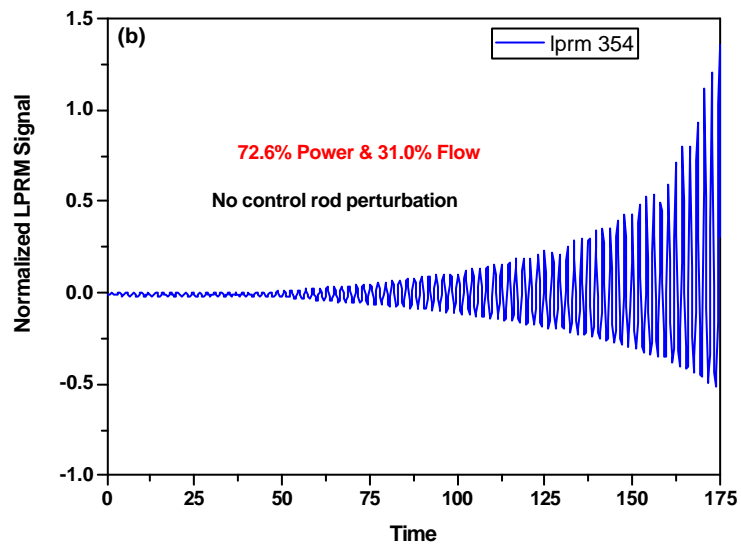
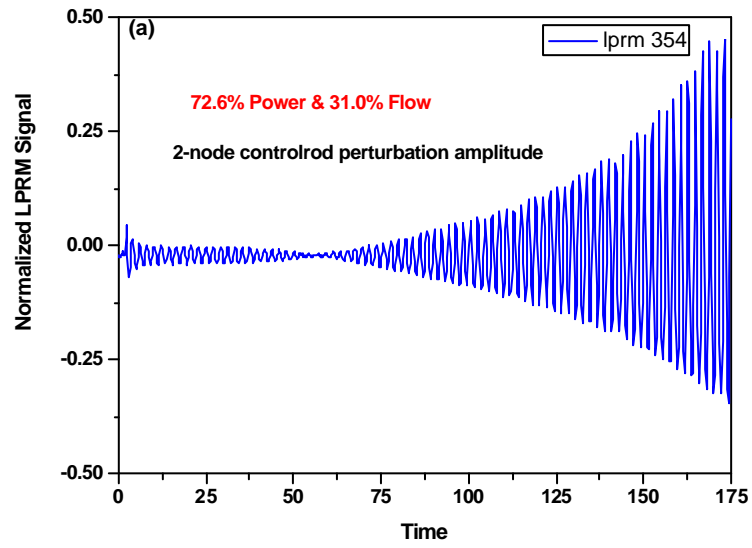


Figure 7-10. $-1\%F$ OP time series of Ringhals-1 LPRM showing an unstable fixed point solution: (a) 2-node control rod perturbation amplitude. (b) No control rod perturbation is induced.

The +3%F OP: 72.6% power and 35.0% mass flow

Figure 7-12 displays the LPRM time series signal at the +3%F OP. It is clear from both parts of the figure that a stable limit cycle is the system solution here. Once more, there is a decrease of the limit cycle amplitude, *viz.* to about 1%.

7.4.2 Interpretation and Discussion

To summarize the above analysis with RAMONA, an unstable fixed point solution is found at the $-1\%F$ OP, while stable limit cycle solutions are observed at the nominal, $+1\%F$ and $+3\%F$ OPs with 6%, 2% and 1% amplitude, respectively. Except for the stable fixed point solution that has not been searched for in the current RAMONA analysis⁴⁸, the solution types are the same as those found using the current reduced order model for a generic case in which a supercritical Hopf bifurcation occurs, as illustrated in Fig. 7-13. The operational points A, B, C and D shown in this figure are located in a region where a supercritical Hopf bifurcation is predicted by the bifurcation code BIFDD.

It should be stressed again that the intention here is to perform a qualitative comparison between the results found using RAMONA and those found using the current reduced order model. By carrying out numerical integration of the ODEs at the four operational points for the generic case, it was found that, as expected, since point A is located in the stable region and the type of bifurcation is supercritical, the solution is a stable fixed point. Point B is inside the linear unstable region but close to the SB, so that a stable limit cycle solution is found here. The same is the case for point C, which is further inside the linear unstable region but still close to the SB, so that again a stable limit cycle solution is observed. However, the amplitude of the stable limit cycle is larger at C than at B. This means that the further the OP is from the SB, the larger is the amplitude of the limit cycle, if found. This is the reason why the limit cycle amplitude at the nominal OP in the Ringhals-1 analysis with RAMONA (Fig. 7-9) is larger than those for the $+1\%F$ and the $+3\%F$ OPs (Figs. 7-11 and 7-12). Thus, one may conclude that the $+3\%F$ OP is the closest to the SB, followed by the $+1\%F$ OP and then the nominal OP.

⁴⁸ It would have been interesting to investigate more operational points by increasing the mass flow further ($> 3\%$) in order to find a stable fixed point solution. Unfortunately, this was not possible since, for operational points with large deviations from the nominal OP, it would have been necessary to provide a new distribution file (containing the nodal distributions on burnup, void history, power and Xenon concentration) for the RAMONA input, and this would have been very time consuming. Hence, the present investigation has been limited to operational points very close to the nominal OP.

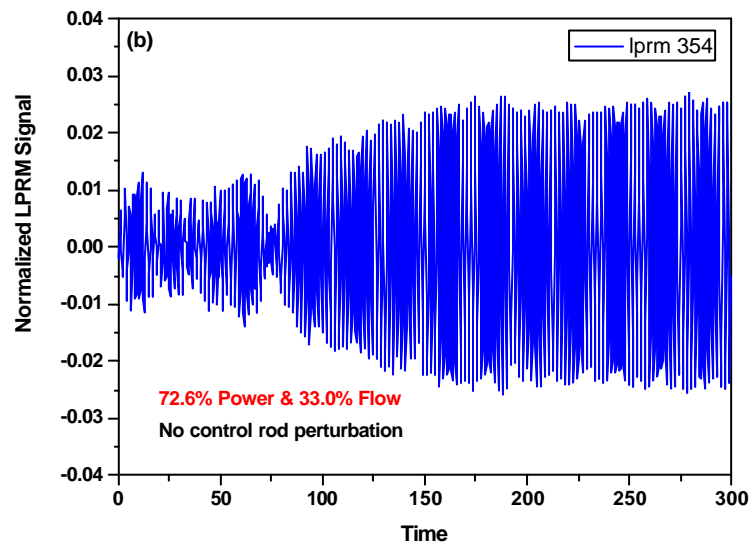
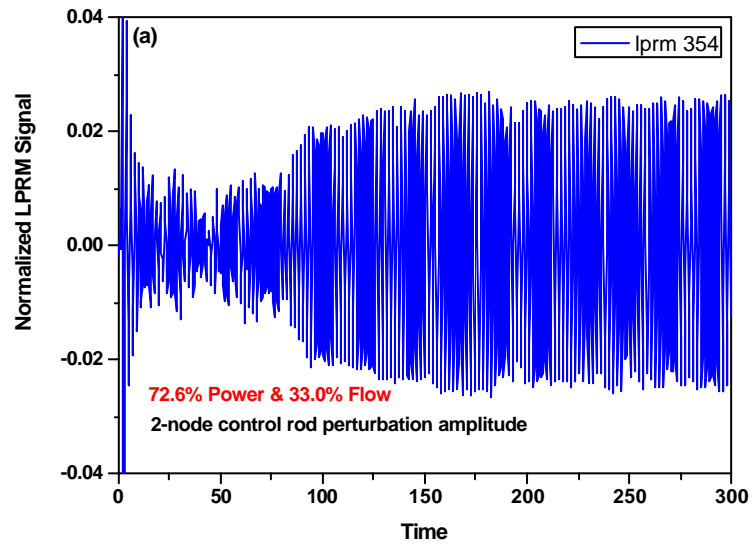


Figure 7-11. +1%F OP time series of Ringhals-1 LPRM showing a stable limit cycle solution with around 2% amplitude: (a) 2-node control rod perturbation amplitude. (b) No control rod perturbation is induced.

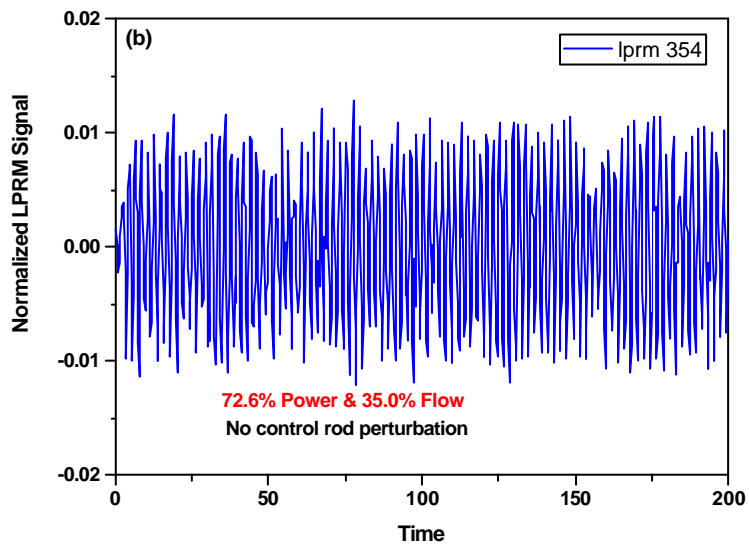
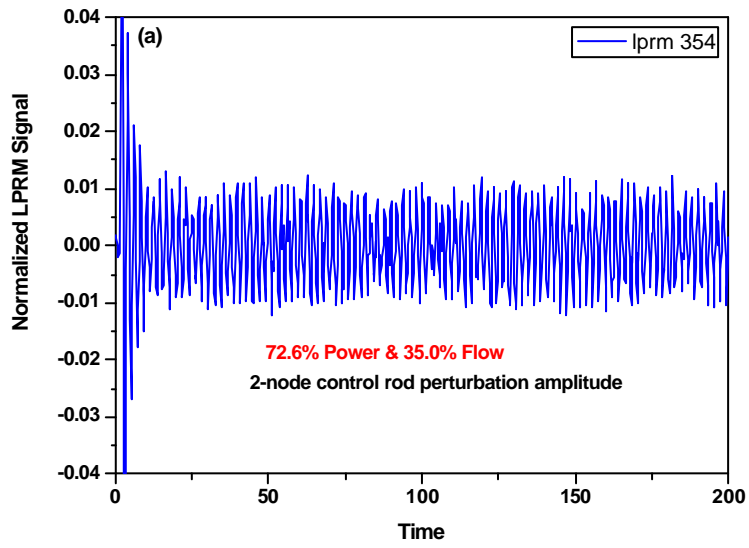


Figure 7-12. +3%F OP time series of Ringhals-1 LPRM showing a stable limit cycle solution: (a) 2-node control rod perturbation amplitude. (b) No control rod perturbation is induced.

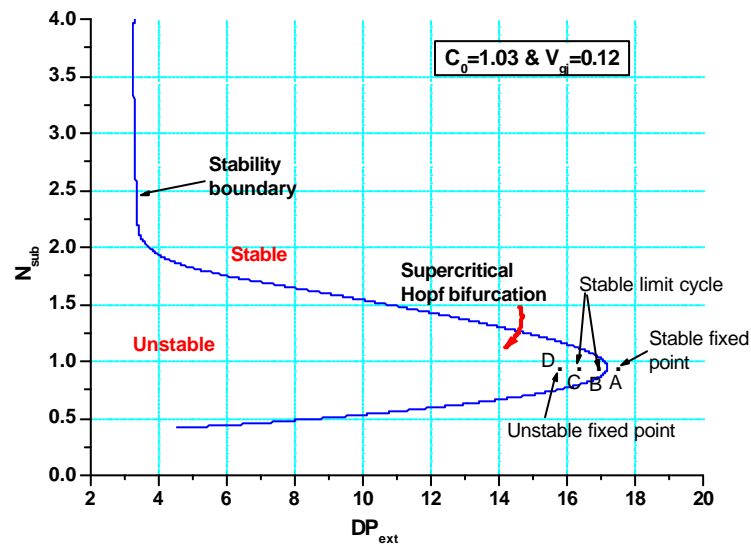


Figure 7-13. Different solution types predicted during the occurrence of a supercritical Hopf bifurcation using the reduced order model for a generic case.

Since the point D in Fig. 7-13 is quite far from the SB inside the linear unstable region, an unstable fixed point is the only possible solution here. This is similar to the Ringhals-1 system behaviour predicted by RAMONA at $-1\%F$ OP. Hence, taking into account the fact that the points A-D analysed with the reduced order model correspond to the occurrence of a supercritical Hopf bifurcation, the only explanation for the change of solution type observed with RAMONA in the Ringhals-1 analysis is the same, *viz.* that a supercritical Hopf bifurcation occurs. The four OPs lie at increasing distances from the SB, $+3\%F$ being the closest, followed by the $+1\%F$, nominal and $-1\%F$ OPs, in that order.

7.5 SUMMARY AND CONCLUSIONS

As a first step, a correspondence hypothesis has been proposed to underline the unique relationship between a stable (unstable) limit cycle solution and the occurrence of supercritical (subcritical) Hopf bifurcation in the modelling of BWR stability behaviour. A detailed local bifurcation analysis has then been carried out using RAMONA in the narrow environment of two representative operational points for the Leibstadt and Ringhals-1 NPPs, respectively. Based on the experience acquired during stability and bifurcation analyses using the current reduced order model, the results found using RAMONA could be explained.

The following are the principal conclusions which can be drawn from the local bifurcation analysis around the nominal Leibstadt OP:

- A qualitative comparison between RAMONA results and those of the reduced order model confirms the occurrence of a subcritical Hopf bifurcation.
- This is the first time that the occurrence of a subcritical Hopf bifurcation has been identified using RAMONA, or any other system code.
- A local SB could thus be determined close to the nominal OP inside the exclusion area.
- The behaviour of the reactor at an operational point close to the SB is very sensitive to parameter variations. For instance, at the nominal OP, the system has a stable fixed point and an unstable limit cycle solution. When increasing the mass flow by only 1% (of the full flow), one sees that the solution becomes a stable fixed point, while by decreasing the mass flow by 0.3%, the solution changes to an unstable fixed point. Consequently, the issue of uncertainties becomes very important concerning the ability of RAMONA to correctly predict the behaviour at such an operational point (close to the SB). The results presented here show that, with a mass flow uncertainty of 2%, RAMONA might predict a stable reactor core for a situation where the system should truly be unstable, or *vice-versa*.

As regards the local bifurcation analysis carried out around the nominal Ringhals-1 OP, the principal findings are:

- A qualitative comparison with the reduced order model results confirms the occurrence of a supercritical⁴⁹ Hopf bifurcation.
- All the OPs analysed using RAMONA are located in the linear unstable region. Since at the +3%F OP the limit cycle has the smallest amplitude, this OP is the closest to the SB. The +1%F OP is the second OP closest, followed by the nominal OP. The 1%F OP is the farthest from the SB, an unstable fixed point being found here.
- It is found that for two OPs (the nominal and +1%F OPs) with a relative difference of as little as 3% in the mass flow (32% and 33% of full flow, respectively), the resulting stable limit cycles have a difference in amplitude of nearly a factor of 3

⁴⁹ Stable limit cycles have, of course, been observed earlier in stability analysis with system codes. This, however, is the first time that, on the basis of the *correspondence hypothesis*, such an observation is being attributed to the occurrence of a supercritical Hopf bifurcation.

(6% and 2% LPRM, respectively). This high sensitivity may, for example, be the explanation for the significant underestimation of the limit cycle amplitude for Ringhals-1 cycle 14 record 9 as investigated by Hennig and Nechvatal using RAMONA3 [15].

As observed in the reduced order model analysis, the present system code investigations have shown that the strip close to the stability boundary where unstable limit cycles may exist in the case of a subcritical Hopf bifurcation is very narrow (< 1% of full mass flow). However, for a supercritical Hopf bifurcation, the strip close to the stability boundary where stable limit cycles exist, is much larger (> 3% of the mass flow).

REFERENCES:

- [1] J. L. Muñoz-Cobo, G. Verdú, "Application of Hopf Bifurcation Theory and Variational Methods to the Study of Limit Cycles in Boiling Water Reactors", *Ann. Nucl. Energy*, **18**, 5, 269, 1991.
- [2] M. Tsuji, K. Nishio, M. Narita, "Stability Analysis of BWRs Using Bifurcation Theory", *J. Nucl. Sci. Tech.*, **30**, 11, 1107-1119, 1993.
- [3] A. A. Karve, Rizwan-uddin, J. J. Dorning, "Stability Analysis of BWR Nuclear Coupled Thermal-Hydraulics Using a Simple Model", *Nucl. Eng. and Design*, **177**, 155-177, 1997.
- [4] D. D. B. van der Bragt, Rizwan-uddin, T. H. J. J. van der Hagen, "Nonlinear Analysis of a Natural Circulation Boiling Water Reactor", *Nucl. Sci. Eng.*, **131**, 23-44, 1999.
- [5] R. Zboray, D. D. B. van der Bragt, Rizwan-uddin, T. H. J. J. van der Hagen, H. van Dam, "Influence of Asymmetrical Axial Power Distributions on Nonlinear BWR Dynamics", *Proc. 9th Int. Topical Mtg. on Nuclear Thermal Hydraulics (NURETH-9)*, San Francisco, USA, October 3-8, 1999.
- [6] D. D. B. van der Bragt, Rizwan-uddin, T. H. J. J. van der Hagen, "Effect of Void Distribution Parameter and Axial Power Profile on Boiling Water Reactor Bifurcation Characteristics", *Nucl. Sci. Eng.*, **134**, 227-235, 2000.
- [7] A. Dokhane, D. Hennig, Rizwan-uddin, R. Chawla, "Nuclear-Coupled Thermal-hydraulic Nonlinear Stability Analysis Using a Novel BWR Reduced Order Model: Part 1 – The Effect of Using Drift Flux versus Homogeneous Equilibrium Models", *Proc. ICONE11*, Tokyo, Japan, April 20-23, 2003.

- [8] T. Lefvert, "Ringhals-1, Stability Benchmark," NEA/NSC/DOC(96)22, Nuclear Energy Agency, 1996.
- [9] D. Hennig, "A Study of BWR Stability Behaviour", *Nucl. Technology*, **126**, 10-31, 1999.
- [10] R. Miró, D. Ginestar, D. Hennig, G. Verdú, "On the Regional Oscillation Phenomenon in BWRs", *Prog. Nucl. Energy*, **36**, 2, 189-229, 2000.
- [11] D. Blomstrand, "The KKL Core Stability Test, Conducted on September 6, 1990," Internal ABB report BR91-245, ABB Atom, 1992.
- [12] M. Johansson, "Data for Stability Benchmark Calculation, Ringhals Unit 1, Cycles 14, 15, 16 and 17," Internal Vattenfall report 0120/94, Vattenfall AB, January 1994.
- [13] R. T. Lahey, Jr. "Applications of Fractals and Chaos Theory in the Field of Multiphase Flow and Heat Transfer," in *Boiling Heat Transfer*, pp. 317-387, edited by R.T. Lahey, Jr., Elsevier Science Publishers, 1992.
- [14] A. H. Nayfeh, B. Balachandran, *Applied Nonlinear Dynamics*, John Wiley & Sons, Inc., New York, 1995.
- [15] D. Hennig and L. Nechvatal, "SWR Stabilitätsanalyse: Methodik der Stabilitätsanalyse und PSI-Ergebnisse zur NEA/NCR Benchmarkaufgabe", Internal PSI report, September 1996.

8 REDUCED ORDER MODEL VS. SYSTEM CODE RAMONA

In Chapter 6, typical standard values were used for BWR operating and design parameters in conducting stability analysis with the current reduced order model. These parameter values were used previously by Karve [1] and are given in Appendix F. This allowed, for the HEM case ($C_0 = 1$, $V_{gj} = 0$), a systematic comparison and validation of the new reduced order model results against those of the Karve model. The principal aim in the present chapter is to make a quantitative comparison between the current reduced order model and the system Code RAMONA for a specific operational point of the Leibstadt NPP. This operational point has been analysed in detail using RAMONA in the previous chapter (Section 7.3) and corresponds to the so-called cycle7 record 4, with 60.5% power and 36.7% mass flow rate (*kklc7_rec4* OP), shown in Fig. 7-1. It is located in the plant's exclusion area and is an OP for which a stability measurement was carried out during cycle 7 reactor start-up, in September 1990. The systematic comparison made here between RAMONA and the current reduced order model allows important conclusions to be drawn regarding the latter's applicability, as well as the limitations.

First, as a bridge between Chapter 6 and the present chapter, as well as to help in drawing the conclusions, Section 8.1 is devoted to a sensitivity analysis in which the effects of certain design and operating parameters on the stability boundary and the nature of Hopf bifurcation are investigated using the reduced order model. After that, in Section 8.2, using RAMONA, the stability behaviour of the *kklc7_rec4* OP analysed in Section 7.3 is recalled by showing the time series of two different LPRMs. Then, in Section 8.3, the same OP is analysed using the current reduced order model, and the stability boundary and bifurcation characteristics are determined. In Section 8.4, a comparative analysis of the results of the reduced order model against those of RAMONA is carried out, and the limitations of the reduced order model are discussed. Finally, in Section 8.5, a summary and conclusions of this comparative study are presented.

8.1 *SENSITIVITY ANALYSIS USING THE REDUCED ORDER MODEL*

Sensitivity of the stability boundary to design and operating parameters for BWRs has been studied extensively [1-3]. These studies showed that the system stability boundary is quite sensitive to certain parameters while it is less affected by others. However, the investigation of parameter effects on BWR bifurcation characteristics has never been reported before. The goal in this section is accordingly to carry out a sensitivity analysis in which the effects of certain parameters on both the stability boundary and the nature of bifurcation are investigated. As a check for the model response to different parameter variations, certain trends are compared with those reported in previous studies. The design and operating parameter values used in this analysis are presented in Appendix G and correspond to the Leibstadt NPP cycle7 record 4 operational point, *i.e.* *kklc7_rec4 OP*.

8.1.1 **Effects of Void Feedback Reactivity**

The impact of a 10% increase in the void feedback reactivity on the BWR stability is shown in Fig. 8-1. Increasing the magnitude of the void feedback reactivity coefficient has a destabilizing effect in the most relevant region ($N_{sub} < 1.5$). This is qualitatively in good agreement with previous findings reported by Yoshimoto *et al.* [5], Karve [1] and van Bragt [3]. For instance, Yoshimoto *et al.* found an increase of the power oscillation amplitude when the void feedback reactivity coefficient is increased by 20%.

Figure 8-2 depicts the effect of increasing the void feedback on the nature of Hopf bifurcation. It is seen in this figure that the nature of Hopf bifurcation is not affected except in a small interval. Only a small shift of the transition point between the sub- and supercritical Hopf bifurcation region is observed when the void feedback gain is increased. Thus, the branch of the SB with $1.9 < N_{sub} < 2.1$, that was associated with supercritical Hopf bifurcation for the reference case, becomes subcritical when the void feedback gain is increased by 10%. This means that increasing the void feedback reactivity makes the Hopf bifurcation more subcritical.

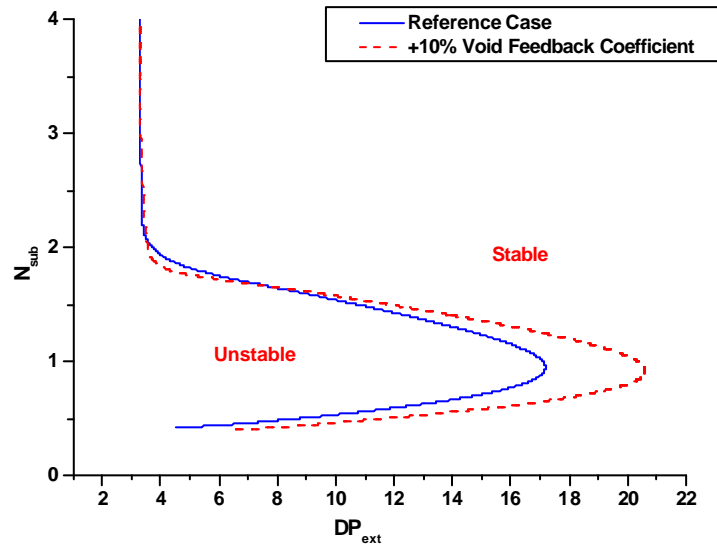


Figure 8-1. Effects of a 10% increase of the void feedback coefficient on the system stability boundary.

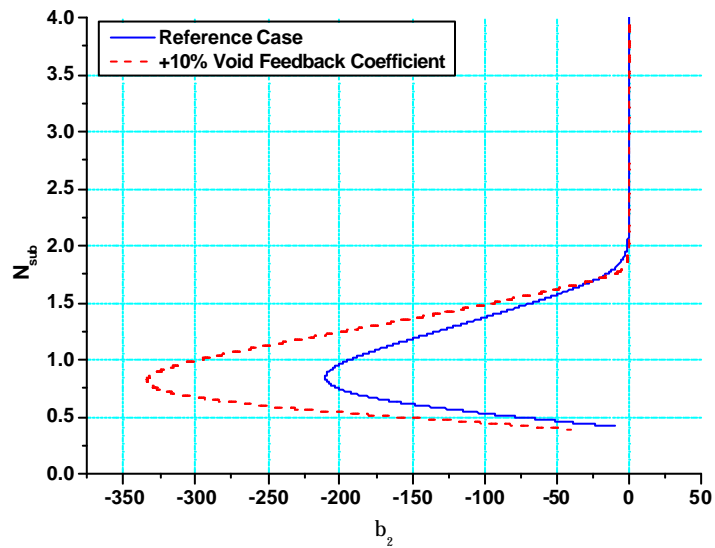


Figure 8-2. Effects of a 10% increase of the void feedback coefficient on the nature of Hopf bifurcation.

8.1.2 Effects of Pellet-Clad Gap Conductance

The effects of a 10% increase in the pellet-clad gap conductance on the stability boundary and the nature of Hopf bifurcation are depicted in Figs. 8-3 and 8-4, respectively. For $N_{sub} < 1.6$, the gap conductance has a destabilizing effect, while it is stabilizing for higher values of N_{sub} ($1.6 < N_{sub} < 2.0$). This may explain the apparently contradicting results reported in previous studies with some of these predicting a stabilizing effect, *e.g.* [1] and [6], and others indicating a destabilizing effect, *e.g.* [2].

Figure 8-4 shows clearly that the gap conductance has a very small effect on the nature of Hopf bifurcation. There is only a small branch of the SB ($2.0 < N_{sub} < 2.1$) which is affected by the change of the gap conductance value.

8.1.3 Effects of Fuel Radial Dimensions

In the following are considered the effects of increasing the fuel radial dimensions by 10% from the reference case values presented in Appendix G. Effectively, the radial dimensions of the fuel pellet, the gap, and the cladding have all been increased by 10%. Figure 8-5 shows that there is a significant effect on the stability boundary. While for low values⁵⁰ of N_{sub} ($N_{sub} < 1.4$), the effect is stabilizing, it is destabilizing for higher values.

Increasing the fuel radial dimensions makes the nature of Hopf bifurcation more supercritical, *i.e.* the SB branch with $2.1 < N_{sub} < 2.3$, that was associated with subcritical Hopf bifurcation for the reference case, becomes supercritical.

8.1.4 Effects of Inlet and Exit Pressure Loss Coefficients

Figures 8-7, 8-8, 8-9 and 8-10 depict the effects on the stability boundary and the nature of Hopf bifurcation of increasing the inlet and exit pressure loss coefficients (K_{inlet} and K_{exit}) by 10% from their reference case values. The current findings for the stability boundary are consistent with those reported by Tsuji *et al.* [2], Yoshimito *et al.* [5] and Karve [1]. Thus, it is seen that increasing the inlet loss coefficient has a stabilizing effect (Fig. 8-7), while increasing the exit pressure loss coefficient has a destabilizing effect (Fig. 8-9). In fact, the same effects were found in the heated channel parametric study carried out in Chapter 5 (see Section 5.5 and [4]).

⁵⁰ As mentioned earlier, these correspond to normal operational points.

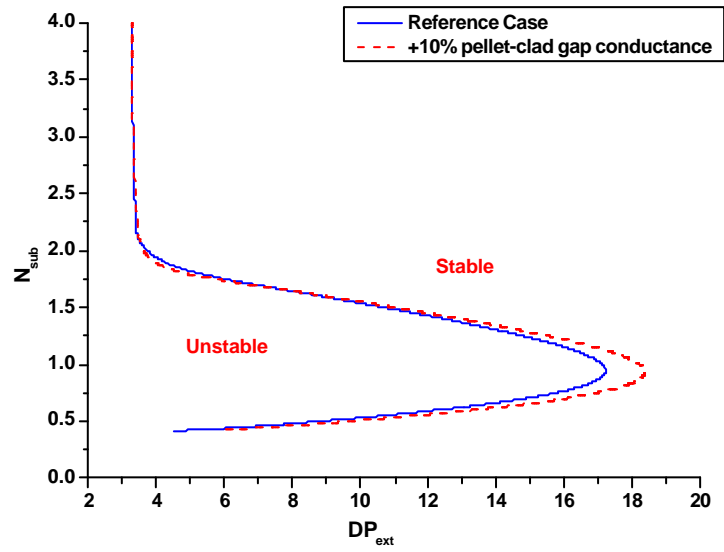


Figure 8-3. Effects of a 10% increase of the pellet-clad gap conductance on the system stability boundary.

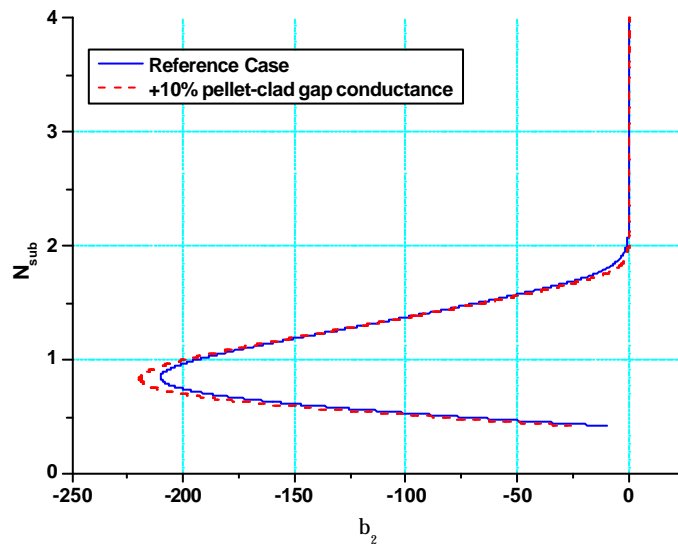


Figure 8-4. Effects of a 10% increase of the pellet-clad gap conductance on the nature of Hopf bifurcation.

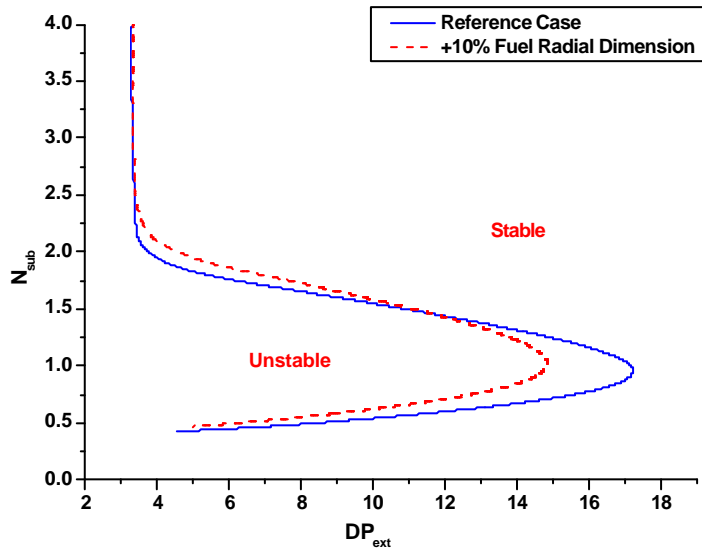


Figure 8-5. Effects of a 10% increase of the fuel radial dimension on the system stability boundary.

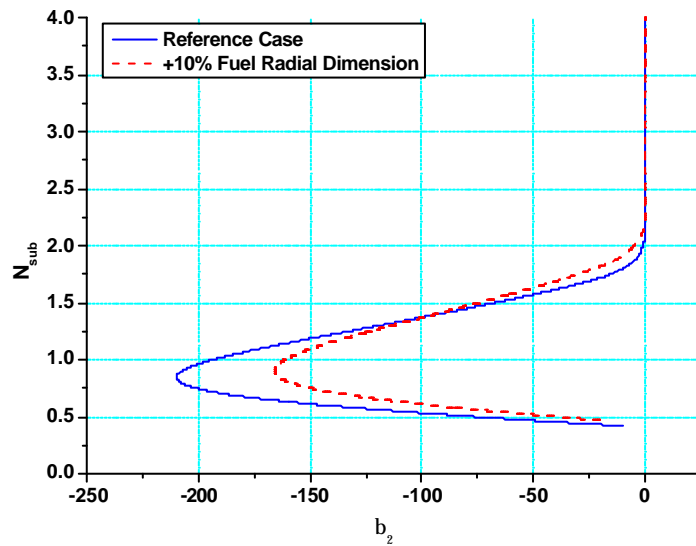


Figure 8-6. Effects of a 10% increase of the fuel radial dimension on the nature of Hopf bifurcation.

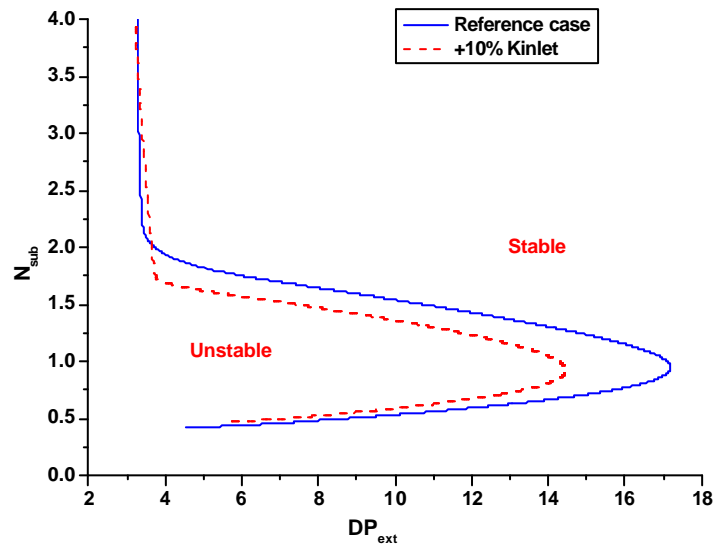


Figure 8-7. Effects of a 10% increase of the inlet pressure loss coefficient on the system stability boundary.

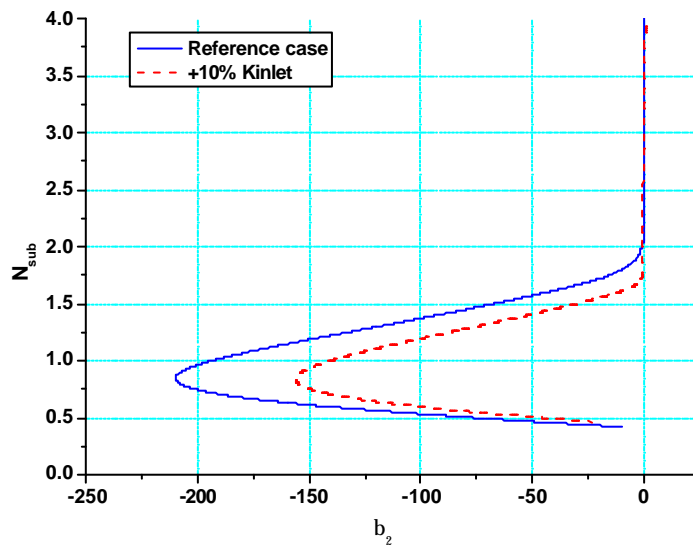


Figure 8-8. Effects of a 10% increase of the inlet pressure loss coefficient on the nature of Hopf bifurcation.

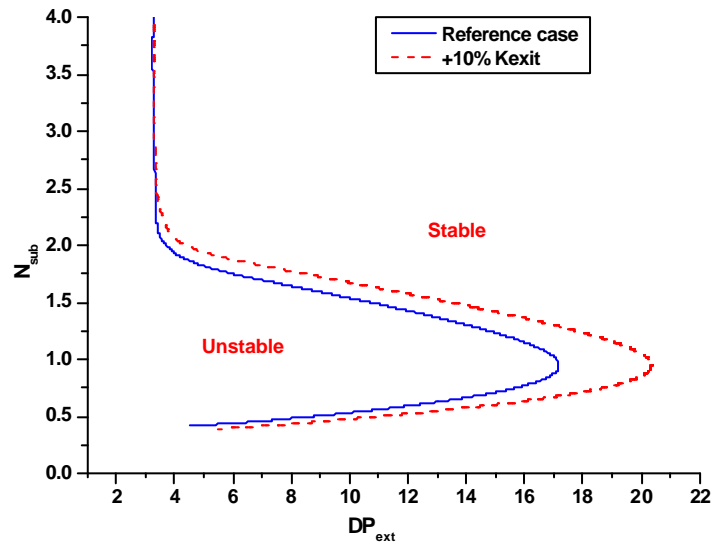


Figure 8-9. Effects of a 10% increase of the exit pressure loss coefficient on the system stability boundary.

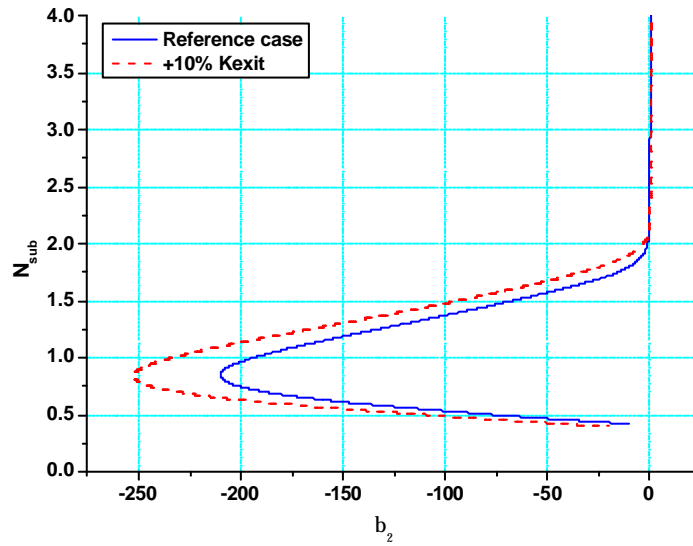


Figure 8-10. Effects of a 10% increase of the exit pressure loss coefficient on the nature of Hopf bifurcation.

The nature of Hopf bifurcation is found to be sensitive to the inlet loss coefficient value in the SB branch with $1.75 < N_{sub} < 2.1$, as shown in Fig. 8-8. This branch, that was associated with the supercritical Hopf bifurcation for the reference case, becomes subcritical when K_{inlet} is increased by 10%. This means that an uncertainty of 10% in the inlet loss coefficient may lead to a discrepancy in predicting the nature of Hopf bifurcation if the operational point has a subcooling number value within the stated interval (1.75 to 2.1).

The effect of K_{exit} on the nature of Hopf bifurcation is quite the opposite to that of K_{inlet} , as depicted in Fig. 8-10. For instance, the branch of the SB with $2.1 < N_{sub} < 2.3$, that was associated with subcritical bifurcation for the reference case, becomes associated with supercritical bifurcation by increasing K_{exit} by 10%. In summary, we can conclude that, while K_{inlet} makes the nature of Hopf bifurcation more subcritical, K_{exit} makes it more supercritical.

8.2 STABILITY BEHAVIOUR OF THE *KKLC7_REC4* OP USING RAMONA

The stability behaviour of the *kklc7_rec4* OP as analysed using the system code RAMONA (see Section 7.3) is recalled here. Figure 8-11 depicts the time series of LPRM84⁵¹ and LPRM354 for two different control rod perturbation amplitudes. This figure clearly shows the excitation of out-of-phase oscillations, *i.e.* when the power increases in LPRM84, it decreases in LPRM354, and *vice versa*. The nature of Hopf bifurcation can be deduced by analysing Figs. 8-11(a) and 8-11(b). While the small amplitude perturbation (0.05-node) decays to the stable fixed point, the large amplitude perturbation (2-node) leads to growing amplitude oscillations. This means that, beside the stable fixed point solution, an unstable limit cycle solution exists at this operational point. Referring to the *correspondence hypothesis*, this implies the occurrence of a subcritical Hopf bifurcation, *i.e.* corresponds to the existence of an unstable limit cycle solution in the linearly stable region in the very close neighbourhood of the SB. Thus, using RAMONA, one can conclude that the *kklc7_rec4* OP is located very close to the local SB in the linear stable region. The oscillation frequency at this OP is found to be 0.58 Hz.

⁵¹ LPRM84 stands for LPRM number 8 located at axial level 4. Level 4 corresponds to the highest level (see Chapter 2).

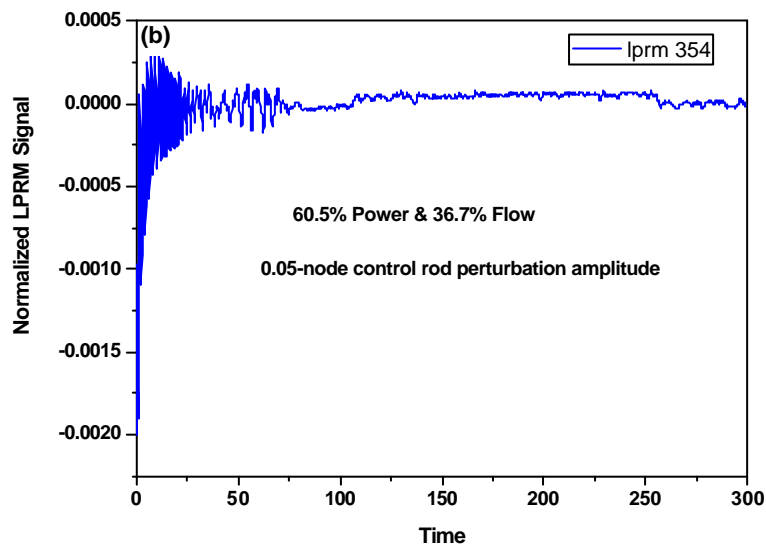
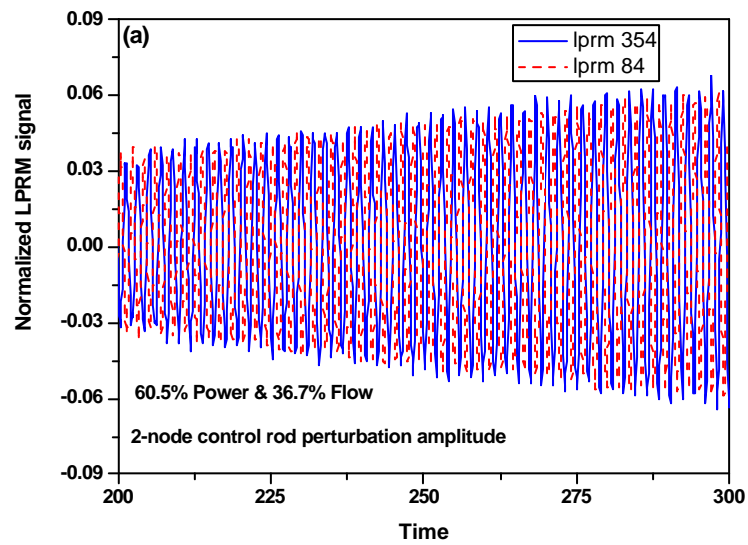


Figure 8-11. Time series of the *kklc7_rec4* LPRMs (RAMONA analysis) showing the occurrence of out-of-phase oscillations with a subcritical Hopf bifurcation. **(a)** 2-node control rod perturbation amplitude. **(b)** 0.05-node control rod perturbation amplitude.

8.3 STABILITY CHARACTERISTICS OF THE *kklc7_rec4* OP USING THE REDUCED ORDER MODEL

In this section, the stability characteristics of the *kklc7_rec4* OP are studied in greater detail using the current reduced order model. In order to achieve the desired modelling, many of the operating and design parameters for this OP have been evaluated in a specific manner. For instance, the single and two-phase friction factors, the two-phase multiplier, the fuel heat capacity, the thermal fuel conductivity and the gap conductance have all been calculated using the correlations used in RAMONA (see Appendix A (A.2.1 and A.3.1)). The inlet and exit loss coefficients have been adjusted to include the spacer pressure losses in the channel at inlet and exit. The void and Doppler feedback reactivities have been calculated based on the methodology proposed in Appendix E. The complete set of design and operating parameters for *kklc7_rec4* OP is given in Appendix G.

Figure 8-12 gives the stability boundary as predicted by the reduced order model for *kklc7_rec4* OP in the $N_{sub} - DP_{ext}$ plane. The *kklc7_rec4* OP is characterized by:

- The subcooling enthalpy is $h_{sat}^* - h_{inlet}^* = 125 \cdot 10^3 J \cdot Kg^{-1}$. This corresponds to a subcooling temperature $T_{sat}^* - T_{inlet}^* = 23.4 K$ and a subcooling number $N_{sub} = 1.55$
- The total pressure drop across the core is $DP_{ext}^* = 0.4497 \cdot 10^5 N/m^2$. This corresponds to a dimensionless total pressure drop across the core $DP_{ext} = 8.57$.

The estimation of the void distribution parameter and drift velocity values at this OP are based on the justifications given in Section 6.4. Thus, the validation of the thermal-hydraulic model against the Saha *et al.* experimental data and several earlier developed analytical models (Section 5.3) showed that for the Set I data, that correspond to an inlet velocity of 0.98 m/s, a value of the void distribution parameter of 1.03 allows the current reduced order model to predict a SB which fits the measurements best. Because, for the *kklc7_rec4* OP, the liquid inlet velocity is also 0.98 m/s, $C_0 = 1.03$ is then clearly a reasonable assumption for the void distribution parameter. On the other hand, based on the relationship between the vapour and liquid velocities used for the slip model in RAMONA (Eq. (A.17) in Appendix A), it was found that the average slip value is 1.35 for the *kklc7_rec4* OP. This corresponds to a drift velocity $V_{gj} = 0.12$.

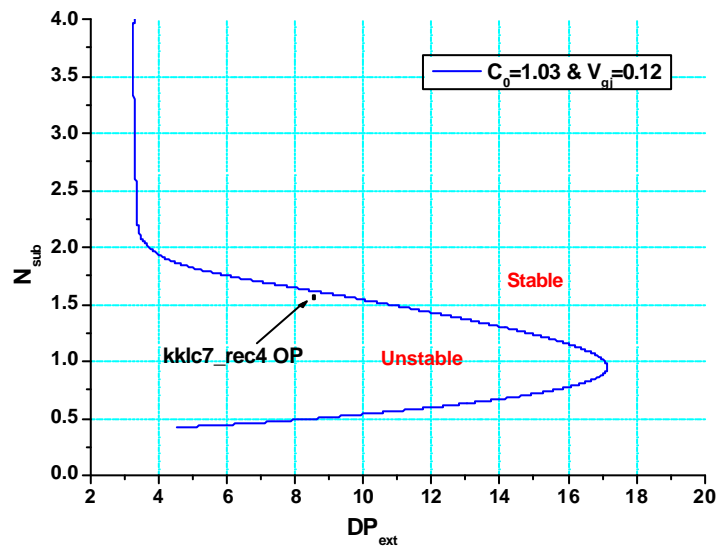


Figure 8-12. Stability boundary in $N_{sub} - DP_{ext}$ plane for operating and design parameters corresponding to the *kklc7_rec4* operational point.

8.3.1 Semi-analytical Bifurcation Analysis

The bifurcation analysis for *kklc7_rec4* OP was then carried out using the bifurcation code BIFDD. As seen in Fig. 8-12, the *kklc7_rec4* OP is located on the unstable side and lies very close to the stability boundary. The transformed stability boundary in the power-flow plane is shown along with the exclusion area in Fig. 8-13. Again, as in Fig. 8-12, the *kklc7_rec4* OP is located in the unstable region. In addition, Fig. 8-14, which shows the nature of Hopf bifurcation along the SB, indicates that for the SB branch with $N_{sub} > 2.1$, the type of Hopf bifurcation is subcritical whereas, for the branch with $N_{sub} < 2.1$, supercritical Hopf bifurcation is expected.

With *kklc7_rec4* located in the unstable region and lying close to the SB branch where a supercritical Hopf bifurcation is expected, one can conclude that a stable limit cycle solution should be found. Note that this OP is not too far from the SB branch where subcritical Hopf bifurcation can occur. Moreover, a close look at the properties of the elements of the eigenvector corresponding to the eigenvalue responsible for the occurrence of the Hopf bifurcation reveals that only in-phase oscillations are expected to be observed when the system loses its stability.

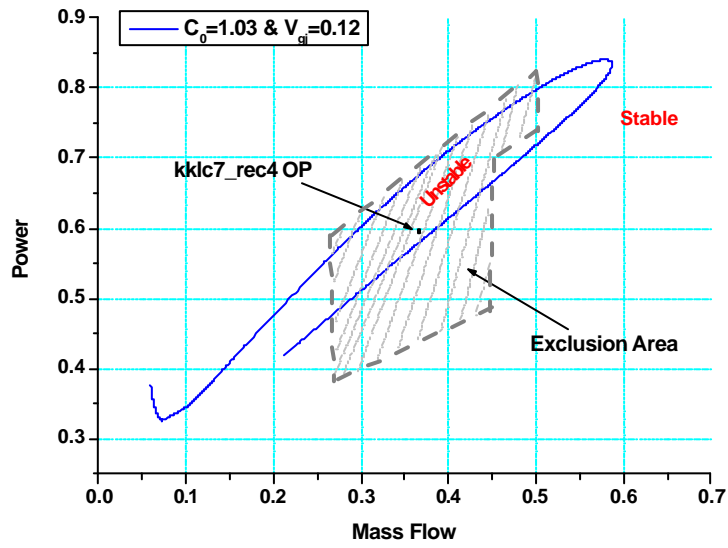


Figure 8-13. Stability boundary in the power-flow map for operating and design parameters corresponding to the *kklc7_rec4* operational point.

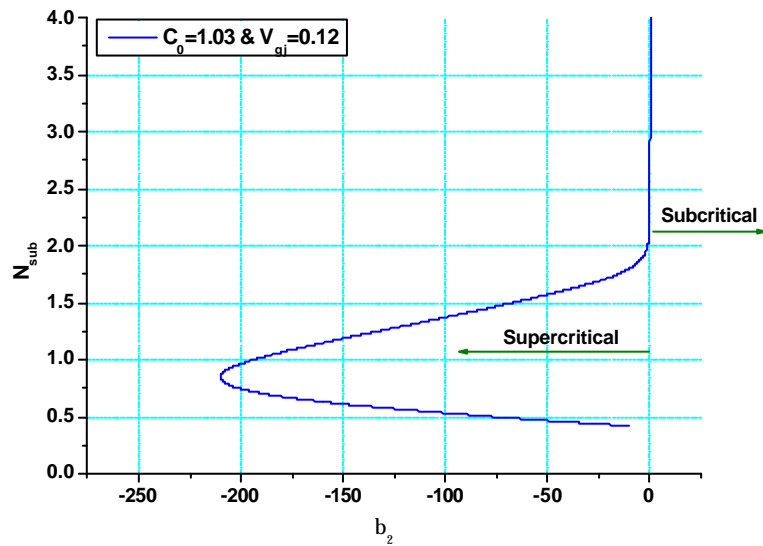


Figure 8-14. Bifurcation characteristics presented in $N_{sub} - b_2$ plane for operating and design parameters corresponding to the *kklc7_rec4* operational point.

Confirmation of these BIFDD predictions of the system behaviour for *kklc7_rec4* is obtained in the following subsection by numerically integrating the set of 22 ODEs at this OP.

8.3.2 Numerical Simulation

Figure 8-15 shows the time evolution of the amplitude of the fundamental and first mode oscillations. The development of a stable limit cycle for $n_0(t)$ is clearly seen here. This is in agreement with the bifurcation analysis prediction (supercritical Hopf bifurcation), as well as with the eigenvector analysis that predicts the excitation of in-phase oscillations. The oscillation amplitude of the first mode, in Fig. 8-15, seems to be zero. However, a zoom of this figure is displayed in Fig. 8-16, showing the development also of a stable limit cycle for $n_1(t)$. Note that, although out-of-phase oscillations are not excited at this OP, the first mode component is not decaying. This is again an illustration of the detailed explanation given earlier (Section 6.3) concerning the relationship between the excitation of in-phase or/and out-of-phase oscillations, and the fundamental and first modes.

The time evolution of the inlet velocities of the two channels is depicted in Fig. 8-17. Both channels are seen to behave in the same manner, *i.e.* the two inlet velocities have the same amplitude and phase. This is further confirmation that the in-phase oscillation mode is excited at this OP. The oscillation frequency from the results obtained using the reduced order model is 0.63 Hz, which is close to the value calculated using RAMONA.

8.4 COMPARISON OF RESULTS AND DISCUSSION

In summary, the system behaviour at the *kklc7_rec4* OP is characterized by:

1. Using the system code RAMONA:
 - a. The out-of-phase oscillation mode is excited.
 - b. The existence of a stable fixed point and an unstable limit cycle solution, *i.e.* the occurrence of a subcritical Hopf bifurcation, is predicted.
 - c. The *kklc7_rec4* OP is very close to the stability boundary.
 - d. The frequency of the oscillations is 0.58 Hz.

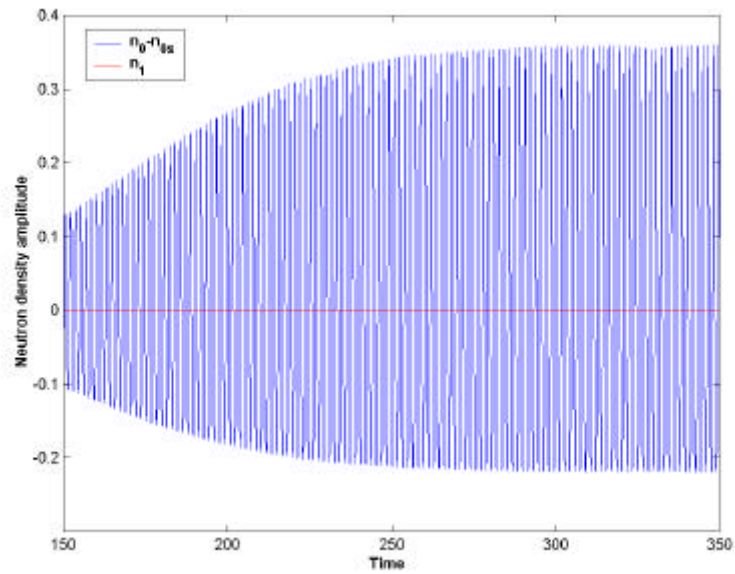


Figure 8-15. Time evolution of the deviation of the fundamental mode amplitude from the steady state value ($n_0 - n_{0s}$) and the first mode amplitude (n_1) at the *kklc7_rec4* operational point (n_{0s} is the steady state value for $n_0(t)$).

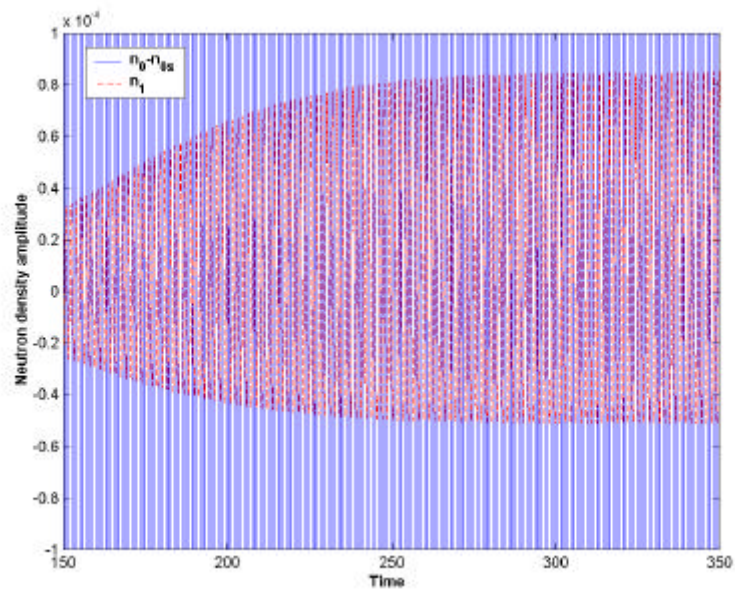


Figure 8-16. Zoom of Fig. 8-15 showing the very small amplitude of the stable limit cycle oscillation of the first mode amplitude (n_1) at the *kklc7_rec4* operational point.

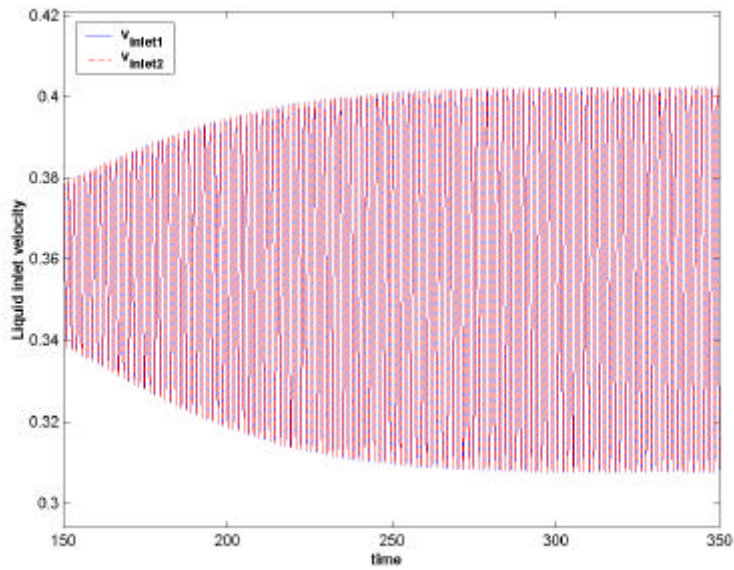


Figure 8-17. Time evolution of the liquid inlet velocity in channel 1 (v_{inlet1}) and channel 2 (v_{inlet2}). The two channels are seen to oscillate in-phase.

2. Using the reduced order model:

- a. The in-phase oscillation mode is excited.
- b. The existence of a stable limit cycle solution, *i.e.* the occurrence of a supercritical Hopf bifurcation, is predicted.
- c. The *kklc7_rec4* OP is very close to the stability boundary.
- d. The frequency of the oscillations is 0.63 Hz.

From the above *kklc7_rec4* OP predictions obtained using RAMONA and the current reduced order model, respectively, one can draw several conclusions. Thus, the reduced order model is seen to yield a good prediction of the location of the OP with respect to the stability boundary, as well as of the oscillation frequency value. However, the discrepancy is obvious between the model results and those of RAMONA concerning the excited oscillation mode (in-phase or out-of-phase) and the nature of Hopf bifurcation. This is not surprising, keeping in mind that (a) the reduced order model is highly simplified with the entire BWR core lumped into two representative channels, and (b) the design and operating parameters used for *kklc7_rec4* OP are core-average values.

The current reduced order model could not predict the out-of-phase oscillations at this OP mainly because of the limitations of the feedback reactivity model for the mode coupling ($\mathbf{r}_{10}(t)$ and $\mathbf{r}_{01}(t)$) as discussed in Appendix E, Section E.3. Accordingly, it is suggested that an improved model for the feedback reactivities in mode coupling be derived for future work.

The discrepancy in predicting the nature of Hopf bifurcation is due mainly to the uncertainties in evaluating the design and operating parameters as core-average values. In Sections 6.4 and 8.1, it was found that changing the value of certain parameters, *e.g.* the drift flux parameters (C_0 and V_{gj}) or the inlet pressure loss coefficient (K_{inlet}), can change the nature of Hopf bifurcation. In other words, a SB branch that was associated with subcritical Hopf bifurcation can become supercritical, or *vice versa*. This means that a small discrepancy in evaluating one or more of such parameters may lead to a wrong prediction of the nature of Hopf bifurcation. In addition, Zhou and Rizwan-uddin [7] showed that the nature of Hopf bifurcation can be very sensitive to the modelling assumptions made. Since the reduced order model does not have completely the same set of modelling assumptions as RAMONA, it is not surprising to observe such a discrepancy between the two models.

8.5 SUMMARY AND CONCLUSIONS

In this chapter, the currently developed reduced order model has been applied to the analysis of a specific Leibstadt operational point (*kklc7_rec4*). The results obtained have been compared to those of the system code RAMONA for the same OP. This comparison has allowed a direct assessment of the performance of the current reduced order model, *viz.* of both its applicability and its limitations.

It is seen that the reduced order model predicts very well the frequency of the oscillations and localizes the analysed OP in an appropriate region close to the SB. However, there is a clear discrepancy between the model results and those of RAMONA as regards the prediction of the oscillation mode (in-phase and out-of-phase) and the nature of Hopf bifurcation at this operational point. The inability to predict the out-of-phase oscillation mode at this OP is due to the limitations of the feedback reactivity model for the mode coupling (Appendix E, Section E.3), while the discrepancy in predicting the nature of Hopf bifurcation is mainly due to the uncertainties in evaluating the design and operating parameters adequately, the latter having been shown to have a considerable

impact on the nature of bifurcation (Section 8.1). These “negative” results concerning the reduced order model’s quantitative performance are in fact not surprising, since the reduced order model is highly simplified with the entire BWR core being lumped into just two representative channels, and the design and operating parameters calculated for a specific OP being core-average values. Consequently, one can conclude that the reduced order model:

- Is most useful for acquiring physical insight into the complex processes determining BWR stability.
- Allows fast and detailed parametric studies.
- Provides a wide range of solutions for the system at various points in a given parameter plane.
- Allows detailed semi-analytical bifurcation analysis using a bifurcation code such as BIFDD.

In addition, the model has been seen to provide good quantitative prediction of:

- The location of the analysed operational point in relation to the stability boundary.
- The oscillation frequency.

In the author’s opinion, however, a detailed quantitative study for a specific operational point is still not possible using a reduced order model, and this remains a big challenge. Thus, reduced order models, with respect to detailed system codes, still need to be considered as *complementary* tools, and *not* as alternatives.

REFERENCES

- [1] A. A. Karve, “Nuclear-Coupled Thermal-Hydraulic Stability Analysis of Boiling Water Reactors”, Ph.D. Dissertation, Virginia University, 1999.
- [2] M. Tsuji, K. Nishio, M. Narita, “Stability Analysis of BWRs using Bifurcation Theory,” *J. Nucl. Sci. and Tech.*, **30**, 11, 1107, 1993.
- [3] D. D. B. van Bragt, “Analytical Modelling of Boiling Water Reactor Dynamics”, Ph.D. Dissertation, Delft University of Technology, 1998.
- [4] A. Dokhane, D. Hennig, Rizwan-uddin, R. Chawla, “A Parametric Study of Heated Channels with Two-Phase Flow Using Bifurcation Analysis”, *Trans. Amer. Nucl. Soc.*, **86**, 131, 2002.

- [5] Y. Yoshimoto, T. Angegawa, O. Yokomizo, S. Ebeta, "Space-dependent Stability Analysis of Core-wide and Regional Modes in BWRs," *Proc. Int. Workshop on Boiling Water Reactor Stability*, CSNI-178, 337, 1990.
- [6] K. Valtonen, "BWR Stability Analysis," Technical Report, Finish Center for Radiation and Nuclear Safety, Helsinki, 1989.
- [7] Quan Zhou, Rizwan-uddin, "Impact of Modelling Assumptions on Stability and Bifurcation Analyses of BWRs," *Trans. Amer. Nucl. Soc.*, **86**, 249, 2002.

9 CONCLUSIONS AND RECOMMENDATIONS FOR FUTURE WORK

A novel analytical, reduced order model has been developed to simulate the different types of instabilities encountered in heated channels and BWRs, *viz.* density wave oscillations (DWOs), as well as in-phase and out-of-phase oscillations in the reactor core. The complete, 22-ODE model comprises three main parts: spatial lambda-mode neutron kinetics with the fundamental and first azimuthal modes, fuel heat conduction dynamics, and core thermal-hydraulics based on a drift flux model representation of the two-phase flow. The recirculation loop has been replaced throughout this study by a constant total pressure drop boundary condition across the reactor core. This assumption is found to be acceptable for out-of-phase instabilities in general, and for small amplitudes in the case of in-phase oscillations.

First, the thermal-hydraulic part of the model was validated and compared with several other analytical models developed earlier for simulating DWO phenomena. The present modelling is based on the assumption that the time-dependent single-phase enthalpy and two-phase quality have spatially quadratic profiles. Stability and *semi-analytical* bifurcation analyses have been carried out for a heated channel using the bifurcation code BIFDD. The impact of the drift flux parameters on both the stability boundary (SB) and the nature of Hopf bifurcation has been investigated. In addition, parametric studies have also been conducted to investigate the effects of different design and operating parameters on the SB and the nature of Hopf bifurcation. Finally, for independent confirmation of the results of the semi-analytical bifurcation analyses, as well as to evaluate the system behaviour in regions away from the SB, the set of ODEs has been integrated numerically using a MATLAB code.

The full, currently developed reduced order model enables the study of BWR instabilities, including out-of-phase oscillations. As such, it is essentially a two-channel, nuclear-coupled thermal-hydraulic model, with each channel representing half of the reactor core. First, stability and semi-analytical bifurcation analyses have been carried out using this model, such as to determine the stability limits for in-phase and out-of-phase oscillation modes. An in-depth investigation has then been carried out of the properties of the elements of the eigenvectors associated with these two modes of oscillations. Next, a comparative study between the use of the homogeneous equilibrium (HEM) and drift flux (DFM) models for the thermal-hydraulics has been performed to investigate the effects of

the drift flux parameters on the SB, the nature of Hopf bifurcation and the mode of oscillation (in-phase or out-of-phase). Moreover, numerical integration of the complete set of 22 system ODEs has been carried out to confirm the results of the semi-analytical bifurcation analysis, a special MATLAB code based on the Gear's algorithm having been developed for the purpose.

In addition, a detailed local bifurcation analysis has been performed at two representative operational points for the Leibstadt and Ringhals-1 NPPs using the complex system code RAMONA. The goal in this analysis has been to demonstrate how the system solution (behaviour) can, in certain situations, vary in a significant manner when a parameter, *e.g.* the mass flow, is changed by small amounts. The results found in this system code analysis could be explained only with the help of the experience which has been accumulated using reduced order models.

Finally, in order to assess the performance of the currently developed reduced order model, it has been applied to the analysis of a specific Leibstadt operational point. The results obtained have been compared to those of the system code RAMONA, such a comparison enabling a direct assessment of both the applicability and limitations of the reduced order model.

9.1 CONCLUSIONS

From the stability and bifurcation analyses carried out for the thermal-hydraulic model, *i.e.* a heated channel problem without neutron kinetics, the following conclusions have been drawn:

- The validation study against the Saha *et al.* experimental data shows that the thermal-hydraulic model predictions are in good agreement with the experimental results for large values of N_{sub} and, for lower values⁵², agree better than most of the earlier analytical models.
- The semi-analytical bifurcation analysis using the bifurcation code BIFDD shows that both sub- and supercritical Hopf bifurcations are encountered along the stability boundary. In addition, the stability boundary is sensitive to the

⁵² in the studied parameter range of the experiments

values of C_0 and V_{gj} . Moreover, the nature of Hopf bifurcation for lower values of N_{sub} is more sensitive to the value of V_{gj} than to that of C_0 .

- In a sensitivity study, it has been shown that the nature of Hopf bifurcation can significantly depend on the values of certain design and operating parameters, e.g. the inlet loss coefficient K_{inlet} and Froude number Fr .
- Numerical integration of the set of ODEs close to the stability boundary confirms the findings of the semi-analytical bifurcation analysis.

From the in-depth stability and bifurcation analyses carried out using the complete BWR reduced order model, it has been concluded that:

- Analysing the properties of the eigenvectors can provide full information as regards the corresponding oscillation modes (in-phase or out-of-phase) *without* solving the set of system ODEs. It has been shown thereby that the excitation of the in-phase (out-of-phase) oscillation mode *does not involve just* the fundamental (first) mode, but, also the thermal-hydraulic and heat conduction components as well. Therefore, a statement such as: “The excitation of the fundamental (first) mode causes the in-phase (out-of-phase) oscillation mode to be excited” is not completely true, since it is also necessary that the amplitude of the fundamental (first) mode is much larger than that of the first (fundamental) mode. Thus, it can happen that, although the fundamental (first) mode is unstable, in-phase (out-of-phase) oscillations are not excited. Moreover, as mentioned, the thermal-hydraulic and heat conduction variables (components) are also involved in the definition of the state (eigenvector properties).

In the author’s opinion, this can be understood more clearly in the frame of the center manifold theorem, in which the full system of 22 ODEs is reduced and lumped at the bifurcation point into just 2 ODEs (Poincaré normal form) which represent the combination of all the 22 original system variables. Consequently, consideration of the properties of the corresponding “lumped” eigenvectors implies that all the system components (variables) are involved. This is a clear argument for the fact that the in-phase and out-of-phase oscillation modes are indeed whole-system mechanisms and not just limited to the excitation of the fundamental or the

first mode. Thus, this leads to a reformulated definition of the in-phase or out-of-phase state based on the properties of the corresponding eigenvector, viz.:

The in-phase (out-of-phase) oscillation mode is an intrinsic state that the reactor can fall into, in which the amplitude of the fundamental (first) mode is larger than that of the first (fundamental) mode, and the thermal-hydraulic and heat conduction variables in one half of the core have the same (opposite) sign and the same absolute value as the corresponding variables in the other half of the core. Furthermore, each mode has its own stability limit.

- Using a DFM, instead of HEM, for the two-phase flow has a significant effect on the stability boundary as well as on the nature of Hopf bifurcation. Moreover, the type of oscillation mode is affected mainly in the higher branch of the stability boundary.
- Both sub- and supercritical Hopf bifurcations are encountered during the loss of system stability.

Because the conditions that a Hopf bifurcation occurs cannot be verified directly when using complex system codes, the *correspondence hypothesis* has currently been proposed, underlining the unique relationship for BWRs between a stable (unstable) limit cycle solution and the occurrence of a supercritical (subcritical) Hopf bifurcation. This hypothesis has been confirmed by carrying out detailed local bifurcation analyses, using the system code RAMONA, in the neighbourhood of the two representative NPP operational points (for Leibstadt and Ringhals-1, respectively). The following are the main conclusions which have been drawn:

- Stability and bifurcation analysis expertise using reduced order models is very important to understand, analyse and explain certain complicated nonlinear phenomena that can arise in simulations using large system codes.
- The qualitative comparison between RAMONA results and those of the reduced order model confirms the *correspondence hypothesis*. As a consequence, a subcritical Hopf bifurcation has been discovered for the first time, to the author's knowledge, while carrying out BWR stability analysis using large system codes.
- Identifying the nature of Hopf bifurcation allows the determination of the location of the local stability boundary inside the power-flow map.

- If the analysed operational point is very close to the local stability boundary, the behaviour of the reactor is very sensitive to small parameter variations as observed at the nominal OP investigated for the Leibstadt NPP. Hence, the issue of uncertainties becomes very important for the ability of a code such as RAMONA to predict the right behaviour at such OPs. For example, with a 2% mass flow uncertainty, the RAMONA prediction could change from that of a stable reactor core to an unstable one, or *vice-versa*.
- The uncertainty issue is also very important in correctly determining the oscillation amplitude in the case of a supercritical Hopf bifurcation. Thus, for example, an uncertainty of a 3% (relative) in the mass flow at such an OP was found to change the RAMONA prediction of the stable limit cycle amplitude by a factor of 3.

Finally, the application of the current reduced order model to the analysis of a specific Leibstadt operational point, and the quantitative comparison of the results obtained with those found using RAMONA, have shown that:

- Although the reduced order model could adequately predict the oscillation frequency and the stability margin for the investigated operational point, it was not able to identify the nature of Hopf bifurcation correctly and to predict the excitation of out-of-phase oscillations. This is mainly because of the highly simplified reactor core geometry, the uncertainties in evaluating the design and operating parameters, as also the limitations of the feedback reactivity model.
- However, the reduced order model does indeed allow a deep insight into the complex processes determining BWR stability, and provides a valuable tool for fast and detailed *semi-analytical* bifurcation analysis.
- As such, for BWR stability analysis, reduced order models should be considered as *complementary* tools to complex system codes, and *not* as alternatives.

9.2 ***RECOMMENDATIONS FOR FUTURE WORK***

Several improvements could be made to the present BWR reduced order model. These improvements would primarily involve the inclusion of additional BWR component models (recirculation loop, several parallel channels, etc.), as well as certain physical phenomena that are known to be important in the stability analysis of BWRs (e.g. a

subcooled boiling model). Accordingly, the following are the main recommendations for further developments:

- In Chapter 5, it was found that the thermal-hydraulic model is in good agreement with experimental data for large values of N_{sub} , while for lower values of N_{sub} , it agrees better than most other models, except for those that include subcooled boiling. It is accordingly recommended that a subcooled boiling model be included into the present thermal-hydraulic model in order to further improve its predictions for lower values of N_{sub} .
- The current reduced order model uses two channels, which is the minimal number needed to simulate out-of-phase oscillations. However, in order to simulate the excitation of higher harmonic modes, *i.e.* the second, the third, etc., it is recommended that a model with a larger number of parallel channels be developed. This would also allow an investigation of the effects of the channel number on the predicted stability behaviour.
- In the current reduced order model development, the recirculation loop was substituted by a constant pressure drop boundary condition across the core. It was shown that this is a valid assumption for out-of-phase oscillations in general but, in the case of in-phase oscillations, valid only for small amplitudes. Therefore, in order to avoid the issue of boundary conditions, it is recommended that the present reduced order model be extended to include the recirculation loop.
- The drift flux parameters, C_0 and V_{gj} , have been used in the present investigations in the sense of parameters which need to be varied in a realistic interval in order to assess their effects. In addition, these two parameters have been shown to have significant impact on the stability boundary, nature of Hopf bifurcation and type of oscillation mode. It is accordingly recommended that, in future studies, a realistic correlation be used to estimate these parameters more accurately.
- In Chapter 8, it was found that the current reduced order model could not predict, as done by RAMONA, the out-of-phase oscillations at the nominal OP investigated for the Leibstadt NPP, largely because of the limitations of the feedback reactivity model. It has been shown that the feedback reactivity for the coupling between the fundamental and first modes based on the linear approximation used currently is quite different from the exact results. Therefore, it is suggested that the reactivity

feedback model be improved further to enable better simulation of out-of-phase oscillations.

During the course of this research several open questions have been encountered. Thus, for example, in Chapter 6, it was reported that using the DFM instead of HEM affects the type of oscillation mode along the stability boundary branch with higher values of N_{sub} . Although this branch is of little importance from the viewpoint of normal BWR operation, further investigations in this context may help provide deeper understanding of the mechanisms behind the excitation of in-phase and out-of-phase oscillations, as well as of the conditions for the transition from one oscillation mode to the other. Moreover, the physical explanation for the transition from sub- to supercritical Hopf bifurcation (and *vice versa*), as a certain physical parameter is changed, remains a challenge. Understanding and explaining such issues clearly requires considerable further efforts.

APPENDIX A RAMONA MODEL DESCRIPTIONS

In this Appendix, the RAMONA-3 (called also RAMONA-3B) models for the neutron kinetics, fuel thermodynamics, and thermal-hydraulics are described. In addition, some of the correlations used in the fuel thermodynamics and thermal-hydraulic modelling are presented. Finally, the new code version, RAMONA-5, is introduced with its specific features and options.

A.1 NEUTRON KINETICS

The neutron dynamics in RAMONA-3B is based on two-group diffusion theory. Hence, the time-dependent diffusion equations for the two-group neutron fluxes are

$$\frac{1}{v_1} \frac{\partial \mathbf{F}_1}{\partial t} = \nabla \cdot D_1 \nabla \mathbf{F}_1 - \mathbf{S}_{r1} \mathbf{F}_1 - \mathbf{S}_{a1} \mathbf{F}_1 + (1 - \mathbf{b}) [\mathbf{n}_1 \mathbf{S}_{f1} \mathbf{F}_1 + \mathbf{n}_2 \mathbf{S}_{f2} \mathbf{F}_2] + \sum_{m=1}^6 \mathbf{l}_m C_m \quad (\text{A.1})$$

$$\frac{1}{v_2} \frac{\partial \mathbf{F}_2}{\partial t} = \nabla \cdot D_2 \nabla \mathbf{F}_2 + \mathbf{S}_{r1} \mathbf{F}_1 - \mathbf{S}_{a2} \mathbf{F}_2 \quad (\text{A.2})$$

$$\frac{\partial C_m}{\partial t} = \mathbf{b}_m [\mathbf{n}_1 \mathbf{S}_{f1} \mathbf{F}_1 + \mathbf{n}_2 \mathbf{S}_{f2} \mathbf{F}_2] - \mathbf{l}_m C_m, \quad m = 1, \dots, 6 \quad (\text{A.3})$$

where

- Φ neutron flux (n/cm² sec),
- D diffusion coefficient (cm),
- \mathbf{S}_r removal cross-section (1/cm),
- \mathbf{S}_a absorption cross-section (1/cm),
- \mathbf{S}_f fission cross-section,
- \mathbf{b}_m fraction of fission neutrons appearing in delayed neutron group m ,
- \mathbf{n} number of neutrons per fission,
- \mathbf{l}_m decay constant for delayed neutron precursor group m ,
- C_m concentration of delayed neutron precursor group m ,
- v neutron velocity,
- t time.

Subscripts 1 and 2 indicate fast and thermal neutron groups, respectively.

In RAMONA-3B, the leakage of thermal neutrons is neglected. This assumption is reasonable because the mean free path of thermal neutrons is usually much smaller than the size of the nodes in the core. This is the reason why this approximation is sometimes called the $1\frac{1}{2}$ energy-group approximation, *i.e.* leakage is assumed to be essentially that of epithermal neutrons.

By spatial discretization, the partial differential equations for neutron diffusion are transformed into ordinary differential equations. These, together with the equations for the delayed neutron precursor concentrations, form a set of nonlinear ordinary differential equations which is solved by a predictor-corrector integration scheme.

A.2 FUEL THERMODYNAMICS

The fuel model calculates the temperature distribution within the fuel pin, and the transport of heat from the fuel into the coolant. The calculated average fuel temperature feeds back into the neutronics (Doppler effect), and the calculated heat flux from the cladding surface enters the hydraulic calculations. The heat conduction in the fuel pin is calculated under the following assumptions:

- Negligible heat conduction in the axial direction.
- Spatially homogeneous heat deposition in the fuel.

Then the heat conduction equation in the fuel is

$$(\mathbf{r}C_p)_f \frac{\partial T_f}{\partial t} = \frac{1}{r} \frac{\partial}{\partial r} (rk_f \frac{\partial T_f}{\partial r}) + q_f \quad (\text{A.4})$$

where \mathbf{r}_f , $C_{p,f}$, k_f and T_f are the density, specific heat, thermal conductivity and temperature of the fuel, respectively. q_f is the power density deposited in the fuel.

The heat transport in the gap is given by

$$\frac{\partial}{\partial r} (k_{gp} \frac{\partial T_g}{\partial r}) = 0, \quad (\text{A.5})$$

and the heat transfer in the cladding by

$$(\mathbf{r}C_p)_c \frac{\partial T_c}{\partial t} = \frac{\partial}{\partial r} \left(k_c \frac{\partial T_c}{\partial r} \right) \quad (\text{A.6})$$

where k_{gp} is the gap heat transfer coefficient. \mathbf{r}_c , $C_{p,c}$, k_c and T_c are the density, specific heat, thermal conductivity, and temperature of the cladding, respectively.

A.2.1 Correlations

The following are the correlations used in the RAMONA-3B fuel model:

1) Fuel heat capacity:

$$(\mathbf{r}C_p)_f = a_1 + a_2 T_f + a_3 T_f^2 + a_4 T_f^3 + a_5 T_f^4 \quad (\text{A.7})$$

with $a_1 = 0.23709 \cdot 10^7$, $a_2 = 0.26470 \cdot 10^4$, $a_3 = -0.28373 \cdot 10^1$, $a_4 = 0.12498 \cdot 10^{-2}$, and $a_5 = -0.12066 \cdot 10^{-6}$ with the heat capacity expressed in $J/m^3 C$ and T_f in $^{\circ}C$.

2) Fuel thermal conductivity

$$k_f = \frac{C_1}{1 + C_2 T_f} \quad (\text{A.8})$$

with $C_1 = 8.5 \text{ W} / \text{m.C}$ and $C_2 = 0.002 \text{ C}^{-1}$.

3) Gap conductance

$$k_{gp} / \mathbf{d} = C_3 + C_4 \cdot \bar{T}_f + C_5 \bar{T}_f^2 \quad (\text{A.9})$$

where currently $C_3 = 6000 \text{ W/m}^2 \text{C}$, $C_4 = 0$, $C_5 = 0$ and \mathbf{d} is the gap width.

Like in the neutron kinetics case, the numerical time-integration for the fuel model is performed using an implicit predictor-corrector scheme.

A.3 THERMAL-HYDRAULICS

The thermal-hydraulic modelling in the RAMONA-3 code is based on a 4-equation non-equilibrium two-phase flow model. The 4 equations are for the vapour and liquid mass balance, and the mixture energy and mixture momentum balance. The model has two main assumptions. First, local variations of system pressure are ignored, *i.e.* acoustic

effects are neglected. This mathematically means that $\nabla p(r,t) = 0$ in the energy equation. The second assumption is that the vapour is assumed to be at saturation, but the liquid in the two-phase mixture is allowed to depart from saturation conditions. Based on the first assumption, the momentum equation is decoupled from the energy equation and integrated along closed contours, one for each hydraulic channel and including the other 6 RAMONA components (see Fig. 2-11).

The four fundamental thermal-hydraulic equations for the standard model are

The mass conservation equations

$$\frac{\partial(\mathbf{a}\mathbf{r}_g)}{\partial t} + \frac{\partial(\mathbf{a}\mathbf{r}_g v_g)}{\partial z} = \Gamma_v \quad (\text{A.10})$$

$$\frac{\partial((1-\mathbf{a})\mathbf{r}_l)}{\partial t} + \frac{\partial((1-\mathbf{a})\mathbf{r}_l v_l)}{\partial z} = -\Gamma_v \quad (\text{A.11})$$

where \mathbf{a} is the void fraction, \mathbf{r} is the density, v is the velocity and Γ_v is the local evaporation rate. Subscripts g and l refer to steam and water, respectively.

The mixture energy conservation equation

$$\frac{\partial}{\partial t} (\mathbf{a}\mathbf{r}_g u_g + (1-\mathbf{a})\mathbf{r}_l u_l) + \frac{\partial}{\partial z} (\mathbf{a}\mathbf{r}_g h_g v_g + (1-\mathbf{a})\mathbf{r}_l h_l v_l) = \frac{q'_w}{A} + q_l'''(1-\mathbf{a}) \quad (\text{A.12})$$

where A is the cross-sectional area, q'_w is the heat input per unit length of the heated wall, q_l''' is the heat per unit volume released directly in the coolant, and u and h are the specific internal energy and specific enthalpy, respectively.

The mixture momentum equation

$$\frac{\partial G}{\partial t} + \frac{\partial}{\partial z} (\mathbf{a}\mathbf{r}_g v_g^2 + (1-\mathbf{a})\mathbf{r}_l v_l^2) = -\frac{\partial}{\partial z} (\mathbf{a}\mathbf{r}_g + (1-\mathbf{a})\mathbf{r}_l) - g(\mathbf{a}\mathbf{r}_g + (1-\mathbf{a})\mathbf{r}_l) - f\Phi^2 \frac{G|G|}{2\mathbf{r}_l d_h} \quad (\text{A.13})$$

where G is the mass flux:

$$G = \mathbf{a} r_g v_g + (1 - \mathbf{a}) r_l v_l \quad (\text{A.14})$$

g is the gravitational constant, f is the single-phase friction factor, Φ^2 is the two-phase multiplier, and d_h is the hydraulic diameter.

A.3.1 Correlations

1) *The single-phase friction factor*

$$f = g_1 \text{Re}^{-g_2} \quad (\text{A.15})$$

where Re is the Reynolds number, $g_1 = 0.184$ and $g_2 = 0.2$.

2) *The two-phase multiplier:*

This can be calculated using one of three different correlations: Becker, Rolstadt, or Martinelli-Nelson. The latter correlation is commonly used and is defined as follows

$$\Phi^2 = 1 + 1.2 \cdot g(G, P) \cdot \left(\frac{r_f}{r_g} - 1 \right) X^{0.824} \quad (\text{A.16})$$

where $g(G, P)$ is a functional of the mass flow and pressure. X is the quality.

Since RAMONA is capable of treating non-homogeneous two-phase flow, the estimation of the slip factor S is of paramount importance. The relation between the vapour velocity and the liquid velocity is

$$v_g = S \cdot v_l + v^0 \quad (\text{A.17})$$

where $v^0 = 0.174$ is the bubble velocity. The slip factor can be calculated with one of the following correlations:

- Bankoff-Malnes correlation
- Bankoff-Jones correlation
- Solberg correlation

For more details on the correlations used in RAMONA-3B, see [1].

The hydraulic equations are integrated using explicit methods for all equations except the momentum equations, which have the option to be integrated either explicitly or implicitly.

A.4 RAMONA-5 VERSION

A new code version called RAMONA-5 is being used since recently at PSI in the framework of the European project NACUSP. This new version is an extension and improvement of the earlier version RAMONA-3B. It is around ten times faster. RAMONA-5 has two options concerning the neutron transport model: the PRESTO1 option which is equivalent to RAMONA-3B but faster, and the PRESTO2 option which is an extended 2-group modal kinetic model as used in the core simulator PRESTO2. In addition, RAMONA-5 has two different thermal-hydraulic models:

1. The standard thermal-hydraulic model used in RAMONA-3B (Section A.3).
2. An advanced thermal-hydraulic model called MONA which is a two-fluid, three-field, non-equilibrium one-dimensional two-phase flow model with constitutive equations for thermodynamic state variables, thermal and hydrodynamic non-equilibrium, as well as heat transfer and vapour generation/condensation.

REFERENCES

- [1] "RAMONA-3B, User Manual", Scandpower, 1993.

APPENDIX B BASIC CONCEPTS OF NONLINEAR DYNAMICS

Fixed point, limit cycle, stable manifold, etc. are all terms which are well known in the area of nonlinear dynamics. To help the non-specialist reader to understand certain aspects related to these concepts more clearly, the definitions of some of the terms are presented in this Appendix.

B.1 FIXED POINTS

Consider the following autonomous system of differential equations

$$\frac{d\bar{x}(t)}{dt} = F(\bar{x}(t), \mathbf{k}) \quad (\text{B.1})$$

where $\bar{x}(t)$ is an n -dimensional state vector and \mathbf{k} is an m -dimensional parameter vector. The *fixed points* of this system are determined by solving the following equation

$$F(\bar{x}(t), \mathbf{k}) = 0 \quad (\text{B.2})$$

The fixed points are also called *stationary solutions*, *critical points*, *constant solutions* and *steady-state solutions* [1]. Consider for $\mathbf{k} = \mathbf{k}_0$, the fixed point \bar{x}_0 . To determine the stability of this fixed point, a small disturbance $\bar{y}(t)$ is introduced

$$\bar{x}(t) = \bar{x}_0 + \bar{y}(t) \quad (\text{B.3})$$

By expanding F in a Taylor series around \bar{x}_0 , and retaining only linear terms, we obtain

$$\frac{d\bar{y}(t)}{dt} = D_x F(\bar{x}_0, \mathbf{k}_0) \cdot \bar{y}(t) + O(\|\bar{y}\|^2) \cong A(t, \mathbf{k}_0) \bar{y}(t) \quad (\text{B.4})$$

This step is called the linearization of the system of nonlinear differential equations. A is the $n \times n$ matrix of first partial derivatives and it is called the *Jacobian matrix*.

The solution of (B.4) can be written in a compact form as

$$\bar{y}(t) = e^{(t-t_0)A} \bar{y}_0 \quad (\text{B.5})$$

where $\bar{y}_0 = \bar{y}(t = t_0)$ is the initial condition. If the eigenvalues of A are all distinct, there exists a matrix L such that $L^{-1}AL = D$, where D is a diagonal matrix in which the eigenvalues λ_i are those of A . Hence, Eq. (B.5) can be rewritten as

$$\bar{y}(t) = Le^{(t-t_0)D}L^{-1}\bar{y}_0 \quad (\text{B.6})$$

The matrix $e^{(t-t_0)D}$ is diagonal, and therefore it is clear from (B.6) that the evaluation of the eigenvalues of the Jacobian matrix determines the local stability of the fixed point \bar{x}_0 . For instance, if all the eigenvalues have negative real parts, the solution $\bar{y}(t)$ will decay to zero. This means that the perturbation will decay to zero and the fixed point is stable. On the other hand, if at least one eigenvalue has a positive real part, $\bar{y}(t)$ will diverge in the direction of the eigenvector that corresponds to that eigenvalue. This means that, the perturbation is growing with time and the fixed point is unstable.

A fixed point is called *hyperbolic fixed point* if all the eigenvalues of the Jacobian matrix at this point have non-vanishing real parts. If at least one eigenvalue has a zero real part, then it is a *nonhyperbolic fixed point*. Three types of hyperbolic fixed points exist. If all the eigenvalues of the Jacobian matrix A have negative real parts, the fixed point is called a *sink*. If all the eigenvalues have positive real parts, the fixed point is called a *source*, and if some of the eigenvalues have positive real parts and the other have negative real parts, the fixed point is called a *saddle point*.

B.2 LIMIT CYCLE

If $\bar{x}(t)$ is a periodic solution of the autonomous system (B.1) with period T , then $\bar{x}(t+T) = \bar{x}(t)$ is a solution of (B.1). This periodic solution corresponds to a closed orbit in R^n such that $\bar{x}(t_0) = \bar{x}(t_0 + T)$ and $\bar{x}(t_0) \neq \bar{x}(t_0 + t)$ for $0 < t < T$. An isolated periodic solution⁵³ is called a *limit cycle*. This limit cycle corresponds to an isolated closed orbit in phase space. Hence, any initial condition that starts close to the limit cycle will be

⁵³ means that there are no other periodic solutions sufficiently close to it

attracted or repelled by this limit depending on its stability characteristics. The stability of the periodic solution is governed by Floquet theory explained below in Section B.4.

B.3 STABLE, UNSTABLE AND CENTER MANIFOLDS

Consider the n -dimensional autonomous system described in Eq. (B.1). Suppose that the Jacobian matrix corresponding to a fixed point has s eigenvalues with negative real parts, u eigenvalues with positive real parts, and c eigenvalues with zero real part. Then the space R^n can be divided into three independent subspaces E^s , E^u and E^c , called *stable*, *unstable* and *center manifold*, respectively. These subspaces are spanned by the eigenvectors associated with the s , u and c eigenvalues, respectively.

The stable manifold of a fixed point is the set of all initial conditions such that the flow⁵⁴ initiated at these points asymptotically approaches the fixed point when $t \rightarrow \infty$, while the unstable manifold of a fixed point is the set of initial conditions such that the flow initiated at these points asymptotically moves away from the fixed point as $t \rightarrow \infty$ [1].

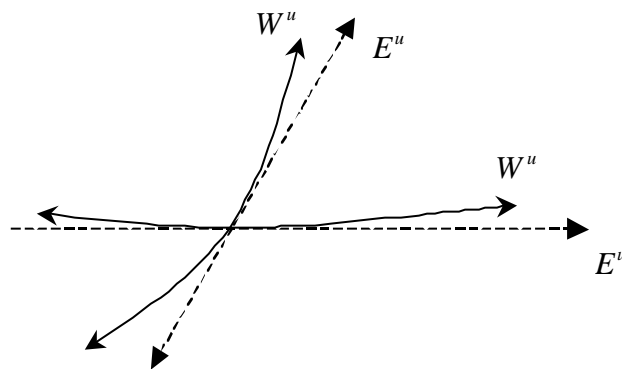


Figure B-1. Illustration of an unstable manifold for a nonlinear system and the corresponding linearized system manifold.

⁵⁴ The term “flow” describes the evolution of the system solution in phase space.

Denoting the stable, unstable and center manifolds for a nonlinear system by W^s , W^u , and W^c , respectively, it can be demonstrated that these manifolds intersect each other at the fixed point and that the corresponding linear manifolds E^s , E^u and E^c are tangential to them [2], as depicted in Figure B-1. As a consequence, in the neighbourhood of the fixed point, the behaviour of a nonlinear system is equivalent to that of the corresponding linearized system. This is equivalent to the Hartman-Großmann theorem [1], which states that a nonlinear system, in a sufficiently close neighbourhood of a hyperbolic fixed point, behaves like a linear one.

B.4 FLOQUET THEORY

Consider the autonomous system of differential equations defined in Eq. (B.1). Suppose, at $\mathbf{k} = \mathbf{k}_0$, there is a periodic solution $\bar{x}_0(t) = \bar{x}_0(t+T)$ with period T . If a perturbation $y(t)$ is superimposed on $\bar{x}_0(t)$, then

$$\bar{x}(t) = \bar{x}_0(t) + y(t) \quad (\text{B.7})$$

By expanding F in a Taylor series around $\bar{x}_0(t)$, and retaining only linear terms, we obtain

$$\frac{d\bar{y}(t)}{dt} = D_x F(\bar{x}_0(t), \mathbf{k}_0) \cdot \bar{y}(t) + O(\|\bar{y}\|^2) \cong P(t, \mathbf{k}_0) \bar{y}(t) \quad (\text{B.8})$$

where P is the matrix of partial derivatives of F (Jacobian matrix). The matrix P is periodic in time and has the same period T as $\bar{x}_0(t)$.

The n -dimensional linear system (B.8) has n linearly independent solutions y_i , where $i = 1, 2, \dots, n$. These solution vectors are usually called a fundamental set of solutions. A matrix $Y(t)$ can be expressed by this fundamental set of solutions and it is consequently called the fundamental matrix solution

$$Y(t) = [\bar{y}_1(t) \ \bar{y}_2(t) \ \dots \ \bar{y}_n(t)] \quad (\text{B.9})$$

If $Y(t)$ is a fundamental matrix solution, then $Y(t+T) = [\bar{y}_1(t+T) \ \bar{y}_2(t+T) \ \dots \ \bar{y}_n(t+T)]$ is also a fundamental matrix solution.

Because the fundamental set of solutions comprises linearly independent solutions, it can be considered as a complete basis. Therefore any vector in this space must be a linear combination of this fundamental set of solutions, so that $Y(t+T)$ can be written as

$$Y(t+T) = Y(t)M \quad (\text{B.10})$$

where M is an $n \times n$ constant matrix called the *monodromy matrix*. Equation (B.10) can be understood as a transformation that maps an initial vector at $t=0$ to another vector at $t=T$. By specifying the initial conditions, the monodromy matrix is simply

$$M = Y(T) \quad (\text{B.11})$$

The eigenvalues \mathbf{I}_m of the monodromy matrix M are called the *Floquet multipliers*. These multipliers provide the local stability of the periodic orbits along their associated eigenvectors ($\bar{\mathbf{v}}_m$). It can be shown that at least one of the Floquet multipliers associated with a periodic solution is always unity. The other multipliers determine the stability of the periodic orbit: stable orbit in the direction $\bar{\mathbf{v}}_m$ for $|\mathbf{I}_m| < 1$, and unstable periodic orbit in the direction $\bar{\mathbf{v}}_m$ for $|\mathbf{I}_m| > 1$. Globally, if all the Floquet multipliers are less than unity, except one that equals one, the periodic orbit is stable. On the other hand, if at least one of these multipliers is larger than unity the periodic orbit is unstable. Sometimes, *Floquet exponents* \mathbf{b}_m are used. Simply, they are related to the Floquet multipliers by $\mathbf{I}_m = e^{\mathbf{b}_m T}$. Hence, for a periodic solution, one Floquet exponent is zero, and the others correspond to stable orbits for all $\mathbf{b}_m < 0$ and an unstable periodic orbit for at least one $\mathbf{b}_m > 0$.

In particular, for examination of the stability of periodic solutions that appear at Hopf bifurcation points, the Floquet theory is of paramount importance. In this case, the original system of ODEs is first reduced to the two-dimensional Poincaré normal form, so that there are two Floquet exponents to be determined. The first trivial one is zero and the second one, called \mathbf{b} , determines the stability of the periodic solution: for $\mathbf{b} < 0$, the periodic solution is stable and the bifurcation is called a *supercritical* Hopf bifurcation, whereas for $\mathbf{b} > 0$, the periodic solution is unstable and the bifurcation is called a *subcritical* Hopf bifurcation.

B.5 SECONDARY HOPF BIFURCATION (NEIMARK BIFURCATION)

It is well known that the Hopf bifurcation of a fixed point leads to generation of a periodic solution. This happens when the pair of complex eigenvalues with the largest real part crosses the imaginary axis of the complex plane. It may happen that a second pair of complex eigenvalue crosses the imaginary axis after the first pair. This phenomenon is called *secondary Hopf bifurcation* or *Neimark bifurcation*. Similar to subcritical and supercritical Hopf bifurcations of a fixed point, there are subcritical and supercritical Neimark bifurcations of periodic solutions.

REFERENCES

- [1] A. H. Nayfeh, B. Balachandran, Applied Nonlinear Dynamics, John Wiley & Sons, Inc., New York, 1995.
- [2] J. Guckenheimer, P. Holmes, “Nonlinear Oscillations, Dynamical Systems, and Bifurcations of Vector Fields,” Springer-Verlag, New York, 1983.
- [3] B. D. Hassard, N. D. Kazarinoff, Y. H. Wan, “Theory and Application of Hopf Bifurcation,” Cambridge University Press, New York, 1981.

APPENDIX C DIMENSIONLESS PARAMETERS

The dimensionless variables and parameters used in the development of the BWR reduced order model are presented in this appendix. The asterisk indicates the original dimensional quantities. The quantities with the subscript jf means that this quantity is defined for both single-phase ($j=1$), and two-phase ($j=2$), regions of the flow channel.

$$A^* = p_c^{*2} - \rho r_c^{*2}$$

$$DP_{ext} = \frac{DP_{ext}^*}{\mathbf{r}_f^* v_0^{*2}}$$

$$Bi_{jf} = \frac{h_{\infty,jf}^* r_1^*}{k_p^*}$$

$$Fr = \frac{v_0^{*2}}{g^* L^*}$$

$$Bi_{c,jf} = \frac{h_{\infty,jf}^* r_c^*}{k_c^*}$$

$$G(z, t) = \frac{G^*(z^*, t^*)}{\mathbf{r}_f^* v_0^*}$$

$$Bi_g = \frac{h_g^* r_g^*}{k_c^*}$$

$$N_{cov,1f} = \frac{h_{\infty,1f}^* L^* T_0^* \mathbf{D} \mathbf{r}^* \mathbf{x}_h^*}{A^* \mathbf{D} h_{fg}^* v_0^* \mathbf{r}_g^* \mathbf{r}_f^*}$$

$$Bi_p = \frac{h_p^* r_g^*}{k_p^*}$$

$$N_{cov,2f} = \frac{2.56 e^{A^* p^* / 6.2 \cdot 10^6} L^* T_0^{*4} \mathbf{D} \mathbf{r}^* \mathbf{x}_h^*}{A^* \mathbf{D} h_{fg}^* v_0^* \mathbf{r}_g^* \mathbf{r}_f^*}$$

$$Bi_{p,jf}^+ = Bi_p \frac{Bi_{c,jf}}{Bi_g + Bi_{c,jf} + Bi_g Bi_{c,jf} \log(r_c / r_g)}$$

$$D(r, t) = \frac{D^*(r^*, t^*)}{L^*}$$

$$N_{f,jf} = \frac{f_{jf} L^*}{2D_h^*}$$

$$D_h^* = \frac{4A^*}{\mathbf{x}_h^*}$$

$$N_r = \frac{\mathbf{r}_f^*}{\mathbf{D} \mathbf{r}^*}$$

$$N_{sbo} = \frac{\mathbf{D}h_{fg}^* \mathbf{r}_g^*}{2c_f^* T_0^* \mathbf{D}\mathbf{r}^*}$$

$$N_{sub} = \frac{(h_{sat}^* - h_{inlet}^*) \mathbf{D}\mathbf{r}^*}{\mathbf{D}h_{fg}^* \mathbf{r}_g^*}$$

$$N_{pch}(t) = \frac{q'' \mathbf{x}^* l^* \mathbf{D}\mathbf{r}^*}{A^* \mathbf{D}h_{fg}^* \mathbf{r}_f^* \mathbf{r}_g^* v_0^*}$$

$$N_r = \frac{\mathbf{r}_g^*}{\mathbf{r}_f^*}$$

$$R = \frac{R^*}{L^*}$$

$$T_{i,jf}(t) = \frac{T_{i,jf}^*(t^*)}{T_0^*}, \quad i = 1, 2, avg, bulk, s$$

$$T_{jf}(r, t) = \frac{T_{jf}^*(r^*, t^*)}{T_0^*}$$

$$T_{sat} = \frac{T_{sat}^*}{T_0^*}$$

$$c_{1mn,l} = c_{1mn,l}^*, \quad l = 1, 2$$

$$c_{2mn,l} = c_{2mn,l}^* \cdot T_0^*, \quad l = 1, 2$$

$$c_q = \frac{c_q^* n_0^* L^{*2}}{k_p^* T_0^*}$$

$$h(z, t) = \frac{h^*(z^*, t^*)}{\mathbf{D}h_{fg}^*}$$

$$h_i = \frac{h_i^*}{\mathbf{D}h_{fg}^*}, \quad i = inlet, sat$$

$$n_k(t) = \frac{n_k^*(t^*)}{n_0^*}, \quad k = 0, 1$$

$$r_i = \frac{r_i^*}{L^*}, \quad i = 1, c, d, g, p$$

$$t = \frac{t^* v_0^*}{L^*}$$

$$\mathbf{u} = \frac{\mathbf{u}^*}{v_0^*}$$

$$v_{inlet}(t) = \frac{v_{inlet}^*(t^*)}{v_0^*}$$

$$z = \frac{z^*}{L^*}$$

$$L = \frac{L^* v_0^*}{L^*}$$

$$\mathbf{a}_c = \frac{\mathbf{a}_c^*}{L^* v_0^*}, \quad \mathbf{a}_c^* = k_c^* / (\mathbf{r}_c^* c_c^*)$$

$$\mathbf{a}_p = \frac{\mathbf{a}_p^*}{L^* v_0^*}$$

$$l = \frac{l^* L^*}{v_0^*}$$

$$\mathbf{m}(t) = \frac{\mathbf{m}^*(t^*)}{L^*}$$

$$\mathbf{r}_m(z, t) = \frac{\mathbf{r}_m^*(z^*, t^*)}{\mathbf{r}_f^*}$$

APPENDIX D INTERMEDIATE EXPRESSIONS

The following are the expressions for $ff_j, j=1,14$ which appeared in the equations of the thermal-hydraulic model in Chapter 4 (Eqs. (4.68), (4.69), and (4.73)).

$$ff_1 = m_{12} \cdot V_{gj}^2 + m_{11} \cdot V_{gj} + m_{10} \quad (\text{D.1})$$

$$ff_2 = v_{12} \cdot V_{gj}^2 + v_{11} \cdot V_{gj} \quad (\text{D.2})$$

$$ff_3 = n_{12} \cdot V_{gj}^2 + n_{11} \cdot V_{gj} \quad (\text{D.3})$$

$$ff_4 = f_{13} \cdot V_{gj}^3 + f_{12} \cdot V_{gj}^2 + f_{11} \cdot V_{gj} + f_{10} \quad (\text{D.4})$$

$$ff_5 = -2 \cdot (d_2 \cdot V_{gj}^2 + d_{11} \cdot V_{gj} + d_0) \quad (\text{D.5})$$

$$ff_6 = m_{22} \cdot V_{gj}^2 + m_{21} \cdot V_{gj} + m_{20} \quad (\text{D.6})$$

$$ff_7 = v_{22} \cdot V_{gj}^2 + v_{21} \cdot V_{gj} \quad (\text{D.7})$$

$$ff_8 = n_{22} \cdot V_{gj}^2 + n_{21} \cdot V_{gj} \quad (\text{D.8})$$

$$ff_9 = f_{23} \cdot V_{gj}^3 + f_{22} \cdot V_{gj}^2 + f_{21} \cdot V_{gj} + f_{20} \quad (\text{D.9})$$

$$ff_{10} = 2 \cdot (d_2 \cdot V_{gj}^2 + d_{21} \cdot V_{gj} + d_0) \quad (\text{D.10})$$

$$ff_{11} = m_{30} \quad (\text{D.11})$$

$$ff_{12} = n_{30} \quad (\text{D.12})$$

$$ff_{13} = f_{30} + f_{31} \cdot V_{gj} + f_{32} \cdot V_{gj}^2 + f_{33} \cdot CC_0^2 + f_{34} \quad (\text{D.13})$$

$$ff_{14} = Fr \cdot (d_{30} + CC_0 \cdot (\mathbf{m}(t) - 1)) \quad (\text{D.14})$$

where

$$m_{10} := (-2 \text{ II3_frac2 } \text{ II0_frac2 } + 2 \text{ II2_frac2 } \text{ III_frac2 }) s1 + (4 \text{ II2_frac2}^2 - 4 \text{ III_frac2 } \text{ II3_frac2 }) s2, \quad (\text{D.15})$$

$$\begin{aligned}
m_{11} := & (-2 \text{II4_frac5 II0_frac2} - 2 \text{II3_frac2 III_frac5} + 2 \text{II3_frac5 III_frac2} \\
& + 2 \text{II2_frac5 II2_frac2}) s^2 + ((-6 \text{II2_frac5 II3_frac2} + 10 \text{II2_frac2 II3_frac5} \\
& - 2 \text{II5_frac5 II0_frac2} - 2 \text{III_frac2 II4_frac5}) s^2 \\
& + (2 \text{II2_frac4 Npch II2_frac2} - 2 \text{II3_frac2 III_frac4 Npch}) C0 \\
& + 2 \text{II3_frac2 II0_frac3} + 2 \text{II3_frac3 II0_frac2} - 2 \text{II2_frac3 III_frac2} \\
& - 2 \text{II2_frac2 III_frac3}) s^1 \\
& + (-4 \text{III_frac2 II5_frac5} - 4 \text{II3_frac5 II3_frac2} + 8 \text{II2_frac2 II4_frac5}) s^2 + (\\
& (2 \text{II2_frac2 II3_frac4 Npch} - 2 \text{II3_frac2 II2_frac4 Npch}) C0 \\
& + 4 \text{III_frac3 II3_frac2} - 8 \text{II2_frac2 II2_frac3} + 4 \text{III_frac2 II3_frac3}) s^2
\end{aligned} \tag{D.16}$$

$$\begin{aligned}
m_{12} := & (-2 \text{II4_frac5 III_frac5} + 2 \text{II2_frac5 II3_frac5}) s^3 + (\\
& (-4 \text{II2_frac5 II4_frac5} - 2 \text{II5_frac5 III_frac5} + 6 \text{II3_frac5}^2) s^2 \\
& + (2 \text{II3_frac5 II2_frac4 Npch} - 2 \text{II4_frac5 III_frac4 Npch}) C0 \\
& - 2 \text{II2_frac5 II2_frac3} - 2 \text{III_frac3 II3_frac5} + 2 \text{II4_frac5 II0_frac3} \\
& + 2 \text{II3_frac3 III_frac5}) s^2 + ((6 \text{II3_frac5 II4_frac5} - 6 \text{II2_frac5 II5_frac5}) s^2 \\
& + ((-2 \text{II5_frac5 III_frac4 Npch} + 2 \text{II3_frac5 II3_frac4 Npch}) C0 \\
& + 2 \text{III_frac3 II4_frac5} + 6 \text{II2_frac5 II3_frac3} - 10 \text{II2_frac3 II3_frac5} \\
& + 2 \text{II5_frac5 II0_frac3}) s^2 \\
& + (2 \text{II3_frac3 III_frac4 Npch} - 2 \text{II2_frac4 Npch II2_frac3}) C0 \\
& + 2 \text{II2_frac3 III_frac3} - 2 \text{II3_frac3 II0_frac3}) s^1 \\
& + (-4 \text{II3_frac5 II5_frac5} + 4 \text{II4_frac5}^2) s^3 + (\\
& (-2 \text{II5_frac5 II2_frac4 Npch} + 2 \text{II4_frac5 II3_frac4 Npch}) C0 \\
& + 4 \text{III_frac3 II5_frac5} - 8 \text{II2_frac3 II4_frac5} + 4 \text{II3_frac5 II3_frac3}) s^2 + (\\
& (2 \text{II3_frac3 II2_frac4 Npch} - 2 \text{II2_frac3 II3_frac4 Npch}) C0 \\
& - 4 \text{III_frac3 II3_frac3} + 4 \text{II2_frac3}^2) s^2
\end{aligned} , \tag{D.17}$$

$$\begin{aligned}
v_{11} := & (-2 \text{II2_frac4 II2_frac2} + 2 \text{II3_frac2 III_frac4}) C0 s^1 \\
& + (2 \text{II3_frac2 II2_frac4} - 2 \text{II2_frac2 II3_frac4}) C0 s^2 , \tag{D.18}
\end{aligned}$$

$$\begin{aligned}
v_{12} := & (2 \text{II4_frac5 III_frac4} - 2 \text{II3_frac5 II2_frac4}) C0 s^2 + (\\
& (-2 \text{II3_frac5 II3_frac4} + 2 \text{II5_frac5 III_frac4}) C0 s^2 \\
& + (-2 \text{II3_frac3 III_frac4} + 2 \text{II2_frac4 II2_frac3}) C0) s^1 \\
& + (2 \text{II5_frac5 II2_frac4} - 2 \text{II4_frac5 II3_frac4}) C0 s^2 \\
& + (2 \text{II2_frac3 II3_frac4} - 2 \text{II3_frac3 II2_frac4}) C0 s^2 , \tag{D.19}
\end{aligned}$$

$$\begin{aligned}
n_{11} := & (2 \text{II3_frac2 II2_frac4} - 2 \text{II2_frac2 II3_frac4}) C0 s1 \\
& + (-2 \text{II2_frac2 II4_frac4} + 2 \text{II3_frac2 II3_frac4}) C0 s2
\end{aligned} \tag{D.20}$$

$$\begin{aligned}
n_{12} := & (2 \text{II4_frac5 II2_frac4} - 2 \text{II3_frac5 II3_frac4}) C0 s1^2 + (\\
& (2 \text{II5_frac5 II2_frac4} - 2 \text{II3_frac5 II4_frac4}) C0 s2 \\
& + (2 \text{II2_frac3 II3_frac4} - 2 \text{II3_frac3 II2_frac4}) C0) s1 \\
& + (-2 \text{II4_frac5 II4_frac4} + 2 \text{II5_frac5 II3_frac4}) C0 s2^2 \\
& + (2 \text{II2_frac3 II4_frac4} - 2 \text{II3_frac3 II3_frac4}) C0 s2
\end{aligned} \tag{D.21}$$

$$\begin{aligned}
f_{10} := & (-2 \text{Npch II2_frac2}^2 + 2 \text{Npch III_frac2 II3_frac2} + 2 \text{II3_frac2 II0_frac2 Vinlet} \\
& - 2 \text{II2_frac2 III_frac2 Vinlet}) C0 s1 \\
& + (4 \text{II3_frac2 III_frac2 Vinlet} - 4 \text{II2_frac2}^2 \text{Vinlet}) C0 s2 + (2 \text{II3_frac2 Npch} \\
& - \text{II2_frac2 Npch } \mu^2 - \text{II2_frac2 Npch } \mu + 2 \text{II2_frac2 Npch } \mu - 2 \text{II3_frac2 Npch } \mu) \\
& C0 CC0 + (-2 \text{II3_frac2 Npch II0_frac1} + 2 \text{II2_frac2 Npch III_frac1}) C0
\end{aligned} \tag{D.22}$$

$$\begin{aligned}
f_{11} := & (2 \text{II4_frac5 II0_frac2 Vinlet} - 4 \text{Npch II3_frac5 II2_frac2} \\
& - 2 \text{II2_frac5 II2_frac2 Vinlet} + 2 \text{II4_frac5 III_frac2 Npch} \\
& + 2 \text{Npch II3_frac2 II2_frac5} - 2 \text{II3_frac5 III_frac2 Vinlet} \\
& + 2 \text{II3_frac2 III_frac5 Vinlet}) C0 s1^2 + ((-4 \text{II4_frac5 Npch II2_frac2} \\
& + 2 \text{II5_frac5 II0_frac2 Vinlet} + 6 \text{II3_frac2 II2_frac5 Vinlet} \\
& + 2 \text{II4_frac5 III_frac2 Vinlet} - 10 \text{II3_frac5 II2_frac2 Vinlet} \\
& + 2 \text{Npch II5_frac5 III_frac2} + 2 \text{Npch II3_frac2 II3_frac5}) C0 s2 + (\\
& -\text{II3_frac5 Npch} + 2 \text{II3_frac5 Npch } \mu - 2 \text{II4_frac5 Npch } \mu - \text{II3_frac5 Npch } \mu^2 \\
& + 2 \text{II4_frac5 Npch}) C0 CC0 + (2 \text{II3_frac2 III_frac4 Npch Vinlet} \\
& - 2 \text{II3_frac4 Npch}^2 \text{II2_frac2} - 2 \text{II2_frac4 Npch Vinlet II2_frac2} \\
& + 2 \text{II3_frac2 II2_frac4 Npch}^2) C0^2 + (-2 \text{III_frac2 II3_frac3 Npch} \\
& - 2 \text{II3_frac2 II0_frac3 Vinlet} + 2 \text{II2_frac2 III_frac3 Vinlet} \\
& + 2 \text{II3_frac5 Npch III_frac1} - 2 \text{II3_frac3 II0_frac2 Vinlet} \\
& + 2 \text{II2_frac3 III_frac2 Vinlet} - 2 \text{II4_frac5 Npch II0_frac1} \\
& + 6 \text{Npch II2_frac2 II2_frac3} - 4 \text{Npch III_frac3 II3_frac2}) C0 \\
& + 2 \text{II3_frac2 II0_frac2} - 2 \text{II2_frac2 III_frac2}) s1 + (\\
& -8 \text{II4_frac5 II2_frac2 Vinlet} + 4 \text{II5_frac5 III_frac2 Vinlet} \\
& + 4 \text{II3_frac2 II3_frac5 Vinlet}) C0 s2^2 + ((-\text{II4_frac5 Npch} + 2 \text{II4_frac5 Npch } \mu
\end{aligned}$$

$$\begin{aligned}
& + 2 \text{II5_frac5} \text{Npch} - 2 \text{II5_frac5} \text{Npch} \mu - \text{II4_frac5} \text{Npch} \mu^2) C0 CC0 + (\\
& 2 \text{II3_frac2} \text{II3_frac4} \text{Npch}^2 + 2 \text{II3_frac2} \text{II2_frac4} \text{Npch} \text{Vinlet} \\
& - 2 \text{II2_frac2} \text{II3_frac4} \text{Npch} \text{Vinlet} - 2 \text{II2_frac2} \text{II4_frac4} \text{Npch}^2) C0^2 + (\\
& -2 \text{II5_frac5} \text{Npch} \text{II0_frac1} - 2 \text{II2_frac3} \text{II3_frac2} \text{Npch} \\
& + 2 \text{II4_frac5} \text{Npch} \text{III_frac1} + 8 \text{II2_frac2} \text{II2_frac3} \text{Vinlet} \\
& - 4 \text{II3_frac2} \text{III_frac3} \text{Vinlet} - 4 \text{II3_frac3} \text{III_frac2} \text{Vinlet} \\
& + 2 \text{II2_frac2} \text{II3_frac3} \text{Npch}) C0 - 4 \text{II2_frac2}^2 + 4 \text{III_frac2} \text{II3_frac2}) s2 + (\\
& \text{II2_frac3} \text{Npch} - 2 \text{II2_frac3} \text{Npch} \mu - 2 \text{II3_frac3} \text{Npch} + \text{II2_frac3} \text{Npch} \mu^2 \\
& + 2 \text{II3_frac3} \text{Npch} \mu) C0 CC0 \\
& + (-2 \text{II2_frac3} \text{Npch} \text{III_frac1} + 2 \text{II3_frac3} \text{Npch} \text{II0_frac1}) C0 \quad (D.23)
\end{aligned}$$

$$\begin{aligned}
f_{12} := & (2 \text{II4_frac5} \text{II2_frac5} \text{Npch} + 2 \text{II4_frac5} \text{III_frac5} \text{Vinlet} - 2 \text{Npch} \text{II3_frac5}^2 \\
& - 2 \text{II2_frac5} \text{Vinlet} \text{II3_frac5}) C0 s1^3 + ((2 \text{Npch} \text{II5_frac5} \text{II2_frac5} \\
& + 4 \text{II4_frac5} \text{II2_frac5} \text{Vinlet} - 2 \text{II4_frac5} \text{II3_frac5} \text{Npch} - 6 \text{II3_frac5}^2 \text{Vinlet} \\
& + 2 \text{II5_frac5} \text{III_frac5} \text{Vinlet}) C0 s2 + (2 \text{II4_frac5} \text{III_frac4} \text{Npch} \text{Vinlet} \\
& - 2 \text{II3_frac5} \text{II2_frac4} \text{Npch} \text{Vinlet} + 2 \text{II4_frac5} \text{II2_frac4} \text{Npch}^2 \\
& - 2 \text{II3_frac5} \text{II3_frac4} \text{Npch}^2) C0^2 + (2 \text{III_frac3} \text{II3_frac5} \text{Vinlet} \\
& + 2 \text{II2_frac5} \text{II2_frac3} \text{Vinlet} + 6 \text{Npch} \text{II3_frac5} \text{II2_frac3} \\
& - 2 \text{II2_frac5} \text{II3_frac3} \text{Npch} - 2 \text{II3_frac3} \text{III_frac5} \text{Vinlet} \\
& - 2 \text{II4_frac5} \text{II0_frac3} \text{Vinlet} - 4 \text{II4_frac5} \text{III_frac3} \text{Npch}) C0 \\
& + 2 \text{II4_frac5} \text{II0_frac2} - 2 \text{II3_frac5} \text{III_frac2} - 2 \text{II2_frac5} \text{II2_frac2} \\
& + 2 \text{II3_frac2} \text{III_frac5}) s1^2 + ((2 \text{Npch} \text{II5_frac5} \text{II3_frac5} - 2 \text{Npch} \text{II4_frac5}^2 \\
& + 6 \text{II5_frac5} \text{II2_frac5} \text{Vinlet} - 6 \text{II3_frac5} \text{II4_frac5} \text{Vinlet}) C0 s2^2 + ((\\
& 2 \text{II5_frac5} \text{II2_frac4} \text{Npch}^2 - 2 \text{II3_frac5} \text{II3_frac4} \text{Npch} \text{Vinlet} \\
& + 2 \text{II5_frac5} \text{III_frac4} \text{Npch} \text{Vinlet} - 2 \text{II3_frac5} \text{II4_frac4} \text{Npch}^2) C0^2 + (\\
& -2 \text{II4_frac5} \text{III_frac3} \text{Vinlet} - 4 \text{Npch} \text{II5_frac5} \text{III_frac3} \\
& + 4 \text{II4_frac5} \text{Npch} \text{II2_frac3} - 6 \text{II3_frac3} \text{II2_frac5} \text{Vinlet} \\
& + 10 \text{II3_frac5} \text{II2_frac3} \text{Vinlet} - 2 \text{II5_frac5} \text{II0_frac3} \text{Vinlet}) C0 \\
& + 6 \text{II2_frac5} \text{II3_frac2} + 2 \text{III_frac2} \text{II4_frac5} + 2 \text{II5_frac5} \text{II0_frac2} \\
& - 10 \text{II2_frac2} \text{II3_frac5}) s2 + (2 \text{II2_frac4} \text{Npch} \text{Vinlet} \text{II2_frac3} \\
& - 2 \text{II3_frac3} \text{II2_frac4} \text{Npch}^2 - 2 \text{II3_frac3} \text{III_frac4} \text{Npch} \text{Vinlet} \\
& + 2 \text{II3_frac4} \text{Npch}^2 \text{II2_frac3}) C0^2 + (2 \text{II3_frac2} \text{III_frac4} \text{Npch} \\
& - 2 \text{II2_frac3} \text{III_frac3} \text{Vinlet} - 4 \text{Npch} \text{II2_frac3}^2 + 4 \text{III_frac3} \text{II3_frac3} \text{Npch} \\
& - 2 \text{II2_frac4} \text{Npch} \text{II2_frac2} + 2 \text{II3_frac3} \text{II0_frac3} \text{Vinlet}) C0 \\
& + 2 \text{II2_frac3} \text{III_frac2} + 2 \text{II2_frac2} \text{III_frac3} - 2 \text{II3_frac2} \text{II0_frac3}
\end{aligned}$$

$$\begin{aligned}
& - 2 \text{II3_frac3 II0_frac2}) s1 \\
& + (4 \text{II5_frac5 II3_frac5 Vinlet} - 4 \text{II4_frac5}^2 \text{ Vinlet}) C0 s2^3 + ((\\
& - 2 \text{II4_frac5 II3_frac4 Npch Vinlet} + 2 \text{II5_frac5 II3_frac4 Npch}^2 \\
& + 2 \text{II5_frac5 II2_frac4 Npch Vinlet} - 2 \text{II4_frac5 II4_frac4 Npch}^2) C0^2 + (\\
& - 4 \text{II3_frac3 II3_frac5 Vinlet} - 4 \text{II5_frac5 III_frac3 Vinlet} \\
& - 2 \text{II2_frac3 II5_frac5 Npch} + 2 \text{II4_frac5 II3_frac3 Npch} \\
& + 8 \text{II4_frac5 II2_frac3 Vinlet}) C0 + 4 \text{III_frac2 II5_frac5} + 4 \text{II3_frac5 II3_frac2} \\
& - 8 \text{II2_frac2 II4_frac5}) s2^2 + ((- 2 \text{II3_frac3 II3_frac4 Npch}^2 \\
& + 2 \text{II2_frac3 II3_frac4 Npch Vinlet} + 2 \text{II2_frac3 II4_frac4 Npch}^2 \\
& - 2 \text{II3_frac3 II2_frac4 Npch Vinlet}) C0^2 + (4 \text{II3_frac3 III_frac3 Vinlet} \\
& - 4 \text{II2_frac3}^2 \text{ Vinlet} - 2 \text{II2_frac2 II3_frac4 Npch} + 2 \text{II3_frac2 II2_frac4 Npch}) \\
& C0 - 4 \text{III_frac2 II3_frac3} - 4 \text{III_frac3 II3_frac2} + 8 \text{II2_frac2 II2_frac3}) s2
\end{aligned} \tag{D.24}$$

$$\begin{aligned}
f_{13} := & (2 \text{II4_frac5 III_frac5} - 2 \text{II2_frac5 II3_frac5}) s1^3 + (\\
& (4 \text{II2_frac5 II4_frac5} + 2 \text{II5_frac5 III_frac5} - 6 \text{II3_frac5}^2) s2 \\
& + (2 \text{II4_frac5 III_frac4 Npch} - 2 \text{II3_frac5 II2_frac4 Npch}) C0 \\
& - 2 \text{II4_frac5 II0_frac3} + 2 \text{II2_frac5 II2_frac3} + 2 \text{III_frac3 II3_frac5} \\
& - 2 \text{II3_frac3 III_frac5}) s1^2 + ((6 \text{II2_frac5 II5_frac5} - 6 \text{II3_frac5 II4_frac5}) s2^2 \\
& + ((- 2 \text{II3_frac5 II3_frac4 Npch} + 2 \text{II5_frac5 III_frac4 Npch}) C0 \\
& + 10 \text{II2_frac3 II3_frac5} - 2 \text{III_frac3 II4_frac5} - 2 \text{II5_frac5 II0_frac3} \\
& - 6 \text{II2_frac5 II3_frac3}) s2 \\
& + (2 \text{II2_frac4 Npch II2_frac3} - 2 \text{II3_frac3 III_frac4 Npch}) C0 \\
& + 2 \text{II3_frac3 II0_frac3} - 2 \text{II2_frac3 III_frac3}) s1 \\
& + (- 4 \text{II4_frac5}^2 + 4 \text{II3_frac5 II5_frac5}) s2^3 + (\\
& (2 \text{II5_frac5 II2_frac4 Npch} - 2 \text{II4_frac5 II3_frac4 Npch}) C0 \\
& - 4 \text{II3_frac5 II3_frac3} - 4 \text{III_frac3 II5_frac5} + 8 \text{II2_frac3 II4_frac5}) s2^2 + (\\
& (2 \text{II2_frac3 II3_frac4 Npch} - 2 \text{II3_frac3 II2_frac4 Npch}) C0 \\
& + 4 \text{III_frac3 II3_frac3} - 4 \text{II2_frac3}^2) s2
\end{aligned} \tag{D.25}$$

$$\begin{aligned}
d_2 := & (\text{II2_frac5 II4_frac5} - \text{II3_frac5}^2) s1^2 + (\\
& (- \text{II3_frac5 II4_frac5} + \text{II2_frac5 II5_frac5}) s2 - \text{III_frac3 II4_frac5} \\
& - \text{II2_frac5 II3_frac3} + 2 \text{II2_frac3 II3_frac5}) s1 \\
& + (- \text{II4_frac5}^2 + \text{II3_frac5 II5_frac5}) s2^2 \\
& + (- \text{III_frac3 II5_frac5} - \text{II3_frac5 II3_frac3} + 2 \text{II2_frac3 II4_frac5}) s2 \\
& - \text{II2_frac3}^2 + \text{III_frac3 II3_frac3}
\end{aligned} \tag{D.26}$$

$$\begin{aligned}
d_{11} := & (III_frac2 II4_frac5 + II2_frac5 II3_frac2 - 2 II2_frac2 II3_frac5) s1 \\
& + (II3_frac5 II3_frac2 + III_frac2 II5_frac5 - 2 II2_frac2 II4_frac5) s2 \\
& + 2 II2_frac2 II2_frac3 - III_frac2 II3_frac3 - III_frac3 II3_frac2
\end{aligned} \tag{D.27}$$

$$d_0 := -II2_frac2^2 + III_frac2 II3_frac2, \tag{D.28}$$

$$\begin{aligned}
d_{21} := & C0 (III_frac2 II4_frac5 + II2_frac5 II3_frac2 - 2 II2_frac2 II3_frac5) s1 \\
& + C0 (II3_frac5 II3_frac2 + III_frac2 II5_frac5 - 2 II2_frac2 II4_frac5) s2 \\
& + C0 (2 II2_frac2 II2_frac3 - III_frac2 II3_frac3 - III_frac3 II3_frac2)
\end{aligned} \tag{D.29}$$

$$m_{20} := (-2 II0_frac2 II2_frac2 + 2 III_frac2^2) s1, \tag{D.30}$$

$$\begin{aligned}
m_{21} := & (-2 III_frac5 II2_frac2 + 4 II2_frac5 III_frac2 - 2 II3_frac5 II0_frac2) s1^2 + (\\
& (-2 II4_frac5 II0_frac2 + 4 II3_frac5 III_frac2 - 2 II2_frac5 II2_frac2) s2 \\
& + (2 II2_frac4 Npch III_frac2 - 2 III_frac4 Npch II2_frac2) C0 \\
& + 2 II0_frac2 II2_frac3 + 2 II0_frac3 II2_frac2 - 4 III_frac3 III_frac2) s1 \\
& + (2 III_frac2 II3_frac4 Npch - 2 II2_frac4 Npch II2_frac2) C0 s2
\end{aligned} \tag{D.31}$$

$$\begin{aligned}
m_{22} := & (-2 II3_frac5 III_frac5 + 2 II2_frac5^2) s1^3 + (\\
& (-2 II4_frac5 III_frac5 + 2 II2_frac5 II3_frac5) s2 \\
& + (2 II2_frac4 Npch II2_frac5 - 2 II3_frac5 III_frac4 Npch) C0 \\
& - 4 II2_frac5 III_frac3 + 2 II3_frac5 II0_frac3 + 2 III_frac5 II2_frac3) s1^2 + (\\
& (2 II3_frac5^2 - 2 II2_frac5 II4_frac5) s2^2 + (\\
& (2 II2_frac5 II3_frac4 Npch - 2 II4_frac5 III_frac4 Npch) C0 \\
& + 2 II2_frac5 II2_frac3 + 2 II4_frac5 II0_frac3 - 4 III_frac3 II3_frac5) s2 \\
& + (2 III_frac4 Npch II2_frac3 - 2 II2_frac4 Npch III_frac3) C0 + 2 III_frac3^2 \\
& - 2 II0_frac3 II2_frac3) s1 \\
& + (-2 II4_frac5 II2_frac4 Npch + 2 II3_frac5 II3_frac4 Npch) C0 s2^2 \\
& + (2 II2_frac4 Npch II2_frac3 - 2 III_frac3 II3_frac4 Npch) C0 s2
\end{aligned} \tag{D.32}$$

$$v_{21} := (2 \text{II1_frac4 II2_frac2} - 2 \text{II2_frac4 III_frac2}) C0 s1 + (2 \text{II2_frac4 II2_frac2} - 2 \text{III_frac2 II3_frac4}) C0 s2 \quad (\text{D.33})$$

$$v_{22} := (-2 \text{II2_frac4 II2_frac5} + 2 \text{II3_frac5 III_frac4}) C0 s1^2 + (-2 \text{II2_frac5 II3_frac4} + 2 \text{II4_frac5 III_frac4}) C0 s2 + (2 \text{II2_frac4 III_frac3} - 2 \text{III_frac4 II2_frac3}) C0 s1 + (2 \text{II4_frac5 II2_frac4} - 2 \text{II3_frac5 II3_frac4}) C0 s2^2 + (2 \text{III_frac3 II3_frac4} - 2 \text{II2_frac4 II2_frac3}) C0 s2 \quad (\text{D.34})$$

$$n_{21} := (2 \text{II2_frac4 II2_frac2} - 2 \text{III_frac2 II3_frac4}) C0 s1 + (2 \text{II2_frac2 II3_frac4} - 2 \text{III_frac2 II4_frac4}) C0 s2 \quad (\text{D.35})$$

$$n_{22} := (2 \text{II3_frac5 II2_frac4} - 2 \text{II2_frac5 II3_frac4}) C0 s1^2 + (2 \text{II4_frac5 II2_frac4} - 2 \text{II2_frac5 II4_frac4}) C0 s2 + (2 \text{III_frac3 II3_frac4} - 2 \text{II2_frac4 II2_frac3}) C0 s1 + (-2 \text{II3_frac5 II4_frac4} + 2 \text{II4_frac5 II3_frac4}) C0 s2^2 + (-2 \text{II2_frac3 II3_frac4} + 2 \text{III_frac3 II4_frac4}) C0 s2 \quad (\text{D.36})$$

$$f_{23} := (-2 \text{II2_frac5}^2 + 2 \text{II3_frac5 III_frac5}) s1^3 + (2 \text{II4_frac5 III_frac5} - 2 \text{II2_frac5 II3_frac5}) s2 + (-2 \text{II2_frac4 Npch II2_frac5} + 2 \text{II3_frac5 III_frac4 Npch}) C0 - 2 \text{II3_frac5 II0_frac3} - 2 \text{III_frac5 II2_frac3} + 4 \text{II2_frac5 III_frac3}) s1^2 + (-2 \text{II3_frac5}^2 + 2 \text{II2_frac5 II4_frac5}) s2^2 + (-2 \text{II2_frac5 II3_frac4 Npch} + 2 \text{II4_frac5 III_frac4 Npch}) C0 + 4 \text{III_frac3 II3_frac5} - 2 \text{II4_frac5 II0_frac3} - 2 \text{II2_frac5 II2_frac3}) s2 + (2 \text{II2_frac4 Npch III_frac3} - 2 \text{III_frac4 Npch II2_frac3}) C0 - 2 \text{III_frac3}^2 + 2 \text{II0_frac3 II2_frac3}) s1 + (2 \text{II4_frac5 II2_frac4 Npch} - 2 \text{II3_frac5 II3_frac4 Npch}) C0 s2^2 + (-2 \text{II2_frac4 Npch II2_frac3} + 2 \text{III_frac3 II3_frac4 Npch}) C0 s2 \quad (\text{D.37})$$

$$f_{22} := (2 \text{II3_frac5 III_frac5 Vinlet} - 2 \text{II2_frac5}^2 \text{Vinlet}) C0 s1^3 + (-4 \text{II4_frac5 II2_frac5 Npch} + 2 \text{II4_frac5 III_frac5 Vinlet} - 2 \text{II2_frac5 Vinlet II3_frac5} + 4 \text{Npch II3_frac5}^2) C0 s2 + (-2 \text{II3_frac4 Npch}^2 \text{II2_frac5} + 2 \text{II3_frac5 II2_frac4 Npch}^2$$

$$\begin{aligned}
& - 2 II2_frac4 Npch Vinlet II2_frac5 + 2 II3_frac5 III_frac4 Npch Vinlet) C0^2 + (\\
& 4 II2_frac5 III_frac3 Vinlet - 2 II3_frac5 II0_frac3 Vinlet \\
& - 2 III_frac3 Npch II3_frac5 - 2 III_frac5 Vinlet II2_frac3 \\
& + 2 II2_frac5 II2_frac3 Npch) C0 + 2 III_frac5 II2_frac2 - 4 II2_frac5 III_frac2 \\
& + 2 II3_frac5 II0_frac2) s1^2 + ((2 II4_frac5 II2_frac5 Vinlet \\
& - 4 Npch II5_frac5 II2_frac5 - 2 II3_frac5^2 Vinlet + 4 II4_frac5 II3_frac5 Npch) \\
& C0 s2^2 + ((2 II4_frac5 III_frac4 Npch Vinlet + 2 II4_frac5 II2_frac4 Npch^2 \\
& - 2 II2_frac5 II4_frac4 Npch^2 - 2 II2_frac5 II3_frac4 Npch Vinlet) C0^2 + (\\
& 2 II4_frac5 III_frac3 Npch + 4 III_frac3 II3_frac5 Vinlet \\
& - 8 Npch II3_frac5 II2_frac3 - 2 II4_frac5 II0_frac3 Vinlet \\
& + 6 II2_frac5 II3_frac3 Npch - 2 II2_frac5 II2_frac3 Vinlet) C0 \\
& + 2 II2_frac5 II2_frac2 - 4 II3_frac5 III_frac2 + 2 II4_frac5 II0_frac2) s2 + (\\
& 2 II3_frac4 Npch^2 III_frac3 - 2 II2_frac4 Npch^2 II2_frac3 \\
& + 2 II2_frac4 Npch Vinlet III_frac3 - 2 III_frac4 Npch Vinlet II2_frac3) C0^2 + (\\
& 2 III_frac4 Npch II2_frac2 + 2 II0_frac3 Vinlet II2_frac3 \\
& - 2 II2_frac4 Npch III_frac2 - 2 III_frac3^2 Vinlet) C0 - 2 II0_frac3 II2_frac2 \\
& - 2 II0_frac2 II2_frac3 + 4 III_frac3 III_frac2) s1 \\
& + (-4 Npch II5_frac5 II3_frac5 + 4 Npch II4_frac5^2) C0 s2^3 + ((\\
& -2 II3_frac5 II4_frac4 Npch^2 - 2 II3_frac5 II3_frac4 Npch Vinlet \\
& + 2 II4_frac5 II3_frac4 Npch^2 + 2 II4_frac5 II2_frac4 Npch Vinlet) C0^2 + (\\
& 6 II3_frac5 II3_frac3 Npch + 4 Npch II5_frac5 III_frac3 \\
& - 10 II4_frac5 Npch II2_frac3) C0) s2^2 + ((2 III_frac3 II3_frac4 Npch Vinlet \\
& - 2 II2_frac4 Npch Vinlet II2_frac3 + 2 III_frac3 II4_frac4 Npch^2 \\
& - 2 II3_frac4 Npch^2 II2_frac3) C0^2 + (-2 III_frac2 II3_frac4 Npch \\
& - 6 III_frac3 II3_frac3 Npch + 2 II2_frac4 Npch II2_frac2 + 6 Npch II2_frac3^2) \\
& C0) s2
\end{aligned} \tag{D.38}$$

$$\begin{aligned}
f_{21} := & (2 II3_frac5 II0_frac2 Vinlet - 4 II2_frac5 III_frac2 Vinlet \\
& + 2 III_frac5 Vinlet II2_frac2) C0 s1^2 + ((-4 II4_frac5 III_frac2 Npch \\
& + 2 II4_frac5 II0_frac2 Vinlet - 4 Npch II3_frac2 II2_frac5 \\
& + 2 II2_frac5 II2_frac2 Vinlet + 8 Npch II3_frac5 II2_frac2 \\
& - 4 II3_frac5 III_frac2 Vinlet) C0 s2 + (2 II2_frac5 Npch \mu + 2 II3_frac5 Npch \\
& - II2_frac5 Npch \mu^2 - II2_frac5 Npch - 2 II3_frac5 Npch \mu) C0 CC0 + (\\
& 2 II2_frac2 III_frac4 Npch Vinlet + 2 II2_frac2 II2_frac4 Npch^2 \\
& - 2 III_frac2 II2_frac4 Npch Vinlet - 2 III_frac2 II3_frac4 Npch^2) C0^2 + (\\
& -2 II2_frac2 II0_frac3 Vinlet - 2 II3_frac5 Npch II0_frac1 \\
& + 2 II2_frac5 Npch III_frac1 + 2 III_frac2 II2_frac3 Npch \\
& - 2 II2_frac3 II0_frac2 Vinlet - 2 III_frac3 II2_frac2 Npch \\
& + 4 III_frac2 III_frac3 Vinlet) C0 + 2 II0_frac2 II2_frac2 - 2 III_frac2^2) s1 + (\\
& 8 II4_frac5 Npch II2_frac2 - 4 Npch II3_frac2 II3_frac5
\end{aligned}$$

$$\begin{aligned}
& - 4 Npch II5_frac5 III_frac2) C0 s^2 + ((-II3_frac5 Npch + 2 II3_frac5 Npch \mu \\
& - 2 II4_frac5 Npch \mu - II3_frac5 Npch \mu^2 + 2 II4_frac5 Npch) C0 CC0 + (\\
& 2 II2_frac4 Npch Vinlet II2_frac2 + 2 II3_frac4 Npch^2 II2_frac2 \\
& - 2 III_frac2 II3_frac4 Npch Vinlet - 2 III_frac2 II4_frac4 Npch^2) C0^2 + (\\
& 4 Npch III_frac3 II3_frac2 - 10 Npch II2_frac2 II2_frac3 \\
& + 2 II3_frac5 Npch III_frac1 - 2 II4_frac5 Npch II0_frac1 \\
& + 6 III_frac2 II3_frac3 Npch) C0) s2 + (-2 III_frac3 Npch \mu - 2 II2_frac3 Npch \\
& + III_frac3 Npch + III_frac3 Npch \mu^2 + 2 II2_frac3 Npch \mu) C0 CC0 \\
& + (2 Npch II0_frac1 II2_frac3 - 2 III_frac3 Npch III_frac1) C0
\end{aligned} \tag{D.39}$$

$$\begin{aligned}
f_{20} := & (2 II0_frac2 Vinlet II2_frac2 - 2 III_frac2^2 Vinlet) C0 s1 \\
& + (-4 Npch III_frac2 II3_frac2 + 4 Npch II2_frac2^2) C0 s2 + (2 II2_frac2 Npch \\
& + 2 III_frac2 Npch \mu - 2 II2_frac2 Npch \mu - III_frac2 Npch - III_frac2 Npch \mu^2) \\
& C0 CC0 + (2 III_frac2 Npch III_frac1 - 2 Npch II0_frac1 II2_frac2) C0
\end{aligned} \tag{D.40}$$

$$d_{30} = INT_rhom C_0 + \mathbf{m}(t) \tag{D.41}$$

$$m_{30} = INT_rhom C_0 N_{pch}(t) Fr \tag{D.42}$$

$$\begin{aligned}
f_{30} := & -(Nf C0^2 Npch(t)^2 INT_rhom_z2 \\
& + (C0^2 Npch(t)^2 + 2 C0^2 Npch(t) Nf Vinlet(t)) INT_rhom_z \\
& + (C0^2 Vinlet(t) Npch(t) + C0^2 Vinlet(t)^2 Nf) INT_rhom - DPext \\
& + Kexit rhom_1 vm_l^2 + \mu(t) Nf_lphi Vinlet(t)^2 + Kinlet Vinlet(t)^2) Fr - \mu(t) \\
& - INT_rhom ,
\end{aligned} \tag{D.43}$$

$$\begin{aligned}
f_{31} := & -2 Nf Npch(t) CC0 INT_z_rhom Fr - 2 Nf Fr Vinlet(t) CC0 INT_l_rhom \\
& - 2 C0 INT_rhom_z Fr Npch(t) Nf - INT_rhom C0 Npch(t) Fr \\
& - 2 INT_rhom Fr C0 Nf Vinlet(t) ,
\end{aligned} \tag{D.44}$$

$$f_{32} := (-INT_l_rhom - INT_rhom) Nf Fr , \tag{D.45}$$

$$f_{33} := (-Npch(t)^2 INT_z2_rhom - 2 Npch(t) INT_z_rhom Vinlet(t) - INT_1rhom Vinlet(t)^2) Nf Fr , \quad (D.46)$$

and

$$f_{34} = -termFr \quad (D.47)$$

where the following are the basic expressions

$$frac1 = \frac{1}{(s_2(t)Z(t)^2 + s_1(t)Z(t) + 1)} , \quad (D.48)$$

$$frac2 = \frac{1}{(s_2(t)Z(t)^2 + s_1(t)Z(t) + 1)^2} , \quad (D.49)$$

$$frac3 = \frac{1}{(s_2(t)Z(t)^2 + s_1(t)Z(t) + 1)(C_0 j(t) + V_{gj})} , \quad (D.50)$$

$$frac4 = \frac{1}{(s_2(t)Z(t)^2 + s_1(t)Z(t) + 1)(C_0 j(t) + V_{gj})^2} , \quad (D.51)$$

$$frac5 = \frac{1}{(s_2(t)Z(t)^2 + s_1(t)Z(t) + 1)^2 (C_0 j(t) + V_{gj})} , \quad (D.52)$$

$$II_j - frac1 = \int_0^{1-m(t)} \frac{Z(t)^j}{(s_2(t)Z(t)^2 + s_1(t)Z(t) + 1)} dZ , \quad (D.53)$$

$$II_j - frac2 = \int_0^{1-m(t)} \frac{Z(t)^j}{(s_2(t)Z(t)^2 + s_1(t)Z(t) + 1)^2} dZ , \quad (D.54)$$

$$II_j - frac3 = \int_0^{1-m(t)} \frac{Z(t)^j}{(s_2(t)Z(t)^2 + s_1(t)Z(t) + 1)(C_0 j(t) + V_{gj})} dZ , \quad (D.55)$$

$$II_j - frac4 = \int_0^{1-m(t)} \frac{Z(t)^j}{(s_2(t)Z(t)^2 + s_1(t)Z(t) + 1)(C_0 j(t) + V_{gj})^2} dZ , \quad (D.56)$$

$$II_j - frac5 = \int_0^{1-m(t)} \frac{Z(t)^j}{(s_2(t)Z(t)^2 + s_1(t)Z(t) + 1)^2 (C_0 j(t) + V_{gj})} dZ , \quad (D.57)$$

$$INT_rhom = \int_0^{1-m(t)} \mathbf{r}_m(Z, t) \cdot dZ , \quad (D.58)$$

$$INT_rhom_z = \int_0^{1-m(t)} Z \cdot \mathbf{r}_m(Z, t) \cdot dZ, \quad (\text{D.59})$$

$$INT_rhom_z2 = \int_0^{1-m(t)} Z^2 \cdot \mathbf{r}_m(Z, t) \cdot dZ, \quad (\text{D.60})$$

$$INT_1rhom = \int_0^{1-m(t)} \frac{1}{\mathbf{r}_m(Z, t)} \cdot dZ, \quad (\text{D.61})$$

$$INT_z_rhom = \int_0^{1-m(t)} \frac{Z}{\mathbf{r}_m(Z, t)} \cdot dZ, \quad (\text{D.62})$$

$$INT_z2_rhom = \int_0^{1-m(t)} \frac{Z^2}{\mathbf{r}_m(Z, t)} \cdot dZ. \quad (\text{D.63})$$

with $Z(t) = z - \mathbf{m}(t)$ and $CC_0 = C_0 - 1$.

The other expressions that are not presented here are very complicated and have therefore been omitted in this Appendix. However, they have been directly transferred to the Fortran code *bwr.f* used in conjunction with BIFDD for bifurcation and stability analyses.

APPENDIX E FEEDBACK REACTIVITY CALCULATIONS

In this thesis, the main feedback reactivity contributions considered are those of void and Doppler due to the void fraction and fuel temperature changes, respectively. As discussed in this Appendix, each of these two feedbacks has been modelled by assuming a linear profile for the reactivity variation with respect to the corresponding parameter. In Section E.3, results obtained using this linear approximation are compared to the exact values calculated using the LAMBDA-REAC code.

The total feedback reactivity of the coupling between modes m and n , defined in Eq. (4.12), can be written as

$$\mathbf{r}_{mn}(t) = \mathbf{r}_{mn}^F(t) = \frac{\langle \mathbf{f}_m^+, (\mathbf{d}M - \mathbf{d}L)\mathbf{f}_n \rangle}{\langle \mathbf{f}_m^+, M_0 \mathbf{f}_m \rangle} = \mathbf{r}_{mn}^V(t) + \mathbf{r}_{mn}^D(t) \quad (\text{E.1})$$

where

$$\mathbf{r}_{mn}^V(t) = \frac{\left\langle \mathbf{f}_m^+, \left(\frac{\partial M}{\partial \mathbf{a}} - \frac{\partial L}{\partial \mathbf{a}} \right) \mathbf{d}\mathbf{a} \mathbf{f}_n \right\rangle}{\langle \mathbf{f}_m^+, M_0 \mathbf{f}_n \rangle} \quad (\text{E.2})$$

is the void feedback reactivity of this coupling, and

$$\mathbf{r}_{mn}^D(t) = \frac{\left\langle \mathbf{f}_m^+, \left(\frac{\partial M}{\partial T_f} - \frac{\partial L}{\partial T_f} \right) \mathbf{d}T_f \mathbf{f}_n \right\rangle}{\langle \mathbf{f}_m^+, M_0 \mathbf{f}_n \rangle} \quad (\text{E.3})$$

is the corresponding Doppler feedback reactivity.

E.1 VOID FEEDBACK REACTIVITY

Based on Eq. (E.2), the void feedback reactivity for the fundamental mode is

$$\mathbf{r}_{00}^V(t) = \frac{\left\langle \mathbf{f}_0^+, \left(\frac{\partial M}{\partial \mathbf{a}} - \frac{\partial L}{\partial \mathbf{a}} \right) d\mathbf{a} \mathbf{f}_0 \right\rangle}{\left\langle \mathbf{f}_0^+, M_0 \mathbf{f}_0 \right\rangle} \quad (\text{E.4})$$

In RAMONA [1], the cross-sections have a second order polynomial form in terms of the void fraction. This is consistent with the assumptions used in [2] and [3] where the analytical expression for the void feedback reactivity is expressed as

$$\mathbf{r}_{00}^V(t) = \sum_k \left(C_1 + C_2 \mathbf{a}_k(t) + C_3 \mathbf{a}_k^2(t) \right) \cdot W_k^P \cdot d\mathbf{a}_k(t) \quad (\text{E.5})$$

where C_i , $i=1,2,3$ are constants, $W_k^P = \frac{P_k^2}{\sum_k P_k^2}$ is a square power weighting factor at the

axial node k , and $d\mathbf{a}_k$ is the void fraction deviation from the steady-state value at this location

E.1.1 Regional Void Feedback Reactivity Contribution

Consider that the reactor core is divided into many regions of the same size and approximately the same steady-state properties. The goal in this section is to deduce the contribution of each core region to the void feedback reactivity. Based on the full core void feedback reactivity formula, *i.e.* Eq. (E.4), the void feedback reactivity of the r^{th} core region [3] for the fundamental mode is

$$\mathbf{r}_{00}^{V,r}(t) = \frac{\left\langle \mathbf{f}_0^+, \left(\frac{\partial M}{\partial \mathbf{a}} - \frac{\partial L}{\partial \mathbf{a}} \right) d\mathbf{a} \mathbf{f}_0 \right\rangle^{(r)}}{\left\langle \mathbf{f}_0^+, M_0 \mathbf{f}_0 \right\rangle} \quad (\text{E.6})$$

where $\langle \quad \rangle^{(r)}$ denotes integration over this core region (r) only.

It is now assumed that the regional void feedback reactivity has the same profile in terms of the void fraction as that given for the full core by Eq. (E.5), *i.e.* second-order polynomial

$$\mathbf{r}_{00}^{V,r}(t) = \sum_k \left(C_1 + C_2 \mathbf{a}_k^{(r)}(t) + C_3 \mathbf{a}_k^{(r)2}(t) \right) W_k^p \mathbf{d}\mathbf{a}_k^{(r)}(t) WD_{00}^{(r)} \quad (\text{E.7})$$

where

$$\sum_k \left(C_1 + C_2 \mathbf{a}_k^{(r)}(t) + C_3 \mathbf{a}_k^{(r)2}(t) \right) \cdot W_k^p \cdot \mathbf{d}\mathbf{a}_k^{(r)}(t) = \frac{\left\langle \mathbf{f}_0^+, \left(\frac{\partial M}{\partial \mathbf{a}} - \frac{\partial L}{\partial \mathbf{a}} \right) \mathbf{d}\mathbf{a} \mathbf{f}_0 \right\rangle^{(r)}}{\left\langle \mathbf{f}_0^+, M_0 \mathbf{f}_0 \right\rangle^{(r)}}, \quad (\text{E.8})$$

and

$$WD_{00}^{(r)} = \frac{\left\langle \mathbf{f}_0^+, M_0 \mathbf{f}_0 \right\rangle^{(r)}}{\left\langle \mathbf{f}_0^+, M_0 \mathbf{f}_0 \right\rangle^{(r)}} \quad (\text{E.9})$$

$WD_{00}^{(r)}$ is the weighting factor that can be viewed as a correction factor to be multiplied to the void feedback reactivity of a core reduced to the r^{th} region.

E.1.2 Generalisation

In this section, Eq. (E.7) is generalized for any given mode coupling assuming the same second-order polynomial in terms of the void fraction. Then the void feedback reactivity of the coupling between modes m and n in the r^{th} core region is

$$\mathbf{r}_{mn}^{V,r}(t) = \sum_k \left(C_1 + C_2 \mathbf{a}_k^{(r)}(t) + C_3 \mathbf{a}_k^{(r)2}(t) \right) W_k^p \mathbf{d}\mathbf{a}_k^{(r)}(t) WD_{mn}^{(r)} \quad (\text{E.10})$$

where the modal reactivity weighting factor is defined as

$$WD_{mn}^{(r)} = \frac{\langle \mathbf{f}_0^+, M_0 \mathbf{f}_0 \rangle^{(r)} \left\langle \mathbf{f}_m^+, \left(\frac{\partial M}{\partial \mathbf{a}} - \frac{\partial L}{\partial \mathbf{a}} \right) d\mathbf{a} \mathbf{f}_n \right\rangle^{(r)}}{\langle \mathbf{f}_m^+, M_0 \mathbf{f}_m \rangle \left\langle \mathbf{f}_0^+, \left(\frac{\partial M}{\partial \mathbf{a}} - \frac{\partial L}{\partial \mathbf{a}} \right) d\mathbf{a} \mathbf{f}_0 \right\rangle^{(r)}} \quad (\text{E.11})$$

This expression for the weighting factor can be approximated by substituting the perturbations in the production and loss operators by average values and by assuming that the steady-state production operator (M_0) can be substituted by an average value for the whole reactor core⁵⁵ [3]. Then Eq. (E.11) becomes

$$WD_{mn}^{(r)} = \frac{\langle \mathbf{f}_m^+, \mathbf{f}_n \rangle^{(r)}}{\langle \mathbf{f}_m^+, \mathbf{f}_m \rangle} \quad (\text{E.12})$$

Typical values of these reactivity-weighting factors that have been computed for *kklc7_rec4* OP assuming just two core regions ($r = 1, 2$) are given in Table E-1. For this, the eigenvectors \mathbf{f}_m and their adjoints for the fundamental and first modes ($m = 1, 2$) were computed using the code LAMBDA [4], the cross-sections being provided by RAMONA.

Table E-1. Weighting distribution factors $WD_{nm}^{(r)}$ for two half-core regions for the Leibstadt *kklc7_rec4* OP calculated using LAMBDA.

$WD_{00}^{(1)}$	$WD_{00}^{(2)}$	$WD_{11}^{(1)}$	$WD_{11}^{(2)}$
0.5005	0.4995	0.4734	0.4726
$WD_{01}^{(1)}$	$WD_{01}^{(2)}$	$WD_{10}^{(1)}$	$WD_{10}^{(2)}$
-0.1272	0.1273	-0.1048	0.1048

Approximation

For the sake of simplicity of the current reduced order model, a linear profile for the void feedback reactivity in terms of the void fraction is assumed as follows.

$$\mathbf{r}_{mn}^{V,r}(t) = \sum_k C_k \cdot \left(\mathbf{a}_k^{(r)}(t) - \mathbf{a}_{k0}^{(r)} \right) \cdot W_k^P \cdot WD_{mn}^{(r)} \quad (\text{E.13})$$

⁵⁵ In [3], this approximation was validated and shown to yield good results.

In fact, this approximation is quite accurate in the case of the fundamental mode, as shown in Figs. E-1 and E-2 where the linear profile void feedback reactivity \mathbf{r}_{00}^V for two different OPs is compared with the corresponding RAMONA results. It should be noted that the linear profile approximation for the void feedback reactivity has been adopted in several previous models, *e.g.* the Karve model [5].

The next goal is the calculation of the void feedback reactivity coefficient C_1 . For this, a new methodology based on the RAMONA code was developed using the option in card 601000 [1], which allows separate perturbations in the void fraction, fuel temperature and the moderator temperature. As a consequence, inducing a perturbation just in the void fraction involves the void feedback reactivity only. For simplicity, this methodology is first applied for the void feedback reactivity for the full-core fundamental mode \mathbf{r}_{00}^V . It will then be generalized to higher modes with two core regions, which is equivalent to the two-channel representation in the current reduced order model. Equation (E.13) can be written for the fundamental mode with a single core region as follows

$$\mathbf{r}_{00}^V(t) = \sum_k C_1 \cdot (\mathbf{a}_k(t) - \mathbf{a}_{k0}) \cdot W_k^p \quad (\text{E.14})$$

Note that, for a single core region, $WD_{00} = \frac{\langle \mathbf{f}_0^+, \mathbf{f}_0 \rangle}{\langle \mathbf{f}_0^+, \mathbf{f}_0^+ \rangle} = 1$.

In the current reduced order model, the flow channel is divided into two axial regions: the single-phase and two-phase regions. The average void fraction in the core is defined as

$$\mathbf{a}(t) = \int_0^1 \mathbf{a}(z, t) \cdot dz = \int_{m(t)}^1 \mathbf{a}(z, t) \cdot dz \quad (\text{E.15})$$

where $m(t)$ is the boiling boundary and $z = 1$ corresponds to the channel exit. Using an averaging approximation based on the following approximation:

$$\mathbf{a}_k(t) = \mathbf{a}(t), \forall k \quad (\text{E.16})$$

$$\mathbf{a}_{k0} = \mathbf{a}_0, \forall k \quad (\text{E.17})$$

the void feedback reactivity can be recast as

$$\mathbf{r}_{00}^V(t) = C_1 \cdot (\mathbf{a}(t) - \mathbf{a}_0) \cdot \sum_{k=1}^{25} W_k^p = C_1 \cdot (\mathbf{a}(t) - \mathbf{a}_0) \quad (\text{E.18})$$

where \mathbf{a}_0 is the reference steady-state average void fraction in the core.

The method for the calculation of C_1 consists of the following steps:

1. At first, a steady-state calculation with RAMONA is performed for a nominal reference operational point. Then the reactivity eigenvalue k_{eff0} and the reference void fraction \mathbf{a}_0 are extracted from the output file.
2. Steady-state calculations are performed for the same nominal operational point, while introducing different values of void perturbation. The corresponding reactivity eigenvalues k_{eff} are then extracted from the output file.
3. Applying first-order perturbation theory [6],

$$\mathbf{r}_{00}^V = \frac{k_{eff} - k_{eff0}}{k_{eff} \cdot k_{eff0}} = C_1 \cdot \mathbf{da} \quad (\text{E.19})$$

Once the void feedback reactivities for different perturbed cases are computed, the value of C_1 is obtained by a linear fitting of \mathbf{r}_{00}^V in terms of \mathbf{da} .

E.1.3 Validation of the Void Feedback Reactivity Coefficient Calculation

In this section, the current void feedback reactivity model is validated against results from the system code RAMONA. This validation comparison (see Figs. E-1 and E-2) clearly shows that using a linear profile for the void feedback reactivity variation with void fraction indeed gives an accurate estimation of void effects for the full core. The two figures are for two different operational points of the Leibstadt NPP, the first one with 59% power and 36% mass flow, and the second with 100% power and 100% mass flow.

E.1.4 Generalization to Two Core Regions

The current BWR reduced order model (Chapter 4) has two channels in order to simulate out-of-phase oscillations. To model the void feedback reactivities in this case, the

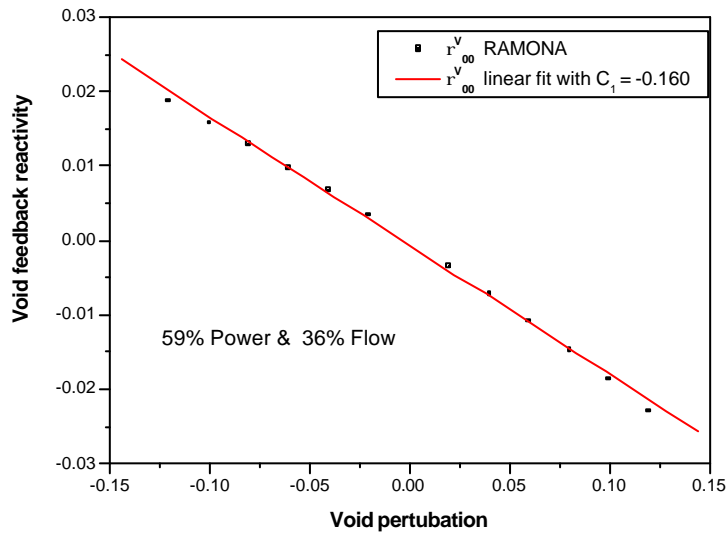


Figure E-1. Validation of the void feedback reactivity calculation against RAMONA results for the Leibstadt NPP operational point with 59% power and 36% flow.

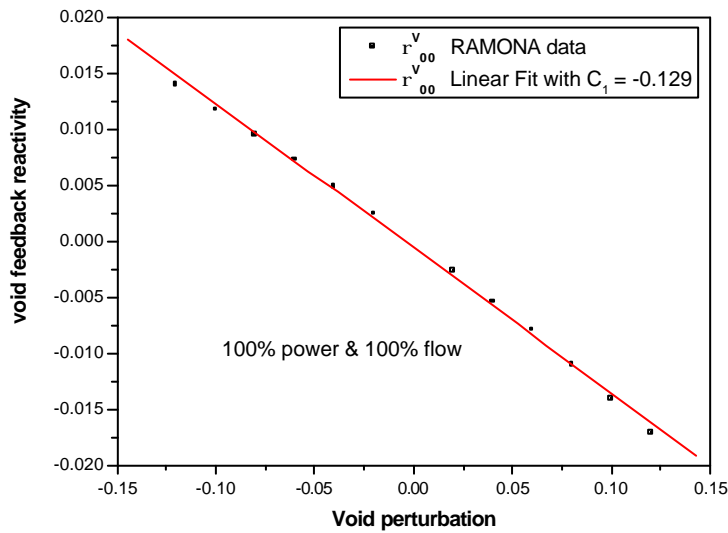


Figure E-2. Validation of void feedback reactivity calculation against RAMONA results for the Leibstadt NPP operational point with 100% power and 100% flow.

core is divided into two similar regions, *i.e.* of the same size and the same steady-state properties. Then the void feedback reactivity in channel l (region (l)) of the coupling of modes m and n , again with the linear profile assumption, may be written as

$$\mathbf{r}_{mn}^{V,l}(t) = C_1 \cdot (\mathbf{a}_l(t) - \mathbf{a}_{0,l}) \cdot WD_{mn}^l = c_{1mn}^l \cdot (\mathbf{a}_l(t) - \mathbf{a}_{0,l}) \quad (\text{E.20})$$

where $c_{1mn}^l = C_1 \cdot WD_{mn}^l$.

Typical values of the void feedback reactivity coefficients are calculated here for the Leibstadt *kklc7_rec4* operational point with 59% power and 36% flow (Table E-2).

Table E-2. Void feedback reactivity coefficients calculated for the Leibstadt OP *kklc7_rec4*.

c_{100}^1	c_{100}^2	c_{111}^1	c_{111}^2
-0.080	-0.080	-0.076	-0.076
c_{101}^1	c_{101}^2	c_{110}^1	c_{110}^2
-0.020	0.020	-0.017	0.017

E.2 DOPPLER FEEDBACK REACTIVITY

The model used for the Doppler feedback reactivity is similar to that developed for void effects. For a given region (r) in the core, the Doppler feedback reactivity can be written as

$$\mathbf{r}_{mn}^{D,r}(t) = \frac{\left\langle \mathbf{f}_m^*, \left(\frac{\partial M}{\partial T_f} - \frac{\partial L}{\partial T_f} \right) dT_f \mathbf{f}_n \right\rangle^{(r)}}{\left\langle \mathbf{f}_m^*, M_0 \mathbf{f}_n \right\rangle} \quad (\text{E.21})$$

As in Eq. (E.10), one can introduce the reactivity weighting distribution factors and a polynomial in terms of the void fraction and the fuel temperature for the r^{th} core region [3] as follows

$$\mathbf{r}_{mn}^{D,r}(t) = \sum_k (D_1 + D_2 \mathbf{a}_k^{(r)}(t) + D_3 \mathbf{a}_k^{(r)2}(t)) W_k^P (\sqrt{T_{f,k}^{(r)}(t)} - \sqrt{T_{f,0,k}^{(r)}}) WD_{mn}^{(r)} \quad (\text{E.22})$$

where D_i , $i=1,2,3$, are constants, $T_{f,k}$ is the average fuel temperature at the axial node k , and $T_{f,0,k}$ is the steady state average fuel temperature for the reference operational point at the axial node k .

Equation (E.22) shows that the Doppler feedback reactivity is proportional to the square root of the fuel temperature. This, in fact, is well consistent with the RAMONA model where the cross-sections have a square root dependence on the fuel temperature [1].

Approximation

As in Section E.2.2, for the sake of simplicity, a linear profile is assumed for the feedback reactivity variation with the parameter of interest, here the fuel temperature, *i.e.*

$$\mathbf{r}_{mn}^{D,r}(t) = \sum_k D_1 \cdot (T_{f,k}^{(r)}(t) - T_{f,0,k}^{(r)}) \cdot W_k^P \cdot WD_{mn}^{(r)} \quad (\text{E.23})$$

It is shown below, in Figs. E-3 and E-4, that using this approximation gives an accurate prediction of the Doppler feedback reactivity for the fundamental mode. It should be noted that a linear profile for the Doppler feedback reactivity in terms of the fuel temperature has been adopted in several earlier models, *e.g.* Karve model [5].

The next goal is the calculation of the Doppler feedback reactivity coefficient D_1 . Similar to the void feedback reactivity case, the coefficient D_1 is first determined for the Doppler feedback reactivity for the fundamental mode (full core). The method is then generalized for higher mode Doppler reactivities in a two-region core. Thus, Eq. (E.23) for the fundamental mode with just one core region can be written as

$$\mathbf{r}_{00}^D(t) = \sum_k D_1 \cdot (T_{f,k}(t) - T_{f,0,k}) \cdot W_k^P \quad (\text{E.24})$$

In order to implement the Doppler feedback reactivity for the current reduced order model in which each channel is divided into two axial regions, two approximations analogous to (E.16) and (E.17) are made, *i.e.*

$$T_{f,k}(t) = T_f(t), \forall k \quad (\text{E.25})$$

$$T_{f,0,k} = T_{f,0}, \forall k \quad (\text{E.26})$$

where $T_f(t)$ is the instantaneous average fuel temperature and $T_{f,0}$ is the steady-state average fuel temperature for the reference case. Consequently, Eq. (E.24) becomes

$$\mathbf{r}_{00}^D(t) = D_1 \cdot (T_f(t) - T_{f,0}) \quad (\text{E.27})$$

The method of calculation of the coefficient D_1 is similar to the method used for the calculation of the void feedback reactivity coefficient C_1 . This means: First, a steady-state calculation with RAMONA is performed for a nominal reference operational point. Then the reactivity eigenvalue k_{eff0} and the reference steady-state average fuel temperature T_{f0} are extracted from the output file. Next, steady-state calculations for the nominal OP, but with different values of fuel temperature perturbations, are performed and the corresponding k_{eff} values are extracted from the output file. Finally, applying first-order perturbation theory,

$$\mathbf{r}_{00}^D = \frac{k_{eff} - k_{eff0}}{k_{eff} \cdot k_{eff0}} = D_1 \cdot dT_f \quad (\text{E.28})$$

where $dT_f = T_f - T_{f0}$ is the fuel temperature perturbation.

Once the Doppler feedback reactivities for different perturbations are computed, the value of D_1 is obtained by a linear fitting in terms of dT_f .

E.2.1 Validation of the Doppler Feedback Reactivity Coefficient Calculation

In this section, the current Doppler feedback reactivity model is demonstrated to be quite accurate for the fundamental mode. This has been done by comparing results with those obtained using RAMONA for the two Leibstadt NPP operational points used earlier. Figures E-3 and E-4 clearly show that good agreement is obtained.

E.2.2 Generalization to Two Core Regions

To model the Doppler feedback reactivities in the context of the current two-channel reduced order model, the core, as for the void reactivity case, is divided into two similar

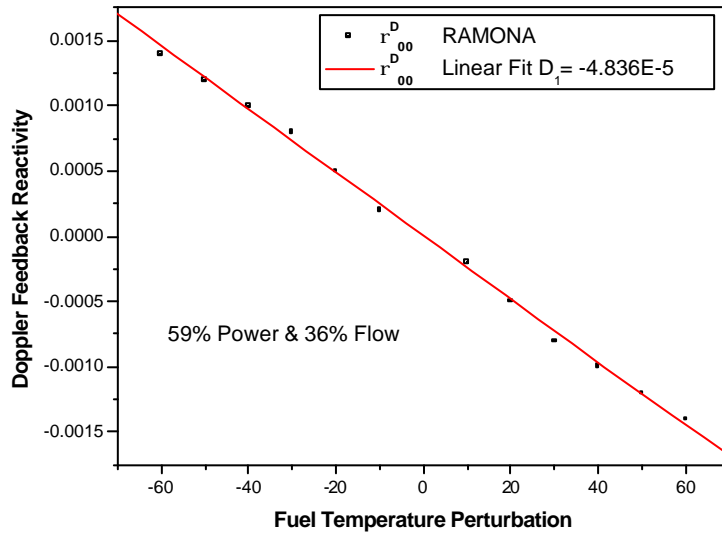


Figure E-3. Validation of the Doppler feedback reactivity calculation against RAMONA results for the Leibstadt NPP operational point with 59% power and 36% flow.

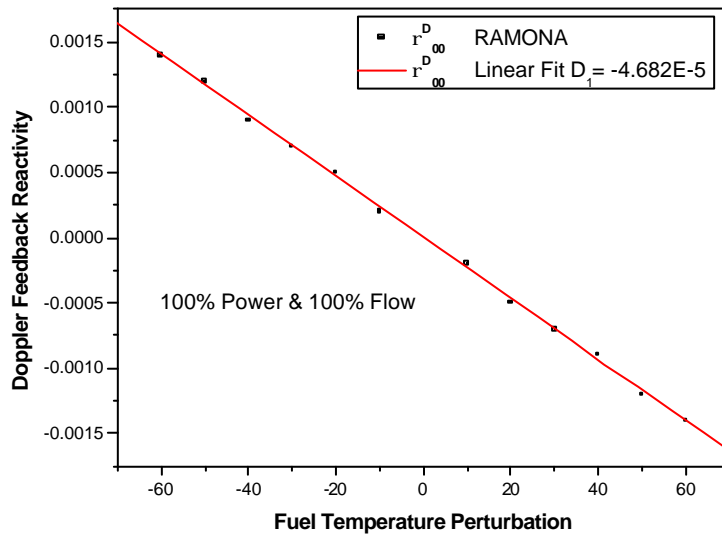


Figure E-4. Validation of the Doppler feedback reactivity calculation against RAMONA results for the Leibstadt NPP operational point with 100% power and 100% flow.

regions. Then the Doppler feedback reactivity in channel l for the coupling of mode m with mode n is:

$$\mathbf{r}_{mn}^{D,l}(t) = D_1 \cdot (T_{f,l}(t) - T_{f,0,l}) \cdot WD_{mn}^l = c_{2mn}^l \cdot (T_{f,l}(t) - T_{f,0,l}) \quad (\text{E.29})$$

where $c_{2mn}^l = D_1 \cdot WD_{mn}^l$.

Typical values of the Doppler feedback reactivity coefficients are calculated here for the Leibstadt *kklc7_rec4* operational point with 59% power and 36% flow (Table E-3).

Table E-3. Doppler feedback reactivity coefficients calculated for the Leibstadt OP *kklc7_rec4*.

c_{200}^1	c_{200}^2	c_{211}^1	c_{211}^2
$-0.242 \cdot 10^{-4}$	$-0.242 \cdot 10^{-4}$	$-0.229 \cdot 10^{-4}$	$-0.229 \cdot 10^{-4}$
c_{201}^1	c_{201}^2	c_{210}^1	c_{210}^2
$-0.062 \cdot 10^{-4}$	$0.062 \cdot 10^{-4}$	$-0.051 \cdot 10^{-4}$	$0.051 \cdot 10^{-4}$

E.3 TOTAL FEEDBACK REACTIVITIES

Based on the approximations assumed for the void and Doppler feedback reactivities, *i.e.* linear profiles for their variation with respect to the average void fraction and fuel temperature, respectively, the total feedback reactivity can be written as

$$\mathbf{r}_{mn}(t) = \sum_{l=1}^2 \mathbf{r}_{mn}^l(t) = \sum_{l=1}^2 c_{1mn}^l \cdot (\mathbf{a}_l(t) - \mathbf{a}_{0,l}) + c_{2mn}^l \cdot (T_{f,l}(t) - T_{f,0,l}) \quad (\text{E.30})$$

To check whether the approximation (E.30) still leads to a good agreement with the results calculated using the exact Eq. (E.1), a comparison has been made between the approximated and exact feedback reactivity values for the Leibstadt NPP *kklc7_rec4* OP (out-of-phase oscillation case). To calculate the exact feedback reactivities, use was made of the code LAMBDA_REAC, developed by Miró *et al.* [7], that allows the calculation of feedback reactivities for higher modes based on Eq. (E.1). For the approximated feedback reactivity calculation, RAMONA was used, in that Eq. (E.30) was applied in conjunction with the void and Doppler feedback reactivity coefficients of Tables E-2 and E-3, on the

one hand, and steady-state and transient values of the average void fraction and fuel temperature extracted from the plot file of RAMONA, on the other.

Figure E-5 shows the time series of the total feedback reactivity of the fundamental mode calculated by the approximated method (\mathbf{r}_{00_appr}) and the exact method (\mathbf{r}_{00_exact}). This figure clearly shows that using the linear approximated method gives good agreement with the exact results for the estimation of the fundamental mode feedback reactivity. In Fig. E-6, the first mode feedback reactivity is depicted as obtained using the two different methods. It is clearly seen that the amplitude of the exact first mode feedback reactivity, \mathbf{r}_{11_exact} , is significantly greater than the approximated first mode feedback reactivity, \mathbf{r}_{11_appr} . However, the oscillation shape of the two is the same, *i.e.* when the amplitude of \mathbf{r}_{11_exact} is growing (decaying), the amplitude of \mathbf{r}_{11_appr} is also growing (decaying).

Figure E-7 depicts the feedback reactivity for the coupling between the first and fundamental modes. The approximated method gives a very small value of the coupled feedback reactivity as compared to the exact one. Moreover, the oscillation shapes of the two feedback reactivities, *i.e.* \mathbf{r}_{10_exact} and \mathbf{r}_{10_appr} , are very different. Thus, while the \mathbf{r}_{10_exact} amplitude is seen to grow over the entire interval, the amplitude of \mathbf{r}_{10_appr} decays from 1 to 30 seconds, then start to grow with relatively small values.

A comparison of the shape of \mathbf{r}_{10_exact} with those of \mathbf{r}_{00_exact} and \mathbf{r}_{11_exact} suggests that the feedback reactivity for the coupling between the first and the fundamental modes is too complicated to be modelled simply, *i.e.* in a manner similar to the feedback reactivity of the fundamental mode. Thus, the approximated method cannot be expected to yield an appropriate simulation of the feedback reactivity for the mode coupling. Accordingly, a bifurcation parameter, $fact_{mn}$, also called the feedback gain parameter, is introduced to serve as multiplier for the corresponding feedback reactivity, *i.e.* to amplify the feedback gain for the coupling between the first and fundamental modes when out-of-phase oscillations are excited. The “corrected” total feedback reactivity then becomes

$$\mathbf{r}_{mn}(t) = fact_{mn} \cdot \sum_{l=1}^2 c_{lmn}^l \cdot (\mathbf{a}_l(t) - \mathbf{a}_{0,l}) + c_{2mn}^l \cdot (T_{f,l}(t) - T_{f,0,l}) \quad (\text{E.31})$$

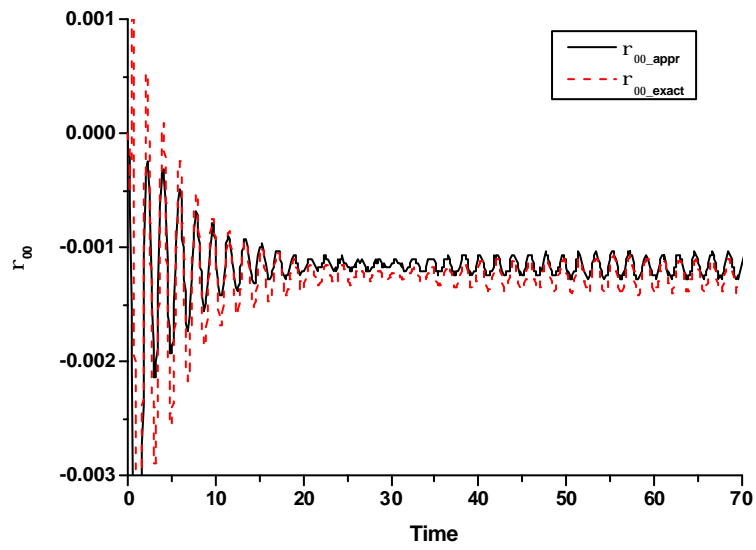


Figure E-5. Validation of the feedback reactivity calculation: comparison between the approximate and the exact feedback reactivity for the fundamental mode.

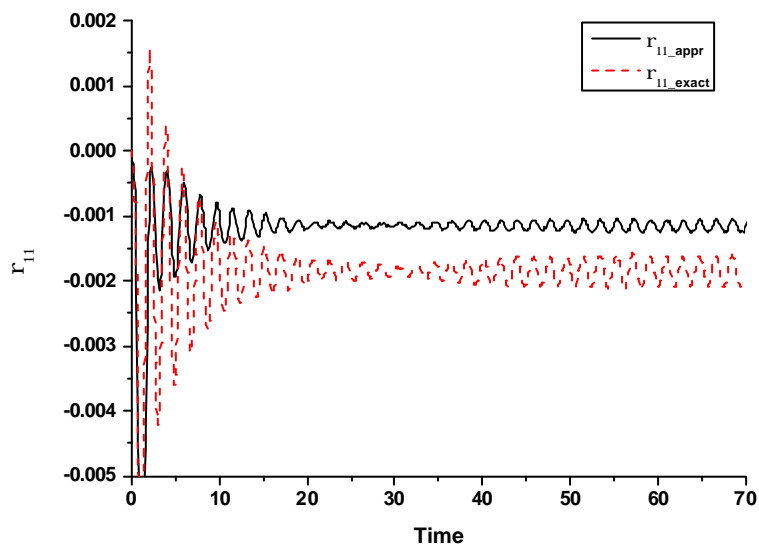


Figure E-6. Validation of the feedback reactivity calculation: comparison between the approximate and the exact feedback reactivity for the first mode.

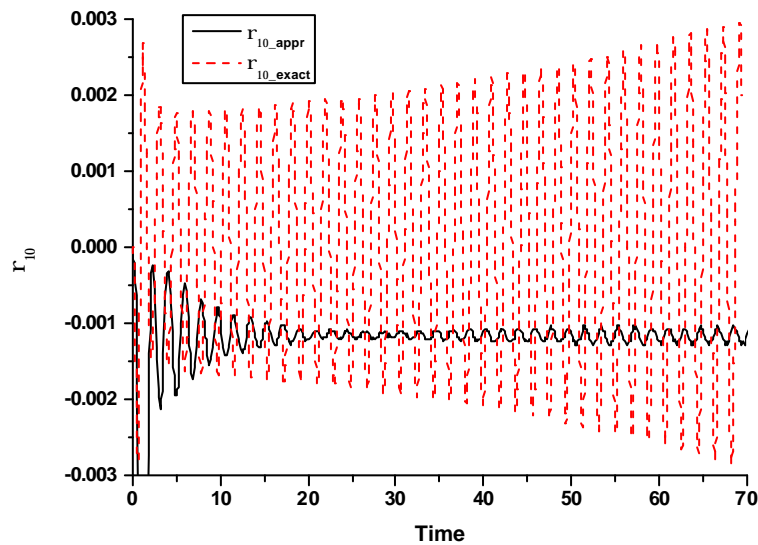


Figure E-7. Validation of the feedback reactivity calculation: comparison between the approximate and the exact feedback reactivity for the coupling between the first and fundamental modes.

REFERENCES

- [1] "RAMONA-3B, User Manual," Scandpower, 1993.
- [2] J. A. Borkowski, N. L. Wade, S. Z. Rouhani, R. W. Shumway, W. L. Weaver, W. H. Rettig, C. L. Kullberg, "TRACBF1 / Mod1, Models and Correlations," NUREG/CR-4391, EGG-2680, 1992.
- [3] J. L. Muñoz-Cobo, O. Rosello, R. Miró, A. Escrivá, D. Ginestar, G. Verdú, "Coupling of Density Wave Oscillations in Parallel Channels with High Order Modal Kinetics: Application to BWR Out-of-phase Oscillations", *Ann. Nucl. Energy*, **17**, 1345-1371, 2000.
- [4] G. Verdú, R. Miró, D. Ginestar, V. Vidal, "The Implicit Restarted Arnoldi Method, an Efficient Alternative to Solve the Neutron Diffusion Equation," *Ann. Nucl. Energy*, **26**, 579-593, 1999.
- [5] A. A. Karve, "Nuclear-Coupled Thermal-Hydraulic Stability Analysis of Boiling Water Reactors," Ph.D. Dissertation, Virginia University, 1999.
- [6] A. F. Henry, *Nuclear Reactor Analysis*, MIT Press, 1975.
- [7] R. Miró, D. Ginestar, D. Hennig, G. Verdú, "On the Regional Oscillation Phenomenon in BWRs", *Prog. Nucl. Energy*, **36**, 2, 189-229, 2000.

APPENDIX F TYPICAL BWR DESIGN AND OPERATING PARAMETERS

In this appendix, standard numerical values are presented of typical BWR design and operating parameters as used in Chapter 6. These parameter values were first used by Karve [1].

$A^* = 1.442 \cdot 10^{-4} m^2$	$c_{200,1}^* = -2.15 \cdot 10^{-5} K^{-1}$
$D^* = 1.424 cm$	$c_{200,2}^* = -2.15 \cdot 10^{-5} K^{-1}$
$L^* = 3.81 m$	$c_{201,1}^* = -9.88 \cdot 10^{-6} K^{-1}$
$R^* = 2.32 m$	$c_{201,2}^* = 9.88 \cdot 10^{-6} K^{-1}$
$T_{inlet}^* = 551 K$	$c_{210,1}^* = -3.28 \cdot 10^{-5} K^{-1}$
$T_0^* = T_{sat}^* = 561 K$	$c_{210,2}^* = 3.28 \cdot 10^{-5} K^{-1}$
$c_{100,1}^* = -5.0500 \cdot 10^{-2}$	$c_{211,1}^* = -2.15 \cdot 10^{-5} K^{-1}$
$c_{100,2}^* = -5.0500 \cdot 10^{-2}$	$c_{211,2}^* = -2.15 \cdot 10^{-5} K^{-1}$
$c_{101,1}^* = -4.5078 \cdot 10^{-2}$	$c_c^* = 330.0 J kg^{-1} K^{-1}$
$c_{101,2}^* = 4.4632 \cdot 10^{-2}$	$c_f^* = 5.307 \cdot 10^3 J kg^{-1} K^{-1}$
$c_{110,1}^* = -7.7116 \cdot 10^{-2}$	$c_p^* = 325.0 J kg^{-1} K^{-1}$
$c_{110,2}^* = 7.6353 \cdot 10^{-2}$	$c_q^* = 4.6901 \cdot 10^{-6} W$
$c_{111,1}^* = -9.8091 \cdot 10^{-2}$	$g^* = 9.81 m s^{-2}$
$c_{111,2}^* = -9.712010^{-2}$	$h_g^* = 5678.2 W m^{-2} K^{-1}$

$$k_c^* = 17.0 \text{ W m}^{-1} \text{ K}^{-1}$$

$$K_{exit} = 1.35$$

$$k_f^* = 0.574 \text{ W m}^{-1} \text{ K}^{-1}$$

$$K_{inlet} = 19$$

$$k_p^* = 2.7 \text{ W m}^{-1} \text{ K}^{-1}$$

$$n_0^* = 3.6245 \cdot 10^7 \text{ cm}^{-3}$$

$$N_{f,1f} = 1.86777$$

$$N_{f,2f} = 2.08256$$

$$p^* = 7.2 \cdot 10^6 \text{ N m}^{-2}$$

$$p_c^* = 16.2 \cdot 10^{-3} \text{ m}$$

$$r_c^* = 6.135 \cdot 10^{-3} \text{ m}$$

$$r_g^* = 5.322 \cdot 10^{-3} \text{ m}$$

$$r_p^* = 5.2 \cdot 10^{-3} \text{ m}$$

$$r_d^* = 0.83 \cdot r_p^*$$

$$v_0^* = 2.67 \text{ m s}^{-1}$$

$$\Delta h_{fg}^* = 1494.2 \cdot 10^3 \text{ J kg}^{-1}$$

$$\Lambda^* = 4.0 \cdot 10^{-5} \text{ s}$$

$$\mathbf{a}_c^* = 7.925 \cdot 10^{-6} \text{ m}^2 \text{ s}^{-1}$$

$$\mathbf{a}_p^* = 7.97 \cdot 10^{-7} \text{ m}^2 \text{ s}^{-1}$$

$$\mathbf{b} = 0.0056$$

$$\mathbf{r}_c^* = 6.5 \cdot 10^3 \text{ kg m}^{-3}$$

$$\mathbf{r}_f^* = 736.49 \text{ kg m}^{-3}$$

$$\mathbf{r}_g^* = 37.71 \text{ kg m}^{-3}$$

$$\mathbf{r}_p^* = 10.422 \cdot 10^3 \text{ kg m}^{-3}$$

$$\mathbf{l} = 0.08 \text{ s}^{-1}$$

$$\mathbf{m}_f^* = 9.693 \cdot 10^{-5} \text{ N m}^{-2} \text{ s}$$

REFERENCES

[1] A. A. Karve, "Nuclear-Coupled Thermal-Hydraulic Stability Analysis of Boiling Water Reactors", Ph.D. Dissertation, Virginia University, 1999.

APPENDIX G DESIGN AND OPERATING PARAMETERS FOR THE NOMINAL LEIBSTADT NPP OPERATIONAL POINT

In this appendix, the numerical values are presented of the design and operating parameters for the Leibstadt OP *kklc7_rec4*, used as input in the analysis carried out in Chapter 8.

$A^* = 1.442 \cdot 10^{-4} m^2$	$c_{200,1}^* = -2.42 \cdot 10^{-5} K^{-1}$
$D^* = 1.424 cm$	$c_{200,2}^* = -2.42 \cdot 10^{-5} K^{-1}$
$L^* = 3.81 m$	$c_{201,1}^* = -0.62 \cdot 10^{-5} K^{-1}$
$R^* = 2.32 m$	$c_{201,2}^* = 0.62 \cdot 10^{-5} K^{-1}$
$T_{inlet}^* = 551 K$	$c_{210,1}^* = -0.51 \cdot 10^{-5} K^{-1}$
$T_0^* = T_{sat}^* = 561 K$	$c_{210,2}^* = 0.51 \cdot 10^{-5} K^{-1}$
$c_{100,1}^* = -8.0 \cdot 10^{-2}$	$c_{211,1}^* = -2.29 \cdot 10^{-5} K^{-1}$
$c_{100,2}^* = -8.0 \cdot 10^{-2}$	$c_{211,2}^* = -2.29 \cdot 10^{-5} K^{-1}$
$c_{101,1}^* = -2.0 \cdot 10^{-2}$	$c_c^* = 330.0 J kg^{-1} K^{-1}$
$c_{101,2}^* = 2.0 \cdot 10^{-2}$	$c_f^* = 5.307 \cdot 10^3 J kg^{-1} K^{-1}$
$c_{110,1}^* = -1.7 \cdot 10^{-2}$	$c_p^* = 476.6 J kg^{-1} K^{-1}$
$c_{110,2}^* = 1.7 \cdot 10^{-2}$	$c_q^* = 4.6901 \cdot 10^{-6} W$
$c_{111,1}^* = -7.6 \cdot 10^{-2}$	$g^* = 9.81 m s^{-2}$
$c_{111,2}^* = -7.6 \cdot 10^{-2}$	$h_g^* = 4937.5 W m^{-2} K^{-1}$

$$k_c^* = 16.0 \text{ W m}^{-1} \text{ K}^{-1}$$

$$K_{exit} = 2.96$$

$$k_f^* = 0.574 \text{ W m}^{-1} \text{ K}^{-1}$$

$$K_{inlet} = 20.1$$

$$k_p^* = 3.79 \text{ W m}^{-1} \text{ K}^{-1}$$

$$n_0^* = 5.01974 \cdot 10^7 \text{ cm}^{-3}$$

$$N_{f,1f} = 2.28$$

$$N_{f,2f} = 2.66$$

$$p^* = 6.97 \cdot 10^6 \text{ N m}^{-2}$$

$$p_c^* = 16.2 \cdot 10^{-3} \text{ m}$$

$$r_c^* = 6.135 \cdot 10^{-3} \text{ m}$$

$$r_g^* = 5.322 \cdot 10^{-3} \text{ m}$$

$$r_p^* = 5.2 \cdot 10^{-3} \text{ m}$$

$$r_d^* = 0.83 \cdot r_p^*$$

$$v_0^* = 2.67 \text{ m s}^{-1}$$

$$\Delta h_{fg}^* = 1494.2 \cdot 10^3 \text{ J kg}^{-1}$$

$$\Lambda^* = 3.0 \cdot 10^{-5} \text{ s}$$

$$\mathbf{b} = 0.0056$$

$$\mathbf{r}_c^* = 6.5 \cdot 10^3 \text{ kg m}^{-3}$$

$$\mathbf{r}_f^* = 736.49 \text{ kg m}^{-3}$$

$$\mathbf{r}_g^* = 37.71 \text{ kg m}^{-3}$$

$$\mathbf{r}_p^* = 10.422 \cdot 10^3 \text{ kg m}^{-3}$$

$$\mathbf{l} = 0.08 \text{ s}^{-1}$$

$$\mathbf{m}_f^* = 9.693 \cdot 10^{-5} \text{ N m}^{-2} \text{ s}$$

$$\mathbf{a}_0 = 0.60$$

$$T_{avg,0}^* = 780 \text{ K}$$

NOMENCLATURE

A	cross-sectional flow area.
ACF	autocorrelation function
AR	autoregressive
ARMA	autoregressive moving-average
B_i	Biot number.
C_i	void feedback reactivity coefficients
C_0	radially non-uniform void distribution parameter
D	flow channel diameter
$D(\vec{r}, t)$	neutron diffusion coefficient
D_h	heated diameter
D_i	Doppler feedback reactivity coefficients
DR	decay ratio
Fr	Froude number
Im	imaginary part
IRF	impulse response function
J	Jacobian matrix
L	flow channel length
N_{cov}	conversion number
N_f	friction number
NF	natural frequency
N_{pch}	phase change number
N_{sub}	subcooling number
P	pressure
PAH	Poincaré-Andronov-Hopf
R	reactor core radius
Re	real part
SB	stability boundary
T	temperature
$U(\vec{r}, t)$	averaged delayed neutron precursor group concentration.

V_{gj}	drift velocity
$a_1(t)$	phase variable: coefficient of the linear term in the single-phase enthalpy profile expression
$a_2(t)$	phase variable: coefficient of the quadratic term in the single-phase enthalpy profile expression.
c_c	clad specific heat
c_f	liquid (coolant) specific heat
c_p	fuel pellet specific heat
c_q	$c_q^* = \frac{q^{m*}}{n_0^*}$
f	friction factor
g	gravitational constant
h_∞	clad surface heat transfer coefficient
h_g	pellet-clad gap conductance
h_{inlet}	coolant inlet enthalpy
h_{sat}	coolant saturation enthalpy
k_c	clad thermal conductivity
K_{exit}	exit pressure loss coefficient
k_f	liquid thermal conductivity
K_{inlet}	inlet pressure loss coefficient
k_p	fuel pellet thermal conductivity
n	neutron number density
p	system pressure
p_c	BWR lattice cell pitch
q''	wall heat flux
q'''	volumetric heat generation rate
r_1	fuel rod radius = r_c
r_c	clad outer radius
r_d	point of discontinuity $0 < r_d < r_p$

r_g	clad inner radius
r_p	fuel pellet radius
$s_1(t)$	phase variable: coefficient of the linear term in the quality profile expression
$s_2(t)$	phase variable: coefficient of the quadratic term in the quality profile expression
t	time
\mathbf{u}	neutron velocity
v	coolant velocity
x	quality
z	channel axial spatial coordinate
DP_{ext}	external pressure drop
Δh_{fg}	vapour-liquid enthalpy difference $\equiv h_g - h_f$
$\Delta \mathbf{r}$	liquid-vapour density difference $= \mathbf{r}_f - \mathbf{r}_g$
Λ	neutron generation time
S_a	macroscopic absorption cross-section
S_f	macroscopic fission cross-section
w	oscillation frequency
\mathbf{a}	void fraction
\mathbf{a}_c	clad thermal diffusivity
\mathbf{a}_p	pellet thermal diffusivity
\mathbf{b}	delayed neutron fraction
q	temperature difference from steady-state value $= T - \tilde{T}$
l	precursor decay constant
l	real part of the eigenvalue with the large real part for the Jacobian matrix of the set of ODEs.
m	boiling boundary
m_f	liquid viscosity
n	average number of neutrons produced per fission
x	volume factor

x_h	heated perimeter = $2pr_c$
r	reactivity
r_c	clad density
r_f	liquid density
r_g	vapor density
r_p	pellet density
G	generation rate

Subscripts

$1f$	single-phase
$2f$	two-phase
avg	average
$exit$	channel exit
ext	external
f	liquid
g	vapor
g	fuel-clad gap
$inlet$	channel inlet
l	left and channel number 1 or 2
m	mixture
o	reference
p	pellet
r	right
s	surface and steady-state
sat	saturation
v	vapour and void

Superscripts

\sim	steady-state value
$*$	dimensional quantity

ACKNOWLEDGEMENTS

This work was carried out within the project STARS in the Laboratory for Reactor Physics and Systems Behaviour of the Paul Scherrer Institute (PSI) and the École Polytechnique Fédérale de Lausanne (EPFL).

This thesis could not have been achieved without the help and support of numerous people. I am particularly grateful to:

- Prof. R. Chawla, Head of Reactor Physics and Systems Behaviour research at PSI/EPFL, for giving me the opportunity to carry out this thesis work and for his support.
- Dr. D. Hennig, my supervisor, for his enthusiastic support, his permanent suggestions and encouragement, and for many valuable discussions. This thesis certainly became to a large extent what it is now due to his keen “fatherhood”.
- Prof. Rizwan-uddin, for the warm hospitality during my stay at the University of Illinois at Urbana-Champaign (UIUC) from July to December 2001. His contribution was very valuable, especially the advice on bifurcation analysis using BIFDD and the many valuable comments and discussions.
- M. A. Zimmermann, the STARS Project Manager, for his interest in my work and his support and fruitful discussions.
- Dr. Y. Aounallah, Dr. A. Dehbi, Dr. M. Dekhane, H. Ferroukhi and O. Zerkak for the time they spent correcting the manuscript and for their valuable discussions.
- STARS colleagues: P. Jacquemoud, K. Hofer, Dr. J. Lebenhaft, Dr. R. Macian and Dr. W. Barten, for their encouragement and interest in my work. Also our secretary Mrs. R. Ringele for her administrative support.
- All my old friends and teachers: Rabah, Messaoud, Fouad, Ammar, Boubekeur; Mmes. N. Boussendal, D. Betite, N. Guechi, H. Mokrane, Keouita, Boudjemline and Mekroud; and Messrs. A. Boutebcha, A. Nechema, K. Saidi, A. Tebiche, Guaneme, Dr. M. Boushaba, K. Guerine and Goumeri, for their advices and encouragement through my different educational stages.
- My wife, Leila, for her constant encouragement and patience. Without her support, the accomplishment of this work would not have been possible.
- My parents for their sacrifices, encouragement and understanding through my whole period in school.

Finally, I would like to thank Profs. B. Deveaud-Plédran, R. Chawla, A. Fasoli, Rizwan-uddin, G. Verdú and Dr. D. Hennig for accepting to form the jury.

CURRICULUM VITAE

Name: Abdelhamid DOKHANE
Date of birth: June 15, 1973
Place of birth: Ferdjioua, Algeria
Address: Weiermattring 6, CH-5200 Brugg
Nationality: Algerian

PROFESSIONAL EXPERIENCE AND EDUCATION

November 1999-January 2004 Ph.D. student at the Laboratory of Reactor Physics and Systems Behaviour, *Swiss Federal Institute of Technology*, Lausanne, and at the *Paul Scherrer Institute*, Villigen, Switzerland.

July 2001-December 2001 Visiting Scholar at the *Department of Nuclear, Plasma, and Radiological Engineering*, *University of Illinois at Urbana-Champaign*, USA.

October 1998-September 1999 Diploma course program at the *International Centre for Theoretical Physics*, Trieste, Italy.

September 1995-July 1998 Teaching Assistant at the *Department of Mathematics*, *University of Constantine*, Algeria.

September 1995-July 1996 DEA (Diplôme d'Etudes Approfondies) in Condensed Matter Physics, *University of Setif*, Algeria.

September 1991-July 1995 DES (Diplôme d'Etudes Supérieures) in Theoretical Physics, *University of Constantine*, Algeria.

July 1991 Baccalauréat in Mathematics, *Lyceé Boudiaf*, *Ferdjioua*, Algeria.

PUBLICATIONS

A. Dokhane, D. Hennig, Rizwan-uddin, R. Chawla, "Bifurcation Analysis using the System Code RAMONA", accepted paper for the *12th International Conference on Nuclear Engineering (ICONE12)*, Virginia, USA, April 25-29, 2004.

A. Dokhane, D. Hennig, Rizwan-uddin, R. Chawla, "Semi-analytical Bifurcation Analysis of Two-phase Flow in a Heated Channel", submitted to the *International Journal of Bifurcation and Chaos* (2003).

A. Dokhane, D. Hennig, Rizwan-uddin, R. Chawla, "Nonlinear Stability Analysis of BWRs on the Basis of System codes and Reduced order models", *Jahrestagung Kerntechnik 2003*, Berlin, Germany, May (2003).

A. Dokhane, D. Hennig, Rizwan-uddin, R. Chawla, "Nuclear-Coupled Thermal-hydraulic Nonlinear Stability Analysis Using a Novel BWR Reduced Order Model: Part 1- The Effects of Using Drift Flux Model Versus Homogeneous Equilibrium Model", *Proc. of the 11th International Conference on Nuclear Engineering (ICONE11)*, Tokyo, Japan, April 20-23, 2003. CD-ROM (2003); Award for "Excellent Presentation" in ICONE11 Student Program.

A. Dokhane, D. Hennig, Rizwan-uddin, R. Chawla, "Nuclear-Coupled Thermal-hydraulic Nonlinear Stability Analysis Using a Novel BWR Reduced Order Model: Part 2- Stability Limits of In-phase and Out-of-phase Modes of Oscillations", *Proc. of the 11th International Conference on Nuclear Engineering (ICONE11)*, Tokyo, Japan, April 20-23, 2003. CD-ROM (2003); Award for "Excellent Presentation" in ICONE11 Student Program.

A. Dokhane, D. Hennig, Rizwan-uddin, and R. Chawla, "Nonlinear Stability Analysis with a Novel BWR Reduced Order Model", *Proc. of the International Conference on the New Frontiers of Nuclear Technology, Reactor Physics, Safety and High-performance Computing (PHYSOR 2002)*, Seoul, KOREA, October 7-10, 2002. CD-ROM (2002)

A. Dokhane, D. Hennig, Rizwan-uddin, R. Chawla, "A Parametric Study of Heated Channels with Two-Phase Flow Using Bifurcation Analysis", *Trans. Amer. Nucl. Soc.*, **86** (2002).

A. Dokhane, D. Hennig, Rizwan-uddin, R. Chawla, "Stability and Bifurcation Analyses of Two-Phase Flow Using a Drift Flux Model and Bifurcation Code BIFDD", *Proc. of the 10th International Conference on Nuclear Engineering (ICONE10)*, Virginia, USA, April 14-18, 2002. CD-ROM (2002).

A. Dokhane, D. Hennig, Rizwan-uddin, and R. Chawla, "Analytical Modelling of Non-Linear Stability Behaviour of Boiling Water Reactors", *PSI Scientific Report 2001, Nuclear Energy and Safety*, **4**, 35-47 (2002).